May 2019

Design and Optimization of Hybrid Foundation for Tall Wind Turbines and Development of New Foundation Through Biomimicry

Shweta Shrestha
Clemson University, shweta102@hotmail.com

DESIGN AND OPTIMIZATION OF HYBRID FOUNDATION FOR TALL WIND TURBINES AND DEVELOPMENT OF NEW FOUNDATION THROUGH BIOMIMICRY

A Dissertation
Presented to
the Graduate School of
Clemson University

In Partial Fulfillment
of the Requirements for the Degree
Doctor of Philosophy
Civil Engineering

---

by
Shweta Shrestha
May 2019

Accepted by:
Dr. Nadarajah Ravichandran, Committee Chair
Dr. Ronald D. Andrus
Dr. Kalyan R. Piratla
Dr. Laura Redmond

ABSTRACT

This study presents a simplified geotechnical design, design optimization, and finite element modeling of the piled-raft foundation intended for a 130 m tall wind turbine for different site conditions. The sites considered are composed of multilayered soil, clayey soil, and sandy soil. The simplified geotechnical design includes the safety checks (vertical load, horizontal load, and bending moment capacities) and serviceability check (total vertical and differential settlements). The simplified design showed that the final design is controlled by differential settlement requirement. Subsequently, a parametric study was also conducted to investigate the effect of soil strength parameter (undrained cohesion for clay and friction angle for sand) and wind speed on the design. The major drawback of this parametric study is that only one variable is changed at a time. However, more than one variable can change at the same time. Therefore, a reliability-based robust design optimization was conducted using Non-dominated Sorting Genetic Algorithm – II (NSGA-II) coupled with Monte Carlo simulation. In the design optimization, the wind speed and soil strength parameter were considered as random variables, radius of raft, length of pile, and number of piles were considered as the design variables, and the total cost of the foundation and the standard deviation of differential settlement were considered as the two objectives to satisfy. This resulted in a set of acceptable designs forming a Pareto front which showed a trade-off relationship between the total cost and standard deviation of differential settlement which can be used to obtain the design as per the cost and safety requirement. The most optimum design can be obtained using the knee point concept. Further, a three-dimensional finite element model of the piled-raft foundation was

developed and analyzed in ABAQUS and the response was compared with the simplified analytical design results. The stress-strain behavior of soil was represented by both linear and nonlinear constitutive models. The soil-structure interfaces were modeled by defining the interaction properties at the interfaces. It was observed that the analytical design resulted in a higher vertical settlement and the horizontal displacement and lower differential settlement and rotation compared to the finite element result. The parametric study conducted subsequently by varying the wind speed and undrained cohesion of soil showed that the difference between the predicted responses from two methods decreases when the load is large and/or soil is soft. Finally, a preliminary study on the development of a new foundation for wind turbine through biomimicry is also presented. Since wind turbine is comparable to a coconut tree, sabal palm tree, and Palmyra tree, the root of these trees is studied to develop simplified configurations with a different number of main roots and sub-roots. The results showed that the performance of the foundation under combined load improved with the increase in the number of main roots while the sub-roots had a negligible contribution to the performance of the foundation.

DEDICATION

To my parents, Keshab Bahadur Shrestha and Gauri Pradhan Shrestha for their endless love, support, and encouragement throughout my journey.

And to my husband, Prabesh Rupakheti for his immense support, encouragement, and belief in me.

ACKNOWLEDGMENTS

I would like to take this opportunity to express my sincere gratitude to many people who have helped me to complete this dissertation. First and foremost, I would like to express my deepest gratitude to my advisor **Dr. Nadarajah Ravichandran (Dr. Ravi)** for his valuable suggestions, motivation, and guidance throughout my journey. I am truly grateful towards him for providing me the opportunity to conduct this remarkable research with him. Not only Dr. Ravi advised me as my research advisor but also selflessly mentored me to prepare for my classes which I taught at Clemson University as Graduate Teacher of Record. He has provided me every single opportunity for my growth at Clemson University. Dr. Ravi truly cares for his students' success. I can't thank him enough for his continuous support and encouragement without which I wouldn't have been able to achieve my goals. I am extremely blessed to be Dr. Ravi's student.

I would also like to thank my committee members **Dr. Ronald D. Andrus**, **Dr. Kalyan R. Piratla,** and **Dr. Laura Redmond** for their support and taking time to review my dissertation. The classes that I took with them and advice were very helpful to develop a better understanding and complete my research.

I would like to extend my sincere gratitude to Shrikhande family for supporting my study through the prestigious **Aniket Shrikhande Memorial Assistantship and Fellowship**. The financial support of the Shrikhande family is gratefully acknowledged. I would also like to convey my great appreciation to the Glenn Department of Civil Engineering for providing me the prestigious **Glenn Teaching Fellowship** and **teaching assistantship**. Further, I want to thank the Office of the Vice President of Research and

the Dean of the Graduate School at Clemson University for selecting me to receive **Doctoral Dissertation Completion Grant** which helped me to complete my dissertation on time. These financial supports were the backbone of my study without which I couldn't imagine completing my study.

My family has been the greatest support through my journey. I want to thank them for their blessings, for believing in me, and constantly supporting my dreams.

Finally, I would like to thank all the faculties, staffs, colleagues, and friends for making my study and stay at Clemson University smooth and enjoyable.

TABLE OF CONTENTS

LIST OF TABLES

LIST OF FIGURES

CHAPTER 1

INTRODUCTION

1.1 Motivation

In 2017, the global energy demand increased by 2.1 %, the majority of which was fulfilled by the non-renewable energy sources such as fossil fuel, oil, natural gas, and coal (IEA, 2018). Figures 1.1 and 1.2 shows the time series of global energy consumption and energy consumption in the United States. It can be seen in the figures that the source of the majority of energy consumption are oil, natural gas, and coal. These sources of energy have a limited lifetime and may not be able to meet the energy demand in the future. Therefore, it is necessary to increase the energy production from renewable and sustainable energy sources. One of the sustainable energy sources with a high potential of producing higher amount of energy is wind. Wind is not only sustainable but also clean energy source which does not cause any harm to the environment. The wind energy production can be increased by increasing the height of the wind turbine tower because the higher and steadier wind can be encountered at the higher altitude and the wind power is directly proportional to the cubic power of wind speed. However, a higher wind turbine tower induces higher design loads (vertical load, horizontal load, and bending moment) at the foundation which makes it challenging to design a safe and economical foundation.

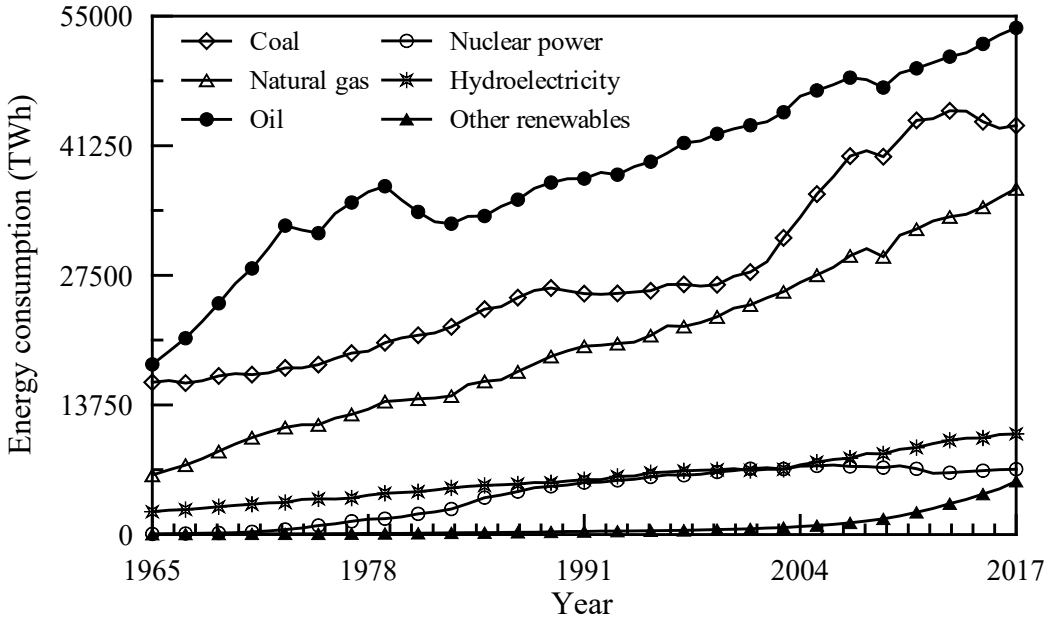

Figure 1.1. Time series of global energy consumption by source (Data source: BP, 2018)

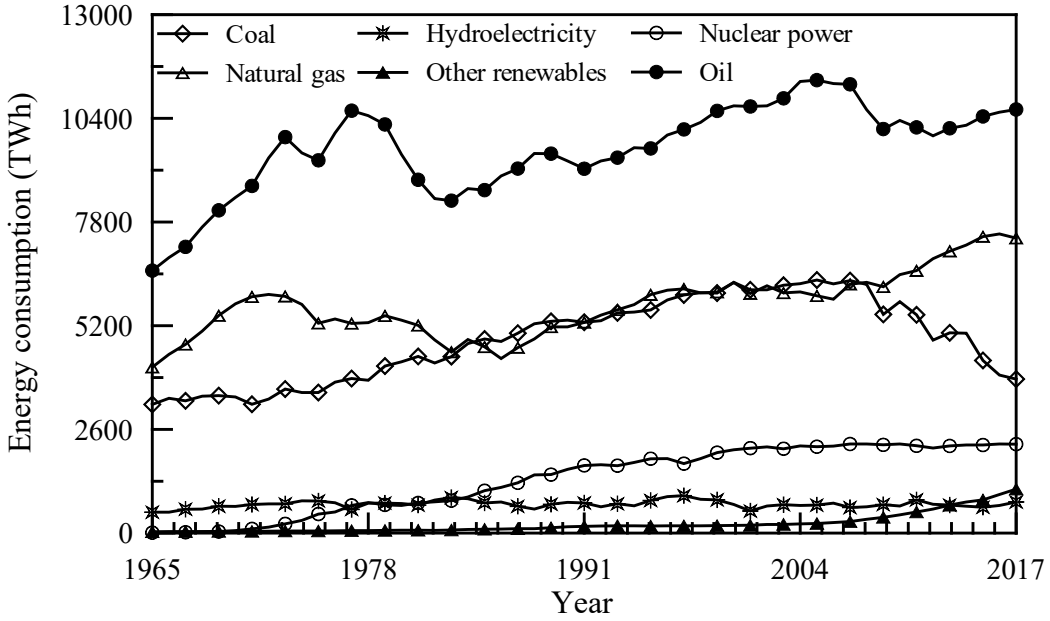

Figure 1.2. Time series of energy consumption by source in the United States (Data source: BP, 2018)

1.2 Research questions

The major research questions of this study listed below.

- How to systematically incorporate the uncertainties in load and soil properties in the analytical design of piled-raft foundation for a tall wind turbine?
- How does analytical design results compare with the nonlinear elastoplastic finite element analysis with advanced interaction modeling results of the piled-raft foundation for a tall wind turbine?
- Piled-raft with the raft and piles looks similar to foundation system of trees. However, piled-raft foundation has vertical piles while tree roots have inclined roots with sub-roots. Is it possible to obtain the configuration inspired from tree root system to develop an effective foundation for tall wind turbines?

1.3 Objectives

The purpose of this study is to design a safe and economical foundation for a tall onshore wind turbine tower. Since the piled-raft foundation has been successfully used in the tall buildings around the world, the use of piled-raft as the foundation for a tall wind turbine tower is primarily explored in this study. Following are the objectives of this study.

- To perform a simplified geotechnical design of the piled-raft foundation subjected to a combined load
- To conduct a reliability-based robust design optimization of the piled-raft foundation
- To compare the performance of a piled-raft foundation with other common foundations for wind turbine such as the raft foundation and pile group foundation

- To perform finite element analysis of the piled-raft foundation
- To perform the preliminary studies on developing a bio-inspired foundation system for a wind turbine

1.4 Analytical design

The analytical design of the piled-raft foundation is a challenging task mainly because of the soil-structure interaction. The soil-structure interaction affects the performance of the piled-raft foundation. Due to the lack of proper understanding of the three-dimensional soil-structure interaction, it is not incorporated in the analytical design procedure. Moreover, it is difficult to predict the load distribution between the raft and piles. Therefore, a proper guideline to design a pile-raft foundation is not yet available. In this study, the analytical geotechnical design of the piled-raft foundation for the wind turbine tower subjected to the vertical load, horizontal load, and the bending moment is presented. The wind turbine tower is assumed to be constructed in a site with clayey soil, sandy soil, and multilayered soil. The method proposed by Hemsley (2000), in which the design procedure proposed by Poulos and Davis (1980) and Randolph (1994) are incorporated was used in this study. However, these methods didn't consider the calculation of differential settlement of the piled-raft foundation due to the bending moment, which is a critical design consideration in the piled-raft foundation to ensure the stability of the foundation and the superstructure. In this study, a new method of calculating the differential settlement of the piled-raft foundation is proposed in which the total bending moment is distributed between the piles and raft. The analytical design procedure

involved the safety and serviceability checks. The detailed analytical design procedure is explained in the upcoming chapters.

1.5 Robust design and optimization of piled-raft foundation

Wind turbine towers are usually constructed in a large number in a wind farm. The wind farm can extend along a huge area in which the large variability in the soil strength parameters and wind speed is expected. The variability in the soil strength parameter may arise due to different soil profile in the large area and due to the limited subsurface exploration. Similarly, wind speed may have seasonal as well as diurnal variations. Therefore, the foundation designed for the wind turbine tower at one location may be over designed or under designed for the wind turbine tower at a different location of the same wind farm due to change in the soil profile and wind speed. Designing the foundation for the soil condition with respect to each location of the wind turbine tower can be expensive and time consuming. Therefore, for the safe and cost-effective design of the wind turbine foundation for a wind farm, the design optimization technique must be used. In this study, the design optimization of the piled-raft foundation was performed by considering the soil strength parameters and wind speed as uncertain parameters or random variables or noise factors. The parameters which are out of control and have an impact on the design results are considered as the uncertain parameters. The goal of design optimization is to produce a set of safe and cost-effective designs of the piled-raft foundation for the range of soil strength parameters and wind speed. In this study, the safety was measured in terms of standard deviation of differential settlement and the cost-effectiveness was measured in terms of total cost of the foundation. These safe and cost-effective designs were represented

graphically using a Pareto front with the total cost and standard deviation of differential settlement as two objectives to be fulfilled. Each point on the Pareto front is a safe design. However, the most optimum design which satisfies both objectives equally can be obtained from the Pareto front from the knee point concept. In this study, first, the robust design and optimization of piled-raft foundation in clayey and sandy soil were performed. In clayey soil, the wind speed and undrained cohesion were considered as uncertainties and in sandy soil, the wind speed and friction angle were considered as uncertainties. This study is discussed in detail in Chapter 2. A similar approach was applied for the piled-raft foundation in the multilayered clay in which the wind speed and the undrained cohesion of the different soil layers were varied. This study is discussed in detail in Chapter 3. Finally, this approach was also applied to perform the cost and performance-based comparison of three typical foundations used to support a wind turbine tower. The foundations considered were a raft, pile group, and piled-raft foundation. This study is discussed in detail in Chapter 4.

1.6 Finite element modeling of the piled-raft foundation

The limitations in the analytical design procedure used in this study are; it doesn't incorporate three-dimensional soil-structure interaction and it doesn't consider the plastic behavior of the soil. In addition, only a limited information can be obtained from the analytical design results. On the other hand, the numerical analysis of the complex problem like the one presented in this study will provide many useful results. In this study, the numerical modeling of the piled-raft foundation was created in the finite element software ABAQUS. While in the analytical design procedure, incorporating soil-structure

interaction was complex, it can be modeled as a contact problem in ABAQUS. The results obtained from the numerical method was compared with the results of the analytical method. The results obtained from the numerical method were further investigated to study pile behavior. The details of this study are discussed in Chapter 5.

1.7 Innovative foundation development through biomimicry

While humans are struggling to design a cost-effective and safe foundation for a tall structure, the natural tree root system has demonstrated the capability to carry the design loads without failure. The comparison of the tall trees such as coconut tree, sabal palm tree, and Palmyra tree with the wind turbine tower shows similarity in their components and the loads acting on them. Inspired from the natural foundation system, this study presents a preliminary study on the development of a new bio-inspired foundation through biomimicry. The preliminary analysis included the creation of simplified configurations for the new foundation and the results are presented in Chapter 6.

1.8 Contributions

This dissertation focusses in the analytical design, robust design optimization, and finite element modeling of the piled-raft foundation. It also presents the preliminary study on the development of ideas for bio-inspired foundation. The key contributions of this dissertation to the existing literature are listed below.

- Analytical design procedure of the piled-raft foundation for onshore tall wind turbine subjected to combined load (vertical load, horizontal load, and bending

moment) with a new method to calculate the differential settlement and rotation of the piled-raft foundation due to bending moment

- Development of a framework for a reliability-based robust design optimization procedure of the piled-raft foundation which allows to select the optimum design as per performance requirement and cost limitation
- Recommendation for the most effective foundation to support wind turbine tower in clayey and sandy soils
- Sophisticated three-dimensional finite element modeling of the piled-raft foundation with accurate modeling of the soil-structure interaction
- Initial development of new foundation for tall wind turbine through biomimicry

1.9 Organization

This dissertation contains seven chapters. Chapter 1 is the introduction where the purpose of this study and objectives are discussed. Chapter 2 is the study on the robust design and optimization of the piled-raft foundation for a tall wind turbine in clayey and sandy soil. This work is published in June 2018 issue of Soils and Foundations journal (Vol. 58, No. 3). In Chapter 3, the geotechnical design and optimization of the piled-raft foundation for a tall onshore wind turbine in multilayered clay are presented. This work was published in November 2018 issue of the International Journal of Geomechanics (Vol. 18, No. 2, DOI: 10.1061/(ASCE)GM.1943-5622.0001061). Chapter 4 includes the performance and cost-based robust design optimization of pile group and raft foundations along with the piled-raft foundation for the tall onshore wind turbine. This work was published in February 2018 issue of the International Journal of Geotechnical Engineering

(DOI: 10.1080/19386362.2018.1428387). Chapter 5 includes the finite element modeling of the piled-raft foundation subjected to combined loads and the comparison of the results with the analytical model. This work is submitted to the International Journal of Geomechanics. Chapter 6 includes the preliminary study to develop a new foundation after a tree root system through biomimicry. Finally, Chapter 7 includes conclusions and recommendations.

CHAPTER 2

ROBUST DESIGN AND OPTIMIZATION PROCEDURE FOR PILED-RAFT FOUNDATION TO SUPPORT TALL WIND TURBINE IN CLAY AND SAND[1]

2.1 Abstract

A geotechnical design and optimization procedure for the piled-raft foundations to support a tall wind turbine in a clayey and sandy soil are presented in this paper. From the conventional geotechnical design, it was found that the differential settlement controlled the final design and considered as the response of concern in the optimization procedure. A parametric study was subsequently conducted to examine the effect of soil shear strength parameters and wind speed (random variables) on the design parameters (number and length of piles and radius of raft). Finally, a robust design optimization was conducted using Genetic Algorithm coupled with Monte Carlo simulation considering the total cost of foundation and the standard deviation of differential settlement as objectives. This procedure resulted in a set of acceptable designs forming a Pareto front which can be readily used to select the best design for a given performance requirement and cost limitation.

[1] A similar version of this chapter is published in the *Soils and Foundations Journal*; Ravichandran, N., Shrestha, S., and Piratla, K. (2018). "Robust design and optimization procedure for piled-raft foundation to support tall wind turbine in clay and sand," 58(3), 744-755.

2.2 Introduction

Wind energy, as an alternative to conventional energy produced by burning fossil fuels, is a renewable and clean energy which produces no greenhouse gas emissions during operation, consumes no water, and uses a little land. With rapidly growing world population, it is essential to increase the energy production using sustainable sources such as wind to meet the demand. One of the cost-effective ways to increase the wind energy production is to build taller towers. Since a higher and steadier wind speed can be accessed at a higher elevation, building a taller tower can increase the wind energy production of a single turbine. The study of Lewin (2010) revealed that an increase in turbine elevation from 80 m to 100 m would result in a 4.6% higher wind speed which translates to a significant 14% increase in power output. A further increase in tower height from 80 m to 120 m would result in 8.5% higher wind speed and 28% increase in power output. It should also be noted that the higher initial construction cost and the lower operational cost of wind turbines makes it economical to build a few taller towers than several normally sized towers to maximize the wind energy production.

Increase in tower height, however, poses significant geotechnical engineering challenges because the foundation design loads (vertical load, horizontal load, and bending moment) increase with the increasing tower height. Larger loads not only result in the larger foundations demanding significant resources to be allocated for the design and construction of the foundation but also present challenges in choosing the appropriate foundation type and optimal design parameters. Among the many foundation types used for supporting wind turbines, a piled-raft foundation is considered to be effective for

supporting tall wind turbines, especially for improving serviceability requirements (Shrestha, 2015). The centrifuge model tests performed by Sawada and Takemura (2014) on three types of model foundations (piled-raft, pile group, and raft alone) subjected to vertical, lateral, and moment loads also show that the vertical bearing capacity of the piled-raft foundation is the largest among the three foundations considered. This may be due to the higher bearing capacity of the raft and increase in pile capacity due to the increase in soil stiffness caused by raft contact stress. The same study also concludes that the settlement due to various loads can be reduced by using piled-raft foundation.

The geotechnical design of a piled raft foundation is complicated, especially when the foundation is subjected to larger horizontal load and bending moment. The complexity increases further when the uncertainties in wind load and soil parameters must be incorporated into the design process to increase its robustness while keeping the cost at the lowest possible value. The selection of suitable design variables such as the number of piles, the length of piles, and the radius of raft for a given loading and soil condition is another challenge because of the existence of a large number of acceptable designs. Selecting the best design that suits the performance and cost limitations is not straightforward in the conventional design. In such situations, the robust design optimization technique can be used to produce a relationship between the measure of robustness and the total cost of the foundation enabling the easy selection of the best design for a given set of performance requirement and cost limitation.

It is well recognized that uncertainties of soil parameters as well as of loads are unavoidable in the design of foundations. In a deterministic design approach, the engineers

use a factor of safety (FS) to cope with the uncertainties in the entire solution process. Usually, a larger FS is used when the uncertainties in soil parameters and loads are higher. Although design optimization is performed in day-to-day engineering profession, the traditional optimization procedure becomes inefficient for the design problem pursued in this study. This is because the pool of acceptable designs in the traditional optimization is small and also the problem is simplified to reduce the number of random and design variables within a manageable range. To consider the uncertainties in a systematic and accurate manner, a reliability-based approach supported by automated computer algorithms must be considered. Researchers have proposed various methods that consider the uncertainties in the soil parameters explicitly for the design of geotechnical as well as other engineering systems (Duncan 2000; Griffiths et al. 2002; Phoon et al. 2003a&b; Fenton and Griffiths 2008; Schuster et al. 2008; Juang et al. 2009 & 2011; Wang et al. 2011; Zhang et al. 2011). Recently, one of the authors and his colleagues developed a reliability-based robust design methodology for the design of an individual drilled shaft in sand considering the uncertainties in soil parameters (Juang et al., 2013). Additional literature on the geotechnical design concept and the design optimization are presented under optimization section.

This methodology is employed in the current study for the design of piled-raft foundation considering not only the uncertainties in soil parameters but also in wind speed which affect the design horizontal load and bending moment. The spatial variation in strength and stiffness properties is unavoidable especially when the foundation design is for constructing a wind farm which covers a large area. Conducting subsurface exploration

to accurately determine the soil properties and designing a piled-raft foundation for each wind turbine is expensive and not recommended in practice. Therefore, it is necessary to develop a design procedure considering possible variations in soil properties so that the design will be accurate. Similarly, the wind speed which affects the horizontal load and bending moment at the base of the tower also varies with location, height, and time. Therefore, the wind speed must also be considered as an uncertain parameter in the design. Both aforementioned uncertain parameters have significant impacts on the selection of an optimum design for a given site condition, performance requirement, and cost limitation. A systematic incorporation of multiple random variables in the design requires an advance optimization procedure with predefined objectives such as cost and performance limitations.

For demonstrating the procedure, a 130 m tall onshore wind turbine in clayey and sandy soil is considered. In the design optimization, the wind speed, undrained cohesion of clayey soil and friction angle of sandy soil are considered as the random variables, while the length of piles, the number of piles, and the radius of raft are considered as the design variables. The differential settlement of the piled-raft, which is a critical overall stability parameter to fulfill serviceability requirement, is considered as the response of concern. The outcome of the optimization is presented in a graphical form as a Pareto front which can be used to select the best design for a given set of performance requirement and cost limitation. The design procedure presented in this study can also be directly applied to other structures which are supported on piled-raft foundation and subjected to combined vertical, lateral, and moment loads.

2.3 Deterministic geotechnical design of piled-raft foundation

2.3.1 Deterministic loads and soil properties

The wind turbine foundation is subjected to vertical load due to self-weight of the superstructure, horizontal load due to the wind force on the above ground components, and bending moment due to wind load. The calculation of each load for the design is discussed below.

The vertical load on the foundation is the dead load due to the weight of all the components above the ground. It is calculated by summing the weights of the tower and other components of the wind turbine such as nacelle and rotor. The sample wind turbine tower considered in this study is a hybrid hollow cylindrical tower with the lower 93 m made of concrete and upper 37 m made of steel. Its diameter gradually varied from 12.0 m at the base to 4.0 m at the top. The weights of nacelle and rotor were obtained from Malhotra (2011). The final dead load of the tower is calculated to be 51.71 MN.

The wind action on the structures above ground induces horizontal load on them which results in a horizontal force and bending moment at the base of the tower. The wind load is calculated following the procedure described in ASCE 7-10 (2010) using the mean survival wind speed of 125 mph. This mean wind speed is considered to be appropriate because most of the wind turbines have the survival wind speed within 112 mph to 134 mph (Wagner and Mathur, 2013) and its range lies between 89 mph and 161 mph. It is general practice to design wind turbine for the survival wind speed and hence the foundation is also designed for the survival wind speed. The cut-off wind speed which is lower than the survival wind speed is not considered in this study. The standard deviation

of wind speed used in this study is 18 mph and the above-mentioned range covers ±2 standard deviations above and below the mean value (used in parametric study and design optimization sections). This range of wind speed considered covers the hurricane of category 1 to 5 (5 being the extreme). The total horizontal load and bending moment are calculated to be 2.26 MN and 144.89 MNm, respectively.

For the design in clayey soil, a unit weight of 18 kN/m^3 and mean undrained cohesion of 100 kPa are assumed. These values represent stiff to very stiff clay. Based on the literature survey (Phoon et al., 2003a, 2003b, 2008), a standard deviation of undrained cohesion is assumed to be 20 kPa. For the parametric study and optimization procedure, the undrained cohesion is varied between 60 kPa and 140 kPa which represent ±2 standard deviations. The modulus of elasticity of the soil is calculated using widely used empirical correlations (USACE, 1990; Duncan and Buchignani, 1976) between the undrained cohesion and modulus of elasticity. For the above-mentioned range of undrained cohesion, the range of modulus of elasticity is calculated to be between 21 MPa and 49 MPa. Similarly, for the design in sandy soil, a site with a single layer of sandy soil is considered with the unit weight and mean friction angle of 17.2 kN/m^3 and 34°, respectively. A standard deviation of 3.4^o is assumed for the friction angle. For the parametric study and design optimization, the friction angle is varied between 27.2^o and 40.8^o which represents ±2 standard deviations. The modulus of elasticity of the sandy soil varied between 1.25 MPa and 62.5 MPa (Wolff, 1989; Kulhawy and Mayne, 1990). These variations in the strength and deformation parameters and loading indicate that a significant variation in performance (safety and serviceability) is possible. This requires a systematic approach to

quantify the variation in the performance and corresponding cost which is the focus of this study.

2.3.2 Geotechnical design procedure

The advantage of a hybrid foundation such as piled-raft for supporting a larger load is that it utilizes the higher bearing resistance of raft to overcome bearing capacity failure and the higher resistance from piles to overcome total and differential settlements. Although the individual design procedures of raft and pile are well documented, the design of piled-raft is complicated, and a limited documentation is available in the literature. The share of the load carried by the raft and the piles and determination of the mobilized strength for a given settlement is the most challenging task in the design. This is mainly due to the lack of understanding of complex soil-raft-pile interaction. Hence, a reliable design guideline is not yet available in the literature, particularly when the piled-raft is subjected to the vertical load, the horizontal load, and the bending moment.

This study includes a preliminary geotechnical design of the piled-raft foundation following the procedure outlined by Hemsley (2000), in which the design procedure proposed by Poulos and Davis (1980) and Randolph (1994) are incorporated. In this procedure, the design variables, i.e. the radius of raft, the length of piles, and the number of piles are assumed and adjusted until all the design requirements are met. To reduce the complication in the design procedure, the type and size of the pile are fixed to be pre-stressed concrete piles of size 0.457 m (18″). The design requirements include checks for the vertical load capacity, bending moment capacity, horizontal load capacity, total and differential settlements, and the rotation of the tower. A minimum factor of safety of 2 is

considered to be safe (Hemsley, 2000) for vertical load, horizontal load, and bending moment capacity checks. The maximum total settlement of 45 mm is allowed. A vertical misalignment within 3mm/m of the tower is considered to be safe against the rotation of the tower (Grunberg and Gohlmann, 2013). For this allowable vertical misalignment, the safe horizontal displacement due to bending moment at the top of 130 m tall tower is calculated to be 390 mm. Hence, the safe rotation of the tower (θ) is determined to be 0.17° calculated using the safe horizontal displacement and the height of the tower.

Check for vertical capacity

To determine the ultimate vertical load capacity of the piled-raft foundation, first the ultimate capacity of individual components (i.e. raft, $P_{u\text{-}R}$ and pile, $P_{u\text{-}P}$) are calculated for the assumed trial dimensions. The ultimate bearing capacity of the raft is calculated using the general bearing capacity equation (Meyerhof, 1963). Since the piled-raft foundation in this study is for a wind turbine tower, a circular raft is considered so that there will be an equal capacity in all directions when the wind turbine rotor rotates. The size of the raft is determined based on the tower base diameter. Since the radius of the base of the tower in this study is 6.0 m, the radius of the raft is considered to be 7.5 m which provides sufficient clearance and doesn't cover a large area. The ultimate vertical pile capacity of a single pre-stressed concrete pile of size 0.457 m is calculated as the sum of skin and toe resistances. The skin resistance is calculated using α and basic friction theory for the pile in clayey and sandy soils, respectively and toe resistance is calculated using Meyerhof's method for both clayey and sandy soils (Das, 2016). Then the ultimate vertical capacity of a block ($P_{u\text{-}B}$) is calculated as the sum of the ultimate vertical capacity of

circular pile group block of soil, raft, and all the piles and the portion of raft lying outside the periphery of the pile group. Finally, the ultimate vertical load capacity of the piled-raft foundation is considered to be the lesser of: (i) the sum of ultimate capacities of the raft and all the piles i.e., $P_{u\text{-}PR} = P_{u\text{-}R} + N_p P_{u\text{-}P}$, where N_p is the number of piles and (ii) the ultimate capacity of the block i.e. $P_{u\text{-}B}$. It should be noted that determination of the number and length of piles is an iterative procedure. The number and length of piles were adjusted until all the design requirements were met. Finally, the factor of safety for vertical load capacity is calculated using Equation 2.1.

$$FS_P = \frac{\min\left(P_{u-PR}, P_{u-B}\right)}{P} \tag{2.1}$$

where P is the design vertical load.

2.3.2.1 Check for moment capacity

The ultimate bending moment capacity of the piled-raft foundation is calculated following a similar procedure used for calculating the ultimate vertical load capacity, i.e. the lesser of: (i) the sum of ultimate moment capacity of raft ($M_{\text{u-R}}$) and all the individual piles in the group ($M_{u\text{-}P}$), i.e., $M_{u\text{-}PR} = M_{u\text{-}R} + M_{u\text{-}P}$, and (ii) the ultimate moment capacity of a block ($M_{\text{u-B}}$). The ultimate moment capacity of the raft, $M_{\text{u-R}}$ for the assumed dimension is calculated using Equation 2.2 (Hemsley, 2000).

$$\frac{M_{u-R}}{M_m} = \frac{27}{4}\frac{P}{P_u}\left[1 - \left(\frac{P}{P_u}\right)^{1/2}\right] \tag{2.2}$$

where M_m is the maximum possible moment that soil can support, P is the applied vertical load, P_u is the ultimate centric load on the raft when no moment is applied. In this study, M_m for a circular raft is calculated by modifying the equation used to calculate M_m for a rectangular raft given in Hemsley (2000). The modified equation for M_m for the circular raft used in this study is given in Equation 2.3.

$$M_m = \frac{q_u D^3}{4}\left(\frac{\pi}{4} - \frac{1}{3}\right) \tag{2.3}$$

where q_u is the ultimate bearing capacity of the raft, and D is the diameter of the circular raft. The ultimate moment of all the piles, $M_{u\text{-}P}$ for the assumed length and number of piles is calculated using Equation 2.4 (Hemsley, 2000).

$$M_{u-P} = \sum_{i=1}^{N_p} P_{uui}\left|x_i\right| \tag{2.4}$$

where P_{uui} is the ultimate uplift capacity of the ith pile, $\left|x_i\right|$ is the absolute distance of ith pile from the center of the group, and N_p is the number of piles. Similarly, the ultimate moment capacity of the block, $M_{u\text{-}B}$ is calculated using Equation 2.5 given below (Hemsley, 2000).

$$M_{u-B} = \alpha_B \overline{p}_u B_B D_B^2 \tag{2.5}$$

where B_B and D_B are the width and depth of the block, respectively, $\overline{p}_u$ is the average lateral resistance of soil along the block, and α_B is the factor depending upon the distribution of ultimate lateral pressure with depth (0.25 for constant distribution of $\overline{p}_u$ and 0.2 for linearly increasing $\overline{p}_u$ with depth from zero at the surface). Hemsley (2000)

proposed Equation 2.5 for designing rectangular raft and pile arrangement. Since in this study raft and pile arrangements are circular, the raft section is converted to an equivalent rectangular section to use Equation 2.5. Finally, the factor of safety is calculated using Equation 2.6.

$$FS_M = \frac{\min(M_{u-PR}, M_{u-B})}{M} \tag{2.6}$$

where M is the design moment.

2.3.2.2 Check for horizontal capacity

Broms' solution outlined in Gudmundsdottir (1981) for the lateral pile analysis in cohesive soil and cohesionless soils was used to determine the lateral capacity of a single pile. Although it is for single pile analysis, it is assumed that all the piles in the group will have similar behavior. The horizontal coefficient of subgrade reaction is used to determine the horizontal load capacity ($V_{u\text{-}P}$) and horizontal deflection (y_H) of a single pile using the procedure described in Gudmundsdottir (1981) for sandy and clayey soils. The horizontal capacity of all the piles in the foundation system is estimated as the sum of horizontal capacities of all the piles i.e., $V_{u\text{-}PR} = N_p V_{u\text{-}P}$ assuming that all the piles in the group will behave in the same way. Finally, the factor of safety is calculated using Equation 2.7.

$$FS_V = \frac{V_{u-PR}}{V} \tag{2.7}$$

where V is the design horizontal load.

2.3.2.3 Pile-raft-soil interaction and resultant vertical load-settlement behavior

The vertical load-settlement behavior of the piled-raft was estimated by the approach proposed by Poulos (2001b) in conjunction with the method used for estimating the load sharing between the raft and the piles presented in Randolph (1994). The stiffness of the piles, raft, and the pile-raft as a block are used to estimate the load sharing between the raft and the piles. The stiffness of the piled-raft, K_{pr} is estimated using the following equation proposed by Randolph (1994):

$$K_{pr} = X K_p; \qquad X = \frac{1 + \left(1 - 2\alpha_{rp}\right) K_r / K_p}{1 - \alpha_{rp}^2 \left(K_r / K_p\right)} \tag{2.8}$$

where K_r is the stiffness of raft, K_p is the stiffness of the pile group, and α_{rp} is the pile-raft interaction factor. In this method, the interaction between the pile and raft is incorporated by using the pile-raft interaction factor. However, the interactions between the raft and soil and the pile and soil which depend on the settlement are not considered. The pile-raft interaction factor is assumed to be 0.8 considering the fact that as the number of piles increases the value of α_{rp} increases and it reaches the maximum value of 0.8 as reported by Randolph (1994). The stiffness of the raft is estimated using the method outlined by Randolph (1994) and the stiffness of the pile group is estimated using the method proposed by Poulos (2001b). In this method, the target stiffness of the piled-raft is first determined by dividing the total vertical load by the assumed allowable settlement and then the Equation 2.8 is solved to determine the stiffness of the pile group. When the foundation is subjected to the vertical load, the stiffness of the piled-raft will remain operative until the load-bearing capacity of the pile is fully mobilized at a load P_A, as shown in Equation 2.9

(also in Figure 2.2). After calculating the values of K_{pr}, K_r and P_A, the load-settlement curve (P vs. S) for the piled-raft foundation is developed using Equation 2.9. Then the settlement of the foundation due to design vertical load is determined by using the load-settlement curve.

$$\left.\begin{array}{l} \text{For } P \le P_A;\ S = \dfrac{P}{K_{pr}} \quad \text{For } P > P_A;\ S = \dfrac{P_A}{K_{pr}} + \dfrac{P - P_A}{K_r} \end{array}\right\} \tag{2.9}$$

2.3.2.4 Pile-raft-soil interaction, differential settlement, and tower rotation

When the piled-raft foundation is subjected to combined loading, piles on one side of the neutral axis will be in tension and the other in compression. The vertical displacement of the piled-raft foundation due to horizontal load and moment affects the vertical resistances of piles in tension and compression sides resulting in a difference in mobilized resistances (Sawada and Takemura, 2014). The difference in the mobilized resistance results in the difference in vertical displacement of piles in tension and compression which results in differential settlement (S_{diff}). During the vertical displacement, there will be interactions among soil, piles, and raft which may have an impact on the capacity of the foundation. The calculation of differential settlement of the combined piled-raft foundation system due to the bending moment considering the interactions among various components is a challenging task in the design of piled-raft foundation. The accurate procedure to estimate the differential settlement of the piled-raft foundation subjected to coupled load (vertical load, bending moment, and lateral load) is not yet available in the literature. This paper proposes a new method to calculate the differential settlement of the piled-raft foundation. In this method, the total applied bending moment is divided between the raft

and the piles such that the differential settlements of the individual components are equal, which is considered as the differential settlement of the piled-raft foundation. The assumption made here is that the pile head is connected rigidly to the bottom of the raft and therefore both piles and raft will rotate by the same amount when the foundation is subjected to bending moment. The estimation of the percentage of moment shared by raft and piles to induce an equal amount of differential settlement is calculated using an iterative procedure in this study. The schematic of the proposed concept is presented in Figure 2.1. The calculation of the differential settlement of individual components (raft and piles) is discussed in the following section.

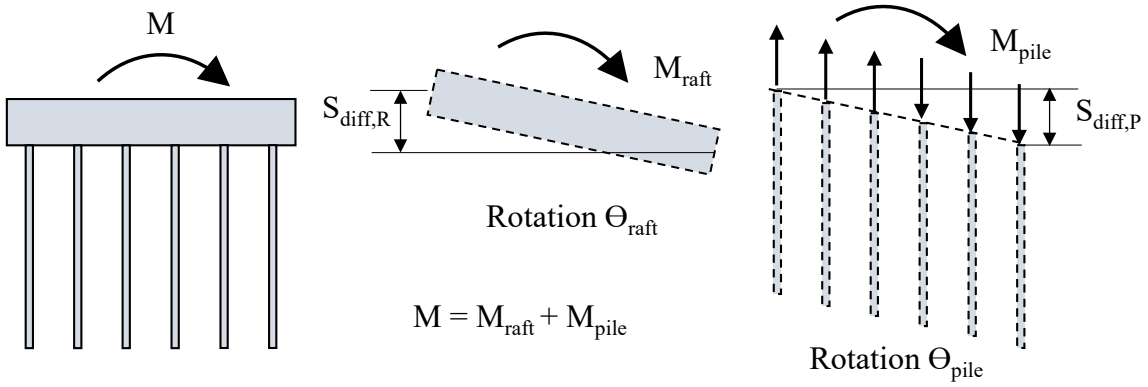

Figure 2.1. Schematic of proposed differential settlement concept for piled-raft foundation

2.3.2.4.1 Differential settlement of raft

The differential settlement of the raft is estimated based on the rotation (θ) due to wind load. The rotation is calculated using Equation 2.10 given by Grunberg and Gohlmann (2013).

$$\theta = \frac{M_{found}}{c_s I_{found}};\ c_s = \frac{E_s}{f' \sqrt{A_{found}}} \tag{2.10}$$

where M_{found} is the fixed-end moment at soil-structure interface (percentage of moment shared by raft to result in an equal differential settlement as that of piles in this study), c_s is the foundation modulus, I_{found} is the second moment of inertia for area of foundation, E_s is the modulus of elasticity of soil, f' is the shape factor for overturning (0.25), and A_{found} is the area of the foundation. After calculating θ, the differential settlement of the raft is determined using a simple trigonometric relationship.

2.3.2.4.2 Differential settlement of piles

The differential settlement profile of the piles as a group is estimated considering the equivalent vertical loads due to the dead load and bending moment shared by the piles. First, the vertical load on each pile is estimated and then the settlement of each pile head is calculated following the procedure outlined by Fellenius (1999). As discussed above, the pile resistance will be different on tension and compression sides which will result in the difference in vertical settlement depending on the location of the pile with respect to the neutral axis. Hence, the settlements of the piles in a vertical section (2-dimensional elevation) are approximated by a straight line to produce the settlement profile for the piles. The above-mentioned procedure is repeated by adjusting the load shared by the pile and the raft until the settlement profiles of raft and piles matched, which is considered as the settlement profile of the piled-raft system.

The allowable differential settlement of the piled-raft foundation considered in this study is 45 mm which is calculated using the allowable rotation (0.17°) and the diameter of the raft (15 m). The allowable horizontal displacement (ΔH) at the top of the tower is 390 mm.

2.3.2.5 Final design of piled-raft foundation

The final design results of the piled-raft foundation for the mean wind speed and soil properties obtained by following the above-mentioned procedure are given in Table 2.1. Based on the vertical capacity and moment capacity check presented earlier, it is found that the final design of the piled-raft foundation is controlled by individual failure (either raft or piles fail, i.e. case 'i' in ultimate vertical and moment capacity determination) on both clayey and sandy soils. In both soils, the thickness of raft is 1.2 m at the depth of 1.5 m. The total settlement (S_{tot}) listed in Table 2.1 is determined using the load-settlement curve for the piled-raft foundation shown in Figure 2.2 for the design vertical load (51.71 MN). It can be observed in Table 2.1 that final designs of the piled-raft foundation in both soils have satisfied the safety and settlement requirements. The total piles are divided equally and arranged circumferentially at radial distances of 5.3 m and 6.7 m at equal spacing maintaining the pile to pile spacing of at least three times the pile size.

Table 2.1. Design results of the piled-raft foundation for mean case

Soil	L_p (m)	N_p	R_r (m)	FS_P	FS_M	FS_V	S_{tot} (mm)	S_{diff} (mm)	ΔH (mm)	y_H (mm)
Clay	20	40	7.5	3.55	3.35	12.94	42.38	44.30	384.71	9.97
Sand	35	36	7.5	7.91	4.32	7.40	42.17	44.90	389.11	27.89

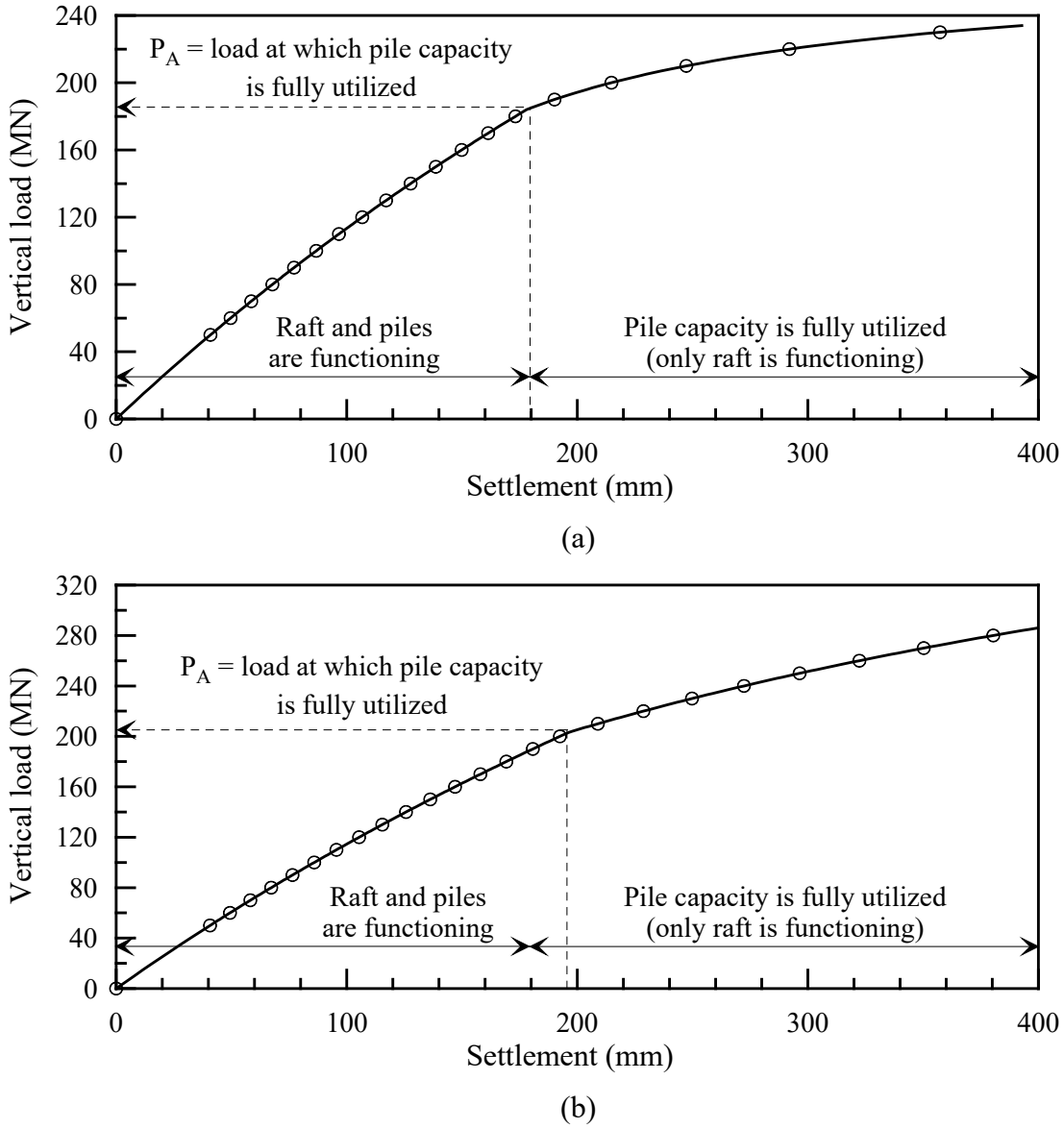

Figure 2.2. Calculated load-settlement curves for piled-raft foundation (a) in clayey soil and (b) sandy soil

It should also be noted in Figure 2.2 that the design vertical load is smaller than P_A (=184.04 MN for clay and = 203.41 MN for sand) which indicates that both the raft and the piles are contributing to support the load and the piles capacity is not fully mobilized

at this vertical load. The sample of pile configuration for the piled-raft foundation in the clayey soil is illustrated in Figure 2.3.

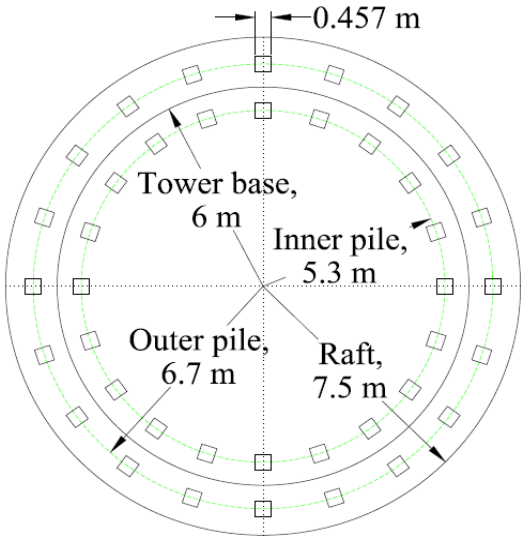

Figure 2.3. Sample plan view of final design outcomes for piled-raft in clay

Although the structural design of the piled-raft foundation is important to ensure the structural safety of the foundation components, it is not considered in this study. This study focusses in performing the geotechnical design of the piled-raft foundation and addressing one of the design issues (differential settlement calculation). Other than structural design, the extreme events such as hurricane and earthquake and a long-term event such as consolidation that the wind turbine may face during its lifetime have not been explored in this study. Nevertheless, the authors' insights on wind turbine performance during the occurrence of these events are briefly discussed here. Although the effect of the hurricane is not explicitly considered in this study, the wind speed range considered for the parametric study (next section) fairly covers the hurricane of category 1 to 5. However, the sustainability of the wind turbine tower during such event is not investigated. Similarly,

the authors believe that the consideration of earthquake in the design will add the horizontal force on the wind turbine tower which induces additional bending moment at the bottom of the tower demanding a larger foundation. In addition, when the wind turbine tower tilts, its center of gravity changes which induces additional bending moment at the base of the tower. However, these components are not considered in this study. Likewise, the long-term consolidation settlement is not considered in this study. The authors believe that if the consolidation settlement is considered then the total and differential settlements will increase.

2.4 Design and Random Variables and conventional Parametric Study

A parametric study is conducted to determine the effect of variation in the loading and soil properties on the design outcomes. The random variables considered are undrained cohesion and wind speed in clayey soil and friction angle and wind speed in sandy soil, and the design variables considered are number of piles-N_p, length of pile-L_p, and radius of raft-R_r for both soils. For each case of the parametric study, the design requirements are met by adjusting only one of the design variables at a time, keeping the rest constant at their mean values. The details of parametric study results for both soils are discussed below.

2.4.1 Variation in undrained cohesion

In this study, the variation in undrained cohesion (c_u) in clayey soil is estimated by considering low site variability. According to SCDOT Geotechnical Design Manual (2010), the coefficient of variation (COV) for low site variability is less than 25%. Hence

for this study, 20% is selected as a reasonable COV (Phoon, 2008). Using the mean c_u value of 100 kPa and COV of 20%, the standard deviation is determined to be 20 kPa. Hence c_u is varied between 60 kPa and 140 kPa, i.e. ±2 standard deviations considering a uniform probability distribution and the designs are performed for each c_u value keeping the wind speed constant at its mean value. The effect of varying c_u on the design variables is shown in Figure 2.4. The results indicate that N_p, L_p, and R_r decrease with increasing c_u because a higher c_u provides a higher bearing capacity of the piled-raft foundation. In Figure 2.4(a), it can be noticed that N_p for the lowest c_u is 66. Dividing these piles equally along the two circumferences of radius 6.7 m and 5.4 m won't satisfy the pile to pile spacing requirement of at least three pile size. The maximum N_p that the circumference of radius 6.7 m and 5.3 m can accommodate while maintaining the required pile spacing are 30 and 24, respectively. Therefore, whenever N_p exceeds 54 (= 30 + 24), the extra piles, i.e. (N_p - 54) are arranged along the third circumference of radius 3.9 m. The radius of the third circumference is determined based on the spacing between previous two circumferences. Moreover, it must be borne in mind that the maximum N_p allowed in the circumference of radius 3.9 m is 18 to maintain the required pile to pile spacing. Hence, whenever N_p exceeds 72 (= 54 + 18), additional circumference is required. It is suggested to add the additional circumference in the inner area until the dimension allows because adding piles inside will not increase the surface area of the foundation. Nevertheless, when the circumference can't be added inside due to size and space constraint, the size of raft should be increased to add piles along outer circumference if necessary. In Figure 2.4 (c),

it can be seen that R_r remained same even with the increase in c_u beyond 100 kPa because it cannot be lower than the bottom diameter of the tower.

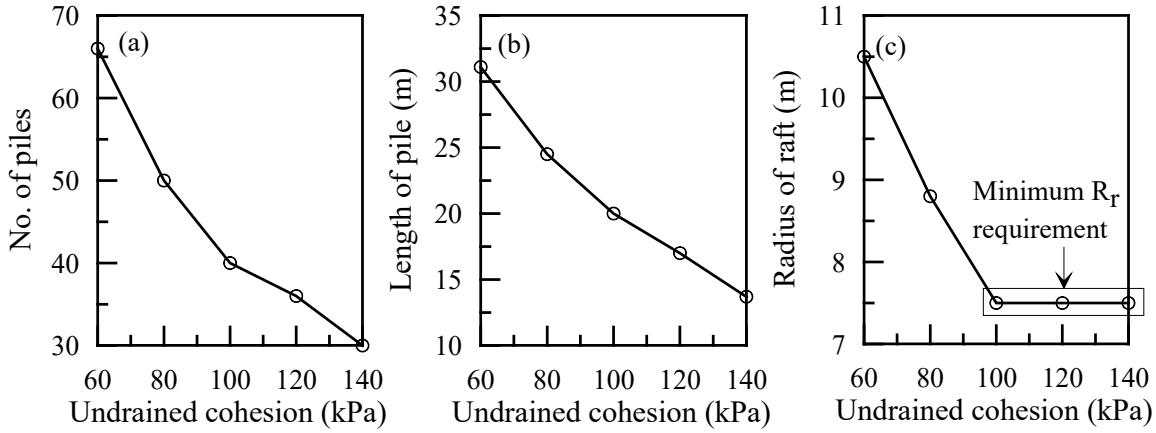

Figure 2.4. Effect of variation in undrained cohesion on (a) number of piles, (b) length of pile and (c) radius of raft in clayey soil

2.4.2 Variation in friction angle

The variation in friction angle (ϕ) in sandy soil is estimated by considering 10% COV, which is a suitable value for friction angle variability (Phoon, 2008). The standard deviation of friction angle is calculated to be 3.4° using a mean value of 34° and COV of 10%. This resulted in the variation of ϕ between 27.2° and 40.8°, i.e. ±2 standard deviations considering a uniform probability distribution. The effect of this possible variation on the design variables is shown in Figure 2.5. The results indicate that N_p, L_p, and R_r decrease with increasing ϕ because a higher ϕ increases the bearing capacity of both the raft and pile resulting in the increase in bearing capacity of the piled-raft foundation. It can be seen in Figure 2.5(a) that N_p required for the lowest ϕ is 68. Hence, for this case the piles are arranged along the three circumferences of radius 6.7 m, 5.3 m, and 3.9 m as discussed in the previous section. It can be observed in Figure 2.5(b) that the decrease in length while

increasing the friction angle from 37.4° to 40.8° is insignificant compared to other increments in friction angle. This is because, for the friction angle of 40.8°, the bending moment requirement is not satisfied for the smaller length of the pile even though it is overdesigned for other design requirements. Hence, the bending moment capacity controlled the design for the highest friction angle limiting the length of the pile to its minimum requirement (when other design variables are kept constant). Similarly, the rate of decrease in R_r is not consistent for all friction angles as can be seen in Figure 2.5(c). The R_r required to fulfill all the design requirements for the lowest friction angle is found to be extremely large because the modulus of elasticity calculated using the correlation (Wolff, 1989; Kulhawy and Mayne, 1990) for the lowest friction angle is very low and hence it required a very large raft to meet the differential settlement requirement. However, it is not practical to construct such a huge raft. Hence it is suggested to increase the length of pile and number of piles in such a case. Similar to the clayey site, the minimum R_r requirement based on the bottom diameter of the tower is maintained for higher friction angles.

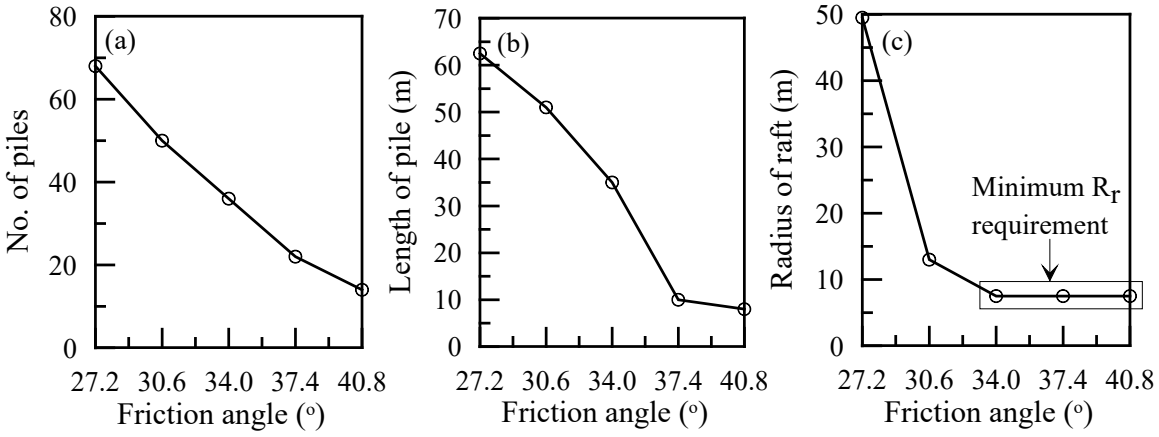

Figure 2.5. Effect of variation in friction angle on (a) number of piles, (b) length of pile and (c) radius of raft in sandy soil

2.4.3 Variation in wind speed

The wind speed (V) is varied between the range of survival wind speed i.e. between 89 mph and 161 mph (±2 standard deviations) with the mean value of 125 mph and standard deviation of 18 mph considering a uniform probability distribution. The designs are performed for each wind speed keeping the undrained cohesion and friction angle constant at their mean values for clayey and sandy soil, respectively and varying only one design variable at a time to meet the design requirement. The adjustment required to be made in N_p, L_p and R_r, with the variation in V are shown in Figures 2.6 and 2.7 for clayey and sandy soils, respectively. For both soil conditions, it is observed that N_p, L_p, and R_r increase with increasing wind speed. It can be seen in Figure 2.6(a) that N_p required for the highest V is 66. Hence the piles are arranged along the three circumferences following the same rule as previous section. It is noticed in Figure 2.7(b) that the rate of increase in the length of pile while increasing the wind speed from 89 mph to 107 mph in case of sandy soil is smaller compared to the other increments in wind speed (107-125, 125-143, and 143-161 mph). This is because it was found that, for the lowest wind speed, decreasing the length of pile below 22 m would result in higher design load compared to the capacity. Hence, the minimum length of the piles required to carry the design axial load due to moment and self-weight were increased although this resulted in overdesign for other design checks. Finally, for lower wind speeds, the radius of raft is maintained at the minimum requirement for both soil conditions based on the bottom diameter of the tower, as shown in Figures 2.6(c) and 2.7(c).

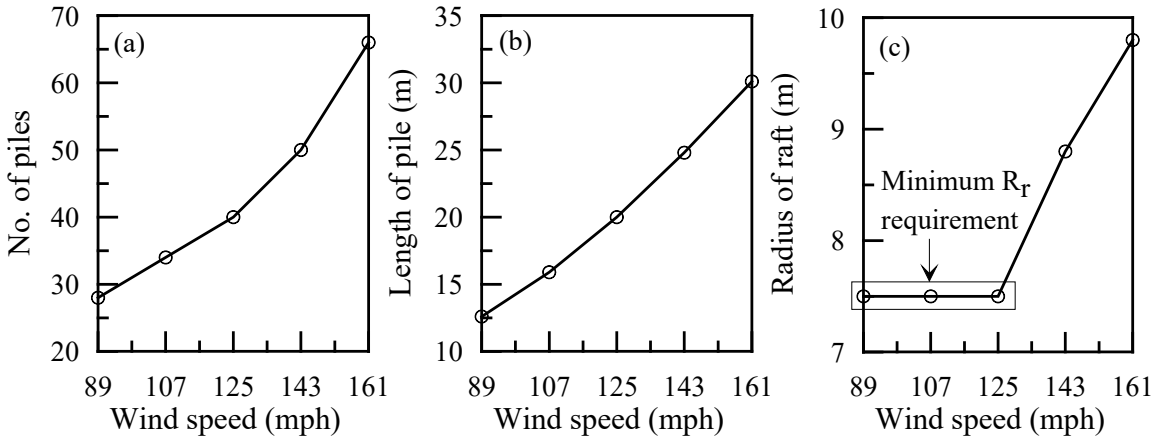

Figure 2.6. Effect of variation in wind speed on (a) number of piles, (b) length of pile and (c) radius of raft in clayey soil

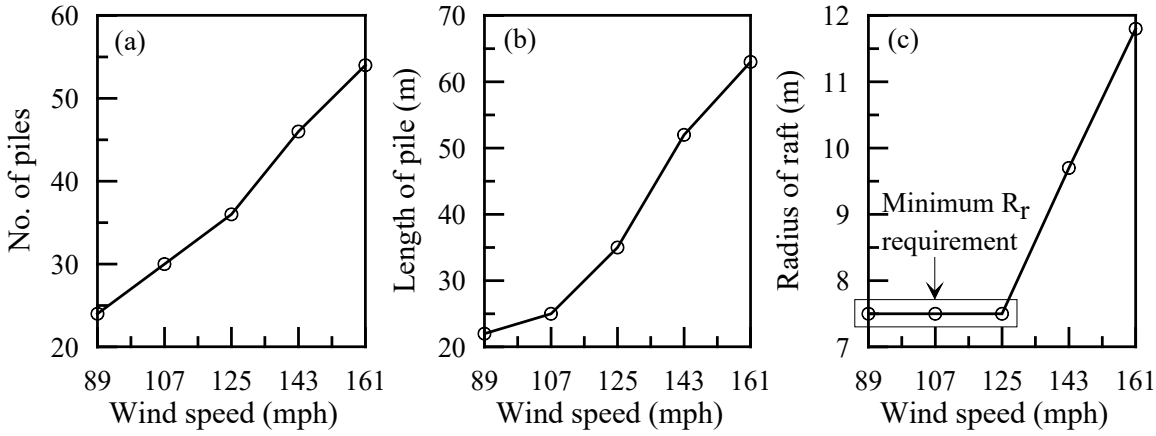

Figure 2.7. Effect of variation in wind speed on (a) number of piles, (b) length of pile and (c) radius of raft in sandy soil

Although the above parametric studies show the change in design variables for the range of possible variations in loads and properties of soils, they only show the effect of a single variable at a time. Also, there is no quantitative measure of variation in the response (differential settlement in this case) for the selected variation in loads and soil properties. Therefore, a procedure that systematically considers randomness in the loads and soil

properties and provides a quantitative measure of performance is needed. Such a procedure is presented in the next section.

2.5 Robust Design Optimization of piled-raft foundation

2.5.1 Concept of Robust Design Optimization

Conventional design of foundations is typically based on trial and error procedures considering cost and safety criteria. The least-cost design that satisfies the safety requirements is then identified and selected as the final design. In order to select the final design out of the pool of acceptable candidate designs, optimization tools can be employed for a desired performance criterion. Valliappan et al. (1999) performed design optimization of the piled-raft foundation on c-ϕ soil. The objective functions in their study were the cost of foundation and the design variables included the thickness of the square raft, cross-sectional area, and length and number of the piles. The optimization was conducted by constraining the settlement and differential settlement within allowable limits. Kim et al. (2001) reported optimal pile arrangements of a piled-raft foundation on clayey soil for different loading conditions. The optimization was performed to minimize the differential settlement. To this end, an implicit function of the location of maximum and minimum settlement of the square raft was considered as the objective function and the locations of piles as design variables. Chan et al. (2009) performed optimization of pile groups in different multi-layer soils using a Genetic algorithm (GA). Their objective was to minimize the material volume of the foundation subjected to several constraints including maximum differential settlement while the design variables considered included location, cross-sectional area and number of piles as well as the thickness of the square pile cap. In another

study by Leung et al. (2010), the piled-raft foundation was optimized using two objectives of maximizing overall stiffness and minimizing differential settlement considering the length of the pile as a design variable. Although several of these previous studies presented efficient optimization approaches for piled-raft design, they ignored to a large extent the uncertainties associated with soil properties as well as the loads. These uncertainties in the input parameters cause uncertainties in the predicted system response and high variability in response may lead to economically inefficient designs. Therefore, along with cost (or material usage) optimization to identify the least sensitive design to uncertainties, the concept of robust design is employed in this paper. As shown in Figure 2.8, introducing robustness in design reduces the variation of system response and prevents the designed system from experiencing unsatisfactory performance.

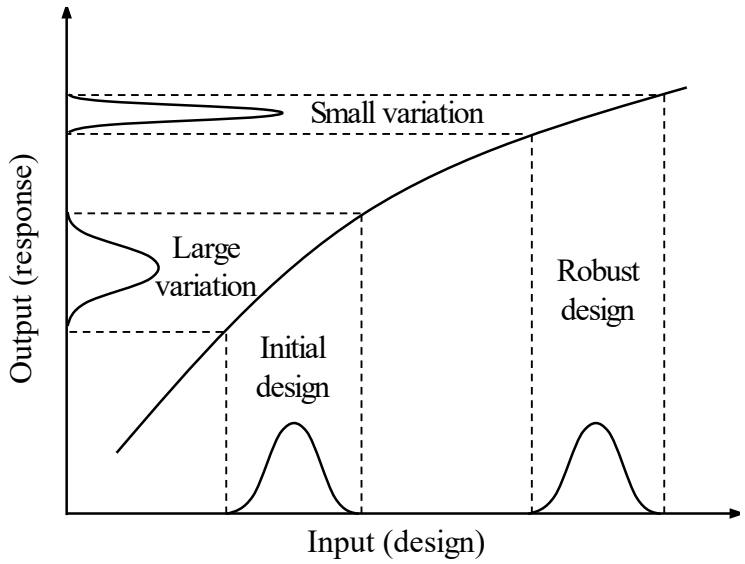

Figure 2.8. Robustness concept (modified after Phadke 1989)

In recent years, reliability-based and robust design of foundations and geotechnical systems have been employed frequently after the concept of uncertainties in soil and robust

design was introduced in geotechnical engineering. Juang and Wang (2013) presented reliability-based robust design optimization method for shallow foundations using Non-dominated Sorting Genetic Algorithm (NSGA-II). They assumed uncertainties in soil parameters such as effective friction angle and undrained shear strength and considered the dimension of foundation as design variables. The objectives of optimization were minimizing the cost of construction and maximizing the robustness, considering standard deviation of failure probability as a measure of robustness. Juang et al. (2013) presented the robust geotechnical design methodology for drilled shafts in sand using NSGA-II. Sandy soil uncertainty such as friction angle was included in that study and the design variables considered were diameter and length of the shaft. The shaft was optimized for cost while the standard deviation of failure probability was constrained to target failure probability. Based on these studies, NSGA-II was found to be an effective and efficient tool for conducting multi-objective optimization and it would result in a set of preferred designs known as the Pareto-optimal front. In their study, the robust geotechnical design methodology was reported as a complementary design approach for conventional trial-and-error design procedures.

2.5.2 Proposed optimization procedure for piled-raft foundation using response surface

In this study, the design optimization of the piled raft-foundation to support tall wind turbine subjected to vertical load, horizontal load, and bending moment at the foundation level is performed considering V (wind speed) and c_u (undrained shear strength) for clayey soil and V and ϕ (friction angle) for sandy soil as uncertainty parameters (or random variables), while N_p, L_p, and R_r are considered as design variables in both soils. The range

and probability distribution of random variables considered for optimization are same as that presented in the parametric study section of this paper, i.e. uniform probability distribution. The uniform probability distribution is considered the simplest distribution among the ones commonly used in robust design optimization. Nevertheless, the uniform distributions for undrained shear strength and friction angle is considered to be appropriate for this study because they have a low coefficient of variations (20% for undrained cohesion and 10% for friction angle) and fairly cover a good range of stiff to very stiff clay and loose to dense sand, respectively. In contrast, the wind speed is better represented by Rayleigh, Weibull, Lognormal, Gamma, and Beta distributions (Morgan et al. 2010). Still, the uniform distribution is used for the wind speed in this study because the aforementioned distribution models are complicated than the uniform distribution and some of them require more than two parameters. A parametric study may be conducted to investigate the effect of probability distribution on the robust design optimization.

A bi-objective robust optimization is performed in this study using NSGA-II, a toolbox in MATLAB, to minimize the effect of uncertainties on the response and to capture the set of optimal designs in terms of cost efficiency and robustness. The first objective considered is the total cost of the piled-raft foundation calculated using unit price data from the RS Means cost database. The unit prices of pre-stressed concrete pile and raft are considered to be \$193.19/m and \$342.13/m^3, respectively (RSMeans, 2013). It should be noted that these unit prices include estimated costs for material, labor, and equipment, but exclude overhead and profit. Since the design of piled-raft foundation is controlled by differential settlement (S_{diff}), it was considered as the response of concern. As reported by Wang et al.

(2014), the standard deviation of response can be considered as an appropriate measure of robustness resulting in the smaller variation in response results corresponding to a more robust design. Thus, in the current study, the standard deviation of differential settlement is considered as the second objective of the optimization. The standard deviation of the differential settlement for numerous design candidates is computed by coupling the optimization program with a Monte Carlo simulation using a code developed in MATLAB. The flowchart of the design and optimization procedure is presented in Figure 2.9 with the details below.

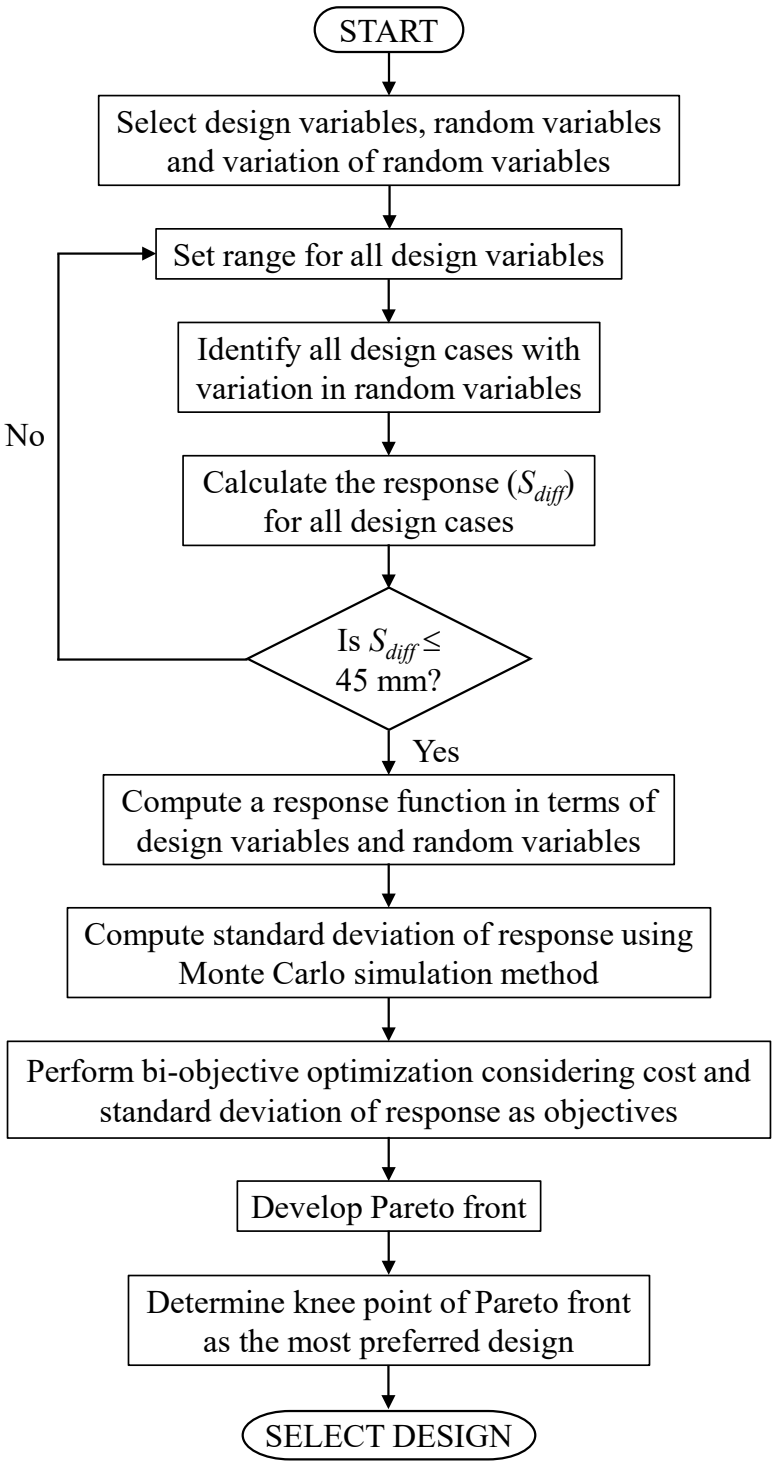

Figure 2.9. Flowchart illustrating the geotechnical design optimization procedure

To predict the approximate behavior of the piled-raft foundation in a simplified manner and avoid thousands of cumbersome calculations, a response surface is developed based on the response and the variables (the random and design variables). For this purpose, several design sets (L_p, N_p, and R_r) are selected and the corresponding differential settlements are determined for variation in the random variables. A regression analysis is subsequently performed on the differential settlement analysis results of both soil types to establish a response surface. For clayey soil, the response surface is established in terms of S_{diff}, V, c_u, L_p, N_p, and R_r, as presented in Equation 2.11. Similarly, for the sandy soil, the response surface is established in terms of S_{diff}, V, ϕ, L_p, N_p, and R_r, as presented in Equation 2.12. The coefficients of determination (or R^2) value obtained from the regression analysis are 0.91 and 0.90 for clayey and sandy soil, respectively which indicate that the proposed response function fitted the data reasonably well.

Foundation in clayey soil:

$$S_{diff} = \exp\left(19.74 + 3.74\ln(V) - 1.87\ln(c_u) - 3.04\ln(L_p) - 3.66\ln(N_p) - 1.28\ln(R_r)\right) \quad (2.11)$$

Foundation in sandy soil:

$$S_{diff} = \exp\left(15.72 + 2.86\ln(V) - 2.19\ln(\phi) - 2.03\ln(L_p) - 2.61\ln(N_p) - 0.54\ln(R_r)\right) \quad (2.12)$$

In this study, 10,000 simulations are performed to compute the standard deviation of response for each design set considering the variation in random variables. From a parametric study, which is not presented in this paper, it was observed that 10,000 simulations produced reasonably smoother Pareto front compared to 1,000 simulations and

therefore 10,000 simulations are considered adequate in this study. The robust design optimization procedure was also subjected to safety constraints of allowable differential settlement ($S_{diff,all}$ = 45 mm) and target reliability (β_t = 3) as the latter has been recommended by Kulhawy and Phoon (1996), to ensure the reliability of the foundation system. The reliability index of the system can be computed using performance function of the system (g) defined as below:

$$g\left(\theta, X\right) = S_{diff,all} - S_{diff}\left(\theta, X\right) \tag{2.13}$$

where θ and X indicate random variables and design variables, respectively. As seen in Equation 2.14, mean value of the performance function (μ_g) is calculated using the mean value of response (differential settlement) which is computed via MC simulation. It should be noted that the standard deviation of the performance function (σ_g) is equal to the standard deviation of the response also calculated by MC calculation ($\sigma_g = \sigma_{S_{diff}}$). The reliability index of the system (β) was then computed as expressed in Equation 2.15 and the values less than β_t were considered unacceptable in optimization.

$$\mu_g = S_{diff,all} - \mu_{S_{diff}} \tag{2.14}$$

$$\beta = \frac{\mu_g}{\sigma_g} \tag{2.15}$$

The preferred designs resulting from the optimization procedure are illustrated graphically in Figure 2.10 in the form of a Pareto front. Figure 2.10 shows that the design with lower cost may have higher vulnerability and higher response variability. It can be observed for the clayey soil in Figure 2.10(a) that the standard deviation of differential

settlement increased from about 4.5 mm to 7.5 mm when the total cost of foundation decreased from about $420,000 to $360,000. Similarly, for sandy soil, as shown in Figure 2.10(b), the standard deviation of differential settlement increased from about 5.0 mm to 8.1 mm when the total cost of foundation decreased from about $670,000 to $540,000. It should be noted that Pareto front changes with the change in mean values of the random variables and the range of design and random variables.

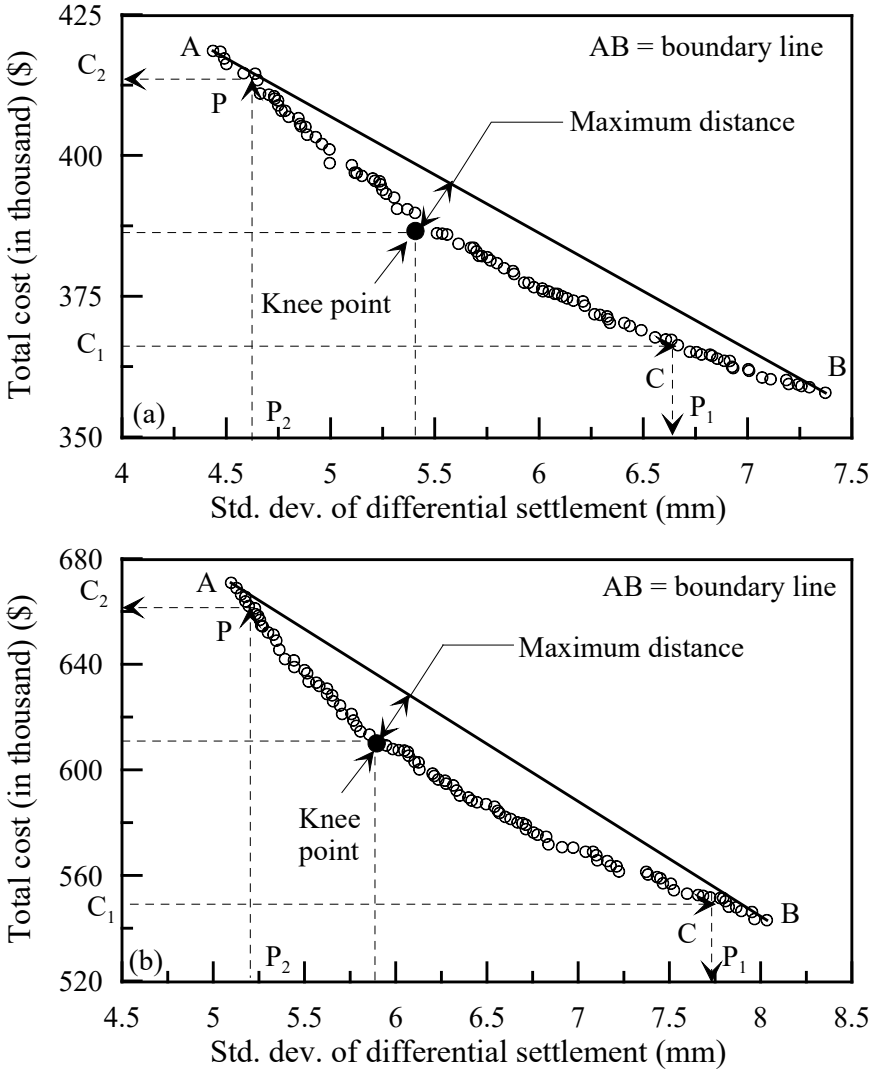

Figure 2.10. Pareto fronts optimized to both total cost and standard deviation (a) piled-raft in clayey soil and (b) piled-raft in sandy soil

The most optimal design (i.e. balancing both objectives) can be obtained from the Pareto front using the knee point concept. Among the various methods available to determine the knee point, normal boundary intersection (NBI) approach, illustrated in Figure 2.10 and also discussed in Juang et al. (2014) and Deb and Gupta (2011), is used in this study. In this method, the boundary line (AB) is created by connecting two extreme points in Pareto front and the distance of each point in Pareto front from the boundary line is calculated. Then the point on the Pareto front with the maximum distance from the boundary line is identified and referred to as the knee point, as marked in Figure 2.10. The optimal cost and standard deviation of response corresponding to the knee point are used to finalize the design solution.

The optimal length of pile, number of piles, and radius of raft for the wind tower designed in this study for clayey soil are found to be 30.4 m, 52, and 8.01 m, respectively, while the cost of that design is estimated to be $386,580. Similarly, sandy soil resulted in a design with 50.9 m long piles, 54 in number and 7.96 m of raft radius with an estimated cost of $610,024. The comparison between conventional geotechnical design results considering mean design parameters and design optimization results considering variation in random variables for clayey and sandy soil is given in Table 2.2. The standard deviation of the response (differential settlement) obtained from the design optimization is also presented in Table 2.2. For both soils, the introduction of variation of the random variable or noise factor in the design resulted in costlier foundation compared to conventional

design for the mean design parameters. However, the variations in the response (differential settlement) are reduced significantly for the foundation in both soils. One may think that the same would have been achieved by using a larger factor of safety but the robust design procedure presented in this paper considers multiple factors (random and design variable) and reduced the variation in response systematically and provides a numerical value for the variation in response.

The use of Pareto front can be extended to determine the cost-based design or the performance-based design. For instance, as shown in Figure 2.10, the client willing to spend C_1 for the construction of foundation can select the design corresponding to point C on the Pareto front with the performance level of P_1. At the same time, the client who demands a certain level of performance, P_2 in Figure 2.10, can select the design corresponding to point P on the Pareto front which will cost C_2 for the construction.

Table 2.2. Comparison of conventional design and optimum design

Soil	Conventional design				Optimized design				
	L_p (m)	N_p	R_r (m)	Total cost ($)	L_p (m)	N_p	R_r (m)	Std. dev of response (mm)	Total cost ($)
Clay	20	40	7.5	227,103	30.4	52	8.01	5.41	386,580
Sand	35	36	7.5	315,971	50.9	54	7.96	5.90	610,024

2.6 Conclusion

A geotechnical design optimization procedure for the piled-raft foundation to support a tall wind turbine on clayey and sandy soil is presented in this paper. The procedure can be easily extended to the geotechnical design of piled-raft foundation to support other structures. The geotechnical design conducted following analytical equations available in the literature indicated that the final design is controlled by the differential

settlement and rotation of the foundation rather than bearing capacity or total settlement. The parametric study showed that for both the soils, design requirements can be met by either increasing the number of piles, the length of pile, or the radius of raft when the wind speed is increased. For a higher undrained cohesion (in clayey soil) and a higher friction angle (in sandy soil), a smaller foundation was enough to meet the design requirements. The robust optimization procedure resulted in an easy-to-use graph called Pareto front which shows a clear trade-off relationship between the cost and standard deviation of the response (differential settlement) for both soils. Although these graphs can be utilized to select the suitable design for a given set of performance requirements (variation in differential settlement) and cost limitation, the best suitable design solution is determined using the knee point concept.

CHAPTER 3

GEOTECHNICAL DESIGN AND DESIGN OPTIMIZATION OF A PILED-RAFT FOUNDATION FOR TALL ONSHORE WIND TURBINE IN MULTILAYERED CLAY[2]

3.1 Abstract

Although, the pile-raft foundation is preferred for supporting tall wind turbine, its geotechnical design and selection of suitable design parameters is a complex procedure. Except the foundation, all the other above ground components are precast members that are assembled at the project site to build a wind turbine. Therefore, it is necessary to consider the possible variations in soil properties and wind speed in the design of foundation. In this paper, a reliability-based robust design procedure for pile-raft foundation that supports a 130-m tall wind turbine on a layered clayey soil is presented. Upon completion of the geotechnical design for the mean wind speed and undrained shear strengths, a parametric study and Monte Carlo simulation were conducted by varying wind speed and undrained cohesion of each layer to establish a relationship among the design variables (number and length of piles and radius of raft) and random variables (wind speed and undrained cohesion). Finally, a reliability based robust design was conducted considering total cost and robustness as the objectives. The standard deviation of the response of concern, which is the differential settlement, was considered as the measure of robustness. The optimization yielded a set of preferred designs known as Pareto front and

[2] A similar version of this chapter is published in the *International Journal of Geomechanics*; Shrestha, S., Ravichandran, N., and Rahbari, P. (2018). "Geotechnical Design and Design Optimization of a Pile-Raft Foundation for Tall Onshore Wind Turbines in Multilayered Clay," 18(2), 04017143.

the suitable design is selected for a given cost limitation and performance requirement using the Pareto front.

3.2 Introduction

Although wind energy is one of the fastest growing clean and renewable energies in the world, it accounts for only 3.3% of total electricity generated worldwide. Nonetheless, according to the 2015 Global Wind Report (GEWC, 2015) the global cumulative installed wind capacity greatly increased by the end of 2015, up to 17% from the preceding year. By the end of 2015, the United States added 4,000 new wind turbines contributing about 8,598 MW of energy, which increase the total installed capacity by 13 % from the end of 2014 (GWEC, 2015). Although a significant number of wind turbines have been installed in the United States, they only account for 4.7% of the total electricity produced nationwide. The selection of suitable locations for onshore wind farms depends on factors such as wind speed, soil condition, availability of construction material, environmental impacts, and other limitations imposed by local and federal agencies.

The energy output of individual wind turbines can be increased by building taller towers to access higher and steadier wind. It is shown that the wind energy is directly proportional to the third power of wind speed, so taller towers can produce significantly higher energy at a small additional cost. Lewin (2010) found that an increase in the turbine height from 80 m to 100 m would result in a 4.6% greater wind speed and a 14% increase in power output, and that an increased height from 80 m to 120 m would result in an 8.5% greater wind speed and a 28% increase in power production. Since the initial construction cost of a wind farm covers the highest percentage of the total cost of the project, it is logical

and cost-efficient to increase the wind energy production by building taller towers which can acquire additional power generated from the same number of wind turbines.

Although building taller towers increases the wind energy production of a single wind turbine, it poses significant challenges to the geotechnical engineer in designing and selecting the most cost-efficient foundation for the given subsurface and wind conditions. A taller wind turbine tower not only increases the vertical dead load but also significantly increases the lateral load and bending moment at the base of the tower. Larger design loads, especially the moment, not only make the foundation design more complex but also make it larger, demanding a significant amount of resources be allotted into foundation design and construction to meet the safety and serviceability requirements. Since a significant percentage of the total cost of installing a wind turbine is allocated for the design and construction of foundation, it is necessary to develop new methodologies to design and select the most cost-efficient foundation for a given set of geotechnical and wind conditions. Typically, the mat (raft) foundation, the pile group foundation, and the pile-raft foundation are used to support wind turbines depending upon the subsurface condition, tower height, and wind speed at the site. The raft foundation is an easy-to-construct foundation and provides significant bearing capacity because of its larger footprint, but its design is controlled by differential and total settlements, especially when subjected to larger loads. In this situation, deep foundations are added to the raft foundation to create what is known as a hybrid foundation or pile-raft foundation, which is economical for supporting tall wind turbines.

Unfortunately, the mobilized capacities of the piles and raft vary with the amount of settlement, which greatly complicates the design of a pile-raft foundation. Also, because of the large number of design variables (radius of raft, number of piles, length of piles etc.), many designs can be produced, leaving the design engineer to pick the design randomly or with little knowledge. Therefore, a proper methodology must be developed to help the engineer select the most appropriate foundation for the given variations in the wind speed and soil conditions. This paper details the efforts of the authors to develop such a methodology for performing reliability-based robust design of pile-raft foundation.

The procedures currently available to perform geotechnical design of pile-raft foundation are broadly classified as simplified methods, approximate computer-based methods (Sinha and Hanna, 2016; Reul, 2004), and more rigorous computer-based methods (Poulos, 2001a). The simplified methods predict the behavior reasonably well when the load is vertical but fail to predict behavior when there are lateral and moment loads. On the other hand, the computer-based methods are widely used in practice for designing pile-raft foundations subjected to combined vertical, lateral, and moment loads. Such computer-based design procedures require knowledge and use of sophisticated finite element or finite difference computer programs that may be unavailable for many practicing engineers. The accurate representation of stress-strain behavior of the supporting soil and the interaction between the raft-soil and pile-soil is the greatest challenge involved in computer-based design. Consequently, practicing engineers develop simplified models that may lead to less accurate results.

The incorporation of uncertainties in the loading (wind speed) and soil properties is also of great importance in the geotechnical design of foundations to support tall wind turbines. Indeed, engineers have great difficulty in selecting a design that is not only economical but also satisfies the performance requirements when there is a significant variability in the soil properties and loading. In particular, the use of pile-raft introduces a significantly large number of design variables (e.g. raft radius, number of piles, arrangement of piles, and length of piles) which greatly increases the difficulty in selecting the appropriate final design. In such situations, a reliability-based robust design optimization technique can be used to shortlist the best candidates and select the most suitable design by imposing appropriate limitations.

In this study, geotechnical design and optimization procedure for a pile-raft foundation are presented for a sample 130 m tall hybrid wind turbine tower with a mean wind speed of 125 mph, at a potential wind farm site in Charleston, SC. A parametric study was also conducted to understand the effect of uncertain parameters known as random variables such as wind speed and soil properties (undrained cohesion in this study) on the design variables such as radius of raft, number of piles, and length of piles and on the material cost of the foundation. In addition, a reliability-based robust design optimization procedure is presented to simplify the selection of design parameters for a site condition.

3.3 Site Condition and design loads

3.3.1 Windfarm Site and Soil properties

A site in the city of Charleston, SC along the east coast of the United State is selected in this study. The soil profile and other necessary subsurface soil properties

required for the design were obtained from a geotechnical report for a location in Charleston, SC (WPC, 2010). It is worth noting that this geotechnical report was produced for the construction of one of the world's largest turbine testing facilities in the world. The site consists of three clay layers beneath a thin sand layer at the surface. The summary of the soil profile and geotechnical parameters are tabulated in Table 3.1. The undrained cohesion (c_u), friction angle (ϕ), and modulus of elasticity (E) tabulated listed in Table 3.1 were calculated using empirical correlations between these parameters and cone tip resistance obtained from CPT7 profile provided in the geotechnical report. However, the modulus of elasticity of the second and third layers were calculated using the empirical correlation between c_u and E obtained from engineering manual (EM 1110-1-1904) for settlement analysis by U.S. Army Corps of Engineers. At this site, the ground water table was located at 1.52 m below the ground surface.

Table 3.1. Generalized soil properties

Layer	Soil	Depth (m)	Unit weight (kN/m^3)	c_u (kPa)	ϕ'(°)	E (kPa)	Poisson's ratio
1	Medium dense sand	0 - 1.22	17.28	-	*50.1	*2.75 x 104	0.4
2	Soft to firm clay	1.22 - 9.15	16.50	98.81	-	1.48 x 104	0.5
3	Cooper Marl	> 9.15	19.64	106.66	-	3.20 x 104	0.5

*Calculated using the CPT data but it was not used in the design because the bottom of the raft rests on the 2nd layer.

3.3.2 Design loads

The loads for the design of foundation for the wind turbine consists of a dead load due to self-weight of the superstructure and lateral load and bending moment due to

horizontal wind. The procedures used to determine these loads for the North Charleston, SC location are detailed in the following section.

3.3.3 Dead load

The dead load was the total vertical load consisting of the weight of the tower, rotor and rotor blades, nacelle with drive train, electronic equipment, and the other wind turbine components. The weight of the tower was calculated based on the volume of the tower and the unit weight of the tower material. The wind turbine tower considered in this study was a hybrid hollow cylindrical concrete and steel tapering tower with the lower 93 m concrete and the upper 37 m steel (Grunberg and Gohlmann, 2013). The tower diameters at the base and top were 12.0 m and 4.0 m, respectively, and the thickness varied between 0.04 m and 1.2 m. The unit weights of concrete and steel used in this study were 23.6 kN/m^3 and 78.5 kN/m^3, respectively. The appropriate weights of nacelle and rotor for the tower height were obtained from Malhotra (2011). The final dead load (P) was calculated to be 51.71 MN.

3.3.4 Wind load

The wind load was calculated considering the mean survival wind speed of 125 mph following the procedure described in ASCE 7-10 (2010). Since most wind turbines have the survival wind speed of 112 mph to 134 mph (Wagner and Mathur, 2013), a wind speed range of 89 mph to 161 mph with the mean survival wind speed of 125 mph was considered appropriate for this study. The wind action on above ground components of the wind turbine such as the tower, blades, and rotor induced lateral load and moment at the base of the tower. These loads were computed by considering the wind load along the tower

height and drag force acting on the nacelle. The total lateral load (V) and the bending moment (M) were calculated to be 2.26 MN and 144.89 MNm, respectively.

3.4 Geotechnical design of pile-raft foundation

The basic idea behind the use of a pile-raft is to increase the bearing capacity of the foundation with the use of a raft and to decrease the total and differential settlements with the use of deep foundations. However, the quantification of the exact percentage of total loads carried by raft and piles is the most challenging aspect in the design of a pile-raft foundation. This is mainly due to a lack of understanding of the complex interaction among the soil, raft, and piles and the mobilized strengths along the interface at a given total and differential settlement values. Thus, a reliable design guideline is not yet available, especially for the foundation subjected to combined moment, lateral, and vertical loads.

In this study, a preliminary geotechnical design of the pile-raft foundation was performed following the procedure outlined by Hemsley (2000) in which the procedures proposed by Poulos and Davis (1980) and Randolph (1994) were incorporated. The factors considered in the preliminary design were the ultimate vertical, moment, and lateral geotechnical capacities, total elastic and differential settlements, the rotation of the tower due to wind load, and the lateral movement of the foundation. The size of raft and the size and number of piles required to satisfy the design requirements were determined in the preliminary design stage. The capacity of pile-raft foundation was checked for vertical load, lateral load, bending moment, total and differential settlements, and rotation. A minimum factor of safety of 2 was considered safe for the vertical load, the lateral load, and the bending moment as suggested by Hemsley (2000), and a vertical misalignment of

3 mm/m was considered safe for the rotational stability of the tower (Grunberg and Gohlmann, 2013). A spreadsheet, the results of which are not included here, was prepared to automate iterative calculations and to perform parametric studies.

3.4.1 Design for vertical load

The vertical capacity of the pile-raft was calculated as the lesser of (i) the sum of ultimate capacities of raft ($P_{u\text{-}R}$) and all the piles ($P_{u\text{-}P}$), i.e., $P_{u\text{-}PR} = P_{u\text{-}R} + P_{u\text{-}P}$ and (ii) the ultimate capacity of a block ($P_{u\text{-}B}$) that consists of piles and raft, plus that of the portion of the raft outside the periphery of the pile group (Hemsley, 2000). The ultimate capacity of raft, $P_{u\text{-}R}$ was calculated using the general bearing capacity equation by Vesic (1973 and 1975), and the ultimate capacity of all the piles, $P_{u\text{-}P}$ was calculated as a sum of ultimate downward capacity of all the piles i.e. $P_{u\text{-}P} = N_p P_{ult\text{-}dn}$, where N_p is the number of piles and $P_{ult\text{-}dn}$ is the ultimate downward capacity of single pile, which is the sum of ultimate skin resistance (P_s) and toe resistance (P_t). In this study, the α method and Meyerhof's method provided in Das (2011) were used to calculate the ultimate skin and toe resistance of a single pile, respectively. Finally, the factor of safety for vertical load was calculated using Equation 3.1.

$$FS_P = \frac{\min(P_{u-PR}, P_{u-B})}{P} \tag{3.1}$$

where P is the design vertical load.

The ultimate vertical capacity calculated by adding the capacities of piles and raft was found to be lower than that calculated assuming the piles and raft as a single block.

The final factor of safety for vertical load capacity was determined to be 3.41, which met the design requirement.

3.4.2 Design for moment load

The ultimate moment capacity of the pile-raft foundation was estimated as the lesser of (i) the ultimate moment capacity of raft plus the ultimate moment capacity of piles and (ii) the ultimate moment capacity of a block containing the piles, raft, and soil. The ultimate moment capacity of the raft, pile group, and block of pile-raft were determined using the method presented in Hemsley (2000). The key equations are summarized below for the sake of completeness.

3.4.2.1 Case I: Ultimate moment capacity of pile-raft considering individual capacity:

The ultimate moment capacity of the raft, $M_{u\text{-}R}$ was calculated using Equation 3.2 (Hemsley, 2000).

$$\frac{M_{u-R}}{M_m} = \frac{27}{4}\frac{P}{P_u}\left[1-\left(\frac{P}{P_u}\right)^{1/2}\right] \tag{3.2}$$

where M_m is the maximum possible moment that soil can support, P is the applied vertical load, P_u is the ultimate centric load on the raft when no moment is applied. For this method, the maximum moment for circular raft, M_m is given by:

$$M_m = \frac{q_u D^3}{4}\left(\frac{\pi}{4}-\frac{1}{3}\right) \tag{3.3}$$

where q_u is the ultimate bearing capacity of raft, and D is the diameter of circular raft.

The ultimate moment of all the piles in the foundation system, $M_{u\text{-}P}$ was estimated using Equation 3.4 (Hemsley, 2000).

$$M_{u-P} = \sum_{i=1}^{N_p} P_{uui} |x_i| \tag{3.4}$$

where P_{uui} is the ultimate uplift capacity of ith pile, $|x_i|$ is absolute distance of ith pile from center of group, and N_p is the number of piles.

The ultimate moment capacity of the pile-raft, $M_{u\text{-}PR}$, system considering individual capacity is given by:

$$M_{u-PR} = M_{u-R} + M_{u-P} \tag{3.5}$$

3.4.2.2 Case II: Ultimate moment capacity of pile-raft considered as a single block:

The ultimate moment capacity of the block, a single unit consisting of the raft and the piles, M_{uB} was estimated using Equation 3.6 given below (Hemsley, 2000).

$$M_{u-B} = \alpha_B \bar{p}_u B_B D_B^2 \tag{3.6}$$

where B_B and D_B are the width and depth of the block, respectively, $\bar{p}_u$ is the average lateral resistance of soil along the block, and α_B is the factor depending upon the distribution of ultimate lateral pressure with depth (0.25 for constant distribution of $\bar{p}_u$ and 0.2 for linearly increasing $\bar{p}_u$ with depth from zero at the surface). It should be noted that Equation 3.6 was proposed for designing rectangular raft and pile arrangement. However, in this study, the raft was circular in shape and therefore the circular section was converted to an equivalent rectangular section to apply the Equation 3.6 to calculate the ultimate moment capacity of the block.

3.4.2.3 Ultimate moment capacity of the pile-raft

It was observed that the design was controlled by individual failure because the ultimate moment capacity calculated for case I was smaller than case II. The final factor of safety for moment capacity was determined to be 3.56 using Equation 3.7, which met the design requirement.

$$FS_M = \frac{\min(M_{u-PR}, M_{u-B})}{M} \tag{3.7}$$

3.4.3 Design for lateral load

The lateral pile capacity of a single pile was determined using the solutions by Broms for cohesive soil outlined in Gudmundsdottir (1981). The ultimate lateral load capacity and lateral deflection of a single pile were calculated using the horizontal coefficient of subgrade reaction. It was assumed that all the piles would behave in the same way under the application of lateral load. Hence the ultimate lateral load capacity of pile group was estimated as the sum ultimate lateral capacity of all the piles present in the group i.e., $V_{u\text{-}PR} = nV_{u\text{-}P}$. The factor of safety for the lateral load was calculated using Equation 3.8.

$$FS_V = \frac{V_{u-PR}}{V} \tag{3.8}$$

The factor of safety was found to be 12.78 and lateral deflection was of 9.12 mm.

3.4.4 Total settlement

3.4.4.1 Elastic settlement

The vertical load vs. total elastic settlement response of the pile-raft foundation was estimated following the approach proposed by Poulos (2001b) in conjunction with the

method of estimating load sharing between the raft and piles presented in Randolph (1994). The load sharing between the raft and the piles can be estimated on the basis of stiffness of the raft, piles, and pile-raft. The stiffness of pile-raft, K_{pr} was estimated using Equation 3.9 proposed by Randolph (1994).

$$\left.\begin{aligned} K_{pr} &= X K_p \\ \text{where } X &= \frac{1+\left(1-2\alpha_{rp}\right)K_r/K_p}{1-\alpha_{rp}^2\left(K_r/K_p\right)} \end{aligned}\right\} \tag{3.9}$$

where K_r is the stiffness of the raft, K_p is the stiffness of the pile group, and α_{rp} is the raft-pile interaction factor. The raft-pile interaction factor was assumed to be 0.8 because as the number of piles in the group increases, the interaction factor increases and tends towards a constant value of 0.8 as reported by Randloph (1994). Among the various methods for estimating the raft stiffness, the method outlined by Randolph (1994) was used. To estimate the stiffness of the pile group, the method proposed by Poulos (2001b) was used, where the target stiffness of the pile-raft was first determined by dividing the total vertical load by the assumed allowable settlement. Equation 3.9 was then solved to determine the stiffness of the pile group, with the stiffness of the pile-raft remaining operative until the pile capacity was fully mobilized at load P_A. With all the known values, the vertical load vs. total elastic settlement relationships established in Equation 3.10 were used to obtain the load vs. settlement (P vs. S) curve for the pile-raft foundation.

$$\left.\begin{aligned} &\text{For } P \le P_A;\ S = \frac{P}{K_{pr}} \\ &\text{For } P > P_A;\ S = \frac{P_A}{K_{pr}} + \frac{P-P_A}{K_r} \end{aligned}\right\} \tag{3.10}$$

The calculated vertical load vs. elastic settlement curve is shown in Figure 3.1. It can be seen from Figure 3.1 that the design vertical load, P is less than the load at which the pile capacity is fully mobilized (P_A), meaning that both the piles and the raft are contributing to the total load bearing capacity to support the applied design load.

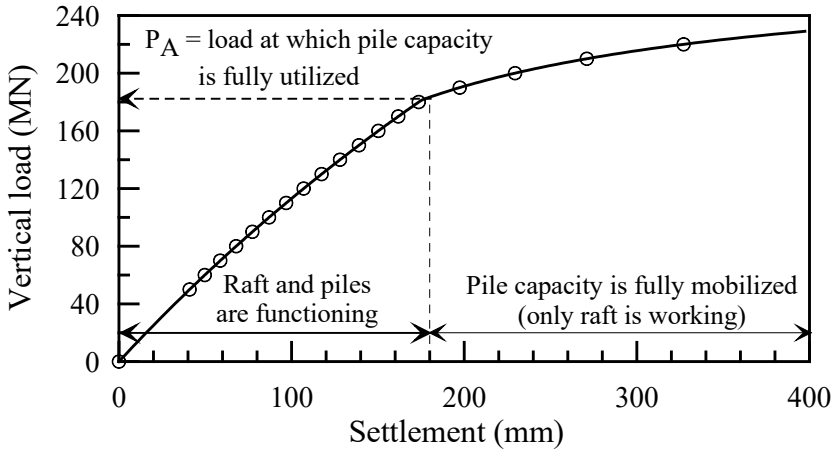

Figure 3.1. Calculated load vs. total elastic settlement curve for piled-raft foundation

From the load vs. total elastic settlement curve, the total elastic settlement of the pile-raft for the total vertical load of 51.71 MN was found to be 42.42 mm.

3.4.4.2 Consolidation settlement

Typically, consolidation settlement is not taken into consideration for deep foundations unless the foundation design is controlled by block failure. However, the proposed study deals with combined raft and pile foundations and therefore the consolidation settlement must be incorporated in the design for obtaining better design especially for meeting the long-term serviceability requirement. Due to the combined loading, the pressure distribution below the raft is non-uniform and the calculation of consolidation settlement due to non-uniform load is complicated. To address this issue

accurately, the differential settlement due to non-uniform pressure distribution must be calculated. However, because of the limitations in the procedures available in the literature, the differential consolidation settlement is not considered in this study. However, the total consolidation settlement due to the average pressure below the raft is calculated and incorporated in the design in this study.

For this study, the consolidation settlements of the second and third clay layers due to increase in stress were calculated at the middle of each layer. The pre-consolidation pressures (σ'_c) of second and third layers were calculated using the correlation between the cone tip resistance and pre-consolidation pressure (Mayne and Kemper, 1988). It was found that both layers are overconsolidated with the final effective stress (σ'_f) less than the pre-consolidation pressure. The compression index (C_c) was calculated using the empirical correlation proposed by Kulhawy and Mayne (1990). Since the swelling index (C_s) is usually 1/5 to 1/10 of C_c (Das, 2011), it was assumed to be 1/8 of C_c in this study. The initial void ratio (e_o) was calculated using the correlation between C_c and e_o proposed by Hough (1957). These consolidation parameters are listed in Table 3.2. Finally, the consolidation settlements (S_c) of the second and third layers were calculated to be 37.62 mm and 16.72 mm, respectively, resulting in a total consolidation settlement of 54.34 mm.

Table 3.2. Consolidation parameters and consolidation settlement

Middle of layer	Thickness (m)	σ'_c (kPa)	σ'_o (kPa)	σ'_f (kPa)	C_c	C_s	e_o	S_c (mm)
2	7.93	424.05	50.53	229.92	0.0907	0.0113	0.57	37.62
3	15.85	504.89	154.92	216.97	0.0907	0.0113	0.57	16.72

The total settlement (elastic plus differential settlements) was calculated to be 96.76 mm which is within the tolerable limit of 100 mm for tall structures (Raju, 2015). Nevertheless, it should be noted that uniform vertical settlement of the entire system may not be hazardous, especially for wind turbines located away from critical infrastructure.

3.4.5 Differential settlement and rotation

There is no accurate procedure available in literature for calculating the differential settlement of the pile-raft foundation system subjected to bending moment. In this paper, a new technique is proposed to calculate the differential settlement of pile-raft foundation. In this method, the percentages of bending moment carried by the raft (M_{Raft}) and piles ($M_{Pile} = M - M_{Raft}$) were adjusted until the differential settlements of both were equal for the applied loads, which is considered as the differential settlement of pile-raft foundation. In practice, the piles are fixed to the bottom of the raft, and the rotation of the piles and the raft are the same. The above idea of adjusting the loads until the rotations are equal replicates the field condition. The vertical shortening and extension of piles from the lateral deflection was assumed as negligible in this study.

3.4.5.1 Differential settlement of raft

To determine the differential settlement of raft, the rotation (θ_{Raft}) from the wind load was first calculated using Equation 3.11 as expressed by Grunberg and Gohlmann (2013).

$$\theta_{Raft} = \frac{M_{Raft}}{c_s I_{Raft}};\ c_s = \frac{E_s}{f^{'}\sqrt{A_{Raft}}} \tag{3.11}$$

where M_{Raft} is the fixed-end moment at the soil-structure interface (the percentage of moment shared by raft to yield an equal differential settlement as piles in this study), c_s is the foundation modulus, I_{Raft} is the second moment of inertia, E_s is the modulus of elasticity of soil, f' is the shape factor for overturning (0.25), and A_{Raft} is the area of the foundation. After calculating θ_{Raft}, a simple trigonometric relationship was used to determine the differential settlement of the raft, assuming that raft rotates about its center line.

3.4.5.2 Differential settlement of piles

The differential settlement of the pile group was estimated on the basis of individual pile settlement profile due to the resultant vertical load induced by the moment carried by the piles (M_{Piles}) using the Fellenius method presented in Coduto (2001). First, the resultant vertical loads acting on each pile were calculated as the sum or difference of vertical load due to dead load and vertical load induced due to bending moment. The difference in the pile settlement of the outer most piles in the direction of moment was considered as the differential settlement of the piles, the concept of which is graphically shown in Figure 3.2. Finally, the rotation of the pile was computed.

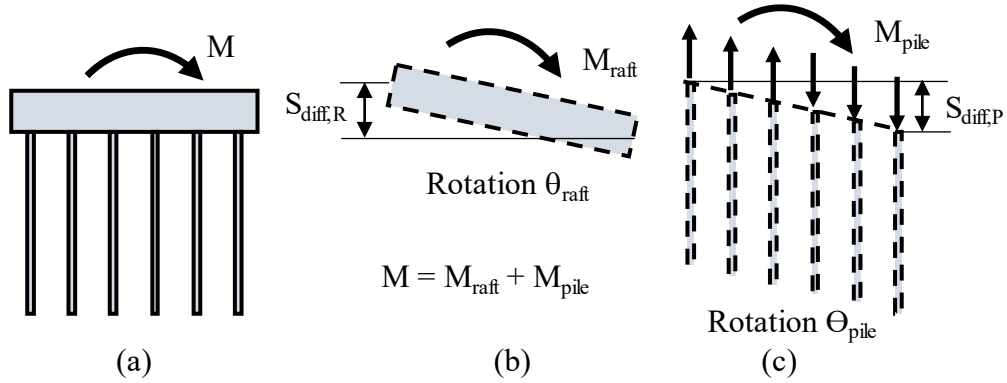

Figure 3.2. Conceptual differential settlement calculation diagram (a) piled-raft, (b) rotation of raft, and (c) rotation of piles

3.4.5.3 Differential settlement of piled-raft

The values of M_{Raft} and M_{Piles} (= M - M_{Raft}) were adjusted until the differential settlement of the raft and the piles were equal. The corresponding final values were considered as moment carried by the piles and the raft, with the final differential settlement deemed to be the differential settlement of the pile-raft foundation. This exercise resulted in differential settlement of 44.23 mm and rotation of 0.17°, a rotation that induced the horizontal displacement of 383.7 mm at the top of the tower, which is within the acceptable limit.

3.4.6 Design outcome

The final design resulted in a raft of radius of 7.5 m and thickness of 1.2 m at a depth of 1.5 m supported by 40 pre-stressed concrete piles of width of 0.457 m and length of 21.8 m arranged equally in the circumference of 5.3 m and 6.7 m. The final design is shown in Figure 3.3.

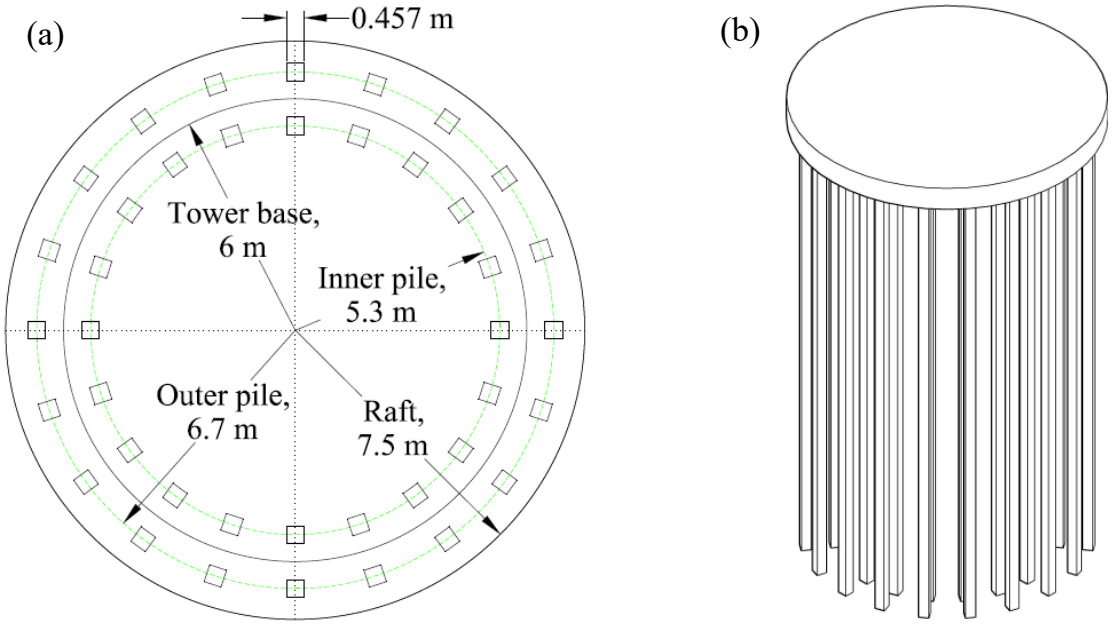

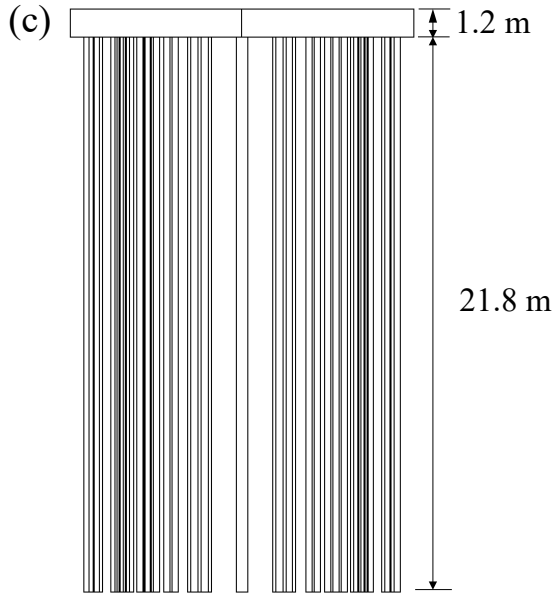

Figure 3.3. (a) Plan, (b) 3D, and (c) front view of designed piled-raft foundation

3.5 Parametric study

To account for the effect of variations in loading and soil properties on the design results, a parametric study was conducted considering possible variations in wind speed and undrained cohesion of the second and third layers of the soil. For each case in the parametric study, only one design parameter (number of piles-N_p, length of pile-L_p, or radius of raft-R_r) was changed at a time to meet all the design requirements. In addition, the variation in total cost of the foundation due to variation in wind speed and undrained cohesion was also studied. The total cost of the foundation includes material cost, labor cost, and equipment cost and was calculated as a sum of total cost of raft and piles using their unit costs. The unit costs for raft and pre-stressed concrete pile used in this study are \$342.19/m^3 and \$192.19/m, respectively obtained from RSMeans (2013). The details of the parametric study and the results are presented below.

3.5.1 Effect of wind speed on the design variables

The wind speed was varied within the range of survival wind speed i.e. between 89 mph and 161 mph with mean (μ_v) of 125 mph and standard deviation (σ_v) of 18 mph. The designs were performed for five wind speeds (89, 107, 125, 143, and 161 mph) which represented $\mu_v \pm 2\sigma_v$ range following the procedure presented in the previous section and keeping the undrained cohesion constant at mean value. The required N_p, L_p, and R_r to fulfill the design requirements for 5 wind speeds and corresponding total cost of foundation are presented in Figures 3.4, 3.5, and 3.6, respectively. The results show that N_p, L_p, and R_r increased with increasing wind speed as did the total cost. The radius of the raft for the lower three wind speeds was the same, as shown in Figure 3.6, because it was the minimum radius requirement based on the bottom diameter of the tower. Thus, the total cost also has a similar trend for lower wind speeds. An investigation of the total cost of the foundation for a different number and length of piles found that for higher wind speeds it is economical to meet the design requirement either by increasing N_p or L_p, rather than by increasing R_r.

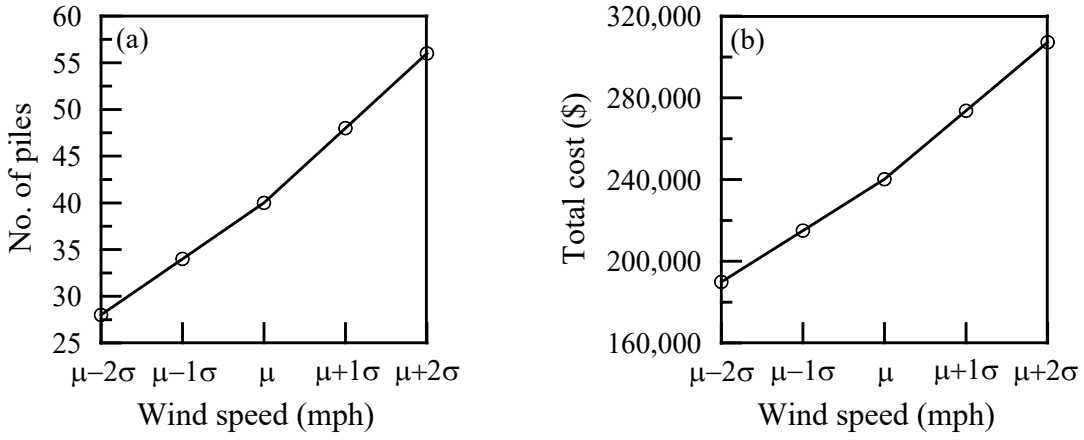

Figure 3.4. Effect of variation in wind speed on (a) number of piles and (b) total cost of piled-raft

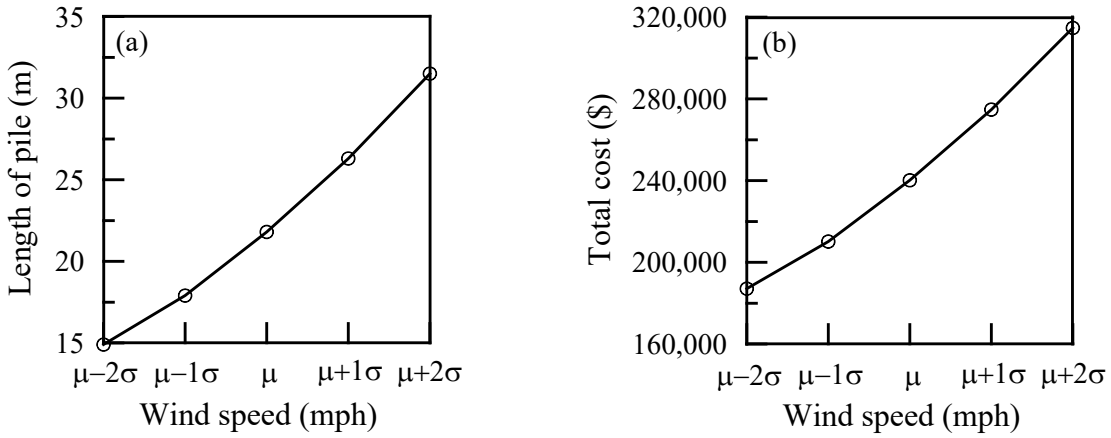

Figure 3.5. Effect of variation in wind speed on (a) length of pile and (b) total cost of piled-raft

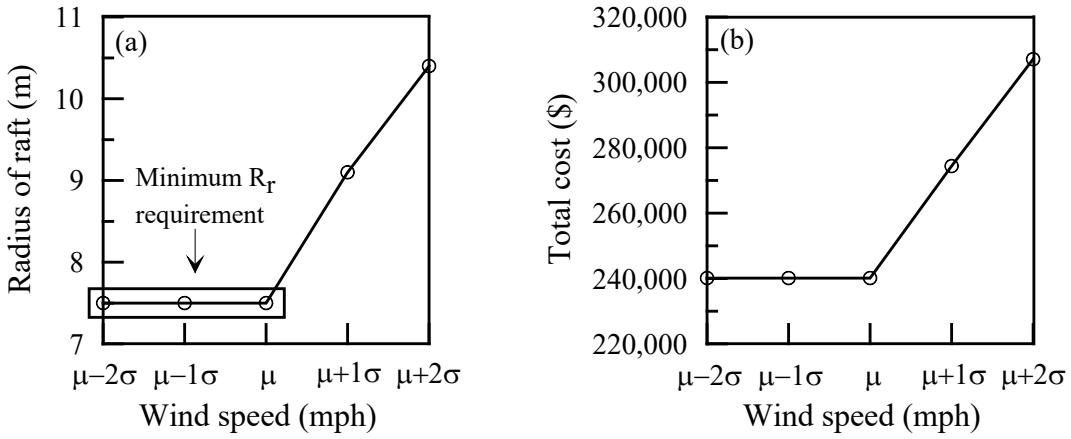

Figure 3.6. Effect of variation in wind speed on (a) radius of raft and (b) total cost of piled-raft

3.5.2 Effect of undrained cohesion on the design variables

Considering the medium site variability, a coefficient of variation (COV) of 25% was assumed to determine the variation in undrained cohesion (c_u) for the last two layers of soil. For the second layer, the standard deviation of c_u (σ_{cu}) was calculated at 24.70 kPa using 25 % COV and the mean c_u (μ_{cu}) of 98.81 kPa. Similarly, the standard deviation of

the third layer was calculated at 26.66 kPa using the same COV and mean c_u of 106.66 kPa. The parametric study was conducted by varying c_u by $\pm 2\sigma_{cu}$ above and below the mean value for both layers. The variation of c_u used in this parametric study is also shown in Figure 3.7.

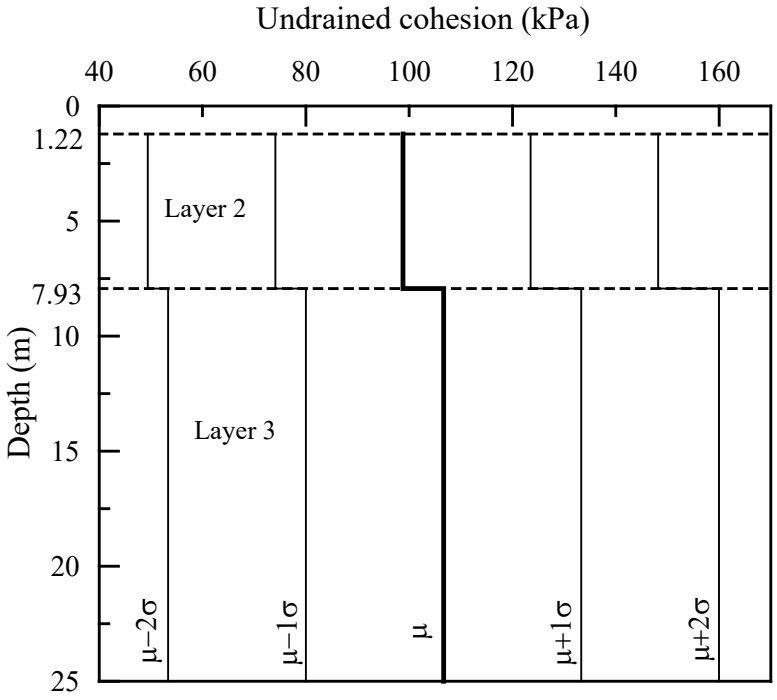

Figure 3.7. Soil profile showing variation in undrained cohesion

As shown in Figure 3.7, for each case of in the parametric study, the c_u of the second and third layer was changed simultaneously while keeping the wind speed constant. Although only the variation up to 25 m depth is shown in Figure 3.7, the c_u for depth greater than that was assumed as the same for the parametric study. The N_p, L_p, and R_r required to meet all the design requirements at 5 undrained cohesions and corresponding total cost of foundation are presented in Figures 3.8, 3.9, and 3.10, respectively. The results indicate that N_p, L_p, and R_r decrease with an increasing c_u along with the total cost of the foundation.

For the lowest c_u in Figure 3.8 (a), piles were arranged in three circumferences to meet all the design requirements without facing a group effect. In Figure 3.10 (a), it can be seen that R_r remains the same even with an increase in c_u because it is the minimum radius requirement based on the bottom diameter of the tower. Similar to the results of the variation in wind speed, adjusting N_p or L_p is the most economical method for meeting all of the design requirements compared to an adjustment of R_r.

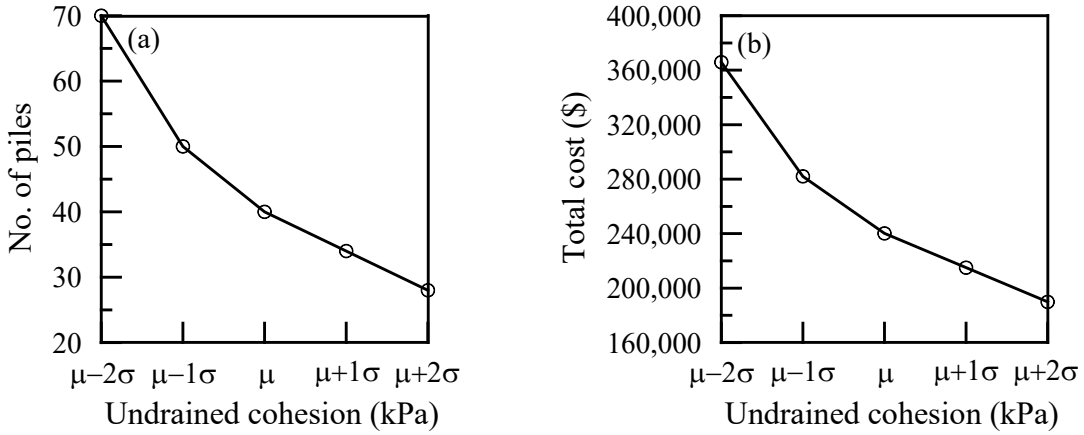

Figure 3.8. Effect of variation in undrained cohesion on (a) number of piles and (b) total cost of piled-raft

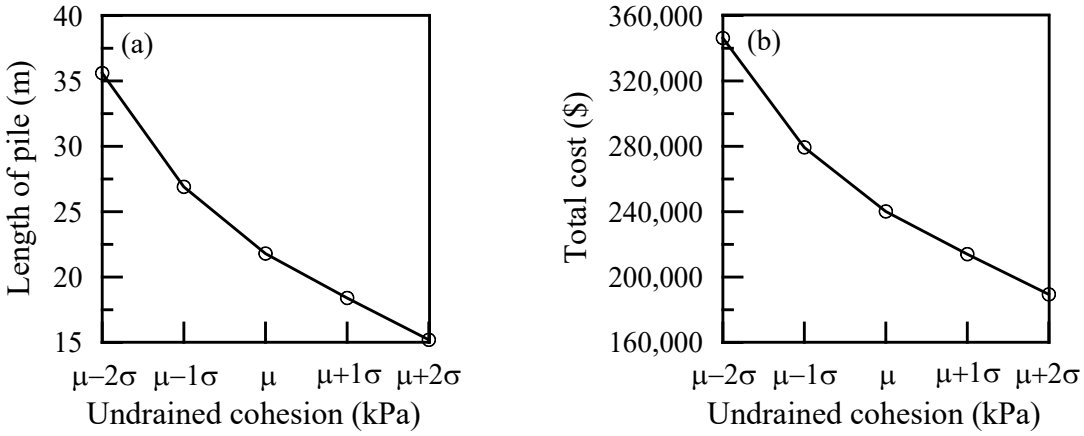

Figure 3.9. Effect of variation in undrained cohesion on (a) length of pile and (b) total cost of piled-raft

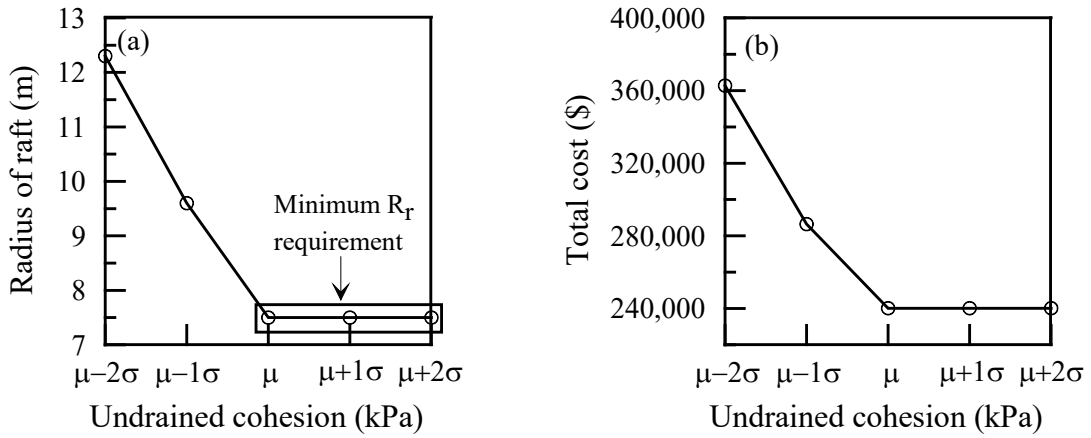

Figure 3.10. Effect of variation in undrained cohesion on (a) radius of raft and (b) total cost of piled-raft

The parametric studies presented above considered the effect of a single variable at a time. A three-dimensional graph can be developed to visualize the effect of two variables. However, in reality, more than two variables may affect the system simultaneously. In such situation, a reliability-based robust optimization procedure can be used to produce an easy-to-use graph for selecting suitable design.

3.6 Design optimization

Although the parametric study results presented in the preceding section shows the effect of variations in soil properties and wind speed on the design outcomes, they do not consider the change in more than one variable at the same time. Moreover, they do not give a clear indication on how to select the most cost-efficient and robust design for a given performance criterion. In such a situation, a reliability-based robust design optimization can be used to develop a criterion to select the most suitable design for the given performance and cost criteria. One such framework is presented in this paper.

In reliability methods, risk or reliability is calculated for a given performance criterion or a performance function. The computational approaches available for conducting a reliability analysis of geotechnical or structural engineering systems with implicit performance functions can be grouped into three. They are: (i) the Monte Carlo simulation, (ii) the response surface approach and (iii) the sensitivity-based analysis. The Monte Carlo and response surface approaches are widely used in geotechnical engineering. The Monte Carlo approach is mostly used when closed-form solution is achievable with reasonable computational effort because the function is developed based on thousands of simulation results. This method may not be effective if obtaining a deterministic solution is time-consuming as in the case of finite element method for complex problems. In such a situation, the response surface method is used in which the function is developed to approximate the performance through a few selected simulations. The inputs for these simulations are selected in the neighborhood of the most likely failure point. Then, a regression analysis of these results is performed. Various methods are available in the literature for performing reliability-based robust design optimization. Some of the latest procedures used for optimizing geotechnical systems along with their robustness measure, safety constraint, random variables, and mathematical models are tabulated in Table 3.3.

Table 3.3. Applications of reliability-based robust design optimization to various geotechnical systems

System	Random variables	Robustness measure	Safety constraint	Optimization method	Reference
Drilled shafts in clay	Soil properties, construction variations, loading	Weighted sensitivity index of response	Target reliability index	Simplified RBRGD in spreadsheet	Khoshnevisan et al. (2016)
Monopile foundation	Undrained shear strength, friction angle, lateral load	Total cost	Failure probability	RBDO by coupling SS method with SA stochastic optimization algorithm.	Overgård et al. (2016)
Drilled shaft	Friction angle, coefficient of lateral earth pressure	Variation in failure probability, feasibility robustness	Failure probability	RGD with NSGA-II	Juang et al. (2013)
Shallow foundation	Undrained shear strength and loads (moment, vertical, horizontal)	Volume of concrete	Target probability of failure	d-RBD with MCS	Ben-Hassine and Griffiths (2012)
Shallow foundation	Undrained shear strength, effective friction angle, coefficient of volume compressibility, vertical central load	Variation in failure probability, feasibility robustness	Failure probability	RGD with NSGA-II	Juang and Wang (2013)
Shallow foundation	Geotechnical parameters (unit weight, friction angle, Young's modulus, Poisson's ratio), loading parameters (dead load, live load), construction tolerance (width, length, depth), model error (ULS and SLS solution)	SI based on gradient of system response to noise factors	Safety margin (difference between resistance and load)	RGD with NSGA-II	Gong et al. (2014)
Spread foundation	Unit weight, effective friction angle, operative horizontal stress coefficient	Construction cost	ULS and SLS requirement	RBD	Wang (2009)

*RBRGD stands for "Reliability-Based Robust Geotechnical Design."

RGD stands for "Robust Geotechnical Design."

NSGA-II stands for "Non-dominated Sorting Genetic Algorithm" version II developed by Deb et al. (2002).

RBDO stands for "Reliability-Based Design Optimization."

SS stands for "Subset Simulation."

Cont.

SA stands for "Simulated Annealing."

d-RBD stands for “direct Reliability Based Design.”
MCS stands for “Monte Carlo Simulation.”
ULS stands for “Ultimate Limit State.”
SLS stands for “Serviceability Limit State.”
COV stands for “Coefficient of variation.”

Although the advantages and disadvantages of these methods vary with the problem, the RBRGD using NSGA-II is used in this study. This method considers the soil properties and wind speed as random variables, standard deviation of the differential settlement and the total cost of foundation as robustness measure, and allowable differential settlement and reliability index as the safety constraint. A framework of design optimization procedure of pile-raft foundation is presented in Figure 3.11 with the procedure discussed below.

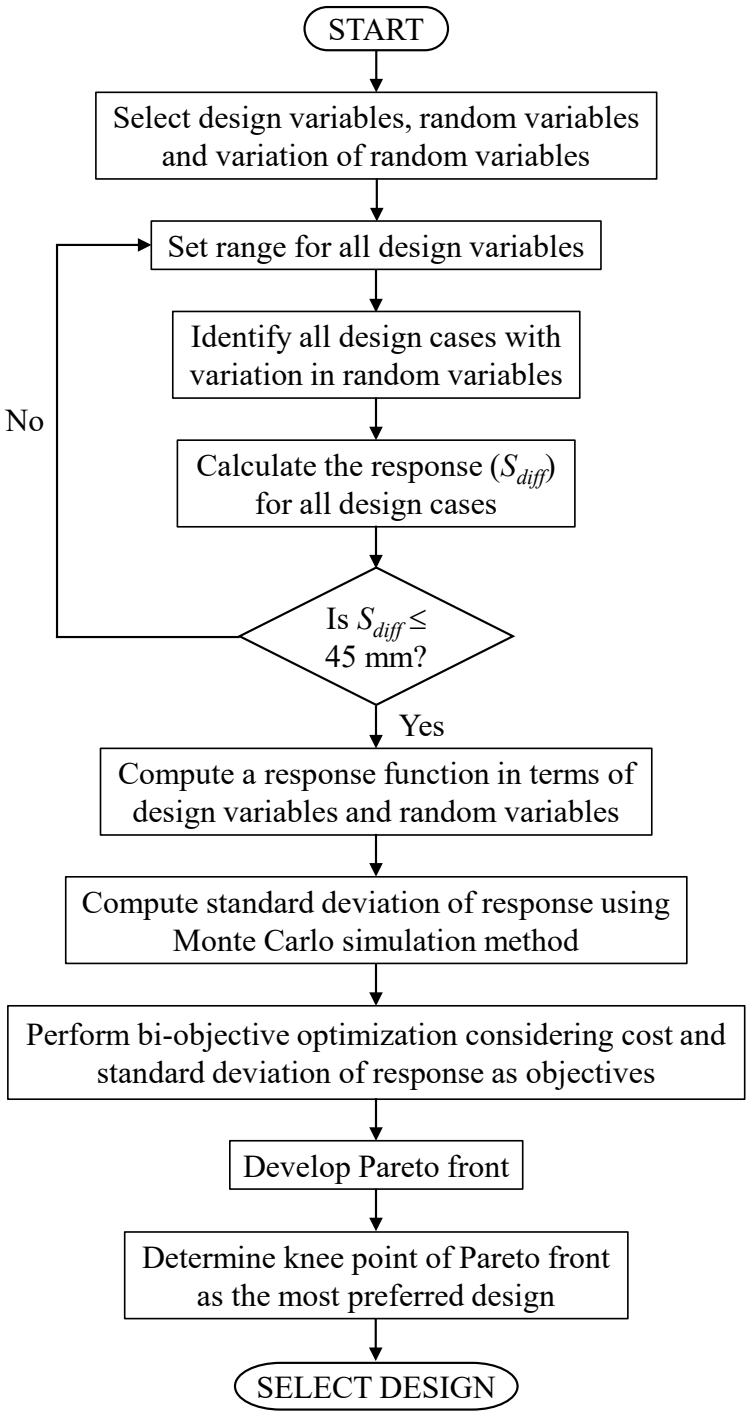

Figure 3.11. Framework illustrating the design optimization procedure

3.6.1 Design variables, random variables and objective functions

The design optimization of pile-raft foundation was performed considering L_p, N_p, and R_r as design variables and V, $c_{u(2)}$, and $c_{u(3)}$ as random variables. The range of design variables used in optimization that would satisfy design requirements for all the possible design sets considering variation in random variables are L_p = 28.4 m to 31.4 m, N_p = 44 to 52, and R_r = 7.5 m to 10.5 m. The maximum and minimum values and standard deviation of random variables used in optimization are the same as those used in the parametric study. Since the excessive differential settlement (S_{diff}) can cause a collapse of the entire turbine, it is considered as the response of concern in this study. A bi-objective optimization was performed using NSGA-II to reduce the effect of uncertainties on response and to capture a set of designs in terms of cost efficiency and insensitivity to uncertain parameters. To achieve this, two objective functions of the total cost of the pile-raft foundation and the standard deviation of the predicted differential settlements were computed and minimized through optimization. The total cost of foundation was considered as one of the objectives because in the wind turbine tower construction, the foundation is the only component that is dependent upon the site subsurface condition. All the other components of the wind turbine are prefabricated and assembled at the site. It implies that the cost of the wind turbine tower is mostly controlled by the cost of foundation. Hence, using the total cost as an objective helps the user to compare costs of different foundations with a range of performance requirement (variation in differential settlement). Thus, the result from design optimization can be used by clients to select the site-specific optimal design within their allocated budget.

3.6.2 Development of response function

To develop a response function for optimization, the response (S_{diff} in this study) of all the possible design sets considering variation in design variables and random variables were first calculated. A regression analysis was then performed using the results of a differential settlement analysis to establish a response function in terms of the design variables (L_p, N_p, and R_r) and random variables (V, $c_{u(2)}$, $c_{u(3)}$). The resulting response function is shown in Eqn. 3.12.

$$S_{diff} = \exp\begin{pmatrix} 11.53 + 3.55\ln(V) - 0.13\ln(c_{u(2)}) - 1.05\ln(c_{u(3)}) \\ -2.07\ln(L_p) - 3.02\ln(N_p) - 1.10\ln(R_r) \end{pmatrix} \quad (3.12)$$

3.6.3 Pareto front and design selection

3.6.3.1 Pareto front

The bi-objective optimization considering total cost and standard deviation of response as objectives for the preferred number of design sets coupled with Monte Carlo method was used to develop Pareto front. The first objective (i.e. the total cost of the foundation) was calculated based on the unit cost of raft and pre-stressed concrete pile, as detailed in the parametric study section of this paper. The second objective, (i.e. the standard deviation of response for each design set) was calculated based on the response function developed as shown in Equation 3.12 for the desired number of Monte Carlo simulations. Here, the number of simulations is the total number of a set of random variables, randomly selected within the provided limits. In this study, 1,000 simulations and 10,000 simulations were used to compute the standard deviation of response for each design set. The preferred designs resulting from optimization procedure are demonstrated

graphically using Pareto front in Figure 3.12 (a) and (b) for these 1,000 and 10,000 simulations, respectively. All the designs in the Pareto front are considered as equally optimum. A clear trade-off relationship between the total cost of foundation and the standard deviation of response can be inferred from the resulted Pareto front shown in Figure 3.12. In other words, decreasing the cost of the foundation may result in designs with a higher vulnerability and response variability against uncertainties. From the 1,000 simulation results, it can be seen that a decrease in the standard deviation of differential settlement from 7.6 mm to 3.5 mm increased the total foundation cost from $340,000 to $460,000. Similarly, the 10,000 simulation results show that a decrease in the standard deviation of differential settlement from 7.0 mm to 3.7 mm increased the total foundation cost from $360,000 to $460,000, which yields a $10,000 difference between the two.

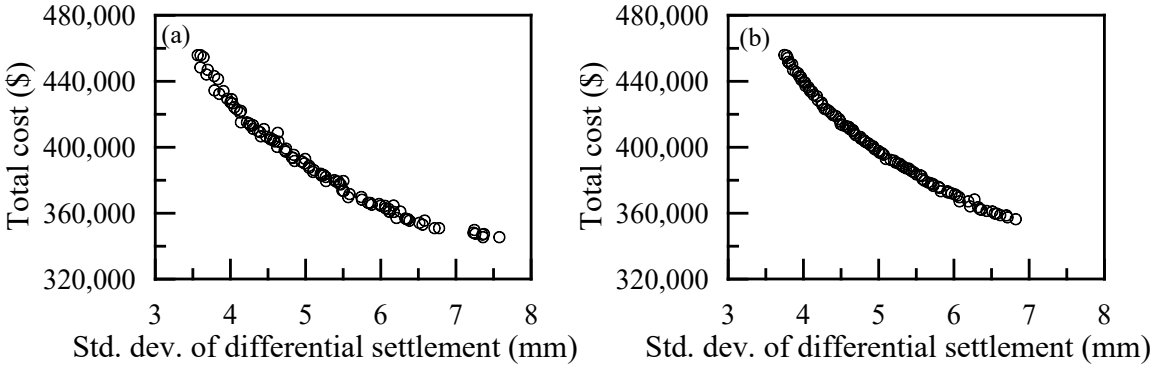

Figure 3.12. Pareto front optimized to both total cost and standard deviation (a) 1,000 simulations, and (b) 10,000 simulations

3.6.3.2 Design selection

The resulting Pareto front can be judged by designers and the final design can be selected based on performance requirements and available funds for the construction of the foundation. The different possible optimum design outcomes that can be extracted from

the Pareto front is presented in Figure 3.13. In this section, the Pareto front for 10,000 simulations is used for demonstration. Generally, to compare the concept of Pareto front with conventional design, it should be noted that the least costly design, which is the most sensitive design on Pareto front (marked as *B* in Figure 3.13), is usually considered as the final design in conventional practices where uncertainties are not involved. Similarly, the design which is the least sensitive but the most expensive of all on the Pareto front (marked as *A* in Figure 3.13) can also be obtained if the client desires to have the most robust design. Nevertheless, the most optimal design that meets the given performance and cost requirements can be obtained from the Pareto front using knee point concept. In this study, the normal boundary intersection (NBI) approach illustrated in Figure 3.14 was used to determine the knee point in the resulting Pareto front. In this method, for each point on the Pareto front, the distance from the boundary line, which connects two extreme upper and lower points of the Pareto front, was computed in the normalized space of the Pareto front. The knee point on the Pareto front, which has the longest distance from the boundary line, was then determined. The knee point determined using NBI approach for the Pareto front with 10,000 simulations is also shown in Figure 3.13 as point *C*.

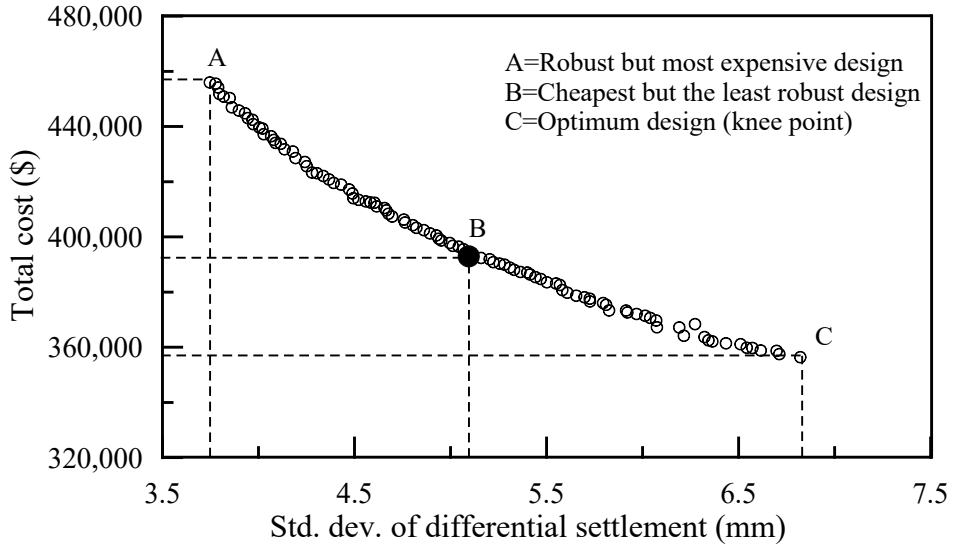

*Pareto front used is for 10,000 simulations.

Figure 3.13. Application of Pareto front for design selection

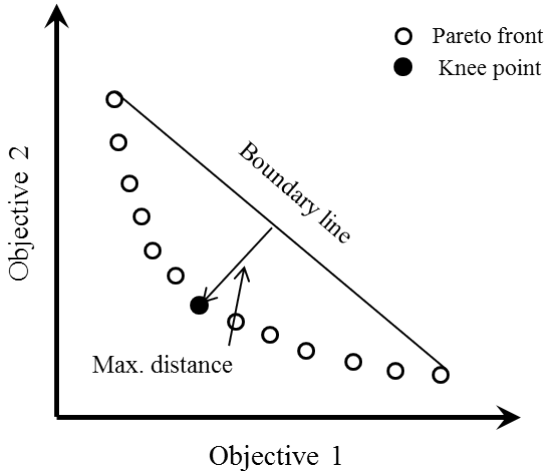

Figure 3.14. Normal boundary intersection approach to determine knee point

The optimum designs for 1,000 and 10,000 simulations obtained via the NBI approach are given in Table 3.4. It is observed that the optimum design for both numbers of simulations has a similar value for both the cost and the standard deviation of response.

Table 3.4. Optimum design obtained from Pareto front

Simulations	L_p (m)	N_p	R_r (m)	Standard deviation of response (mm)	Total cost ($)
1,000	29.87	52	7.93	5.57	369,742
10,000	31.25	52	7.91	5.09	392,929

3.7 Conclusion

A reliability-based robust design optimization of pile-raft foundation for a tall wind turbine on clayey soil was presented in this paper. Based on the deterministic geotechnical design outcomes, it was found that the final design is controlled by the differential settlement and rotation. The use of the pile-raft which takes advantage of both the raft and piles to control the bearing capacity and settlement, respectively, was found to be the best option for meeting the design requirements. The results of the parametric study showed that the design requirements can be met by increasing either the number of piles, length of piles, or radius of the raft for higher wind speeds. The results of the Pareto front created from the design optimization results showed a clear trade-off relationship between the total cost of the foundation and the standard deviation of response (differential settlement). Such a relationship is useful for selecting the preferred design for the given condition using knee point concept.

CHAPTER 4

PERFORMANCE AND COST-BASED ROBUST DESIGN OPTIMIZATION PROCEDURE FOR TYPICAL FOUNDATIONS FOR WIND TURBINE[3]

4.1 Abstract

The cost and performance-based comparisons of three typical foundations (raft, pile group, and piled-raft) for a tall wind turbine on clayey and sandy soils are presented in this paper. The conventional geotechnical designs of the three foundations showed that the final design is controlled by differential settlement and hence it is considered as the response of concern in a robust design optimization procedure. The piled-raft foundation was found be the most economical based on the comparison of foundations based on conventional design procedure. The robust design optimization was carried out using Non-dominated Sorting Genetic Algorithm II (NSGA-II) coupled with Monte Carlo simulation to incorporate the unpredictable nature of geotechnical properties of soil and wind speed. The total construction cost of the foundation and standard deviation of differential settlement were considered as two objectives of interest to be minimized. This procedure resulted in a set of acceptable designs for all three foundation types resting on clayey and sandy soils which can be readily used to select the best design for a given performance requirement and cost limitation. Results indicated that the pile group or piled-raft foundation is economical for design with higher robustness while the raft foundation is economical for design with lower

[3] A similar version of this chapter is published in the *International Journal of Geotechnical Engineering*; Ravichandran, N. and Shrestha, S. (2018). "Performance-and-cost based robust design optimization procedure for typical foundations for wind turbine," 1-14.

robustness. The optimum designs of the foundations were determined using the knee point concept.

4.2 Introduction

Wind turbine is the source of environment friendly, renewable, and sustainable energy. Its popularity has increased over the past few decades due to its advantages over fossil fuel such as no greenhouse gas emission during operation and no consumption of fuel. The increasing energy demand of ever rising world population obliges the governmental and non-governmental agencies fulfilling the energy demand to focus in producing energy from a sustainable source such as wind. One of the cost-effective way to increase the wind energy production is by building taller towers. Since higher and steadier wind speed can be accessed at higher altitude, building taller tower can increase the energy production with a small additional cost because the wind power is directly proportional to the cubic power of wind speed. The bright side of building taller tower is that it increases the wind energy production per tower which will eventually increase the capacity of wind farm with same number of higher towers. On the contrary, the challenges tagged along with the taller tower such as design and selection of economical and safe foundation to sustain larger loads acting on the tower can't be avoided. The literature indicates that the suitable foundations to support a tall wind turbine tower are raft foundation, pile group foundation, and piled-raft foundation (Shrestha, 2015). Hence in this study, these three foundations are investigated for their cost and performance based on robustness.

The conventional geotechnical design of the foundation does not consider the geotechnical site variability and load variability. However, soil is very erratic and the

physical, mechanical, and engineering properties of the soil can change even within a short distance. Similarly, the loading on the wind turbine tower due to wind also exhibits seasonal as well as diurnal variations. In addition, for a big project extending to very large area, it may not be economical and feasible to conduct subsurface exploration at many locations which leads to imprecise site characterization. Similarly, human error during the work is also another source of uncertainty. The uncertainties due to spatial variability in geotechnical parameters, load variability, inadequate site characterization, and human error have a direct impact on the final foundation design. In conventional design approach, the factor of safety is used to incorporate the uncertainties in the system. As a result, the foundation designed according to conventional design principles will always be over designed or under designed, both of which are undesirable situations. Hence, a robust design concept is introduced in such situations where the uncertainties are involved. The design which is insensitive to the variations in uncertain parameters is called robust design. The objective of the robust design procedure is to incorporate uncertainties and increase the robustness, i.e. to minimize the variation design outcome while maintaining the cost at lowest possible value. In robust design procedure, it is challenging to select a suitable design because there can be substantial number of acceptable designs. Hence in such situations, a tradeoff relationship between the measure of robustness and the total cost of the foundation is developed enabling the easy selection of the best design for a given set of performance requirement and cost limitation.

In recent years, the reliability based robust design optimization has gained popularity in the field of geotechnical engineering. Juang and Wang (2013) performed the

reliability-based design optimization of shallow foundation using Non-dominated Sorting Genetic Algorithm (NSGA-II) considering undrained cohesion and effective friction angle as uncertain parameters for foundations on saturated clay and sand, respectively. They considered dimension of foundation as design variable. Recently, one of the authors of this paper and his colleagues developed the robust geotechnical design methodology for the design of drilled shaft in sand considering the uncertainties in drained friction angle and earth pressure coefficient at rest (Juang et al., 2013). They considered drained friction angle and earth pressure coefficient at rest as uncertain parameters and depth and diameter of drilled shaft as design parameters. The same authors of this paper and his colleagues have also worked in the development of seismic robust geotechnical design of cantilever retaining wall where they have considered soil properties and dynamic load parameter as the uncertain parameters and dimensions of retaining wall as design variables (Rahbari et al., 2017 and Rahbari et al., 2018, accepted for publication). Liu et al. (2012) performed optimization of pile foundation by using Automatic Grouping Genetic Algorithms (AGGA) with the constrains such as vertical bearing capacity of pile and maximum and differential settlements. In their study, the number of piles, length of piles, diameter of piles, and layout of piles were considered as the design variables and total cost as the objective to minimize. In another study by Chan et al. (2009), the optimization of pile groups in multi-layer soils was performed using Genetic algorithm (GA). Their objective was to minimize the material volume of the foundation subjected to several constraints including maximum differential settlement. The design variables considered included location, cross-sectional area and number of piles, and the thickness of the square pile cap.

Similarly, in the optimization of piled-raft foundation performed by Leung et al. (2010), the objectives were to maximize overall stiffness and minimize the differential settlement considering the length of piles as design variable. Although the above-mentioned researchers added valuable optimization techniques in the field of geotechnical engineering, some of them ignored the uncertainties in the loading. Therefore, a reliability based robust design optimizations of raft, pile group, and piled-raft foundations are presented in this paper considering the uncertainties in both soil properties and loading.

The objective of this study is to perform a reliability based robust geotechnical design optimization of typical foundations used to support the wind turbine tower and compare their cost and performance. The conventional geotechnical designs of these three foundations for a hybrid 130 m tall wind turbine tower on clayey and sandy soils are presented in this study followed by the robust design optimization. In the design optimization procedure, wind speed, undrained cohesion for clayey soil and friction angle for sandy soil were considered as uncertain parameters. The outcomes of the design optimization of all the foundations are presented in the form of Pareto fronts and are compared.

4.3 Conventional Geotechnical Design of Foundations

4.3.1 Design Loads and Soil Properties

4.3.1.1 Design Loads

The loads acting on the wind turbine foundation are vertical load due to the self-weight of the superstructure and horizontal load and bending moment due to the wind load acting on the tower body. These loads were calculated based on the tower dimension and

wind speed. The wind turbine tower considered in this study is a hybrid hollow cylindrical tower with the lower 93 m made of concrete and upper 37 m made of steel. Its diameter gradually varies from 12.0 m at the base to 4.0 m at the top. The total vertical load acting on the tower was calculated as the sum of concrete and steel part of tower and other components such as nacelle and rotor taken from Malhotra (2011). The final dead load of the tower was calculated to be 51.71 MN. The horizontal load due to wind acting on the tower body was calculated following the procedure described in ASCE 7-10 (2010) for a mean survival wind speed of 128.5 mph (category 4 hurricane). This is a very high wind speed and the wind turbine may occasionally experience it in the events such as hurricane and tornado. Still this wind speed was considered because the wind turbines are designed to withstand survival wind speed and the most wind turbines have survival wind speed of 112 mph to 145 mph (http://energy-alaska.wikidot.com/wind-power-technology-overview). The horizontal load was calculated as the sum of all the horizontal loads acting on the tower and the bending moment was calculated by multiplying the horizontal loads with the respective moment arms to the base of the tower. The total horizontal load and bending moment were calculated to be 2.39 MN and 153.11 MNm, respectively for the wind speed of 128.5 mph.

4.3.1.2 Soil Properties

Two sample sites composed of clayey and sandy soil were assumed in this study. The clayey soil was assumed to have a unit weight of 18 kN/m^3 and mean undrained cohesion of 80 kPa. The modulus of elasticity of clay calculated using widely used correlation (USACE, 1990; Duncan and Buchignani, 1976) between the undrained

cohesion and modulus of elasticity was 28 MPa. Similarly, the sandy soil was assumed to have the unit weight and mean friction angle of 17.2 kN/m^3 and 34°, respectively. The modulus of elasticity of sand was calculated to be 30 MPa (Wolff, 1989; Kulhawy and Mayne, 1990).

4.3.2 Geotechnical Design of Foundations

The geotechnical design of raft, pile group, and piled-raft foundations are presented in this section. The basic design approach involved checks for vertical capacity, lateral capacity, bending moment capacity, total and differential settlements (S_{tot} and S_{diff}), and rotation of the tower (θ). A minimum factor of safety (FS) of 2 was considered to be safe for vertical load, horizontal load, and bending moment capacity requirements. (Hemsley, 2000). A vertical misalignment within 3 mm/m of the tower was considered to be safe against the rotation of the tower (Grunberg and Gohlmann, 2013). It means for a 130 m tall tower, a horizontal displacement of 390 mm at the top of tower is considered to be safe and so is the corresponding rotation and differential settlement resulting from this horizontal displacement.

4.3.2.1 Design of Raft Foundation

The geotechnical design of raft foundation was performed by using the general bearing capacity equation (Meyerhof, 1963) given in Equation 4.1.

$$q_u = c' N_c F_{cs} F_{cd} F_{ci} + q N_q F_{qs} F_{qd} F_{qi} + \frac{1}{2} \gamma B N_\gamma F_{\gamma s} F_{\gamma d} F_{\gamma i} \quad (4.1)$$

where q_u is the ultimate bearing capacity, c' is cohesion, N_c, N_q, and N_γ are bearing capacity factors, F_{cs}, F_{qs}, and $F_{\gamma s}$ are the shape factors, F_{cd}, F_{qd}, and $F_{\gamma d}$, are the depth

factors, F_{ci}, F_{qi}, and $F_{\gamma i}$, are the load inclination factors, q is the effective stress at the bottom of foundation, γ is the unit weight of the soil, and B is the width or diameter of the foundation. The nacelle at the top of wind turbine tower can rotate according to the wind direction which changes the eccentricity direction. Therefore, to begin the design, first the shape of the raft was fixed to be circular so that the capacity will be equal along all directions. Then a trial dimension of raft was assumed and tested for factor of safety, eccentricity, total and differential settlements, and rotation requirements. The factor of safety against bearing capacity failure (FS_{bc}) was calculated as the ratio of ultimate bearing capacity to the maximum soil pressure under the foundation. The total elastic settlement was calculated using Janbu et al. (1956) for the foundation in clayey soil and Bowle's (1987) method in sandy soil. The differential settlement of the raft was calculated based on the rotation (θ) of the foundation due to wind load. The rotation was calculated using Equation 4.2 given by Grunberg and Gohlmann (2013).

$$\theta = \frac{M_{found}}{c_s I_{found}};\ c_s = \frac{E_s}{f' \sqrt{A_{found}}} \tag{4.2}$$

where M_{found} is the bending moment at soil-structure interface, c_s is the foundation modulus, I_{found} is the second moment of inertia of the foundation, E_s is the modulus of elasticity of soil, f' is the shape factor for overturning (0.25), and A_{found} is the area of the foundation. After calculating θ, the differential settlement of the raft was calculated using a simple trigonometric relationship and assumed dimension.

The final design results of the raft foundation in clayey and sandy soils after several trials are presented in Table 4.1 and the sketch is shown in Figure 4.1. For both soil, the

thickness of raft is 1.5 m located at the depth of 2.0 m. The design results presented in Table 4.1 show that all the design requirements are fulfilled. Although total settlement is higher than differential settlement for raft in clayey soil, it is assumed to be acceptable because for a tall structure, the differential settlement is more critical than total settlement because it can add additional bending moment at the foundation.

Table 4.1. Design results of raft foundation

Soil	R_r (m)	FS_{bc}	S_{tot} (mm)	S_{diff} (mm)	ΔH (mm)
Clay	12.0	2.12	65.32	42.85	232.09
Sand	11.5	8.63	38.97	43.54	246.12

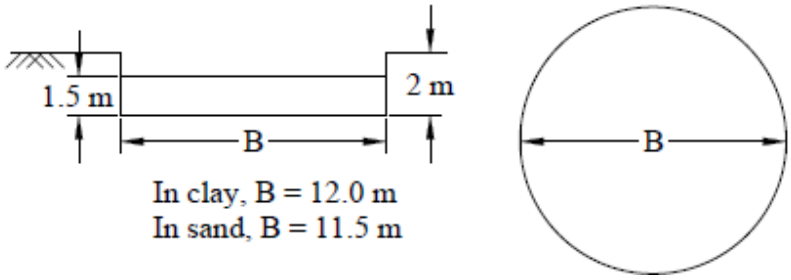

Figure 4.1. Final design of raft foundation

4.3.2.2 Design of Pile Group Foundation

Pile group foundation was designed following a simplified procedure available in literature in which the pile group capacity was checked for the combined vertical load due to self-weight and bending moment. To reduce the complexity of design, the type and size of pile were fixed to be a closed-ended pipe pile with outside diameter of 0.406 m (16″) and thickness 0.013 m (0.5″). The design steps involved adjustment of length (L_p), number (N_p), and configuration of piles until the design requirements are met. First, a trail number, length, and configuration of piles were assumed. Then a single pile capacity on clayey and sandy soils was calculated as a sum of ultimate skin and toe resistances. The skin resistance

was calculated using α method and friction theory for the pile group foundation in clayey and sandy soils, respectively and the toe resistance was calculated using Meyerhof's method for both soil conditions (Das, 2016). The resultant vertical load acting on each pile was calculated as a sum of self-weight on each pile (total vertical load/number of piles) and vertical load contribution from bending moment using Equation 4.3 given by Roa (2011).

$$P_i = \frac{P}{N_p} \pm \frac{M\ x_i A_i}{I} \tag{4.3}$$

where P_i is the axial load on the i^{th} pile, P is the total vertical load, N_p is the number of piles in the group, M is the bending moment, A_i is the area of cross-section of the i^{th} pile, x_i is the horizontal distance of i^{th} pile with respect to the center of gravity of the pile group, and I is the moment of inertia of the pile group. The resultant vertical load was checked with ultimate downward or upward pile capacity ensuring a factor of safety of at least 1 for each pile. The ultimate vertical capacity of pile group foundation was determined as the lesser of: *(i)* the sum of ultimate downward capacities of each individual pile and *(ii)* the ultimate downward capacity of a block containing all the piles. The factor of safety for the vertical load (FS_P) was calculated as the ratio of ultimate vertical capacity of pile group and total vertical load. It should be noted that the pile center to center spacing was kept at least three times the pile diameter to reduce the effect of overlapping stress zones on the capacity. Then the lateral capacity of pile group foundation was determined using Brom's method outlined in Gudmundsdottir (1981) for clayey and sandy soils. In this method, the horizontal coefficient of subgrade reaction was used to calculate the lateral displacement

(y_H) and the lateral pile capacity which was used to calculate the factor of safety against lateral load (FS_H). After that, the settlement profile of the piles in the group due to resultant vertical load calculated using Equation 4.3 was calculated using the procedure given by Fellenius (1999). When the bending moment acts on the pile group foundation, piles located towards the direction of moment will be in compression and the piles on the other side will be in tension. This will result in differential settlement of the foundation which was calculated as the difference between the maximum settlement and the minimum settlement of the piles at the extreme opposite ends. This process was repeated until the design requirements were met. The final design results are presented in Table 4.2 and the sketch of pile group foundation in clayey soil is shown in Figure 4.2. The pile group foundation in sandy soil will also have similar sketch but with different number and length of piles. For pile group in both soils, the radius of pile cap was considered to be 7.5 m with the thickness of 1.0 m located at the depth of 1.5 m below the ground surface. The radius of pile cap was deemed to be 7.5 m based on the radius of base of the tower which is 6.0 m. The total piles were distributed along the two circumferences of radius 6.7 m and 5.3 m. Table 4.2 shows that all the design requirements are fulfilled for pile group foundations on both soils.

Table 4.2. Design results of pile group foundation

Soil	L_p (m)	N_p along radius of		FS_P	FS_H	S_{diff} (mm)	ΔH (mm)	y_H (mm)
		6.7 m	5.3 m					
Clay	33.3	32	26	2.12	13.55	39.19	339.60	5.39
Sand	45.5	34	28	8.63	8.87	43.24	374.75	10.99

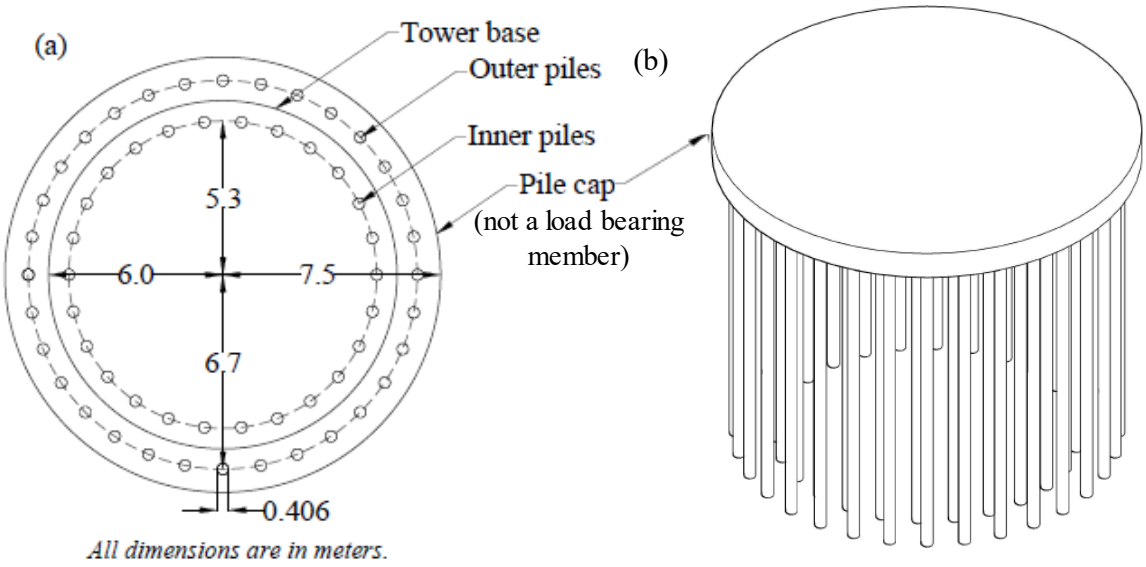

Figure 4.2. Final design of pile group foundation in clay (a) Plan view and (b) 3D view (length of pile is not to scale)

4.3.2.3 Design of Piled-raft Foundation

The advantage of hybrid foundation such as piled-raft for supporting larger load is that it utilizes the bearing resistance from raft and piles to maximize the bearing capacity and to minimize total and differential settlements, respectively. However, it is challenging to quantify the contributions from each component towards the resistance due to the complex interaction among soil, raft, and soil. Hence, the design of piled-raft foundation is mostly conducted using the computer-based methods such as finite element and finite difference method. As a result, a reliable design guideline to design a piled-raft foundation is not yet available, especially when it is subjected to the vertical load, horizontal load, and bending moment.

In this study, a preliminary geotechnical design of the piled-raft foundation was conducted by following the procedure outlines by Hemsley (2000), in which the design procedure proposed by Poulos and Davis (1980) and Randolph (1994) are incorporated.

Similar to raft and pile group foundation, a circular raft and a closed-ended pipe pile with outside diameter of 0.406 m (16″) and thickness of 0.013 m (0.5″) were first fixed. Then a trial dimensions such as radius of raft, length of pile, and the number of piles were assumed and adjusted until all the design requirements were met. An elaborated description of the procedure of designing piled-raft foundation adopted in this study can be found in Shrestha et al. (2017). Here the procedure is described briefly.

First a trial dimensions of piled-raft foundation were assumed. The ultimate bearing capacity of the raft and piles were calculated similar to that described for first two foundations in previous design sections. The vertical load capacity of the piled-raft foundation was determined as the lesser of: (i) the sum of ultimate capacities of raft and all the piles and (ii) the ultimate capacity of a block containing soil, all the piles, and raft portion lying outside the pile group circumference. Then factor of safety of piled-raft foundation for vertical load (FS_P) was calculated as the ratio of ultimate vertical load capacity of piled-raft foundation and design vertical load. Then the foundation was checked for the moment capacity. The bending moment capacity of the piled-raft foundation was calculated following a similar procedure used for calculating the vertical load capacity, i.e. the lesser of: *(i)* the sum of ultimate moment capacity of raft ($M_{u\text{-}R}$) and all the individual piles in the group ($M_{u\text{-}P}$), i.e. $M_{u\text{-}PR} = M_{u\text{-}R} + M_{u\text{-}P}$ and *(ii)* the ultimate moment capacity of a block ($M_{u\text{-}B}$). The ultimate moment capacity of the raft, $M_{u\text{-}R}$ was calculated using Equation 4.4 (Hemsley, 2000).

$$\frac{M_{u-R}}{M_m} = \frac{27}{4}\frac{P}{P_u}\left[1-\left(\frac{P}{P_u}\right)^{1/2}\right] \tag{4.4}$$

where M_m is the maximum possible moment that soil can support, P is the applied vertical load, P_u is the ultimate centric load on the raft when no moment is applied. The ultimate moment capacity of all the piles were calculated as the sum of product of ultimate uplift capacity of each pile and its respective distance from the center. The ultimate moment capacity of the block, $M_{u\text{-}B}$ was calculated using Equation 4.5 given below (Hemsley, 2000).

$$M_{u-B} = \alpha_B \overline{p}_u B_B D_B^2 \tag{4.5}$$

where B_B and D_B are the width and depth of the block, respectively, $\overline{p}_u$ is the average lateral resistance of soil along the block, and α_B is the factor depending upon the distribution of ultimate lateral pressure with depth (0.25 for constant distribution of $\overline{p}_u$ and 0.2 for linearly increasing $\overline{p}_u$ with depth from zero at the surface). Finally, the factor of safety for moment (FS_M) was calculated as the ratio of ultimate moment capacity of piled-raft foundation and the applied bending moment. Then the horizontal load capacity was determined using the method discussed in the design of pile group foundation, i.e. Broms' method. After this, the piled-raft foundation was tested for the serviceability requirements, i.e. total and differential settlements. The vertical load-settlement behavior of the piled-raft was estimated by the approach proposed by Poulos (2001b) along with the method used for estimating the load sharing between the raft and the piles presented in Randolph (1994) using the stiffness of the piles, raft, and piled-raft block. The stiffness of the piled-raft, K_{pr} is estimated using Equation 4.6 proposed by Randolph (1994):

$$K_{pr} = X K_p; \qquad X = \frac{1 + \left(1 - 2\alpha_{rp}\right) K_r / K_p}{1 - \alpha_{rp}^2 \left(K_r / K_p\right)} \tag{4.6}$$

where K_r is the stiffness of raft, K_p is the stiffness of the pile group, and α_{rp} is the pile-raft interaction factor. The pile-raft interaction factor is assumed to be 0.8 considering the fact that as the number of piles increases the value of α_{rp} increases and it reaches the maximum value of 0.8 as reported by Randolph (1994). Then the load-settlement curve (P vs. S) for the piled-raft foundation was developed using Equation 4.7.

$$\left.\begin{array}{l} \text{For } P \le P_A;\ S = \dfrac{P}{K_{pr}} \\ \text{For } P > P_A;\ S = \dfrac{P_A}{K_{pr}} + \dfrac{P - P_A}{K_r} \end{array}\right\} \tag{4.7}$$

where P_A is the load at which pile capacity is fully mobilized and only raft is contributing for resistance. The resultant vertical load - settlement curve for the raft foundation on clay and sand are shown in Figure 4.3. The total settlement for the given design vertical load, P can be determined from Figure 4.3. It can be seen in Figure 4.3 that the load-settlement curve for piled-raft in both soils is overlapping up to P_A and beyond that the curve for piled-raft foundation in sand is steeper than in clay. It should be noted that for piled-raft foundation in both clayey and sandy soils, the design vertical load, P is smaller than P_A, i.e. both raft and piles are functioning to carry the load.

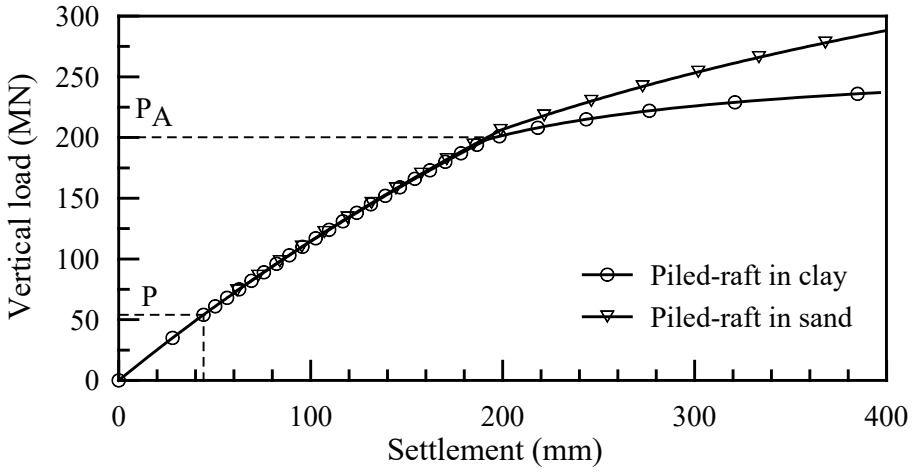

Figure 4.3. Load-settlement curves for piled-raft foundation in clayey soil sandy soil

The piled-raft foundation was then checked for the differential settlement requirement. The calculation of differential settlement of the combined piled-raft foundation system due to the bending moment is a challenging task because it is difficult to quantify the amount of load carried by raft and piles. This paper proposes a new method to calculate the differential settlement of the piled-raft foundation. In this method, the total applied bending moment is divided between the raft and the piles such that the differential settlements of the individual components are equal, which is considered as the differential settlement of the piled-raft foundation. The assumption made here is that the pile head is connected rigidly to the raft and both components will rotate by an equal amount when the foundation is subjected to bending moment. The estimation of percentage of moment shared by raft and piles to induce equal amount of differential settlement is an iterative procedure in this study. The differential settlement of the raft was calculated using Equation 4.2 and the differential settlement profile of the piles in the group was estimated following the procedure described earlier for pile group foundation, i.e. as a difference

between the settlement due to maximum and minimum load. The final design results of piled-raft foundation on clayey and sandy soils meeting all design requirements are given in Table 4.3 and the sketch is shown in Figure 4.4. For both soils, the plan view of the piled-raft foundation will be same because there are same number of piles but the length is different. In both soils, the thickness of raft is 1.0 m and it is placed at the depth of 1.5 m from the ground surface. The total piles are divided equally and arranged along two circumferences of radius 6.7 m and 5.3 m.

Table 4.3. Design results of piled-raft foundation

Soil	R_r (m)	L_p (m)	N_p	FS_P	FS_M	FS_H	S_{tot} (mm)	S_{diff} (mm)	ΔH (mm)	y_H (mm)
Clay	7.5	29	52	3.31	3.20	10.06	42.20	40.63	352.08	5.42
Sand	7.5	41	52	7.94	3.90	7.11	42.14	41.06	355.86	9.47

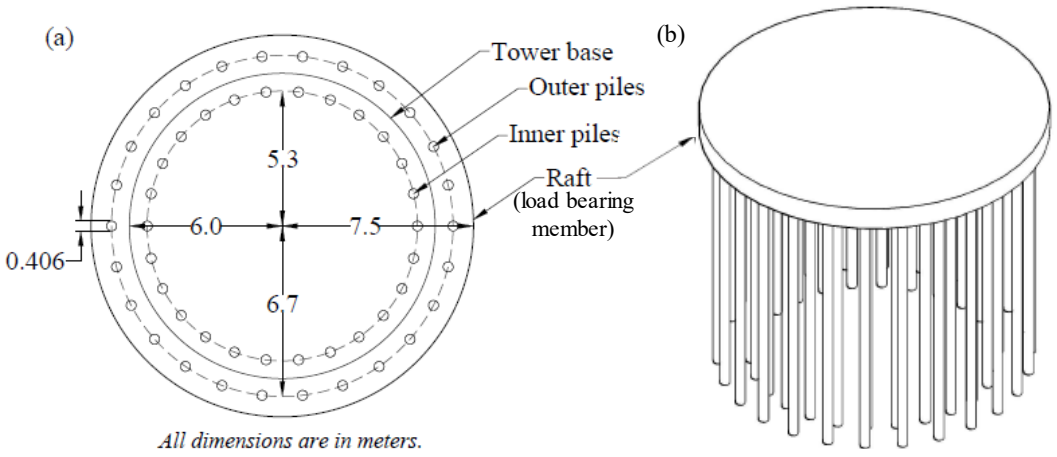

Figure 4.4. Final design of piled-raft foundation (a) Plan view and (b) 3D view (length of pile is not to scale)

4.3.3 Comparison of foundations based on conventional design

The conventional geotechnical design of foundation focusses on meeting all the safety criteria with the minimum material consumption. The foundations designed based on the conventional design concept can be compared based on the volume of material

required and their respective costs. In this study, the total cost of foundation was calculated using the unit price of the foundation components obtained from RSMeans (2013). The unit prices of raft, closed-end pipe pile, and pile cap obtained from RSMeans (2013) are \$342.13/m^3, \$265.95/m, \$250.97/m^3, respectively. It should be noted that these unit prices include estimated costs for material, labor, and equipment, but exclude overhead and profit. The comparison of volume and cost of three foundations are presented in Table 4.4.

Table 4.4. Comparison of foundations based on conventional design

Soil	Raft		Pile group			Piled-raft		
	Vol. (m^3)	Total cost (\$)	Vol. of cap (m^3)	Vol. of pile (m^3)	Total cost (\$)	Vol. of raft (m^3)	Vol. of pile (m^3)	Total cost (\$)
Clay	678.58	232,163	176.71	31.00	558,005	176.71	24.20	461,510
Sand	623.21	213,219	176.71	45.28	794,594	176.71	34.22	627,463

The comparison of total cost of foundation based on conventional geotechnical design showed that the piled-raft foundation is the most economical foundation for the loading and soil conditions considered in this study followed by pile group and raft foundation for both clayey and sandy soils. Nevertheless, this result may or may not be always true because the effect of variation in soil properties and loading conditions which is the real scenario, are not incorporated in the conventional design methodology. Therefore, it is necessary to conduct the reliability based robust design optimization to address the effect of variation in soil properties and loading on the final design. The next section of this paper focusses on the robust design optimization of the raft, pile group, and piled raft foundation.

4.4 Robust Design Optimization of Foundations

4.4.1 Background - Need of Reliability Based Design

The basic concept behind designing most of the engineering systems is to achieve two goals: *(i)* maximizing safety and *(ii)* minimizing cost, i.e. to determine the optimum design. In the conventional foundation design, several trial and error procedures are conducted to determine the final dimensions which give minimum cost and provides required strength. However, the parameters on which the strength of the foundation depend and affect its performance such as soil properties and dynamic loads are uncertain, i.e. they can have spatial and seasonal variations. The parameters which vary naturally or which are liable to change during the life of the system and can change the performance of the system are called the uncertain parameters. In traditional deterministic design of foundation, these uncertainties are accounted in terms of factor of safety. Nevertheless, the use of empirical factor of safety in the design of foundation doesn't guarantee that the system will perform satisfactorily for different loading and soil conditions. In addition, it doesn't provide any information on how different uncertain parameter affect the factor of safety. Hence these days, engineers are focusing on reliability based robust design procedure to achieve the fundamental goals of design i.e. minimum cost and safety.

In engineering, a design is considered to be robust when the effect of variations in the response is minimized, i.e. the design which is insensitive to the variations of uncertain parameters which are difficult (or impractical) to control is called robust design. The concept of robust design can be explained with the help of Figure 4.5. Let us consider that the gradient of curve *OP* represents the variation in design/uncertain parameters. In the

robust design procedure, even when the variations in uncertain parameters are considered, the response may vary largely due to large variation in uncertain parameters or not strategically defined design variables limits. In Figure 4.5, the portion *ab* of the curve has higher variation (higher gradient) in the uncertain parameters or the design variables, thus resulting in large variation in the response which doesn't satisfy the requirement of robust design. The variation in the response can be minimized by either reducing the variation in the uncertain parameters or by adjusting the limits of the design variables. In Figure 4.5, the portion *cd* of the curve has lower variation (lower gradient) in the uncertain parameters or the design variables, thus resulting in small variation in the response and hence it is called the robust design.

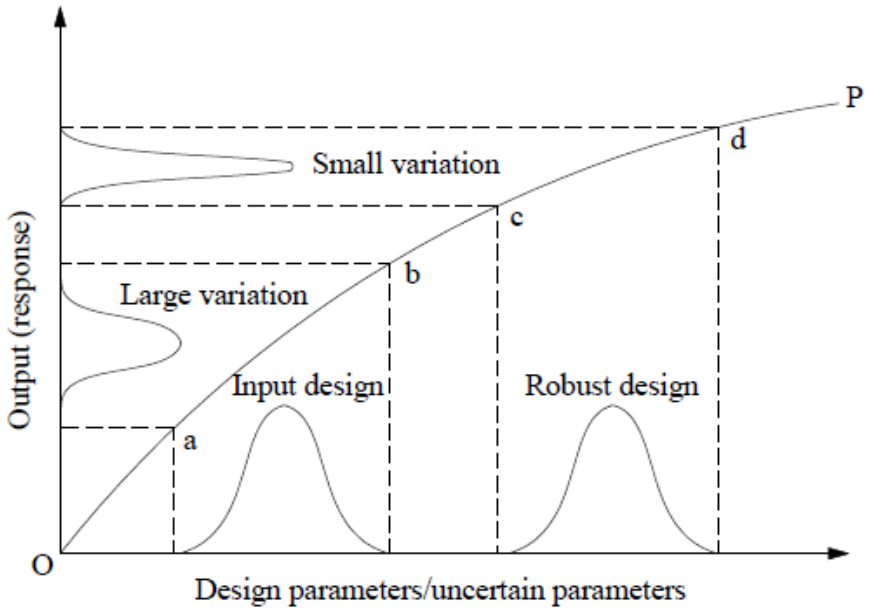

Figure 4.5. Robustness concept

In this study, multi-objective robust design optimization of three foundations under study was performed using Non-dominated Sorting Genetic Algorithm - II (NSGA - II)

developed by Deb et al. (2002) coupled with Monte Carlo (MC) simulation. The variation in the response was minimized by adjusting the limits of design variables. Steps in robust design optimization are shown in Figure 4.6 using a flowchart. Each step in the flowchart are discussed in detail in the relevant sections.

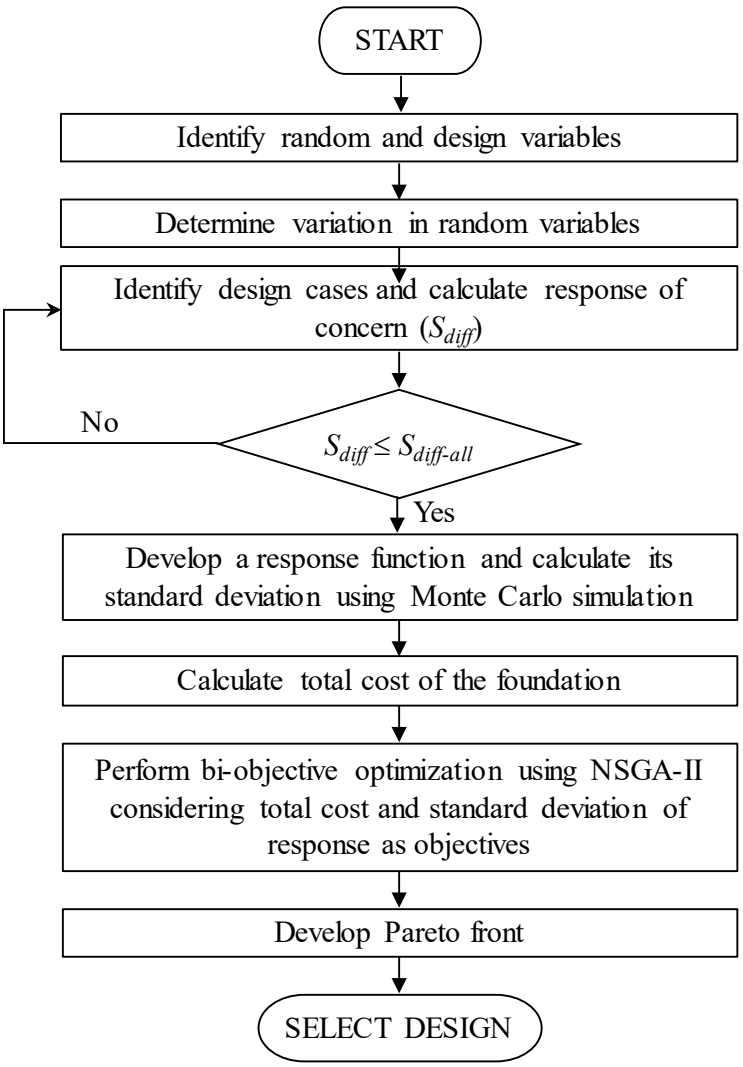

Figure 4.6. Framework of robust geotechnical design optimization

4.4.2 Identification of Uncertain Parameters and their Distribution

The first step in the probabilistic design approach is to identify all the uncertainties that have impact on the design of geotechnical system such as shallow foundation, deep foundation, retaining wall, tunnel, etc. and gather required statistical information about them. In the design of geotechnical system, the uncertainties may arise due to natural phenomena such as varying soil profile, inadequate subsurface exploration, human error during subsurface exploration, different applied loads such as wind load, rainfall, snow fall, etc. These uncertainties can directly impact the performance of the system. In this study, two major parameters were identified to have maximum impact on the foundation performance, they are soil properties and wind speed. For clayey soil, wind speed (V) and undrained cohesion (c_u) were considered as uncertain parameters and for sandy soil V and effective friction angle (ϕ') were considered as uncertain parameters. The uncertain parameters are also referred as random variables because they can have different outcomes. In the probabilistic design approach, various outcomes of random variables or different possible variables of the random variables have certain probability of occurrence which depends on the type of distribution. Hence it is important to accurately represent the random variable using appropriate probability distribution which is modeled in terms of mean and standard deviation.

In this study, the undrained cohesion of clayey soil was estimated to have low site variability. Hence the coefficient of variation (COV) of undrained cohesion for low site variability was assumed to be 20% (Phoon, 2008). Using the mean c_u value of 80 kPa and COV of 20%, the standard deviation was determined to be 20 kPa. For this study, all the

random variables were varied between ± 2 standard deviations from their mean value in the design optimization process because it will represent wide range values that affect the optimum design. Hence undrained cohesion was varied between 40 kPa and 120 kPa considering normal probability distribution. Similarly, the variation in friction angle (ϕ) in sandy soil was estimated by considering 10% *COV*, which is a suitable value for friction angle variability (Phoon, 2008). With the mean friction angle of 34° and *COV* of 10 %, the standard deviation was calculated to be 3.4°. This resulted in the variation of friction angle between 27.2° and 40.8°, i.e. ± 2 standard deviations considering normal probability distribution. Finally, the wind speed (V) was varied between the range of survival wind speed, i.e. between 112 mph and 145 mph (± 2 standard deviations) with the mean value of 128.5 mph and standard deviation of 8.25 mph considering normal probability distribution. It is well known fact that in normal distribution, the value can range from negative infinity to positive infinity because of which it is better to represent the soil properties and wind speed using lognormal distribution which only has positive value. Still, the normal probability distribution was used in this study because the minimum values of random variables are positive and the range of random variables were clearly defined during the computer simulation (details of computer simulation is discussed later).

4.4.3 Identification of Design Variables and their Range

The variables that influence the objectives of design such as minimum cost and safety requirement are referred as design variables. During the design optimization procedure, these variables are allowed to change for different loading and soil conditions to obtain the number of safe designs, out of which the optimum design is selected. In this

study, the design variables that have the maximum impact on the objectives of the optimization were carefully selected for the three foundations on both soils (clayey and sandy soils) under study. The design variable for the raft foundation was considered to be the radius of raft (R_r) while the depth and the thickness of the raft were kept constant. For the pile group foundation, length of pile (L_p) was considered to be the design variable keeping the size (0.406 m outside diameter), number of piles (52 in clay and sand), and radius of pile cap (7.5 m) constant. Similarly, for the piled-raft foundation, the length of pile (L_p) and radius of raft (R_r) were considered to be the design variables keeping the number (52 in clay and sand) and size of piles (0.406 m outside diameter), thickness (1 m) and, depth of raft (1.5 m) constant.

In the optimization process, it is important to shrewdly define the design space or possible design options or in other words, the upper and lower limits of all the design variables. While defining the bounds of the design variables, one should be cautious not to pick the value that can waste the simulation time of computing the solutions which are not significant. In this study, the design variables are set in such a way that they satisfy the safety requirements for various combination of random variables (worst, medium, and best-case scenarios). The upper and lower bounds of design variables for all three foundations on clayey and sandy soils are listed in Table 4.5.

Table 4.5. Upper and lower bounds of design variables for foundations on clay and sand

Soil	Raft	Pile group	Piled-raft	
	R_r (m)	L_p (m)	L_p (m)	R_r (m)
Clay	17 - 30	45 - 80	30 - 50	7.5 – 12.0
Sand	23 - 33	67 – 92	55 - 75	7.5 – 12.0

4.4.4 Response function development

The design outcome that can explicitly measure the performance of the system is called the response of concern. For a tall structure, the tilting of the super structure is very critical which induce differential settlement of the foundation. The tilting can induce additional bending moment at the foundation which can eventually cause failure of the foundation if exceeded beyond the limit. This statement is supported by the results of conventional geotechnical design of all three foundations presented in the previous section of this paper which indicated that the final design is controlled by the differential settlement. For this reason, differential settlement was selected as suitable response of concern for all three foundations in the optimization procedure. The response or the differential settlement is the function of random variables and design variables because of which it will also be a random variable. The exact relation of the response with the random and design variables may not be known in all cases. Hence, the response surface methodology was adopted in this study to establish a functional relationship among response, random variables, and design variable using a known mathematical model. For this purpose, several design sets were selected for each foundation and corresponding differential settlements were calculated. Here, the design set means one set of random and design variables within the limit discussed in the previous parts of this paper. The selected design sets include the best case (highest c_u/ϕ, lowest - V, and highest design variables), worst case (lowest c_u/ϕ, highest - V, and lowest design variables), and medium case (medium c_u/ϕ, medium - V, and medium design variable). Then, a non-linear regression analysis was conducted on differential settlement analysis results for each foundation in

both soils to establish a nonlinear response function or differential settlement relationship with random and design variables. While conducting the regression analysis, it was found that the pile group foundation in clay didn't result in reliable response function while using same number of design sets as pile group foundation in sand. Hence, additional design sets were selected to increase the number of data points for regression analysis in order the improve the quality of the response function. This exercise resulted in better response function for pile group foundation in clay. The response functions (differential settlement functions) for raft, pile group, and piled-raft foundations in clayey soil are given in Equation 4.8, 4.9, and 4.10, respectively which has the corresponding coefficient of determination (or R^2) values of 0.93, 0.88, and 0.99. Similarly, the differential settlement functions for raft, pile group, and piled-raft foundations in sandy soil are given in Equation 4.11, 4.12, and 4.13, respectively which has the corresponding coefficient of determination (or R^2) values of 0.92, 0.91, and 0.98. High R^2 value (close to 1) indicate that the function fitted the data reasonably well.

Foundation in clayey soil:

Raft: $$S_{diff} = \exp\left(5.47 + 1.48\ln(V) - 1.05\ln(c_u) - 1.78\ln(R_r)\right) \quad (4.8)$$

Pile group: $$S_{diff} = \exp\left(-0.14 + 4.42\ln(V) - 1.88\ln(c_u) - 2.95\ln(L_p)\right) \quad (4.9)$$

Piled-raft: $$S_{diff} = \exp\left(10.16 + 5.84\ln(V) - 3.73\ln(c_u) - 4.47\ln(L_p) - 1.80\ln(R_R)\right) \quad (4.10)$$

Foundation in sandy soil:

Raft: $$S_{diff} = \exp\left(26.64 + 0.85\ln(V) - 6.42\ln(\phi) - 1.83\ln(R_r)\right) \quad (4.11)$$

Pile group: $$S_{diff} = \exp\left(22.41 + 6.64\ln(V) - 5.55\ln(\phi) - 7.60\ln(L_p)\right) \quad (4.12)$$

Piled-raft: $$S_{diff} = \exp\left(28.16 + 4.36\ln(V) - 7.11\ln(\phi) - 4.62\ln(L_p) - 1.27\ln(R_R)\right) \quad (4.13)$$

The response functions of pile group and piled-raft foundations were also plotted in a 2D plot to study the effect of different variables on the response and to inspect if they are providing reasonable results. The response, i.e. differential settlement was plotted against wind speed, soil parameter, and length of pile as shown in Figures 4.7, 4.8, and 4.9, respectively for both soils. For the variation of differential settlement with the wind speed, the length of pile and the soil parameter were kept constant. Similarly, for the variation of differential settlement with soil parameter, the wind speed and length of pile were kept constant and for variation of differential settlement with length of pile, the wind speed and soil parameter were kept constant. The radius of raft in the piled-raft foundation was fixed at 7.5 m in these plots. All the variables were varied within their range as discussed in the previous sections. The plots presented in Figures 4.7, 4.8, and 4.9 showed that the differential settlement for the pile group foundation is higher than the piled-raft for identical loading and soil conditions for foundations in both clay and sand. The reduction in the differential settlement of the piled-raft foundation is due to the contribution of the raft to resist some percentage of the bending moment.

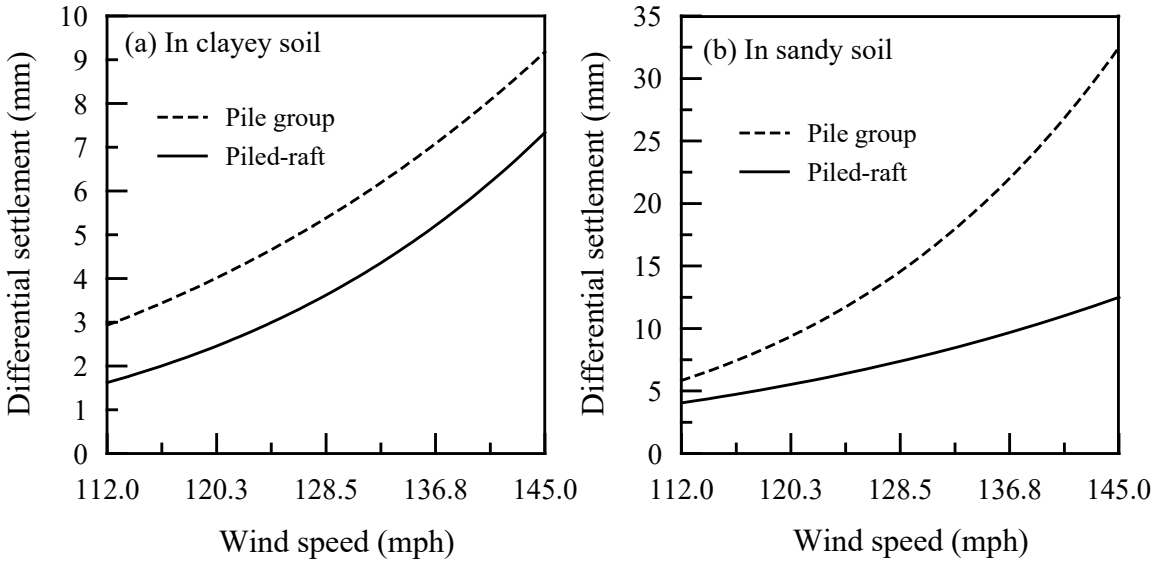

Figure 4.7. Differential settlement vs. wind speed for pile group and piled-raft foundations in (a) clay and (b) in sand.

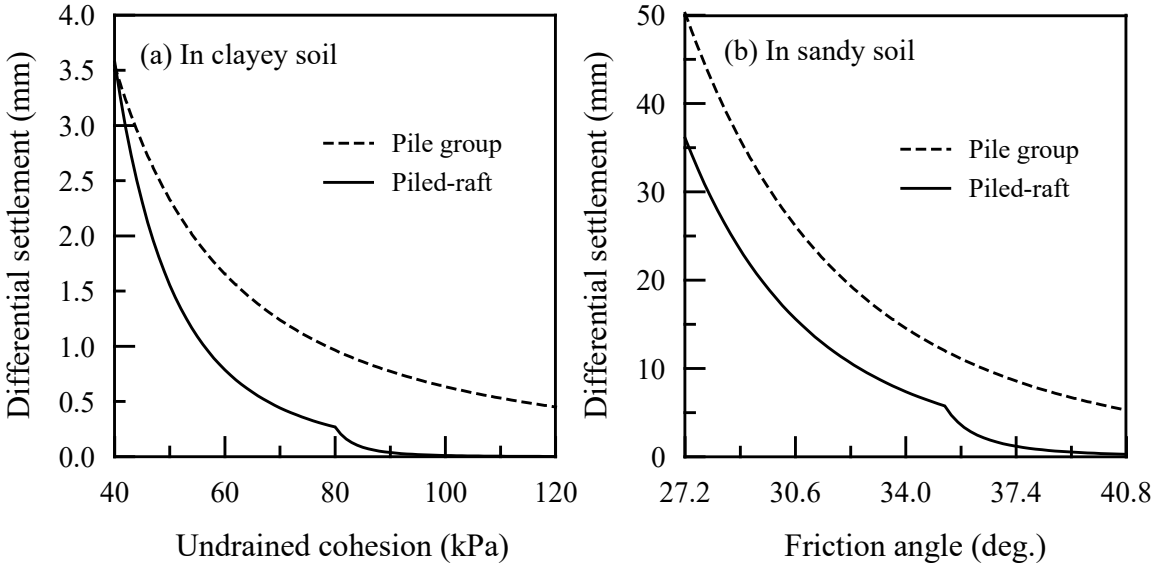

Figure 4.8. Differential settlement vs. undrained and friction angle for pile group and piled-raft in (a) clay and (b) in sand, respectively

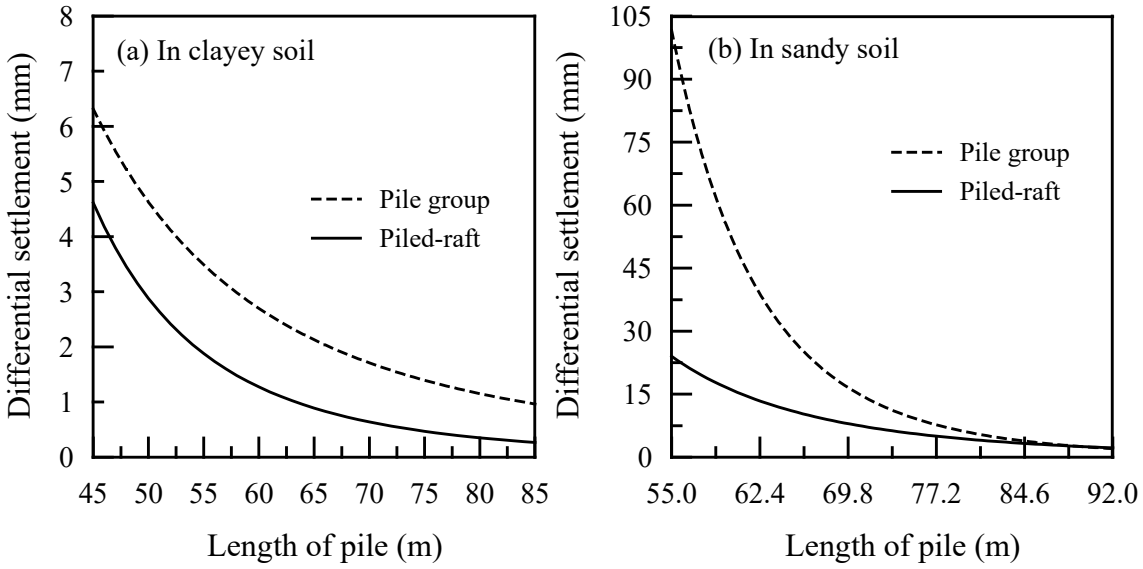

Figure 4.9. Differential settlement vs. length of pile for pile group and piled-raft in (a) clay and (b) in sand

It can be seen in Figure 4.8(a) that both pile group and piled-raft foundations have the same differential settlement for undrained cohesion of 40 kPa. The reason behind this could be due to use of mathematical model or the differential settlement functions to generate these plots. The mathematical models for differential settlement were established based on number of data. The accuracy level is sensitive to the number of data used to produce the model. As discussed earlier, the issue related to pile group foundation in clayey soil to establish reliable response function led the authors to use the higher number of data compared to others. The differential settlement functions for the pile group foundation and the piled-raft foundation on clay have different R^2 values which means that they have different level of accuracy. Hence the plots generated using these equations may have some discrepancies like one seen in Figure 4.8(a), where the differential settlement of the piled-raft foundation should have always been lower than that of pile group foundation for identical soil and loading conditions.

4.4.5 Multi-objective Optimization using NSGA-II Algorithm Coupled with Monte Carlo Simulation

The objective of the robust design optimization is to determine a set of non-dominated designs which are cost efficient, robust, and meet all safety requirements and select the optimum design. The optimum design can be obtained through multi-objective optimization where the cost is minimized and the robustness in maximized while meeting the safety constraints. In this study, the multi-objective optimization was conducted by using the genetic algorithm NSGA-II (Deb et al., 2002) procedure in MATLAB. The concept of NSGA-II procedure is shown in Figure 4.10. In this technique, first the parent population (P_o) or the first trial designs of size N is selected and the genetic algorithm operations such as mutations and crossover are performed on the P_o to generate offspring population (Q_o) of same size. Then parent population is refined using an iterative procedure (also referred as generation) to generate parent and offspring population at t^{th} generation, i.e. P_t and Q_t, respectively. They are then combined to form a combined population R_t of size $2N$ which is sorted according to nondomination (F_1, F_2, …, F_{2N}) or according to the hierarchy. The best N elements of the sorted population are then selected as parent population for the next generation (P_{t+1}). This process is repeated until the parent population is converged and the parent population at final generation is used to generate the Pareto front. Pareto front is the collection of non-dominated designs in which each design is safe. In this study, the size of population (N) was considered to be 100 and the number of generations were considered to be 200 for all three foundations in both soils.

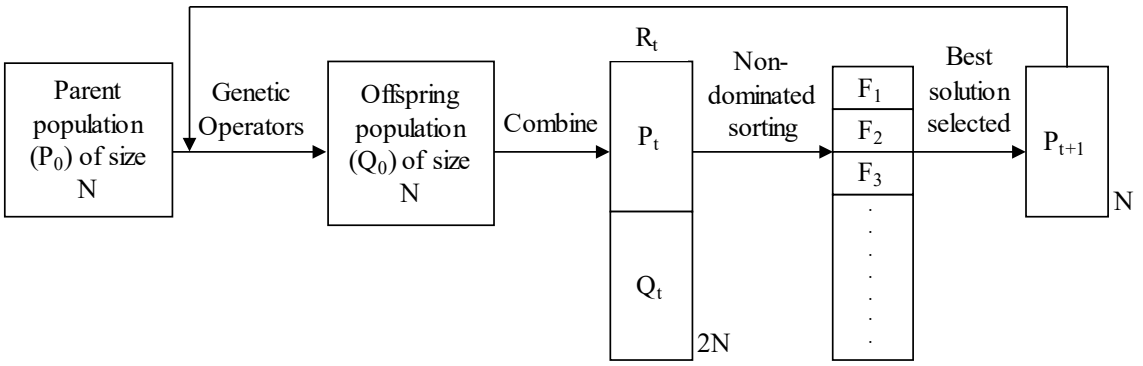

Figure 4.10. NSGA-II Procedure (modified after Deb et al. 2002)

The multi-objective optimization was conducted considering the total cost and standard deviation of differential settlement (response) as two objectives which are the measure of the cost efficiency and robustness, respectively. The first objective, i.e. the total cost of foundation was calculated using the unit price of the foundation components obtained from RSMeans (2013). The unit prices of raft, closed-end pipe pile, and pile cap obtained from RSMeans (2013) are \$342.13/m3, \$265.95/m, \$250.97/m^3 respectively as mentioned before in this paper. The second objective, i.e. the standard deviation of differential settlement was calculated by coupling the NSGA-II algorithm with Monte Carlo (MC) simulation. The MC simulation technique can not only be used to calculate the standard deviation of differential settlement but also the reliability of foundation. In MC simulation, each random variable is selected randomly according to its probability distribution function and repeated for number of cycles to compute the desired results. The basic steps of MC simulation technique as noted in Haldar and Mahadevan (2000) are as follows:

- Defining response in terms of random variables.

- Determining probabilistic characteristics of random variables in terms of probability distribution function and its statistical properties.
- Generating random variables.
- Computing desired results for each simulation cycle.
- Extracting the probabilistic information of the response from desired number of cycles.
- Determining the accuracy and efficiency of the simulation.

The first two steps, i.e. defining all random variables and their probability distribution functions are already discussed in the previous section of this paper. Then the random variables are generated according to the probability distribution function used for each random variable. Then the numerical experiment is conducted for *M* number of each random each variable which will give *M* number of responses for each set of input variables. Here, the input variables are referred to the design variables and response is referred to differential settlement. These *M* responses are used to estimate the probabilistic information of the response such as statistical properties, probability distribution function, probability of failure, reliability index, etc. In this study, we are interested in calculating the standard deviation of differential settlement and reliability index of the foundation. The standard deviation of differential settlement is used as the second objective in the multi-objective optimization procedure and the reliability index is used as measure of reliability of the foundation. The accuracy of the numerical experiment increases when the value of *M* goes to infinity which is not possible practically. For this study, 10,000 simulation cycles were performed to compute the required output which is the standard number in MC

simulation and considered to be adequate. The safety constraints of allowable differential settlement ($S_{diff,,all}$ = 45 mm) and target reliability (β_t = 3), as the latter has been recommended by Kulhawy and Phoon (1996), to ensure the reliability of the foundation system were also incorporated in the MC simulation. The reliability index of the system was computed using performance function of the system (g) defined as below:

$$g\left(\theta, X\right) = S_{diff,all} - S_{diff}\left(\theta, X\right) \tag{4.14}$$

where θ and X indicate random variables and design variables, respectively. The reliability index (β) can be computed as the ratio of mean value (μ_g) and standard deviation (σ_g) of performance function g, as given in Equation 4.15. The mean value of the performance function was calculated using the mean value of response (differential settlement) as shown in Equation 4.16 and the standard deviation is equal to the standard deviation of the response i.e. $\sigma_g = \sigma_{S_{diff}}$. In the optimization process, the values of reliability index less than target reliability index were considered unacceptable.

$$\beta = \frac{\mu_g}{\sigma_g} \tag{4.15}$$

$$\mu_g = S_{diff,all} - \mu_{S_{diff}} \tag{4.16}$$

The MC simulation is used as an inside loop of the NSGA-II algorithm, i.e. for each design set or each member of parent population set, 10,000 simulations were conducted to compute 10,000 responses which were used to calculate standard deviation of differential settlement and reliability index. Also, the set of parent population went through 200 iterations or generations process for refinement of the population. Finally, the population

set at the end of 200th generation which passes all the safety constraints is presented in the form of Pareto fronts as shown in Figures 4.11 and 4.12 and discussed in the next section.

4.4.6 Comparison of Pareto fronts of Foundations on Clayey and Sandy Soils

The Pareto front is a plot of non-dominated design sets which shows a tradeoff relationship between two objectives, i.e. one objective can't be improved without compromising the other. The concept of Pareto optimality is to find the best solution of multi-objective problem for the given conditions. In Pareto front, the total cost measures the cost efficiency and the standard deviation of differential settlement measures the robustness. The term robustness is defined as the insensitivity of response of the system when it is subjected to adverse condition such as variation in random variables. In this study, the robustness is measured in terms of standard deviation in differential settlement. Lower standard deviation of differential settlement means higher robustness and vice versa. Usually, it is desired to have the minimum cost for maximum level of robustness. However, this is not possible due to the tradeoff relationship between the cost and robustness measure. For the easiness of comparison of the total cost of three foundation at different level of robustness, the Pareto fronts for all foundations are plotted in the same graph.

4.4.6.1 Pareto front of Foundations in Clayey Soil

The Pareto fronts for foundations on clayey soil are illustrated graphically in Figure 4.11. It can be seen for all foundations that the lower costs have higher response variability as indicated by higher values of standard deviation of differential settlement. For the raft foundation, the standard deviation of differential settlement increased from about 1.5 mm to 4.0 mm when the total cost decreased from about $ 1,440,000 to $ 450,000. In case of

the pile group foundation, the standard deviation of differential settlement increased from about 0.4 mm to 2.8 mm when the total cost of the foundation decreased from $ 1,220,000 to $ 660,000. Similarly, for the piled-raft foundation, the total cost decreased from about $ 840,000 to $ 750,000 when the standard deviation of differential settlement increased from 1.5 mm to 2.7 mm. The interesting point to notice here is that the Pareto front for raft foundation is above the Pareto front for piled-raft foundation which is above the Pareto front for pile group foundation. This means that the pile group foundation is the most economical foundation followed by the piled-raft and the raft foundation but only for common standard deviation of differential settlement, i.e. between 1.5 mm to 4.0 mm. This result is contradicting from the result of conventional design results which proves that the results may deviate from conventional design results when the uncertainties are incorporated in the design. The other noticeable fact in Figure 4.11 is that at about standard deviation of differential settlement of 2.6 mm (at *a*), the Pareto fronts for raft and piled-raft foundations are intersecting, i.e. they have the same total cost of $760,000 (at a_C). Similarly, at about standard deviation of differential settlement of 3.0 mm at *b*), the Pareto fronts for raft and pile group foundations are intersecting, i.e. they have the same total cost of $640,000 (at b_C). Decision making during such situation may be ambiguous. The professional and experienced judgement play an important role to select the foundation in such case. For instance, in the wind farm many wind turbines are constructed in large area in certain pattern. In such case, constructing a very large raft foundation may not be feasible because a single foundation can cover large area of the wind farm. So, the raft foundation can be omitted. Next, the pile foundation may have longer piles which may be difficult to

drive and can add other unseen costs. At the same time, the piled-raft can also have longer piles, but the raft can provide more strength compared to pile cap. Hence one can come to final decision based on different scenarios when the foundations have the same total cost for same level of robustness in the Pareto front.

In addition, it can be comprehended from Figure 4.11 that for the standard deviation of differential higher than 3.0 mm, i.e. for lower robustness, the raft is cheapest of all. But for the higher robustness, the pile group or the piled-raft foundation are economical. The Pareto fronts of pile group and piled-raft foundations are extended using the best fit trend line which is represented by dotted line in Figure 4.11. However, it should be bore in mind that this may not be ideal thing to do as the Pareto front is dependent on the range of design variables selected and variation of uncertain parameters. Nevertheless, it is done in this study for the comparison of Pareto front at different standard deviation of differential settlement as the Pareto fronts for three foundations do not cover the same range of standard deviation of differential settlement. Doing this it was found that the piled-raft foundation is the most economical for the standard deviation of differential settlement lower than about 1.2 mm (at *c*), i.e. for high robustness.

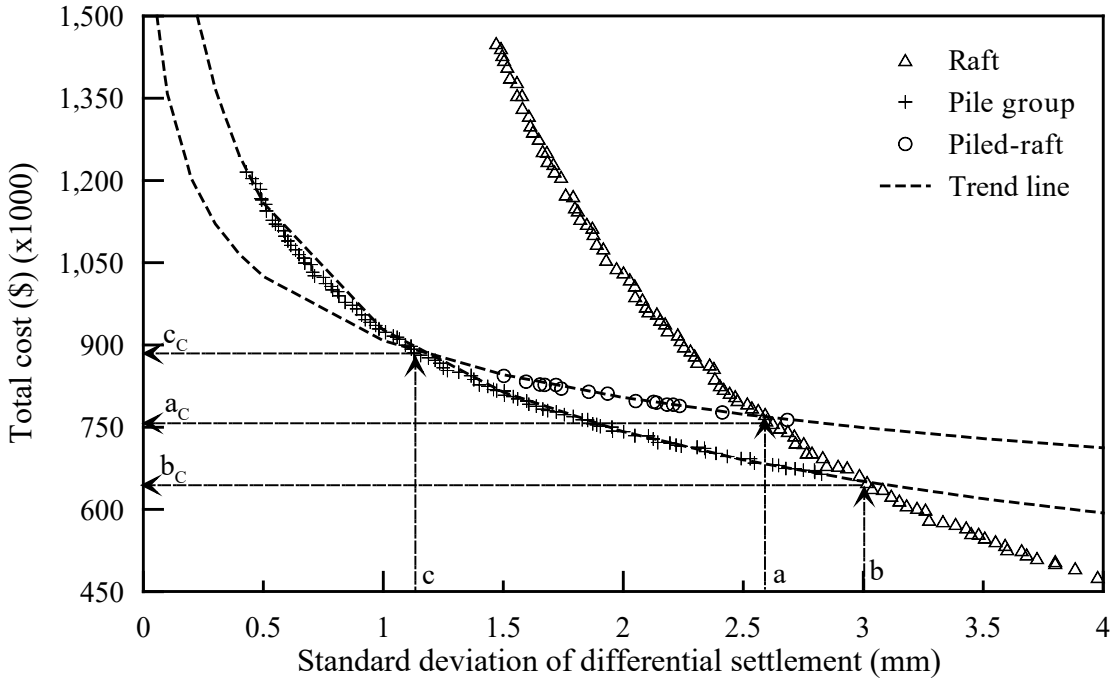

Figure 4.11. Pareto fronts optimized to total cost and standard deviation of response for foundations on clayey soil

4.4.6.2 Pareto front on Sandy Soil

The Pareto front for foundations on sandy soil is illustrated graphically in Figure 4.12. Like the previous case, the tradeoff relationship between the two objectives can be observed. For raft foundation, the standard deviation of differential settlement increased from about 3.0 mm to 4.8 mm when the total cost decreased from about $ 1,180,000 to $ 700,000. In case of pile group foundation, the standard deviation of differential settlement increased from about 1.1 mm to 5.0 mm when the total cost of the foundation decreased from $ 1,315,000 to $ 1,110,000. Similarly, for the piled-raft foundation, the total cost decreased from about $ 1,180,000 to $ 1,110,000 when the standard deviation of differential settlement increased from 2.5 mm to 4.0 mm. In the case of foundations in sandy soil, it can be observed that the Pareto front for all three foundations intersected at

standard deviation of differential settlement of about 3.0 mm (at *a*) at which all the foundations have equal total cost of about $1,140,000 (at a_C). Above this value of standard deviation of differential settlement, the raft foundation is found to be the most economical followed by piled-raft and pile group foundation. Below the standard deviation of differential settlement of 3.0 mm, the pile group and the piled-raft foundation have similar total costs and the raft has the highest total cost (estimated from trendline of Pareto front of raft). When the standard deviation of differential settlement falls below 2.5 mm (at *c*), i.e. high robustness, the pile group foundation is found to be the most economical compared to other two foundations.

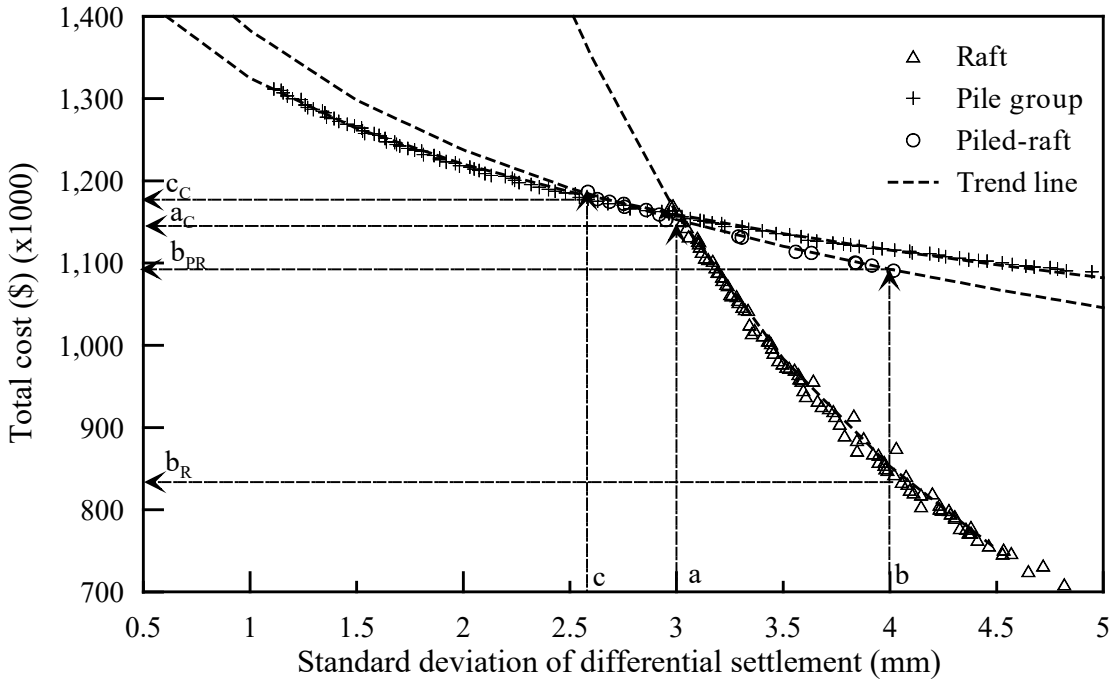

Figure 4.12. Pareto fronts optimized to total cost and standard deviation of response for foundations on sandy soil

Using the Pareto front, the client can select the desired design for the given cost and performance limitation. By investigating the Pareto fronts for three foundations in clay and sand, it was found that the raft foundation is economical for lower robustness and pile group or piled-raft is economical for higher robustness. The selection of the final design will be based on numerous factors such as availability of area, easiness in construction, and most importantly the cost and performance limitation. It should be noted that the results and discussions presented above are for the given problem with the assumed random and design variables. The results may not follow the same trend if any of the input factor is changed.

4.4.7 Determination of the Optimum Design

If the client desires to obtain the most optimum design, i.e. the design in which both objectives are compromised equally, it can be obtained from Pareto front using knee point concept. Among the various methods available to determine the knee point, normal boundary intersection (NBI) approach, illustrated in Figure 4.13 and also discussed in Juang et al. (2014) and Deb and Gupta (2011), is used in this study. In this method, the boundary line (*AB*) is created by connecting two extreme points in the normalized space of the Pareto front and the distance of each point in Pareto front from the boundary line is calculated. Then the point on the Pareto front with the maximum distance from the boundary line is referred to as the knee point, as marked in Figure 4.13. The optimum cost and the standard deviation of response corresponding to the knee point are used to finalize the design solution.

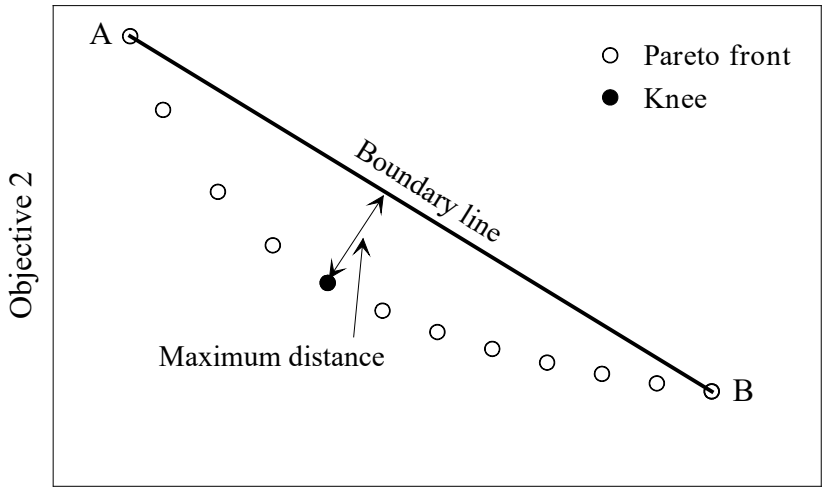

Figure 4.13. NBI method of determining knee point

The optimum design obtained using NBI method for all three foundations in clayey and sandy soil are given in Table 4.6. Since the robustness measure, i.e. the standard deviation of differential settlements for optimum designs of different foundations are not equal, the comparison of the optimum total cost of foundation presented in Table 4.6 is not relevant. Nevertheless, it gives freedom to the clients to select the suitable foundation that satisfies their objectives.

Table 4.6. Optimum designs using NBI method

Foundation	Clay			Sand		
	Dimension (m)	Std. dev of S_{diff} (mm)	Total cost ($)	Dimension (m)	Std. dev of S_{diff} (mm)	Total cost ($)
Raft	R_r = 22.56	2.42	820,299	R_r = 28.49	3.85	872,291
Pile group	L_p = 61.05	1.13	885,415	L_p = 81.41	2.78	1,165,990
Piled-raft	R_r = 10.88 L_p = 46.61	2.48	769,281	R_r = 11.06 L_p = 71.69	3.46	1,119,090

For both soils, the introduction of variation of random variable or noise factor in the design resulted in costlier foundation compared to conventional design for the mean

design parameters. In clayey soil, the piled-raft foundation was found to have lowest optimum cost followed by raft and pile group foundation. However, the difference is not a lot. Similarly, in clayey soil, the raft foundation was found to have the lowest optimum cost followed by piled-raft and pile group. This may entice the client to select the raft foundation. However, the constraint such as availability of area to construct such a large raft foundation (radius of 28.49 m) in a wind farm may direct the client to used either pile group or piled-raft foundation. Hence the selection is completely based on the given scenario. It can be observed that the total cost of construction of foundation in sandy soil is higher than that in clayey soil.

4.5 Conclusion

A multi-objective design optimization of the typical foundations used for onshore tall wind turbine tower is presented in this study. The conventional geotechnical design conducted by using analytical equations showed that the final design is controlled by the differential settlement and rotation of the foundation rather than the bearing capacity or total settlement. The reliability based robust geotechnical design optimization of all three foundations was conducted using NSGA-II algorithm coupled with Monte Carlo Simulation. It resulted in the Pareto front which showed a clear tradeoff relationship between the total cost and standard deviation of differential settlement (robustness measure). It is a convenient tool to make the final design decision based on the cost and performance requirements. For both soils, the raft foundation was found to be the most economical for lower robustness and pile group or piled-raft foundation was found to be the most economical for higher robustness. The optimum design can be obtained from

Pareto front using knee point concept. In clayey soil, the optimum design for the piled-raft foundation was found to be the cheapest among all the foundations and in sandy soil the optimum design of raft foundation was found the be the cheapest. The procedure presented in this study to conduct the robust design optimization of different foundations for tall structures can also be extended to design the foundation to support other tall structures.

CHAPTER 5

INVESTIGATION OF SETTLEMENT BEHAVIOR OF PILED-RAFT FOUNDATION FOR TALL WIND TURBINES USING 3D NONLINEAR FINITE ELEMENT MODELING AND ANALYTICAL METHOD[4]

5.1 Abstract

Geotechnical design of piled-raft foundation is typically performed using simplified semi-empirical equations that don't consider the soil-structure interaction and the effect of bending moment on the differential settlement. In this study, the settlements and rotations computed using analytical and linear and nonlinear finite element methods were compared. First, the piled-raft foundation for supporting a 130 m-tall wind turbine was designed using a simplified analytical method and then a nonlinear finite element model was created in ABAQUS and analyzed. In the finite element modeling, the stress-strain behavior of the soil was represented by linear elastic and nonlinear elastoplastic Drucker-Prager models. The soil-structural interfaces were modeled as two bodies in the contact. The results showed that the vertical and the horizontal displacements from the analytical procedure were significantly higher than that from the finite element method, while the differential settlement and rotation were lower. The parametric study conducted by varying the wind speed and undrained cohesion of the soil indicated that the difference between the predicted responses decreases when the load is large and/or soil is soft.

[4] A similar version of this chapter is submitted to the *International Journal of Geomechanics*; Shrestha, S. and Ravichandran.

5.2 Introduction

The importance of meeting the energy demand through clean and sustainable sources has been well recognized in recent years. Among the many sustainable sources, the wind is gaining popularity around the world particularly in the USA and Europe. The wind energy production can be increased either by building taller turbine towers to access steadier and higher wind speed or many turbines. Selection of site for building a wind farm depends on site-specific wind characteristics and subsurface condition that affects the design and construction of the foundation for supporting the wind turbines. In some areas, the wind characteristics may be favorable, but the subsurface condition may not be suitable for transferring the larger vertical load, horizontal load and moment to the subsurface soil. This will result in a larger and uneconomical foundation, especially when the foundation must support tall turbines that induce larger moment at the base of the tower.

Mat foundation, pile group foundation, and piled-raft foundation are commonly used for supporting wind turbines. Out of these three foundation types, the piled-raft foundation that has a large mat at the top of a number of deep foundations is economical for tall onshore wind turbine, especially when the subsurface soil is weak (Shrestha and Ravichandran, 2016). Higher bearing resistance is derived from the mat foundation while higher settlement resistance is derived from the deep foundation. Although the combined mat and deep foundation is better for meeting the safety and serviceability requirements effectively, the geotechnical design of piled-raft foundation is complicated because of the complex load transfer and soil-structure interaction mechanisms. The load sharing between the piles and raft are not well understood especially when the piled-raft is for supporting

wind turbine that induces shear and moment loads in addition to the vertical load. There are a few analytical methods available for the design of piled-raft foundation in the literature (Poulos and Davis, 1980; Poulos, 2001a; Randolph, 1994; Burland, 1995; Hemsley, 2000). The details of these methods are given in the analytical design section.

Although these simplified methods can be used to perform designs to a reasonable extent for certain geometric and loading conditions, the literature still lacks in a reliable method that considers the complex load transfer and interaction mechanisms accurately. In such situations, a numerical method can be used for gaining insights into the behavior of piled-raft foundation subjected to complex loading conditions. With the rapid advancement in computer technology and efficient algorithm development for accurately representing the interaction between contacting surfaces, computer models of piled-raft foundation can be developed and analyzed within a reasonable time. Prakaso and Kulhawy (2001) analyzed the piled-raft foundation using 2D plane strain finite element (FE) model using PLAXIS in which the rectangular raft was represented by strip and the row of piles was represented by an equivalent plane pile. By comparing the computed results with that of the corresponding 3D model, they concluded that the plane strain model overestimates the displacement by 5% to 25% for different raft rigidity, the plane strain (center-edge) differential settlement is about 2/3 of the center-corner differential settlement, and the bending moment was similar to that across the raft. However, a piled-raft foundation problem is a 3D problem in which the 3D pile-raft-soil interaction affect the performance of the foundation. Therefore, a 3D finite element analysis (FEA) is considered precise compared to 2D FEA.

Ruel and Randolph (2003) presented a comparative study of a 3D FEA results of three instrumented piled-raft foundations by implementing ABAQUS. They found a reasonable agreement of the overall settlement and differential settlement obtained from the FEA and in-situ measurements for all three foundations. However, the proportion of the total load carried by piles obtained from FE results was higher than that obtained from the in-situ measurements. But only 15 % of the piles being instrumented, it is questionable if all the piles will behave in the same way. Lee et al. (2009) studied the bearing behavior of piled-raft foundation on soft clay under vertical loading by developing a 3D FE model using ABAQUS. In their study, the pile-soil interface slip was allowed and the length of pile, number of piles, pile configuration, and load on the raft were varied to study the effects of pile-soil slip. They concluded that the slip analysis resulted in the higher average settlement and the lower maximum pile loads compared to no slip analysis. The loading pattern (uniform or point load) and pile configuration also affected the pile load distribution. Sinha and Hanna (2016) developed a 3D model of a piled-raft foundation considering the pile-soil-raft interaction to examine the effect of the parameters such as foundation geometry, pile length, pile size, pile spacing, pile diameter, raft thickness, cohesion, and friction angle on the settlements (center, corner, and differential settlements) of the foundation under vertical loading. They concluded that the pile shape has the negligible effect on the settlements while the increase in the pile spacing resulted in the increase in settlements. On the other hand, the increase in pile length and friction angle and cohesion of soil resulted in the decrease in settlements. Similarly, the use of thicker raft

minimized the differential settlement but at the same time imposed an additional load on some of the piles leading to ununiform settlement of the raft.

The aforementioned methods accounted for the pile-soil-raft interaction by using the interaction property or using the rough contact but didn't consider the effect of bending moment on the differential settlement. For the tall structures, the design approach should also consider the bending moment as it is the major factor contributing to the differential settlement of the foundation. Moreover, either a rectangular or square raft is considered with the pile configuration in a grid pattern in the previous studies. This study presents the development of a three-dimensional FE model of the piled-raft foundation in ABAQUS by accounting the pile-soil interaction and the combined loading (vertical load, horizontal load, and bending moment). The raft considered in this study is circular which is appropriate for a wind turbine tower and the piles are arranged in a circular pattern. Two constitutive models were used to represent the stress-strain behavior of the soil: linear elastic (LE) and nonlinear elastoplastic Drucker-Prager (DP) model. The objectives of this study are to: ***(i)*** perform the analytical design of the piled-raft foundation, ***(ii)*** conduct the finite element analysis of the piled-raft foundation using LE and DP constitutive models for soil, ***(iii)*** to compare the analytical design results with the finite element analysis results, ***(iv)*** conduct a parametric study by varying the wind speed and the undrained cohesion in order to investigate the effect on the response, and ***(iv)*** investigate the results from FEA to obtain the useful information which may not be possible to obtain from the experiments.

5.3 Current design procedures

In theory, the piled-raft foundation is economical and shows better performance compared to conventional raft or pile group foundation for supporting larger combined loads. The principal working theory of the piled-raft foundation is that the raft provides significant bearing resistance and the piles provide significant settlement resistance. Hence, the combined pile-raft system provides superior bearing and settlement resistance. Although reasonably accurate equations and procedures are available for the geotechnical design of raft and single pile or group of piles, only a few simplified procedures are available to design piled-raft foundation in the literature. This is mainly due to the lack of understanding of the three-dimensional complex pile-soil-raft interaction that greatly influences the load sharing between the raft and piles. The major challenge during the design of piled-raft foundation is the quantification of load shared by the raft and piles and the mobilized strength of each component, all of which depends on pile-soil-raft interaction. The challenges in designing the piled-raft foundation further increase when it is subjected to the combined vertical load, horizontal load, and bending moment. As a result, reliable design guidelines are not yet available to design piled-raft foundations.

The methods available in the literature to design piled-raft foundation are broadly classified into three categories: simplified methods, approximate methods, and more rigorous computer-based methods (Deka, 2014). The simplified method of analyzing a piled-raft foundation include the analytical equations based on the elastic theory proposed by Poulos and Davis (1980), Poulos (2001b), Randolph (1994), Burland (1995), and Hemsley (2000). The approximate method is based on the strip on spring or plate on spring

where the raft is represented either by plate or strip and piles are represented by spring. The rigorous computer-based methods include the use of numerical solution using the commercially available software based on the finite element, finite difference, and boundary element methods. With the rapid development of computer technologies over the past few decades, a three-dimensional finite element method has gained popularity among the designers to solve the complex piled-raft problem.

In this study, the settlement response of piled-raft foundation for supporting a tall wind turbine predicted by the simplified method and linear and nonlinear finite element methods were compared to investigate the relative accuracy of the models. The finite element model was then used to gain further insights into the behavior of piles-raft-soil system such as load sharing between piles and raft, slip and separation at the pile-soil interface and the deformation behavior of soil and pile.

5.4 Design Loads and Soil Properties

The piled-raft foundation in this study is designed for a 130 m tall hybrid wind turbine tower made of lower 93 m of concrete and upper 37 m of steel. The wind turbine specifications (diameter, height, and material) were obtained from Grunbeg and Gohlmann (2013). It is assumed that the wind turbine is constructed at a hypothetical site with a clayey soil deposit. During the operation of the wind turbine, it will be subjected to vertical load due to self-weight of the superstructure and turbine components, horizontal load due to wind action on the components above the ground, and bending moment induced by the horizontal wind load. The calculation of each load and the soil properties for the analytical and FE modeling are discussed below.

5.4.1 Design loads

The piled-raft foundation will be subjected to the vertical load due to the weight of the tower and other turbine components and the horizontal load and bending moment due to the wind acting on the tower body. The vertical load was calculated by adding the weights of the tower and other components of the wind turbine such as nacelle and rotor. The weight of the tower was calculated using the tower dimension and corresponding unit weights of the tower components and the weights of nacelle and rotor were obtained from Malhotra (2011). The final dead load was calculated to be 51.71 MN.

The wind action on the structures above the ground induces horizontal load on them which results in a horizontal load and bending moment at the base of the tower. The wind load was calculated following the procedure described in ASCE 7-10 (2010) using the mean survival wind speed of 201.3 km/h. This mean wind speed is considered to be appropriate because most of the wind turbines have the survival wind speed within 180.3 km/h to 215.7 km/h (Wagner and Mathur, 2013) and its range lies between 143.3 km/h and 259.2 km/h. The total horizontal load and bending moment were calculated to be 2.26 MN and 144.89 MNm, respectively. It should be noted that a parametric study was conducted by varying the wind speed for comparing the predictions for a wide range of horizontal load and bending moment.

5.4.2 Soil properties

A site composed of a single layer of clayey soil was considered in this study. The unit weight and mean undrained cohesion for the clayey soil were assumed to be 18 kN/m^3 and 100 kPa, respectively. The modulus of elasticity of the soil was determined using the

correlation between undrained cohesion and modulus of elasticity obtained from USACE (1990) and was calculated to be 3.5 x 10^4 kPa. The determination of the nonlinear elastoplastic constitutive model parameters is described in the finite element modeling section. A parametric study was also conducted by varying the undrained cohesion and corresponding modulus of elasticity to investigate the effect of soil properties on the predicted performance.

5.5 Design of piled-raft foundation using Analytical Method

The geotechnical design of the piled-raft foundation (determination of dimensions of raft, type of piles, dimensions of piles, number of piles, and arrangement of piles) was conducted using the simplified approach proposed by Hemsley (2000) in which the design procedures proposed by Poulos and Davis (1980) and Randolph (1994) are incorporated. In addition, a new iterative procedure was developed to calculate the differential settlement of the piled raft foundation due to the bending moment. At first, the radius of the raft, the length of the piles, the number of piles, and arrangement of the piles were assumed and adjusted until all the design requirements were met. The design requirements include stability checks (vertical load capacity, horizontal load capacity, and bending moment capacity) and serviceability checks (total and differential settlements, and the rotation of the tower per unit length). A minimum factor of safety of 2.0 was considered to be safe (Hemsley, 2000) for vertical load, horizontal load, and bending moment capacity checks. A vertical misalignment within 3 mm/m of the tower was considered to be safe against the rotation of the tower which yielded the allowable rotation and differential settlement of

0.172° and 45 mm (Grunberg and Gohlmann, 2013) for the problem considered in this study.

5.5.1 Stability check

5.5.1.1 Vertical load capacity

The vertical load capacity of the piled-raft is the smaller of: ***(i)*** the sum of ultimate capacities of the raft and all the piles and ***(ii)*** the ultimate capacity of the piled-raft system as a single block. For case ***(i)***, the ultimate bearing capacity of the raft was calculated using the general bearing capacity equation and that of piles was calculated using the α-method for clayey soil. For case ***(ii)***, the ultimate capacity of the block was calculated as the ultimate capacity of the block that consists of raft, piles, portion of the raft outside the periphery of the piles and the soil. For the soil properties and loading considered in this study, the final design was controlled by the individual component failure (either raft or piles fail) that is the case ***(i)***. The vertical load capacity determined using this procedure was then compared with the design vertical load. The calculated factor of safety was determined to be 4.06, which meets the design requirement.

5.5.1.2 Moment load capacity

The moment capacity of the piled-raft foundation was calculated following a similar procedure used for calculating the vertical load capacity. The moment capacity of the individual components and the block were first determined using the method presented in Hemsley (2000). Then, the moment capacity of the piled-raft foundation was determined as the smaller of: ***(i)*** the ultimate moment capacity of the raft and the individual piles and ***(ii)*** the ultimate moment capacity of the piled-raft foundation as a single block. Based on

the calculations it was found that the design was controlled by individual component failure and the resulting factor of safety was 4.23 that meets the design requirement.

5.5.1.3 Horizontal load capacity

The horizontal capacity of the piled-raft foundation was estimated following Broms' solution outlined in Gudmundsdottir (1981) for the lateral pile analysis in cohesive soil. Although this method is for single pile analysis, it was assumed that all the piles in the group will have similar behavior. The horizontal coefficient of subgrade reaction was used to determine the horizontal load capacity and horizontal deflection of the pile. The horizontal load capacity of the piled-raft was compared with the design horizontal load and the factor of safety was found to be 14.23 and the horizontal deflection was found to be 7.10 mm.

5.5.2 Serviceability check

5.5.2.1 Vertical settlement of the piled-raft

The vertical load-settlement behavior of the piled-raft was estimated by the approach proposed by Poulos (2001b) in conjunction with the method used for estimating the load sharing between the raft and the piles presented in Randolph (1994). The stiffness of the piles, raft, and pile-raft as a single block was used to estimate the load sharing between the raft and the piles. The stiffness of the piled-raft, K_{pr} was estimated using Equation 5.1 proposed by Randolph (1994).

$$K_{pr} = X K_p; \qquad X = \left\{ \frac{1 + \left(1 - 2\alpha_{rp}\right) K_r / K_p}{1 - \alpha_{rp}^2 \left(K_r / K_p\right)} \right\} \tag{5.1}$$

where K_r is the stiffness of raft, K_p is the stiffness of the pile group, and α_{rp} is the pile-raft interaction factor. The pile-raft interaction factor was assumed to be 0.8 considering the fact that when the number of piles in the group increases the value of the interaction factor increases and it reaches a constant value of 0.8 as reported by Randolph (1994). The stiffness of the raft was estimated using the method outlined by Randolph (1994) and the stiffness of the pile group was estimated using the method proposed by Poulos (2001b). In this method, the target stiffness of the piled-raft was first determined by dividing the total vertical load by the assumed allowable settlement and then the Equation 5.1 was solved to determine the stiffness of the pile group.

To introduce the effect of inelastic behavior of soil, it was assumed that the load-settlement relationship is hyperbolic in nature. Hence the stiffness of piles and raft were replaced by secant stiffness using the hyperbolic factors shown in Equation 5.2.

$$K_p = K_{pi}\left(1-\frac{R_{fp}P_p}{P_{pu}}\right) \;;\; K_r = K_{ri}\left(1-\frac{R_{fr}P_r}{P_{ru}}\right) \tag{5.2}$$

where K_{pi} and K_{ri} is the initial stiffnesses of pile group and raft, respectively. R_{fp} and R_{fr} are the hyperbolic factors for piles and raft, respectively. P_p and P_r are the loads carried by piles and raft, respectively. P_{pu} and P_{ru} are the ultimate capacities of the piles and raft, respectively. In this study, the hyperbolic factors of 0.2 and 0.9 were used for piles and raft, respectively. When the foundation is subjected to the vertical load, the stiffness of the piled-raft will remain operative until the load-bearing capacity of the pile is fully mobilized at load P_A as shown in Equation 5.3 (also in Figure 5.1). After calculating the values of K_p,

K_r, K_{pr}, and P_A, the load-settlement curve (P vs. S) for the piled-raft foundation was developed using the Equation 5.3 and the resultant vertical load-settlement curve is shown in Figure 5.1.

$$\left.\begin{array}{l} \text{For } P \le P_A;\ S = \dfrac{P}{K_{pr}} \\ \text{For } P > P_A;\ S = \dfrac{P_A}{K_{pr}} + \dfrac{P - P_A}{K_r} \end{array}\right\} \tag{5.3}$$

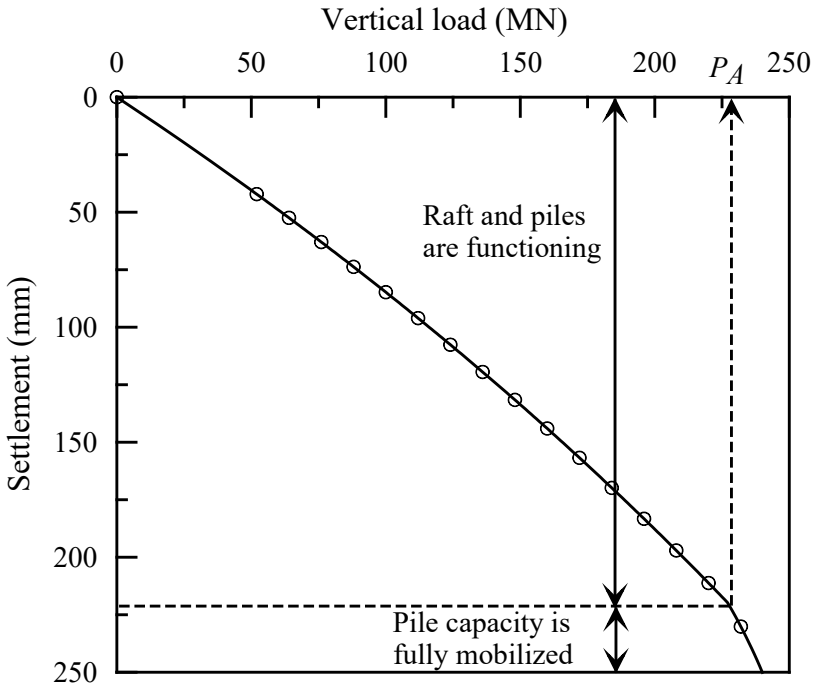

Figure 5.1. Load-settlement curve for the piled-raft foundation based on the analytical model

From the above load-settlement curve, it was determined that the piled-raft foundation considered in this study would settle vertically by 41.90 mm when subjected to the design vertical load of 51.71 MN. It should be noted that the design vertical load is smaller than P_A (= 227.04 MN) which indicates that both the raft and piles are contributing to support the load and the piles capacity is not fully mobilized at this vertical load.

5.5.2.2 Differential settlement and rotation of the piled-raft

The calculation of differential settlement of the combined piled-raft foundation system due to the bending moment is another challenging task in the geotechnical design of piled-raft foundation. The accurate procedure to estimate the differential settlement due to bending moment is not yet available in the literature. This paper proposes a new method to calculate the differential settlement of the piled-raft foundation due to the bending moment. In this method, the total applied bending moment is converted into vertical forces (their magnitude varies with distance to the pile from the center) and divided between the raft and the piles such that the differential settlements of the individual components (i.e., raft and piles) are equal, which is considered as the differential settlement of the piled-raft foundation. The calculation of the differential settlement of individual components (raft and piles) is discussed in the following section.

5.5.2.3 Differential settlement of raft

The differential settlement of the raft was estimated based on the rotation (θ). The rotation was calculated using Equation 5.4 given by Grunberg and Gohlmann (2013).

$$\theta = \frac{M_{found}}{c_s I_{found}};\ c_s = \frac{E_s}{f' \sqrt{A_{found}}} \tag{5.4}$$

where M_{found} is the fixed-end moment at soil-structure interface (percentage of moment shared by raft to result in an equal differential settlement as that of piles in this study), c_s is the foundation modulus, I_{found} is the second moment of inertia for area of foundation, E_s is the modulus of elasticity of soil, f' is the shape factor for overturning (0.25), and A_{found}

is the area of the foundation. After calculating θ, the differential settlement of the raft was determined using simple trigonometric relationship.

5.5.2.4 Differential settlement of piles

The differential settlement profile of the piles as a group was estimated considering the equivalent vertical loads due to the dead load and bending moment shared by the piles. First, the vertical load on each pile was estimated and then the settlement of each pile head was calculated following the procedure outlined by Fellenius (1999). Finally, the settlements of the piles in a vertical section (2D elevation) were approximated by a straight line to produce the settlement profile for the piles. The above-mentioned procedure was repeated by adjusting the bending moment shared by the piles and the raft until the settlement profiles of raft and piles matched. The final settlement profile is considered as the settlement profile of the piled-raft system. After several iterations, it was found that the raft takes 12.46 % and piles take 87.54 % of the total bending moment to yield an equal differential settlement. The differential settlement of the piled-raft system was found to be 10.55 mm which gives a rotation of 0.04°. For the 130 m tower height, this rotation of 0.04° induces a horizontal displacement of 91.41 mm at the top of the tower which is within the acceptable limit.

The final design that meets all the geotechnical design requirements (safety and serviceability) resulted in a raft of radius of 7.5 m and thickness 1.2 m at a depth of 1.5 m supported by 44 pre-stressed concrete piles of width 0.457 m and length 28.0 m arranged equally along the circumferences with radii of 5.3 m and 6.7 m. The final design is shown in Figure 5.2.

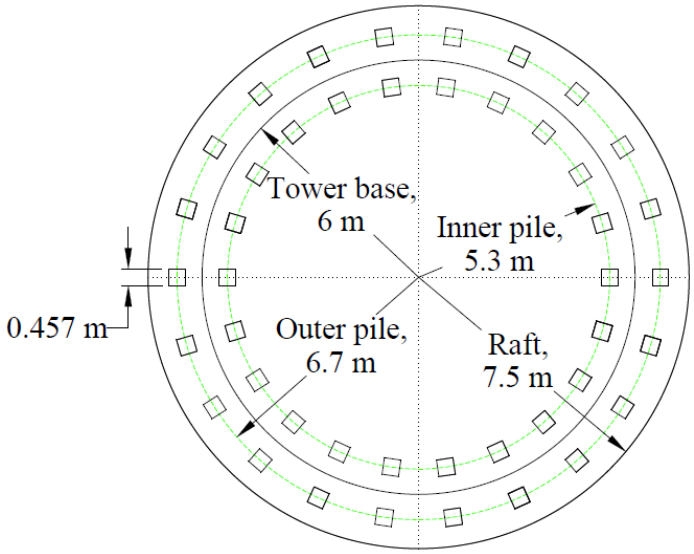

Figure 5.2. Plan view of designed piled-raft foundation

5.6 Analysis of piled-raft foundation using Coupled Finite Element Method

5.6.1 Modeling tool

A three-dimensional finite element model of the piled-raft foundation system including the supporting soil was developed using ABAQUS, a general-purpose finite element software widely used in Civil and Mechanical Engineering fields. ABAQUS has many desirable features suitable for this study. These features include: ***(i)*** inbuilt material model library with many constitutive models which facilitates the user to use the appropriate material model for the problem in hand and ***(ii)*** various interaction models to represent the interaction between two different surfaces which is important for accurately analyzing the soil-pile and soil-raft interactions. The ability to incorporate the interaction among piles, raft, and soil is one of the key advantages of the finite element modeling over the analytical method. Moreover, a three-dimensional model can be developed in ABAQUS which is required for this problem due to asymmetric loading even though the

foundation geometry is symmetrical about the vertical axis. The steps involved in the development of the finite element model of the piled-raft foundation in ABAQUS are discussed below.

5.6.2 Finite element model development and boundary conditions

The dimensions of the piled-raft foundation (size of the raft, size of the piles, and location of the piles) obtained from the analytical design were used to develop its FE model in ABAQUS. First, three-dimensional models of each of the components of the piled-raft foundation were created and spatially discretized using 8-nodehexahedral brick elements. For the supporting soil, the diameter and the height of the simulation domain was determined to be 50 m and 56 m, respectively, based on an initial size sensitivity study. The purpose of the size sensitivity study was to ensure that the simulation domain size and its boundaries do not affect the computed responses. Although a half-model can be used with appropriate boundary conditions along the vertical plane of shear and bending moment, a full 3D model was used in this study because of unsymmetrical location of the piles.

The individual components were then assembled at their respective locations in the assembly module. While assembling, it is important to ensure that there is space for raft and piles in the soil body, i.e. the part of the soil which will be occupied by the raft and piles must be removed. To achieve this, cut instance technique was used to cut the soil with raft and pile which resulted in a new soil part with required spaces for raft and piles. Finally, the new soil part, raft, and piles were assembled as shown in Figure 5.3. In the analytical design, a 1.2 m thick raft is positioned at the depth of 1.5 m from the ground surface which

implies that there will be a 0.3 m thick soil above the raft. However, in Figure 5.3, the soil above the raft can't be seen because it wasn't modeled as a soil body. Instead, it was modeled as a uniform vertical pressure equivalent to the weight of the 0.3 m thick soil which was later applied to the model before applying the vertical and lateral loads. This was done to reduce/eliminate the numerical instabilities that may occur near the surface during the numerical analysis.

The bottom of the simulation domain was fixed in all directions, i.e. no translation in x, y, and z directions. The vertical sides of the simulation domain were fixed in x and y directions (i.e., in the lateral direction) and allowed to move freely in z-direction (vertical direction). The top of the simulation domain was free. Figure 5.3 shows these boundary conditions in addition to various parts and dimensions of the simulation domain.

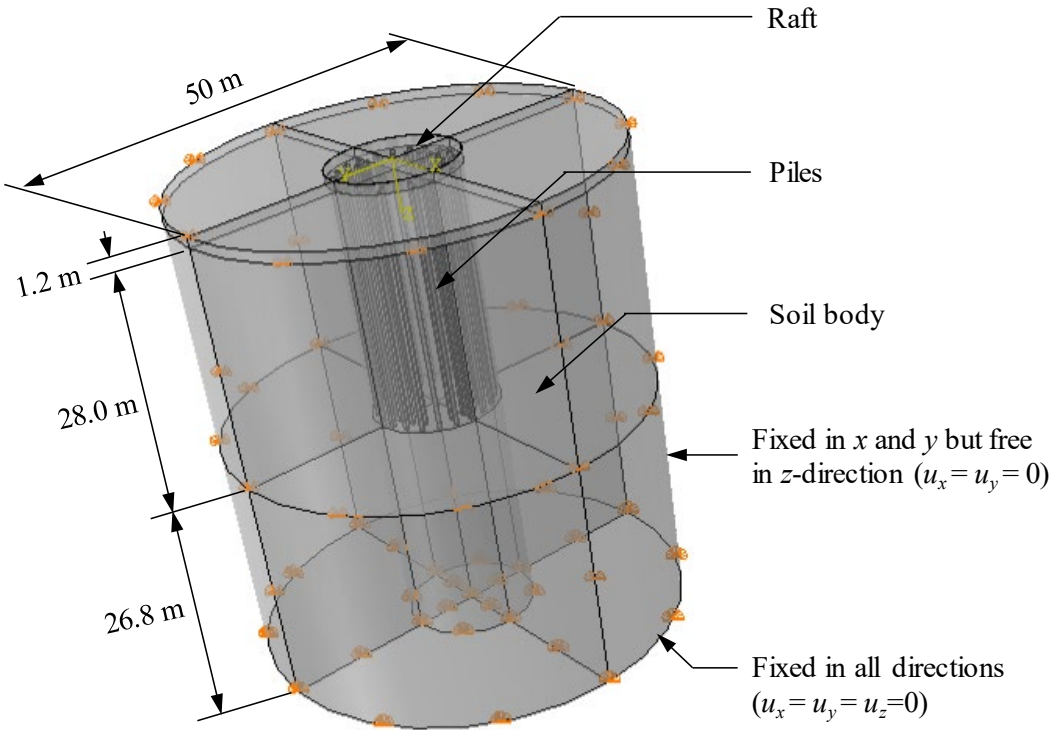

Figure 5.3. Three-dimensional view of the piled-raft system in ABAQUS

5.6.3 Constitutive models for the soil and structural components

The mathematical representation of the stress-strain behavior of the soil and the structural elements is critical for accurately predicting the response of the piled-raft systems using finite element method. The selection of the material model depends on the expected and/or observed behavior of each component for a given load range and material properties. In general, a geotechnical system may show nonlinear elastoplastic behavior at higher load and/or lower material stiffness (i.e., the system undergoes large strain). On the other hand, the same system may show linear behavior at smaller loads and/or higher material is stiffness (i.e., the system undergoes small strain). The linear elastic relationships are simple, computationally efficient, numerically stable, and determination of their model parameters are straight forward. On the other hand, the nonlinear elastoplastic relationships are complex, computationally expensive, numerically unstable, and determination of their model parameters requires significant effort with advanced laboratory tests. In this study, the structural components, i.e. raft and piles were represented by an in-built linear elastic constitutive model because in most of the structural designs the structural components are only allowed to behave in the linear elastic range. The properties of the raft and piles are listed in Table 5.1.

Table 5.1. Structural components model parameters

Component	Density (kg/m^3)	Young's modulus (N/m^2)	Poisson's ratio
Pile	2549.3	3.00×10^{10}	0.15
Raft	2549.3	3.28×10^{10}	0.15

The supporting soil was represented by two constitutive models: linear elastic (LE) and elastoplastic Drucker-Prager (DP) models to compare the predicted results. The

purpose of using LE model to represent the soil in this study was to compare the results of the finite element simulation with the results of analytical design. Since the analytical design procedure is based on the elastic theory, the use of LE model in FEA will enable us for appropriate comparison. Since soil exhibits nonlinear elastoplastic behavior at larger deformation range, an elastoplastic DP model was also used in this study to accurately represent the stress-strain relationship of the soil and to compare the predictions with that of LE and analytical models. DP model is superior to the linear elastic-perfectly plastic Mohr-Coulomb (MC) and LE models because it can model the modulus reduction with increasing strain. Since the experimental stress-strain relationship was not available, the DP model parameters were calibrated using the basic geotechnical strength and deformation parameters to ensure that the elastoplastic model parameters are consistent with that of linear elastic models. It should be noted that one may use laboratory test results such as triaxial test results to accurately calibrate the elastoplastic DP model parameters.

First, the linear elastic-perfectly plastic MC stress-strain relationship was developed in EXCEL using the initial elastic modulus and shear strength parameters that define the yielding. Then, the DP stress-strain relationship was formulated by using the hyperbolic relationship between the vertical strain and deviatoric stress. The calibrated stress-strain curves for the MC and DP models are shown in Figure 5.4 (a). The use of the DP model in ABAQUS requires the hardening model, i.e. yield stress vs. plastic strain curve as one of the inputs. To obtain the yield stress vs. plastic strain curve, first, the initial yield stress was estimated as the deviator stress at which the stress-strain curve starts to exhibit nonlinear behavior. From Figure 5.4 (a), the initial yield stress is found to be 30

kN/m^2. Then, the plastic strains for corresponding stresses were calculated by subtracting elastic strain from the total strain. The elastic strain at each stress was calculated by dividing the stress by the initial elastic modulus. The final DP hardening curve obtained through this procedure is shown in Figure 5.4 (b). The other constitutive model parameters for both the LE and DP models are listed in Table 5.2.

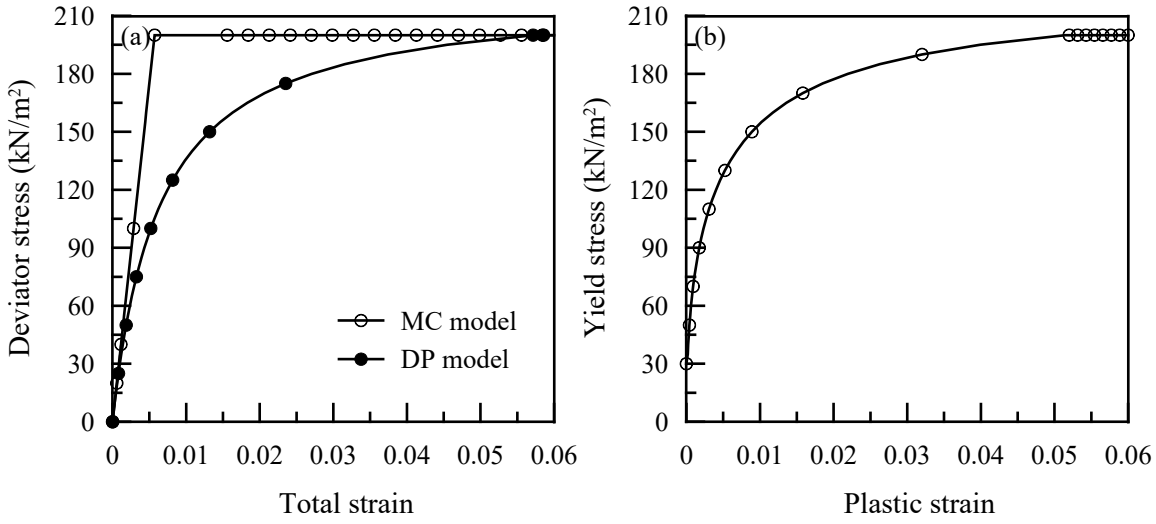

Figure 5.4. (a) Calibrated MC and DP models and (b) DP hardening model inputs

Table 5.2. Constitutive model parameters for linear elastic and Drucker-Prager models

Model	Parameter	Value
Linear elastic	Density (kg/m^3)	1835.5
	Young's modulus (kN/m^2)	3.50 x 10^7
	Poisson's ratio	0.45
Drucker-Prager	Shear criterion	Linear
	Flow potential eccentricity	0.1
	Friction angle (°)	0
	Flow stress ratio	1
	Dilation angle (°)	0
	Yield stress vs plastic strain	Graphically shown in Figure 5.4(b)

5.6.4 Spatial discretization and simulation domain

The simulation domain was discretized using the linear 8-noded hexahedral brick element (C3D8R) with reduced integration and hourglass control for all the components. While generating the mesh, the nodes at the interface between contacting surfaces must coincide or be within allowable distance. To achieve this, partition technique was used to divide the components into pieces as shown in Figure 5.5. An equal number of elements were assigned to the overlapping surfaces. The finite element mesh was refined to decrease the size of the elements in the areas where higher stress and/or deformation gradient was expected such as in the raft and along the soil-pile region. A coarser mesh was created in the areas where the stress concentration was expected to be lower such as the soil towards the sides and bottom. This was done by using the bias feature available in ABAQUS which allows generating gradually increasing or decreasing element size in the desired direction. The partition of the model and the finite element mesh generated with the internal mesh view are shown in Figure 5.5. The final finite element mesh consisted of 370,979 nodes and 288,360 three-dimensional brick elements.

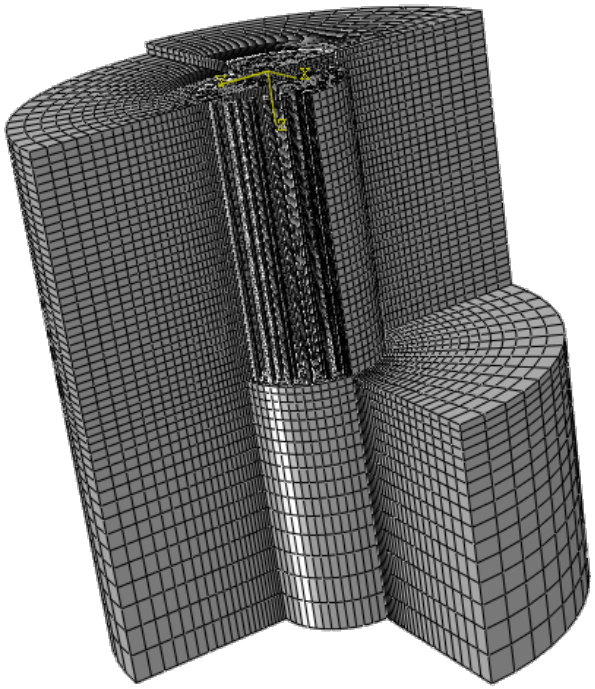

Figure 5.5. Finite element mesh (with internal mesh view)

5.6.5 Soil-structure interface modeling

There are three interfaces exist in piled-raft foundation. They are: raft-pile interface, raft-soil interface, and pile-soil interface. The external loads are first taken by the raft and then the raft transfers the loads to the piles through the *raft-pile interface* and to the soil through the *raft-soil interface*. The loads transferred to the piles are then transferred to the soil through the *pile-soil interface*. The accurate modeling of these interfaces is critical in the modeling of piled-raft foundation for a realistic prediction of its overall behavior.

In this study, soil-structure (raft-soil and pile-soil) and structure-structure (raft-pile) interfaces were modeled using a surface to surface contact which is used to define contact between two deformable surfaces or between a deformable surface and a rigid surface. This method uses a master-slave concept in which one of the contacting surfaces is defined as

master surface and the other as slave surface. The general rule of selecting master and slave surfaces is to define the surface with coarser mesh as master surface and the one with finer mesh as slave surface or to use the stiffer body as the master surface. Also, while defining the contact constraint with the master-slave concept, the master surface can penetrate the slave surface, while the slave surface can't penetrate the master surface. The details of soil-structure and structure-structure contact are given below.

5.6.5.1 Soil-structure interface

The soil-structure interfaces in the piled-raft foundation are raft-soil and pile-soil which are modeled using the surface to surface contact. In both raft-soil and pile-soil contact pairs, soil surface was defined as the slave surface and raft (side and bottom) and pile (skin and tip) surface as the master surface. The interaction between raft-soil and pile (skin)-soil contact pairs was defined using mechanical contact in which normal and tangential behavior of the contacting surface can be defined. The interaction between pile (tip)-soil was defined using tie constraint (more detail about tie constraint is provided in the next section). The normal behavior dictates the load transfer in the normal direction and the tangential behavior dictates the load transfer in tangential direction when there is relative motion. Since the load can transfer in the normal direction only when the two surfaces are in contact, "hard" contact was used to define the normal behavior. It ensures that the surfaces are always in contact and the loads are always transferred during the simulation. The tangential behavior was defined by using "penalty" friction formulation which allows some relative motion or elastic slip of the contacting surfaces.

The friction formulation available in ABAQUS follows Coulomb's friction model, according to which two contacting surfaces can tolerate shear stress up to critical shear stress (τ_{crit}) within which the contacting surfaces stick to each other. Once the shear stress exceeds the critical shear stress, the sliding of the surfaces begins. As per Coulomb's friction model, the critical shear stress is defined as, $\tau_{crit}=\mu p$, where μ is defined as the coefficient of friction and p is the contact pressure. In this study, the coefficient of friction of 0.48 was used which is common in clay-structure interaction problem. Further, a critical shear displacement or an allowable elastic slip of 5 mm was defined which is a default value in ABAQUS. This allows relative motion of the surface, but it is still computationally efficient and provides accurate results (Jozefiak et al. 2015).

5.6.5.2 Structure-structure interface

The structure-structure interface in the piled-raft foundation is the raft-pile interface. In this contact pair, raft (bottom) surface was defined as the master surface and pile (head) surface was defined as the slave surface. The contact between these surfaces was defined by surface to surface based tie constraint. A tie constraint ties two surfaces in contact together throughout the simulation. It makes the translation and rotation motion equal for the surfaces in contact.

5.6.6 Key steps of the simulation

The analysis was carried out in three steps: initial step, geostatic step, and loading step. The initial step is the default step in ABAQUS which is created automatically. In the initial step, the boundary conditions, interactions, and constraints are already activated which are propagated into the next step. The geostatic step establishes the equilibrium of

gravitational loads and forces and verifies the initial stresses. A uniformly distributed load representing the soil mass above the raft was also applied in this step. The last step is the loading step where the design loads (vertical load, horizontal load, and bending moment) were applied in the desired directions and locations. At first, the vertical load was applied at the center node of raft without applying the horizontal load and bending moment. Then the vertical load was kept constant and the horizontal load and bending moment were applied. To transfer the bending moment applied on the raft, an MPC beam constraint was applied between center node (on the top surface) and top nodes of the raft which ties the center node with all the nodes on the top surface. All the loads were applied in time steps. In LE model, a larger time step of 0.1 was used because there is no failure due to which there will not be numerical instability. However, for DP model, smaller time steps of 0.001 and 0.0001 were used as there can be numerical instability due to a larger increment of load. After successfully developing a 3D model of the piled-raft foundation, a job was created and submitted for the analysis in Palmetto cluster which is Clemson University's high-performance computing resource. It was found that the difference in the results with the time step of 0.001 and 0.0001 was within 1% however, the difference in wall clock time was almost six hours. Therefore, the model with the time step of 0.001 was selected for DP model in this study.

5.7 Results and discussions

The vertical and differential settlements, horizontal displacement, and rotation of the piled-raft foundation are the key results obtained from the finite element simulation. The deformed shape of the piled-raft foundation obtained with nonlinear elastoplastic DP

soil model showing vertical displacement contours at the end of loading is shown in Figure 5.6. The deformation scale factor used for the deformed shape in Figure 5.6 is 150 and the legend is for the vertical displacement (U3) in meter. A similar deformed shape was obtained for the piled-raft model with LE soil model which is not shown here. Due to the combined vertical load, bending moment, and horizontal load, the piled-raft foundation is settling down as well as rotating in the vertical plane of the application of the loads. The rotation in the pile can also be observed near the pile head which is the expected behavior of the pile under a bending moment. It can be seen in Figure 5.6 that the displacement is the highest at the compression side and lowest at the tension side of the foundation. A gradual increase in the vertical settlement can be seen from the tension side to the compression side.

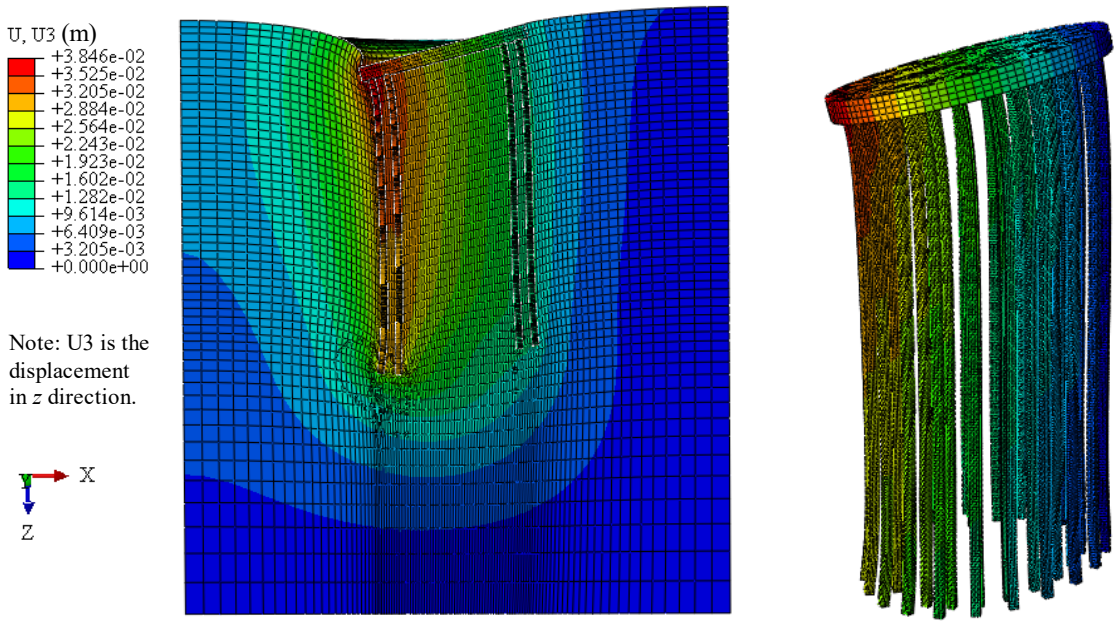

(a) (b)

Figure 5.6. Deformed shape with vertical deformation contours using DP soil model (a) cross section of the model domain and (b) piled-raft only (deformation scale factor = 150)

5.7.1 Settlement response due to vertical load

The vertical load-settlement curves for the piled-raft foundation with linear elastic (LE) and nonlinear elastoplastic DP soil models obtained by applying the vertical load is shown in Figure 5.7. The vertical load-settlement curves shown in Figure 5.7 is only for the vertical load before the application of bending moment and horizontal load. It can be observed in Figure 5.7 that up to the vertical load of about 30 MN both LE and DP soil models are exhibiting linear load-settlement behavior. Beyond that, the LE soil model continues to show the linear behavior while the DP soil model displays a nonlinear behavior due to the reduction in soil modulus with increasing strain. At the design vertical load, i.e. at 51.71 MN, a uniform vertical settlement of 22.67 mm was observed on the raft surface when the LE soil model was used while this value was 25.44 mm when the nonlinear elastoplastic DP soil model was used. The difference between the vertical settlements due to the LE and DP models is found to be 2.77 mm at the vertical load of 51.71 MN. However, this difference will not be the same for other vertical loads due to the nonlinear load-settlement curve for the DP soil model.

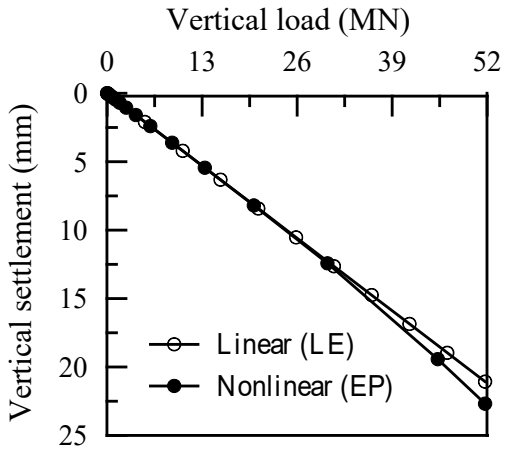

Figure 5.7. Vertical settlement response of the piled-raft foundation from ABAQUS

5.7.2 Settlement and rotation responses due to bending moment and horizontal load

The bending moment and horizontal load were applied at the end of the vertical load. While applying the bending moment and horizontal load, the vertical load was kept constant at its design value. The horizontal displacement, differential settlement, and rotation responses of the piled-raft foundation with the LE and DP soil models for different bending moments and horizontal loads are shown in Figure 5.8 (a) and (b). The horizontal displacement was obtained as the displacement of the raft in the direction of horizontal load (x-direction in this study) while the differential settlement was calculated as the difference between the vertical settlements at the extreme ends of the raft. The rotation was calculated using the differential settlement and dimension of the raft. Similar to the vertical settlement response, for the LE soil model, a linearly increasing trend of the horizontal displacement, differential settlement, and rotation were observed with increasing load. While for the DP soil model, a nonlinear settlement and rotation responses were observed. For all the loads, the DP model resulted in higher settlement and rotation compared to the LE model. At the end, the loading, the piled-raft model with the LE soil model resulted in a horizontal displacement of 5.64 mm, differential settlement of 23.05 mm, and the rotation of 0.18°. On the other hand, the piled-raft model with the DP soil model resulted in a horizontal displacement of 7.29 mm, differential settlement of 26.00 mm, and the rotation of 0.20°. The difference between the horizontal displacement due to the LE and DP model at the design horizontal load of 2.26 MN is found to be 1.65 mm and the difference in the differential settlement at the design bending moment of 144.89 MNm is found to be 2.95

mm. Similar to the case of the vertical load-settlement curve, this difference will not be the same for other loads due to nonlinear DP model.

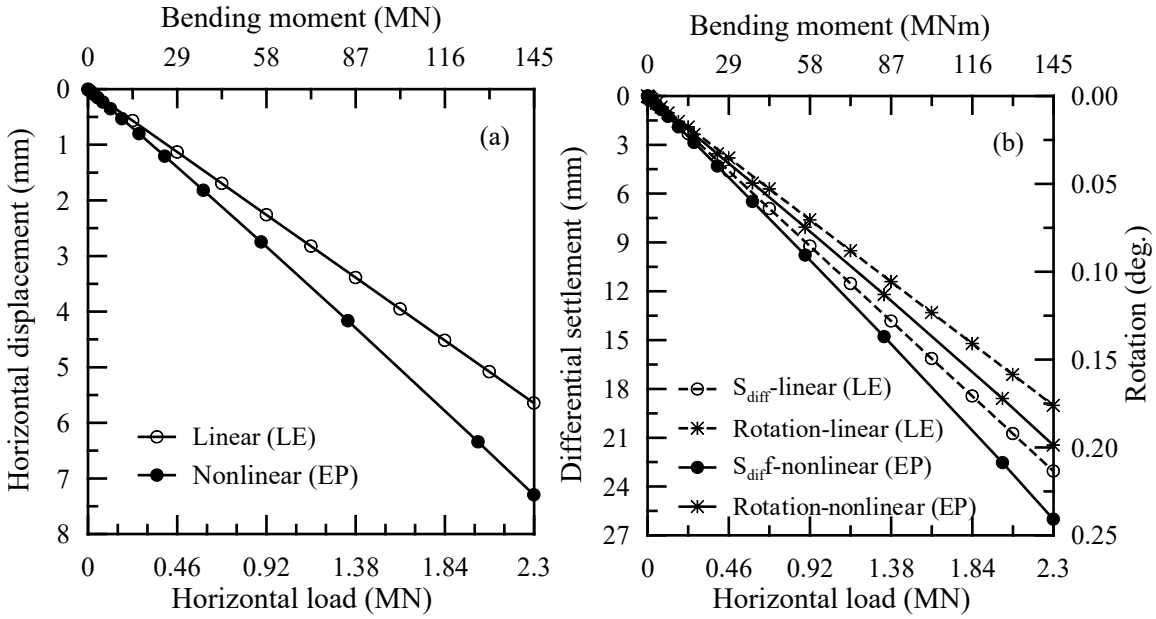

Figure 5.8. (a) Horizontal displacement response and (b) differential settlement and rotation responses of the piled-raft foundation from ABAQUS

5.8 Comparison of analytical and Finite Element Simulation results

It was observed in the analytical design that the serviceability requirements control the final design of the piled-raft foundation. Hence, the serviceability requirements such as the vertical settlement, horizontal displacement, differential settlement, and the rotation of the piled-raft foundation for the design loads obtained from the analytical design method and finite element simulation were compared. In addition, the results obtained with the LE and DP soil models were compared. The comparison between them is presented in Table 5.3. In Table 5.3, the results for both linear and nonlinear soil models are presented for both methods. The linear response for the vertical settlement obtained from the analytical

method was determined by performing the vertical settlement analysis without hyperbolic factors, i.e. entering $R_{fr} = R_{fp} = 0$ in Equation 5.2 and the nonlinear response was obtained by entering $R_{fr} = 0.9$ and $R_{fp} = 0.2$ in Equation 5.2. The analytical method presented in this study to calculate the differential settlement, rotation, and horizontal displacement do not consider the nonlinear soil response. Therefore, these values are not presented in Table 5.3. Further, the linear response from the finite element simulation was obtained by using the LE soil model and the nonlinear response was obtained by using the elastoplastic DP soil model. It should be noted that the vertical settlements for both methods shown in Table 5.3 are due to the vertical load only.

Table 5.3. Comparison between the analytical method and FEM results

Method	Vertical settlement (mm)		Differential settlement (mm)		Rotation (deg.)		Horizontal displacement (mm)	
	Linear	Non-linear	Linear	Non-linear	Linear	Non-linear	Linear	Non-linear
Analytical	40.00	41.90	10.55	-	0.04	-	7.10	-
ABAQUS	22.67	25.44	23.05	26.00	0.18	0.20	5.64	7.29
ABAQUS/ Analytical	0.57	0.61	2.18	-	4.5	-	0.79	-

It was observed that the finite element simulation with the LE soil model under-predicts the vertical settlement by 43.33 % and with the elastoplastic DP soil model under-predicts the vertical settlement by 39.28 % compared to the analytical method. The horizontal displacement with the LE soil model was also underpredicted by the finite element model by 20.56 %. On the other hand, the finite element predictions resulted in 118.48 % and 350.00 % higher differential settlement and rotation compared to the analytical results, respectively. It can be observed in Table 5.3 that the predictions with the LE soil model are always smaller than that of with the elastoplastic DP model.

Further, the vertical load-settlement responses obtained from the analytical (with and without hyperbolic factor) and finite element methods (with LE and DP soil models) at different vertical loads were compared and presented in Figure 5.9. The same dimensions of the piled-raft foundation were used to perform this analysis. It can be observed that the vertical settlement obtained using the analytical method without the hyperbolic factor is lower compared to that obtained using the hyperbolic factor. However, the difference is almost negligible for lower vertical loads and increases with the increase in load. Moreover, it can also be observed that the vertical load-settlement curve from the analytical method without the hyperbolic factor is linear unlike the one with the hyperbolic factor which is nonlinear. Hence it can be concluded that the hyperbolic factor may be contributing to the nonlinear plastic deformation at the higher vertical loads. The vertical load-settlement curves obtained from the finite element simulation are also plotted in Figure 5.9. It can be observed that while using the LE soil model, the finite element simulation resulted in a linear load-settlement curve while the use of the DP soil model resulted in a nonlinear response. When using the DP soil model, the gradient of the vertical-load settlement curve increased as the vertical load increased. As a result, the difference between the vertical settlements with the LE and DP model changes with the change in load. It can be seen in Figure 5.9 that for lower loads (up to about 40 MN), the LE model result and DP model result is overlapping. This is because, at the lower loads, the LE and DP stress-strain relationship of soil overlaps as shown in Figure 5.4 (a). Moreover, the vertical settlement obtained from the finite element simulation is lower than the analytical solution for both the LE and DP soil models except for the vertical settlement at vertical loads higher than

about 170 MN for the simulation with the DP soil model. For the vertical load higher than 170 MN, the vertical settlement obtained from the ABAQUS simulation with the DP soil model is higher than the analytical solution without the hyperbolic factor.

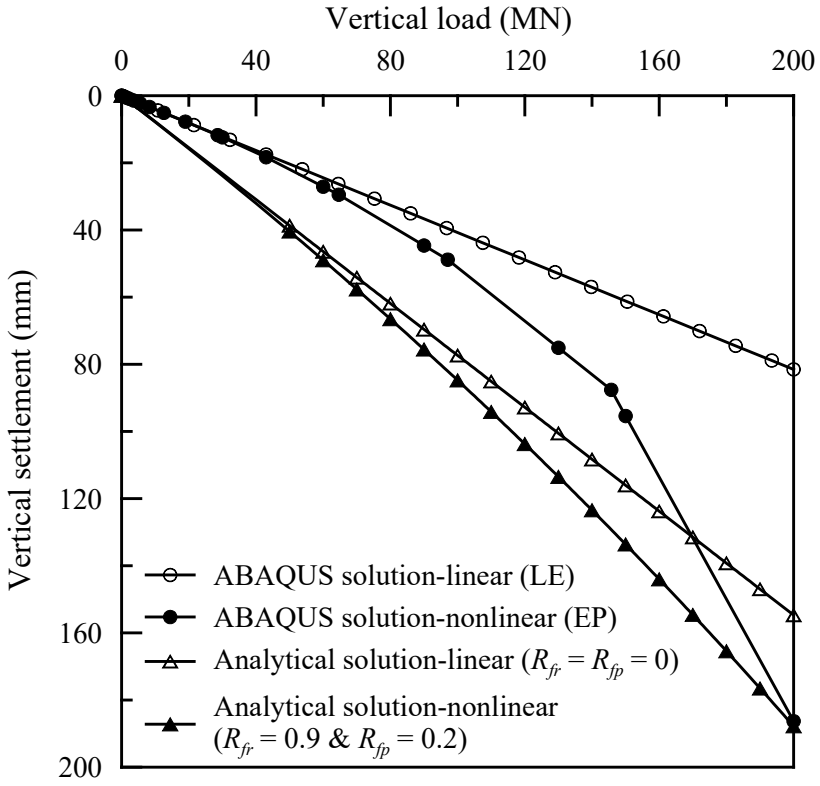

Figure 5.9. Comparison of vertical load-settlement curve from analytical method and ABAQUS

The comparison presented above is for the mean soil properties and load. To investigate the effect of variation in soil properties and loading and to calibrate the finite element model for a range of loading and soil strength and deformation, a parametric study was conducted by considering the variation in undrained cohesion and wind speed and presented in the next section.

5.9 Effect of wind speed and undrained cohesion on the predicted responses

The wind turbine is constructed in groups in a wind farm which extends over a large area. Hence, there will be a variation in soil strength parameter (undrained cohesion and corresponding modulus) and wind speed. The difference between the analytical result and the finite element simulation may not always be the same when the undrained cohesion and the wind speed change. Therefore, a parametric study was conducted to examine the effect of varying undrained cohesion and wind speed on the differential settlement over the wide range so that the accurate conclusion can be made. For this purpose, the mean design (length of pile, radius of raft, and number of piles) of piled-raft foundation for mean undrained cohesion and loading was used. The piled-raft foundation with the mean design was analyzed analytically and numerically for the range of undrained cohesion and wind speed. The undrained cohesion was varied between 40 kPa and 160 kPa at the interval of 20 kPa which fairly covers the clay with medium to very stiff consistency. Since the variation of the undrained cohesion affects the modulus of elasticity of the soil, the correlation between modulus of elasticity and the undrained cohesion obtained from the USACE (1990) was used to determine the corresponding modulus of elasticity for different undrained cohesion. Similarly, the wind speed was varied between 114.3 km/h and 288.2 km/h at the interval of 28.98 km/h. This range of wind speed covers the survival wind speed and all the category of hurricane. The corresponding design loads (horizontal load and bending moment) were calculated for each case of wind speed.

5.9.1 Effects of undrained cohesion on the predicted response

The piled-raft foundation designed considering the mean wind speed and undrained cohesion (N_p = 44, L_p = 28m and R_r = 7.5 m) was used for investigating the effect of undrained cohesion. The finite element simulations were conducted by varying the undrained cohesion of the soil while keeping the wind speed at its mean value. The variation of the differential settlement obtained from the analytical method and the finite element method (with LE and DP soil models) are plotted in Figure 5.10 (a). The dispersion of the ratio of the differential settlement obtained from the finite element simulation and the analytical solution from the linear line ($x = y$ line) and the linear best fit line for the dispersion are plotted in Figure 5.10 (b). For the range of undrained cohesion considered, the differential settlement obtained from ABAQUS with the DP soil model was found to be higher than that obtained from ABAQUS with the LE soil model. However, the difference in the differential settlements obtained from the LE and DP soil models small when the undrained cohesion is between 120 kPa to 160 kPa. The difference seems to increase when the undrained cohesion is between 60 kPa to 120 kPa. It can be seen in Figures 5.10 (a) and (b) that the differential settlement obtained from ABAQUS with LE and DP soil models is higher for the stronger/stiffer soil (c_u > 80 kPa) than that of the analytical method. However, for the weaker/softer soil (c_u = 60 kPa), the result was the opposite. From Figure 5.10 (b), it can be seen that the difference between the differential settlements obtained from the two methods increase when the undrained cohesion is decreasing from the highest value. But for the undrained cohesion of 60 kPa, the opposite trend is observed (ABAQUS result < analytical solution) and the difference is smaller. This

could be because for the undrained cohesion of 60 kPa, the single pile capacity is reduced by 1.2 times compared to the capacity at 80 kPa that will result in significant reduction in capacity for the piled-raft in which there are 44 piles. This reduction in pile capacity results in a sudden increase in the differential settlement. Further, it can be noticed in Figures 5.10 (a) and (b) that the results for the undrained cohesion of 40 kPa is not present. This is because, while calculating the differential settlement using the analytical method, the settlement fell into the failure zone. As a result, it was not possible to calculate the differential settlement from the analytical method. Therefore, the differential settlement obtained from ABAQUS for the undrained cohesion of 40 kPa (which is 55.37 mm for LE model and 70.15 mm for DP model) was not presented as well.

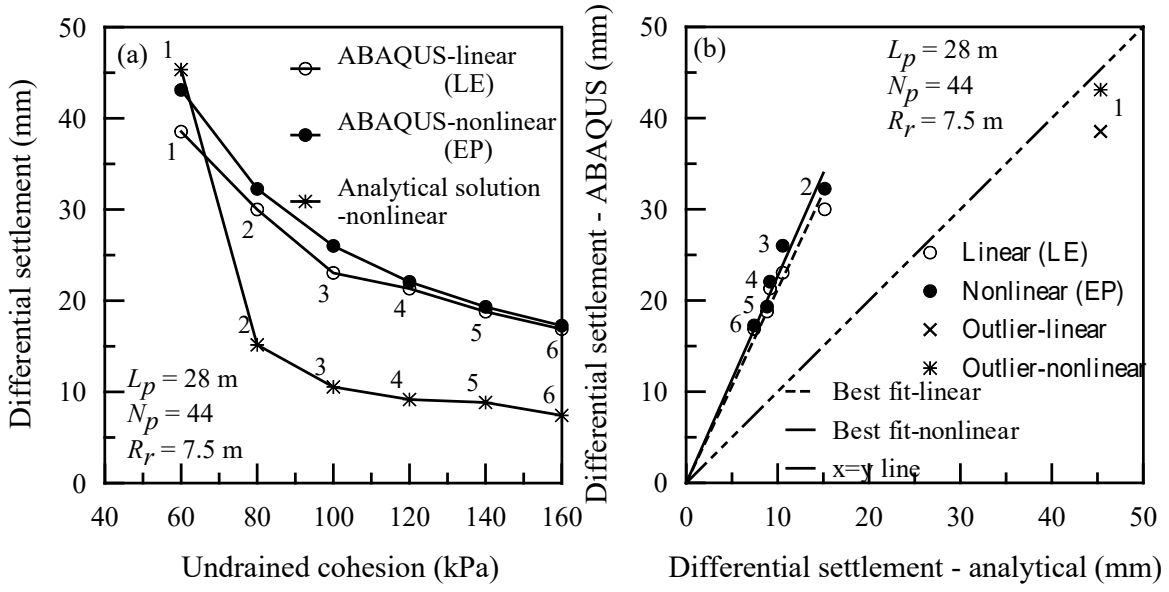

*Note: 1: 60 kPa, 2: 80 kPa, 3: 100 kPa (mean), 4: 120 kPa, 5: 140 kPa, 6: 160 kPa

Figure 5.10. Effect of undrained cohesion on differential settlement (a) comparison between analytical and ABAQUS results and (b) dispersion around $S_{diff\text{-}analytical} = S_{diff\text{-}ABAQUS}$ line

5.9.2 Effect of wind speed on the predicted response

The effects of variation in wind speed on the differential settlements obtained by keeping the undrained cohesion at its mean value from the analytical procedure and ABAQUS (with LE and DP soil models) are plotted in Figure 5.11 (a). From the figure, it is observed that the differential settlement is higher for the higher wind speed (i.e. higher lateral loads) and lower for the lower wind speed. The dispersion of the ratio of the differential settlement obtained from the ABAQUS simulation and analytical method from the linear line ($x = y$ line) and the linear best fit line for the dispersion are plotted in Figure 5.11 (b). It can be observed in Figure 5.11 (a) that the differential settlements obtained from the finite element simulation by using the LE and DP soil models are nearly the same up to the wind speed of 143.3 km/h and the difference between them increases when the wind speed increases beyond 143.3 km/h. Further, the differential settlements obtained from the finite element simulation (both LE and DP soil models) for the range of wind speed considered in this study are always higher than that obtained from the analytical method. This observation is consistent with the previous parametric study in which the undrained cohesion was varied while keeping the wind speed at its mean value. However, the difference in the differential settlements obtained from the two methods is not always equal. With the increase in wind speed, the difference in the differential settlements obtained from the two methods slightly increased up to the wind speed of 230.23 km/h and then decreased when the wind speed increased from 230.23 km/h as can be observed in Figure 5.11 (a) and (b). At the wind speed of 259.2 km/h, the finite element simulation results with the LE soil model and analytical method converge. Moreover, a sudden

increase in the differential settlement while increasing the wind speed from 230.2 km/h to 259.2 km/h for the analytical solution can also be observed. This could be because for the higher wind speed the load on the pile also increases but the soil strength remains the same. This results in an increase in differential settlement. It can be observed in Figure 5.11 that the differential settlement for the highest wind speed of 288.2 km/h is not presented because similar to the case of the undrained cohesion variation, the analytical solution resulted in an unsafe design for the largest wind speed, i.e. the settlement fell on the failure zone. Hence, it was not possible to calculate the differential settlement from the analytical method for the maximum wind speed. Therefore, the differential settlement obtained from the finite element simulation for the wind speed of 288.2 km/h (which is 50.96 mm for the LE model and 58.95 mm for the DP model) was not presented as well.

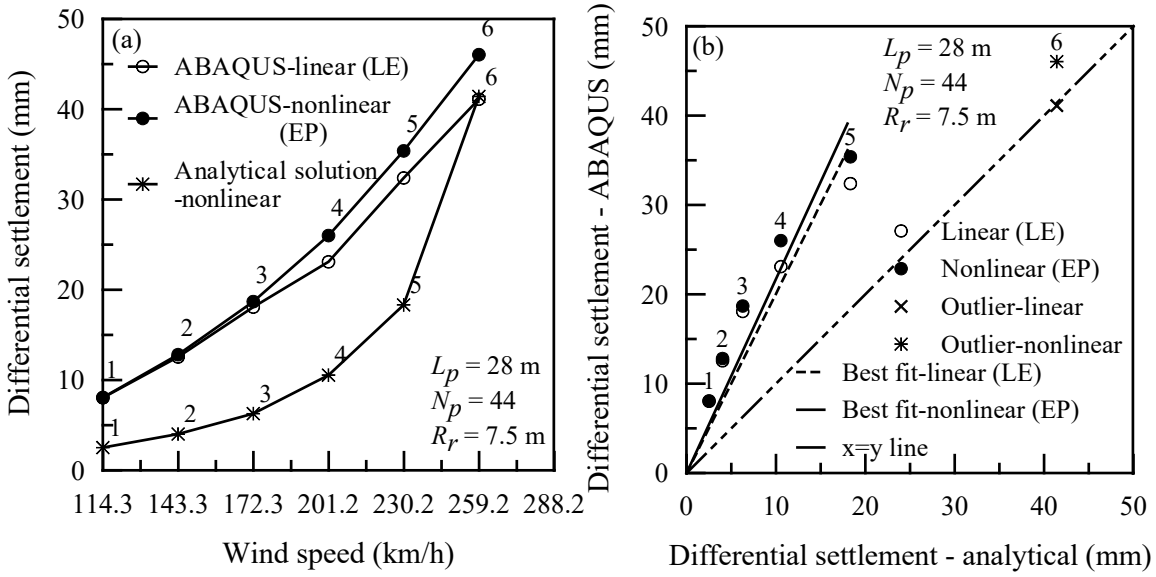

Note: 1: 114.3 km/h, 2: 143.3 km/h, 3: 172.3 km/h, 4: 201.3 km/h (mean), 5: 230.2 km/h, 6: 259.2 km/h

Figure 5.11. Effect of wind speed on differential settlement (a) comparison between analytical and ABAQUS results and (b) dispersion around $S_{diff\text{-}analytical} = S_{diff\text{-}ABAQUS}$ line

5.10 Further investigation of piled-raft foundation using finite element model

The application of the computer software in the analysis of a complex problem has gained popularity with the development of the competent finite element program. For the complex problem in geotechnical engineering involving the soil-structure interaction and the combined loading like the one demonstrated in this study, an experimental analysis is challenging and expensive. A successful experimental study of a piled-raft-soil system under the application of the combined load needs careful pre-experiment planning and resources and yet the results may lack some data for analysis. In such a case, the experimental analysis may be expensive and impractical. An advanced validated/verified finite element model is a valuable tool. It can be used for gaining further insights that could not be possible or is expensive to obtain from an experimental method. The ABAQUS results for the mean design case was used for further investigating the behavior of the piled-raft foundation.

5.10.1 Behavior of critical piles

The piles in the piled-raft foundation under the bending moment are either in tension or in compression depending on the location of the piles and the direction of the moment. Among all the piles in the pile group, the piles located at the extreme edge of the raft along the direction of the bending moment are considered as critical piles in this study because they are under the highest tension or compression force and hence expected to have the minimum or the maximum settlement. The critical piles are shown in Figure 5.12 where piles 1 and 2 are in compression and piles 3 and 4 are in tension.

5.10.1.1 *Vertical deformation of critical piles*

In Figure 5.12, the un-deformed shape and the vertical deformation of the piled-raft foundation (only critical piles) using DP soil model are shown. The other piles were removed for visualization of critical piles only. Figure 5.12 shows that the whole foundation has settled down vertically due to the vertical load and rotated due to the bending moment and horizontal load. A similar response was observed for the LE soil model which is not shown here.

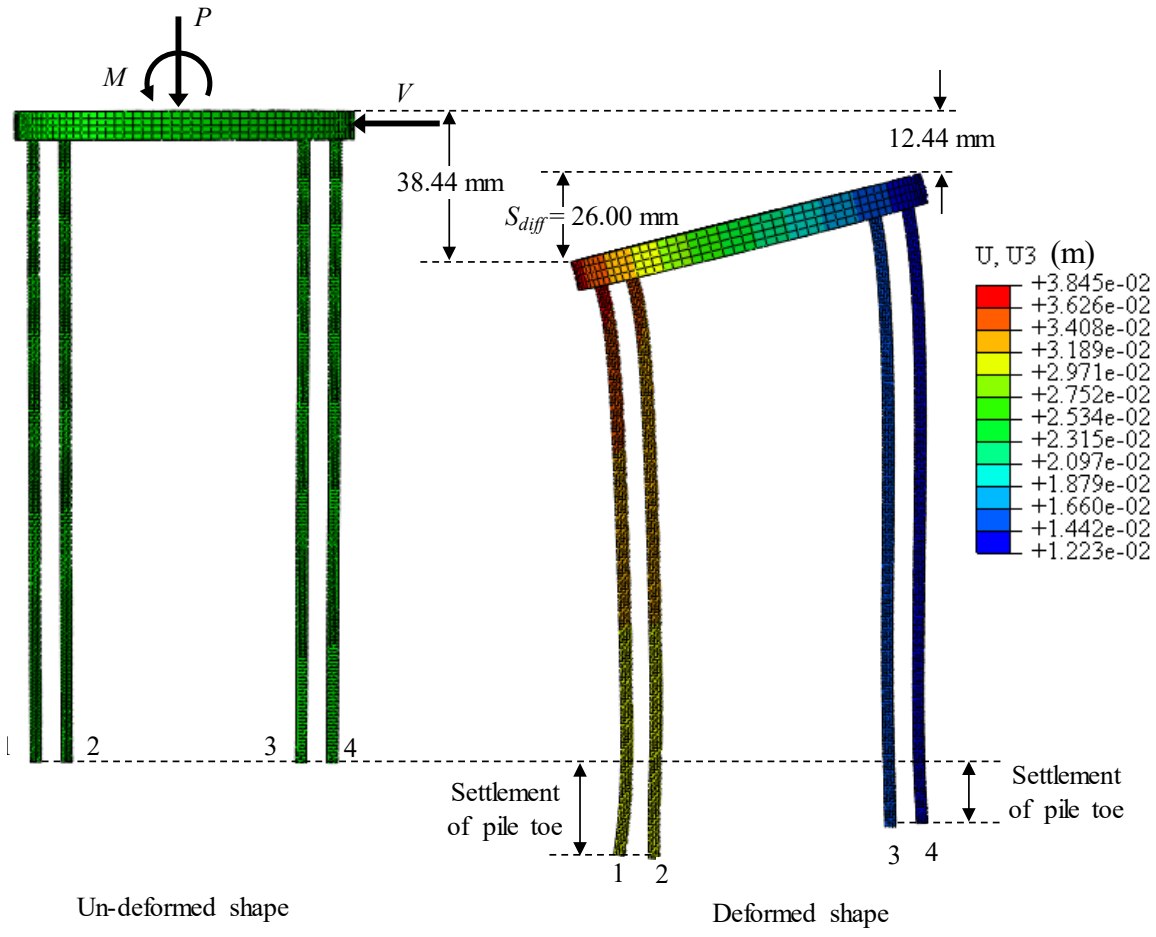

Figure 5.12. Vertical deformation of the critical piles using DP soil model (other piles are removed for visualization purpose; deformation scale factor = 150)

The critical piles can either be compressed or elongated due to the combined action of vertical load, horizontal load and bending moment. To identify if a pile is compressed or elongated, the initial and final lengths of the pile are calculated based on the vertical coordinates of the pile top and tip at the end of the simulation and compared. The results of this analysis using both the LE and DP soil models are given in Table 5.4. It was found that the final lengths of all the critical piles under consideration are smaller than the initial length for both the LE and DP soil models. This indicates that these piles are in compression. The amount by which these piles have compressed are also tabulated in Table 5.4. It was found that for both the LE and DP soil models, pile no. 1 which is the farthest pile from the center of the foundation in the direction of the bending moment has the maximum compression. On the other hand, pile no. 4 which is the farthest pile from the center of the foundation opposite to the direction of the bending moment has the minimum compression. Further, piles no. 2 and 3 have the compression between the maximum and the minimum values. Hence it can be interpreted that the compression of all the other piles in between decrease from pile no. 1 to pile no. 4. Moreover, it can be observed that the use of DP soil model resulted in lower compression compared to the LE soil model. This result can be used to analyze the structural safety of the pile. For instance, it can be determined if the pile will still be intact when compressed or elongated by a certain amount.

Table 5.4. The final condition of critical piles

Pile no.*	Initial length (mm)	Linear elastic model		Drucker-Prager model	
		Final length (mm)	Compressed by (mm)	Final length (mm)	Compressed by (mm)
1	28000.0	27993.4	6.6	27993.62	6.38
2		27996.2	3.8	27996.35	3.65
3		27999.0	1.0	27999.16	0.84
4		27999.4	0.6	27999.68	0.32

Note: *Refer to Figure 5.12 for pile no.

5.10.1.2 Separation and slip study between soil and pile

Furthermore, the separation and slip of the pile from the soil were also investigated. Since piles no. 1 and 4 have the maximum and the minimum settlement, respectively, they were taken as the sample to study the slip and separation at the soil-pile interface. Three locations were selected along the length of the pile to calculate the relative movement as shown in Figure 5.13. These nodes lie on the cross-section of the pile. The common nodes to pile and soil are numbered from 1 to 8 on the left and 1′ to 8′ on the right at various locations along the length of pile. Nodes 1 to 3 and 1′ to 3′ are near the top of the pile, nodes 4 to 5 and 4′ to 5′ are around the middle of the pile, and nodes 6 to 8 and 6′ and 8′ are near the bottom of the pile.

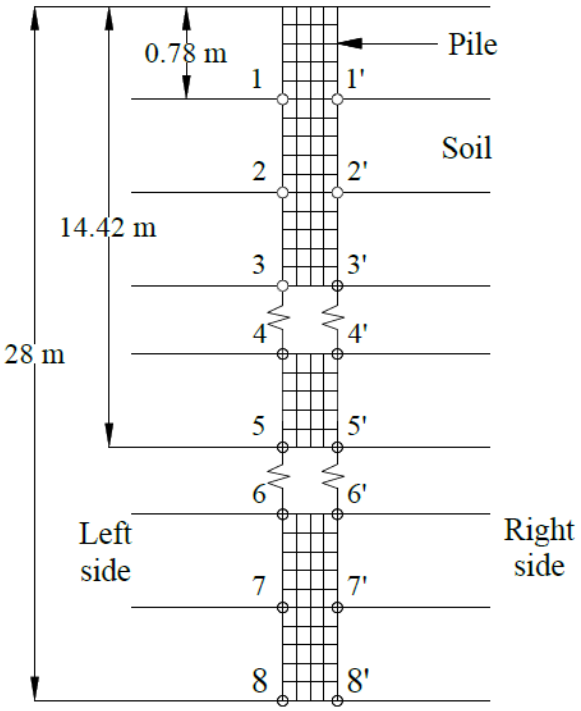

Figure 5.13. Nodes defined for pile for slip and separation study

The slip and separation were calculated as the difference between the initial and final coordinates in the vertical and horizontal directions, respectively. The separation and slip values calculated from the finite element simulation with the LE and DP soil models are presented in Table 5.5. Similar results were observed in both cases (LE and DP soil models) except for no slip at all on the right-side nodes while using the DP soil model. It was found that for pile no. 1 there is a separation and slip near the top on both sides (except node 3 and 1' for LE model where no slip is observed) while middle section has no slip and separation except for node 5 with the LE soil model. Similarly, no slip was observed near the bottom of the piles except at node 6. While a separation of 0.01 mm was observed at nodes 6, 6', and 7' with the LE soil model and at node 7 with the DP soil model. For pile no. 4, a separation was observed at upper three nodes for both the LE and DP soil models

and a slip was observed at nodes 1, 2, 3 with both the LE and DP soil models (except node 3 with DP soil model) and at node 1' with the LE soil model. For other nodes at the middle and bottom parts, the separation and slip were not observed except at nodes 6 and 6' with the DP soil model where a negligible separation was observed. For both the piles, the maximum observed separation and slip is 0.02 mm for the LE soil model and 0.03 mm and 0.05 mm, respectively for the DP soil model. In summary, separation and slip were observed near the top of the pile while the bottom portion didn't exhibit any separation or slip. The separation and slip have the tendency to decrease the pile capacity. Nevertheless, it can be predicted that there was no significant reduction in the pile capacity during the simulation because the separation and slip were negligible, and no unusual deformation was observed around the pile at the end of the simulation.

Table 5.5. Separation and slip of the critical piles (piles 1 and 4)

Pile no.*	Node**	Separation (mm)		Slip (mm)		Node**	Separation (mm)		Slip (mm)	
		LE	DP	LE	DP		LE	DP	LE	DP
1	1	0.02	0.03	0.01	0.05	1'	0.01	0.01	0	0
	2	0.02	0.02	0.01	0.01	2'	0.02	0.03	0.01	0
	3	0.01	0.01	0	0.01	3'	0.01	0.01	0.01	0
	4	0	0	0	0	4'	0	0	0	0
	5	0.01	0	0	0	5'	0	0	0	0
	6	0.01	0.01	0	0	6'	0.01	0.01	0	0
	7	0	0.01	0	0	7'	0.01	0.01	0	0
	8	0	0	0	0	8'	0	0	0	0
4	1	0.01	0.01	0.02	0.02	1'	0.02	0.01	0.01	0
	2	0.02	0.02	0.01	0.01	2'	0.01	0.01	0	0
	3	0.01	0.01	0.01	0	3'	0.01	0.01	0	0
	4	0	0	0	0	4'	0	0.01	0	0

Table 5.5 (Cont.)

4	5	0	0	0	0	5'	0	0	0	0
	6	0	0.01	0	0	6'	0	0.01	0	0
	7	0	0	0	0	7'	0	0	0	0
	8	0	0	0	0	8'	0	0	0	0

Note: *Refer to Figure 5.12 for pile no.
**Refer to Figure 5.13 for node no.

5.10.2 Surface manifestation around the foundation

Several views of the deformed shape of the piled-raft foundation and surrounding soil obtained from the finite element simulation with the elastoplastic constitutive model are shown in Figure 5.14. From the figure, it can be seen that the system is settling down due to the vertical load and rotating due to lateral loads. A similar deformed shape was observed from the finite element simulation with the LE soil model which is not shown here.

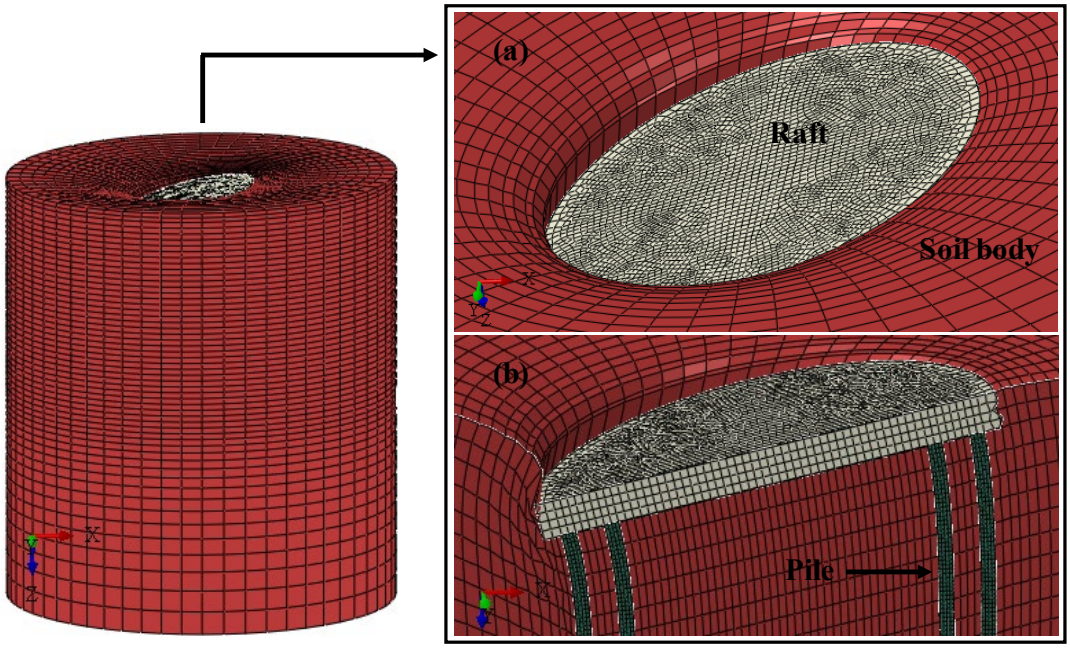

Figure 5.14. Surface manifestation at the ground surface for DP soil model (a) top view and (b) cross-section

5.10.3 Contribution of raft and piles in the settlement response of piled-raft foundation

The major drawback in the currently available analytical design of the piled-raft foundation is that the load sharing between the raft and piles can't be calculated. The determination of the load sharing between the raft and piles is complicated because the raft and pile capacities are mobilized at different settlements. The fact that the pile tip and pile head capacity are mobilized at different settlements, makes the determination of load sharing more complicated. If the load shared between the raft and piles was computable, then the raft and piles could be designed as a separate component to resist the shared load. This paper presents the use of validated sophisticated finite element model to determine the contribution of raft and piles in carrying the vertical load, horizontal load, and bending moment. To conduct this study, the computer models of pile group only and raft only with the same dimension as the mean design were created and then the vertical load up-to 150 MN, lateral load up-to 7 MN, and bending moment up-to 250 MNm were applied (one load at a time, not combined load). In the case with only piles, the pile head was fixed replicating the pile head connection. The piled-raft foundation was also subjected to the same loads (one load at a time). Then settlement responses (vertical, lateral, and differential settlements) of the individual components and the piled-raft foundation using LE and DP models were studied to understand the contribution of each component in the piled-raft foundation.

5.10.3.1 Vertical load-settlement responses of pile, raft, and piled-raft

The vertical load-settlement responses of the three models (raft only, piles only, and piled-raft) obtained from ABAQUS using LE and DP soil models are plotted in Figure

5.15. The foundations with LE model for soil resulted in a linear load-settlement response while the foundations with DP model for soil resulted in a nonlinear load-settlement response. In Figure 5.15 (b), the load-settlement curve for the raft shows that the maximum vertical load is 90 MN. The curve was intentionally cut up to that point because the vertical settlement of the raft with DP soil model at 150 MN was computed to be 29,539.06 mm, which is extremely high to include in the plot. With no doubt, the vertical settlement obtained for the piled-raft foundation was the lowest of three cases for both LE and DP soil models followed by piles and raft foundation. The raft being load bearing component and the piles being settlement reducing component clearly justify why the raft resulted in higher settlement than the piles. At the vertical load of 90 MN, the vertical settlements observed in the pile-raft, piles, and raft using LE soil model were 36.69 mm (S_{PR}), 42.83 mm (S_P), and 89.93 mm (S_R), respectively as shown in Figure 5.15 (a). This indicates that the addition of raft to the piles contributed to the reduction of settlement by 14.4 % while the addition of piles to the raft contributed to the reduction of settlement by 59.2 %. This result is also true for other vertical loads shown in Figure 5.15 (a). On the other hand, at the same vertical load of 90 MN with DP soil model, the vertical settlements observed in piled-raft, piles, and raft were 44.64 mm, 52.45 mm, and 298.23 mm respectively. This indicates that while using DP constitutive model for soil, the addition of raft to the piles contributed to 14.89 % reduction in the settlement while the addition of piles to the raft contributed in 85.03 % reduction in the settlement. However, the percentage reduction in the settlement is not the same for other loads like in the case of LE soil model due to nonlinear load-settlement curve. By studying the result with both LE and DP soil models, it can be concluded that

the piles have a higher contribution in reducing vertical settlement (also differential settlement) compared to the raft. The investigation of the deformed shapes of the three foundations at the end of vertical loading also didn't show an unusual pattern.

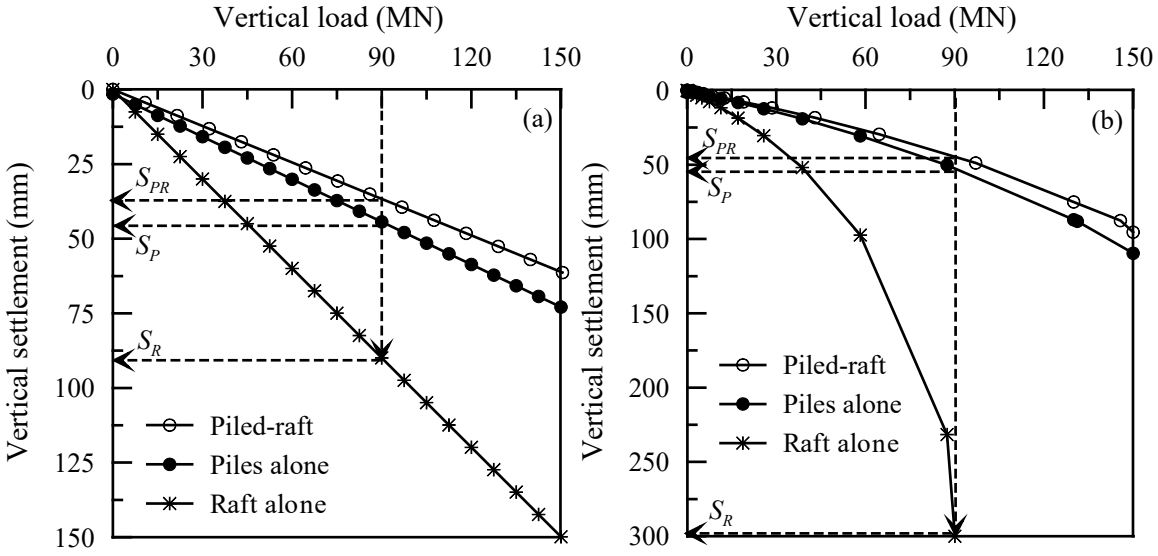

Figure 5.15. The vertical load-settlement responses of piled-raft, piles, and raft with (a) LE model and (b) DP model

5.10.3.2 Horizontal load-settlement/displacement responses of pile, raft, and piled-raft

The horizontal load-displacement responses of the three models (raft only, piles only, and piled-raft) obtained from ABAQUS using LE and DP soil models are plotted in Figure 5.16 (a) and (b), respectively. Similar to the vertical load-settlement plot, a linear load-settlement response was observed in the case of LE soil model and a nonlinear load-settlement response was observed in the case of DP soil model. It can be seen in Figure 5.16 that the piled-raft foundation exhibited the lowest horizontal displacement followed by raft and piles foundations. At the horizontal load of 5 MN, the horizontal displacements observed in the piled-raft, piles, and raft were 5.30 mm ($S_{lat\text{-}PR}$), 6.62 mm ($S_{lat\text{-}P}$), and 5.98 mm ($S_{lat\text{-}R}$), respectively in the case of LE soil model. This indicates that the addition of

raft to the piles contributed to 20 % reduction in the horizontal displacement while the addition of piles to the raft contributed to 11.4 % reduction in the horizontal displacement. This result is also true for other horizontal loads shown in Figure 5.16. At the same horizontal load of 5 MN, the horizontal displacements observed in the piled-raft, piles, and raft while using the DP soil model were 5.77 mm, 6.87 mm, and 6.69 mm, respectively. This indicates that while using the DP soil model, the addition of raft to the piles resulted in 15.92 % reduction in the horizontal displacement and the addition of piles to the raft resulted in 13.72 % reduction. However, the percentage reduction in the horizontal displacement is not the same for other loads due to the nonlinear settlement curve. Thus, based on the observations of the results with the LE and DP constitutive models for the soil, it can be concluded that the raft has a higher contribution in reducing horizontal settlement compared to the piles.

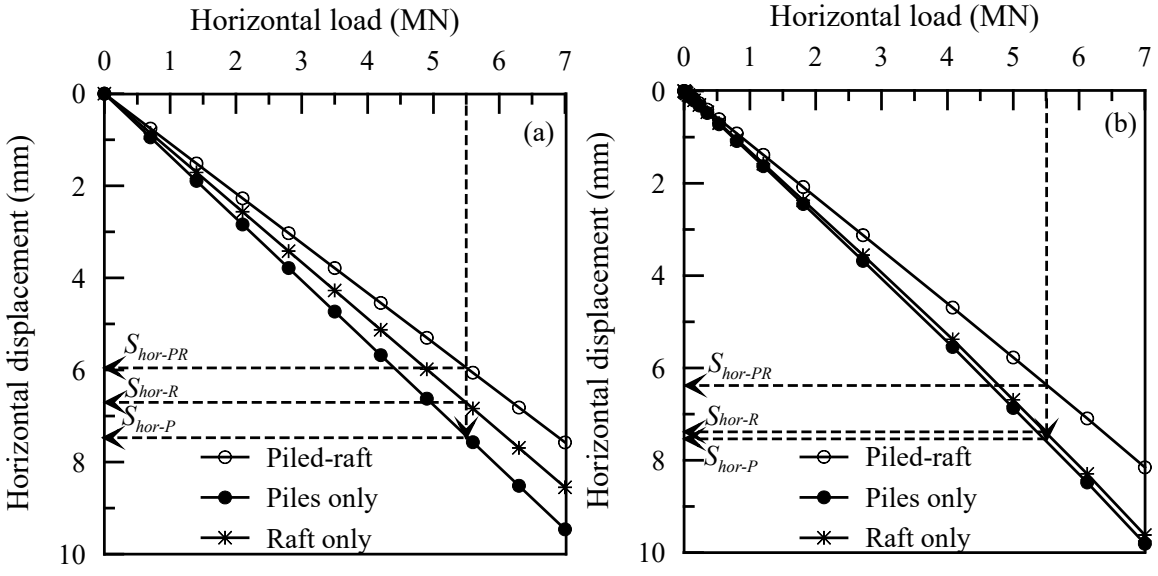

Figure 5.16. The horizontal load-displacement responses of piled-raft, raft, and piles with (a) LE model and (b) DP model

5.10.3.3 Bending moment-differential settlement responses of pile, raft, and piled-raft

The bending moment-differential settlement responses of the three computer models of raft only, piles only, and piled-raft foundations with the LE and DP soil constitutive models are shown in Figure 5.17 (a) and (b), respectively. Similar to the previous load-settlement responses, a linear response is observed for this case as well while using the LE soil model and a nonlinear response is observed while using the elastoplastic DP soil model. In Figure 5.17 (b), the load-settlement curve for the raft shows that the maximum bending moment is 175 MNm. Similar to the case with vertical load, the curve was intentionally cut up to that point because the differential settlement of the raft with the DP soil model at 250 MNm was computed to be 599.97 mm, which is very high to include in the plot. The raft foundation is exhibiting the highest differential settlement of all the three foundations. It is interesting to observe that the differential settlement computed for the piled-raft foundation is slightly higher than the differential settlement computed for the piles only for both LE and DP soil model. This observation elucidates that the addition of raft to the piles is not contributing to reducing the differential settlement and piles are the only contributing factor in controlling the differential settlement in the piled-raft foundation. Nevertheless, it should be noted that the method of the application of bending moment may also affect the result. For instance, in the piled-raft foundation, the bending moment was applied as a concentrated bending moment acting at the center of the raft which was transferred to the raft and piles by using the MPC bean constraint. While in the pile group, the vertical load induced due to the bending moment on each pile was

calculated and applied as couples. These couple forces acting on the piles would provide the same bending moment. Further, in the case of piles only, the pile cap was not included while in the case of piled-raft foundation, the raft was included in the simulation. For a bending moment of 150 MNm, both the piled-raft and piles are exhibiting a differential settlement of about 22.30 mm ($S_{diff\text{-}PR/P}$) and the raft is exhibiting a differential settlement of 75 mm ($S_{diff\text{-}R}$) while using the LE soil model. In this case, the addition of the piles to the raft resulted in 70 % reduction in the differential settlement which is also true for other load cases. At the same bending moment value, with DP soil model, both the piled-raft and piles are exhibiting a differential settlement of about 23.06 mm ($S_{diff\text{-}PR/P}$) and the raft is exhibiting a differential settlement of 138.16 mm ($S_{diff\text{-}R}$). In this case, the addition of piles to the raft resulted in 82.78 % reduction in the differential settlement. However, unlike the case with LE soil model, the percentage reduction is not the same for the other load cases while using the DP soil model due to the nonlinear load-settlement curve.

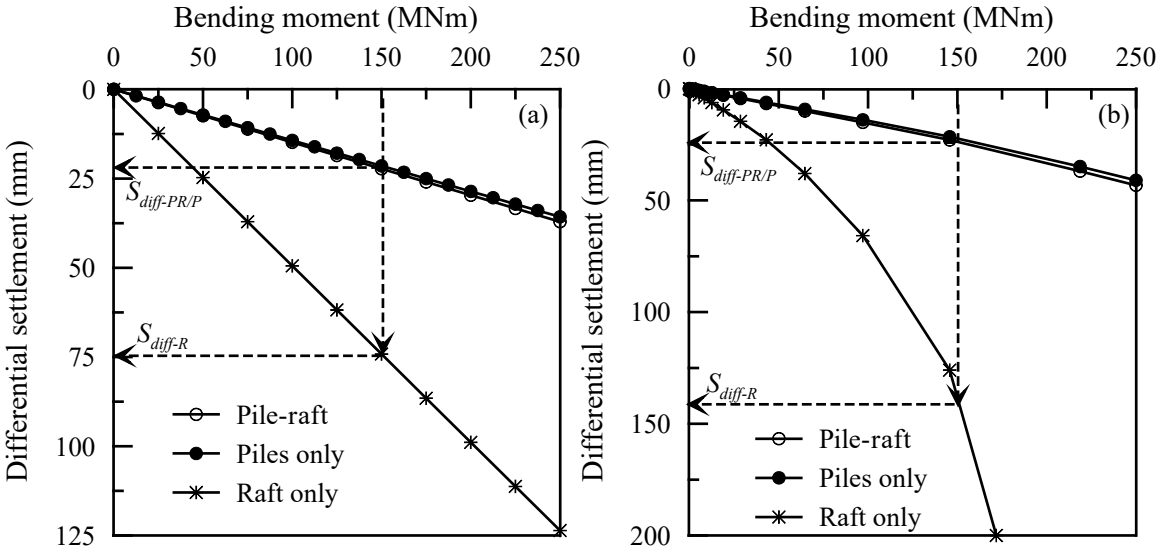

Figure 5.17. The bending moment-differential settlement responses of piled-raft, raft, and piles with (a) LE model and (b) DP model

5.11 Conclusion

In this study, a piled-raft foundation for a tall wind turbine tower in a clayey soil was designed using a simplified analytical method which showed that the differential settlement controlled the final design. The finite element analysis of the piled-raft foundation with both linear elastic (LE) and nonlinear elastoplastic Drucker-Prager (DP) constitutive models for the supporting soil was performed using ABAQUS. The comparison of the serviceability requirements obtained from the two methods for the mean loading and soil condition showed that the analytical method resulted in a higher vertical settlement and horizontal displacement compared to that obtained from ABAQUS with both the soil models. The differential settlement and rotation obtained from the analytical method were found to be lower than that of ABAQUS with both the soil models. Likewise, in the parametric study where the undrained cohesion of the soil and the wind speed were varied one at a time, the differential settlement obtained from the analytical solution was

higher than that of finite element simulation with both LE and DP soil models. However, the result was opposite for the lower undrained cohesion (60 kPa). For all the load cases, the finite element simulation with the DP soil model was predicting higher response compared to the LE soil model. The further investigation of the finite element analysis with the mean soil properties and load indicated that all the piles in the piled-raft foundation are under compression for both LE and DP soil models. The piled-raft foundation with DP soil model resulted in lower compression compared to the one with LE soil model. The amount by which the piles are compressed decreased from the extreme piles in the direction of the bending moment towards the piles in the opposite direction. Such a result can be used to perform the structural stability analysis of the piles. Moreover, it was found that there is insignificant to no slip and separation between the pile and soil with both soil models and hence it can be predicted that there was no significant decrease in pile capacity. Further, the deformation of the ground surface around the raft didn't show any unusual behavior. The investigation of the vertical load carrying capacity of the individual components, i.e. raft and piles showed that there is a higher contribution from piles in reducing the vertical settlement of the piled-raft foundation compared to the raft for both soil models. Similarly, it was found that the raft is contributing more in reducing the horizontal displacement of the piled-raft foundation for both soil models. Furthermore, it was found that only piles are contributing in controlling the differential settlement of the piled-raft foundation.

CHAPTER 6

DEVELOPMENT OF A NEW FOUNDATION FOR TALL STRUCTURES THROUGH BIOMIMICRY – PRELIMINARY STUDIES

6.1 Abstract

The sustainable solutions to many complex human challenges have been inspired by nature's tested strategies and patterns. This study presents the preliminary studies on the development of a new foundation for wind turbine subjected to combined loads (vertical load, horizontal load, and bending moment) through biomimicry. At first, the preliminary study was conducted in which the conventional pile group foundation along with many modified configurations with piles battered at different angles and arranged at different locations were analyzed using GROUP, a foundation engineering software widely used in the industry for designing pile groups. The results showed that the performance of the foundation is affected by the orientation of the piles. Then simplified configurations of new foundation were created with different number and orientation of main root and sub-roots (roots branch out from the main roots). The first model consisted of six main roots inclined at an angle of 20° with the horizontal. The second model consisted of twelve main roots inclined at an angle of 37.5°. The third model consisted of eighteen main roots to the bottom part of the bulb at an angle of 55°. Then two sub-roots were added per main root for each of the previous models. A vertical drilled shaft was placed right at the center of each model which contributes significantly to the vertical load capacity. The results showed that the performance of the foundation under combined vertical load, horizontal load, and

bending moment improved with the increase in the number of main roots. On the other hand, the addition of sub-roots resulted in negligible improvement in the performance of the foundation.

Keywords: finite element analysis, ABAQUS, biomimicry, tree root system

6.2 Introduction

"Nature has inspired humankind for literally hundreds of years before the vertical flight machine we now know as a helicopter became a practical reality," these are the words of Prof. J. Gordon Leishman. Yes, the dragonfly's wings inspired the successful design of helicopter after overcoming many challenges. Similarly, bullet train was inspired from kingfisher's beak, signal transfer under water was inspired from dolphin, the Eastgate Centre (shopping center) was inspired from termite mound to control the temperature naturally inside the building. And there are many more successful and sustainable bio-inspired innovations made by human where the nature's patterns and strategies have provided the solutions to human challenges and this approach is called 'biomimicry'.

Although there are many successful bio-inspired innovations made in other fields, it is a very young area in the field of geotechnical with a huge potential to explored. DeJong et al. (2017) have presented examples of applying bio-inspired concepts in geotechnical engineering. They have demonstrated an example of a tree root system that could be used as a biological analog to design geotechnical engineering foundation and anchorage system. In their study, the tree root system is characterized in terms of physical components (lateral root branches, root tip, and overall root geometry and spacing), their physiological processes, and purpose and importance of each component. Burrall et al. (2018) have

conducted the vertical pullout tests on the rootstock of Lovell, Marianna, and Myrobalan tree species for the bio-inspired foundation idea. They measured the ground displacement, extraction force, and trunk displacement for different tree species. They observed that the root systems formed root-soil blocks while extracted, the sum of individual root capacity had a major contribution to the ultimate capacity, and the uprooting resistance continued to be significant up to a large vertical trunk displacement. However, these studies didn't perform analysis on developing the bio-inspired foundation.

Inspired from such studies, this study focusses on developing potential bio-inspired foundation by mimicking the tree root system. Nature has been demonstrating the mechanism of a tree root system to support the loads on the tree since long time. When the humans are struggling to design the efficient and economical foundation for the structures subjected to a large lateral load, nature, on the other hand, has so many naturally formed reliable and inexpensive foundations successfully flaunting its capability. The tree root system is bearing different loads such as wind, earthquake, and its self-weight without failure. This study is inspired by the tree root system to apply a similar concept to develop a new foundation to support a wind turbine. Preliminary study shows that coconut tree, palmyra tree, date tree, and sabal palm tree as shown in Figure 6.1 have similar components as wind turbine tower. The tower can be represented by the stem of the tree, the weight of generator and nacelle at the top can be represented by the weight of fruit on the top of the tree, and the blades by the branches and leaves as shown in Figure 6.2.

(a) Coconut tree (b) Palmyra tree (c) Sabal palm tree (d) Wind turbine

Figure 6.1. Similarities among tall tree and tall wind turbine

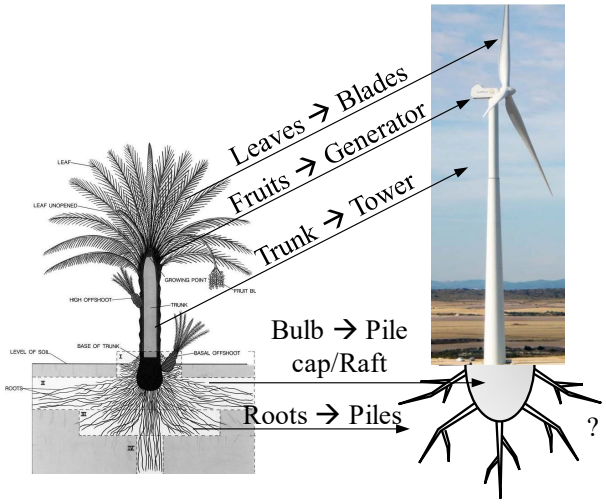

Figure 6.2. Comparison of tree and wind turbine components

A study conducted by the University of Florida revealed that the sabal palm tree exhibited the highest survival rate between 80 % to 100 % among thirty-five species of trees after experiencing hurricanes with wind speed ranging from 130 km/hr to 265 km/hr (Duryea and Kampf, 2017). Therefore, the new foundation configuration presented in this study is inspired by the tree root system of the sabal palm tree as well as a coconut tree, as coconut tree has similar root system as the sabal palm tree.

The primary objective of this study is to conduct a preliminary study to develop a new and effective foundation through biomimicry. In the initial part of this study, the conventional pile group foundation with many modified configurations were analyzed in GROUP. Then the simplified configurations of the new foundation were identified with a different number and orientation of roots. These configurations were analyzed in finite element software ABAQUS.

6.3 Study of tree root system

The first step towards achieving the objective is to carefully study the tree root system. As discussed before, the sabal palm tree has strong roots resilient to high winds. Therefore, the initial configuration is inspired by sabal palm tree root. Its tree root system has an underground short and bulbous stem (termed as a bulb in this study) which is surrounded by a dense mass of contorted roots which commonly has the diameter of 1.2 to 1.5 m and can penetrate to the depth of 4.6 m to 6.1 m. A smaller but tough root develops from this mass which usually has the diameter of 13 mm and can penetrate to the depth of 4.6 m to 6.1 m (Wade and Langdon, 1990). Although there are some ideas on the geometry of tree roots, it is painstaking task to characterize different types of roots (such as main root and sub-root) in term of their physical properties, mechanical properties, and most importantly their purposes. As discussed before, DeJong et al. (2017) characterized tree roots according to only three aspects out of several aspects. The growth of the roots may be in search of nutrition or to ensure stability or sometimes they may divert the direction of growth due to presence of strong soil layer. In this study, an effort is made to identify the level of contribution of different roots in improving the performance of the foundation.

6.4 GROUP analysis

A preliminary study was conducted using a computer-based finite element difference software GROUP. The GROUP analysis allowed for the smooth transition from conventional foundation to the bio-inspired foundation. In this study, a conventional pile group foundation was modified with the use of battered piles. First, the analytical design of the pile group foundation was performed to obtain the initial dimensions of the foundation. Then, the pile orientation and location were changed to obtain many modified designs which are close to the tree root system. A three-dimensional model of all the designs were created in the GROUP and analyzed.

6.4.1 Problem formation

The foundation considered in this study is intended for wind turbine tower of height 130 m subjected to the wind speed of 90 mph. The design loads were calculated using similar method as described in Chapter 2, 3, and 4 of this dissertation. The design vertical load, horizontal load, and bending moment were calculated to be 51.7 MN, 1.2 MN, and 76.3 MNm, respectively. The foundation is assumed to be constructed in a site with multilayered soil as shown in Table 6.1.

Table 6.1. Soil profile

Layer	Depth (m)	Unit weight, γ (kN/m^3)	Undrained cohesion, c_u (kN/m^2)	Friction angle, ϕ (°)	Modulus of elasticity, E (kN/m^2)
Medium dense sand	0-1.22	17.28	-	34	6.00 X 10^4
Soft to firm clay	1.22-9.15	16.5	100	-	3.74 X 10^4
Cooper Marl	> 9.15	19.64	100	-	3.00 X 10^4

6.4.2 Geotechnical design of pile group

The geotechnical design of the pile group was performed using the procedure described in Chapter 4 of this dissertation. The final design resulted in 40 closed-end steel pipe piles of length 30 m. Out of 40 piles, 18 were distributed along the circumference of 5.3 m and 22 were distributed along the circumference of 6.7 m at equal spacing. The pile cap was considered to have a radius of 7.5 m and a thickness of 1.2 m. For this design, the factor of safety for the vertical load capacity (which includes the bending moment) was calculated to be 1.75 and the factor of safety for the horizontal load capacity was calculated to be 17.83. Under the given design loads, this design would result in the horizontal displacement of 4.83 mm and the differential settlement of 7.53 mm. The plan of the pile group foundation is shown in Figure 6.3.

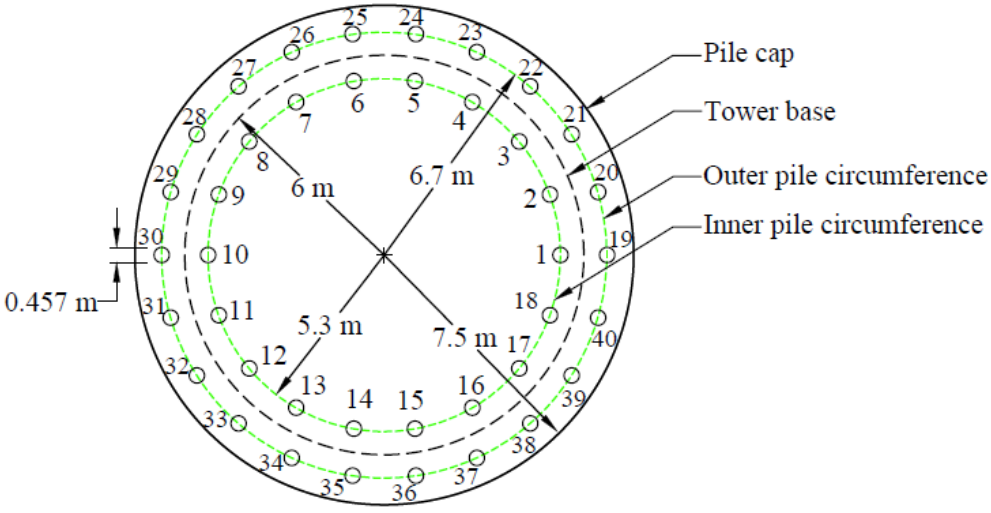

Figure 6.3. Plan view of pile group configurations

6.4.3 Key steps in generation of 3D numerical model in GROUP

While creating a 3D numerical model of the designed pile group foundation in GROUP, first the pile section was defined and pile properties were assigned followed by defining pile head connection. A fixed head connection was used in this study. Then the piles were added by defining the coordinates of the pile head. Next, the design loads were applied in the appropriate direction. The properties shown in Table 6.1 were used to define the soil layers.

6.4.4 Models generated in GROUP

The abovementioned procedure was used to generate a numerical model of designed pile group foundation, i.e., with vertical piles. Since the objective of this study is to mimic the tree root system, additional numerical models of pile group foundation were created by modifying the geometry of the initial pile group foundation. The modification was done by varying the inclination of outer piles with the horizontal plane (β) between 30° to 75° at an interval of 15°. It resulted in overall five models which are listed in Table 6.2.

Table 6.2. Models created in GROUP

Model name	β (°)	
	Inner pile	Outer pile
D1M01	90	90
D1M02	90	75
D1M03	90	60
D1M04	90	45
D1M05	90	30

A 3D view of the pile group models generated in GROUP is shown in Figure 6.4. These models were analyzed and the results are discussed below.

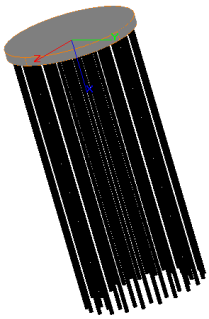

(a) D1M01

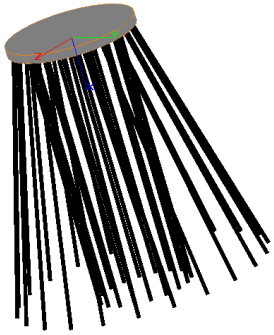

(b) D1M02

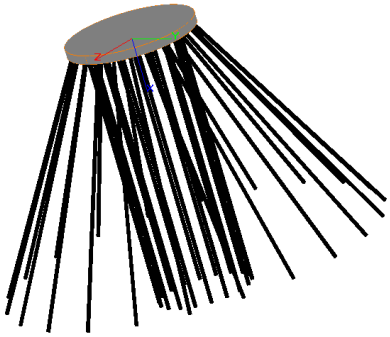

(c) D1M03

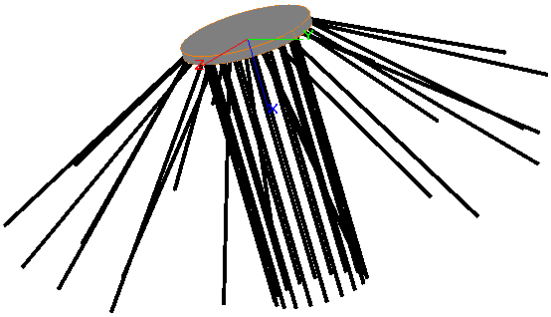

(d) D1M04

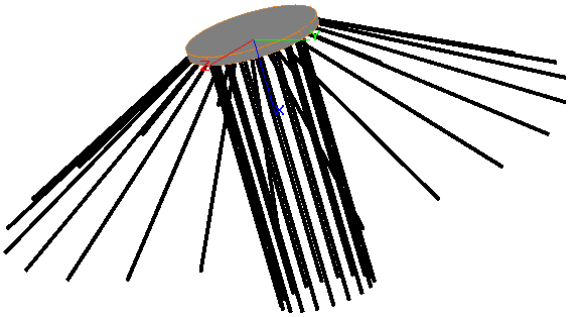

(d) D1M05

Figure 6.4. 3D view of models generated in GROUP

6.4.4.1 Results and discussions

GROUP can provide many results. However, only the relevant results are discussed here such as differential settlement, rotation, stress, axial force, shear force, and bending moment. The differential settlement, maximum rotation, and maximum stress observed in the pile group foundation for the models generated are shown in Figure 6.5 (a), (b), and (c), respectively. Both straight line and smooth curve fitting lines are shown in the figure. It is observed that decreasing the outer pile inclination with the horizontal plane from 90° to 60° resulted in the decrease in differential settlement and rotation. Further decreasing the outer pile inclination from 60° to 30° didn't improve the performance, i.e., the

differential settlement and maximum rotation increased. From this observation, it can be concluded that the pile inclination of 60° is the most effective one for the given loading and soil condition. The maximum stress observed in the pile for different inclinations of the outer pile is presented in Figure 6.5 (c). The pile number at which the maximum stress is observed is also shown in the figure against each data point. For all the configurations, the maximum stress is observed in pile number 19 (see Figure 6.3), which lies along the outer circumference in the direction of bending moment. It is found that the stress is increasing with the decrease in the outer pile inclination.

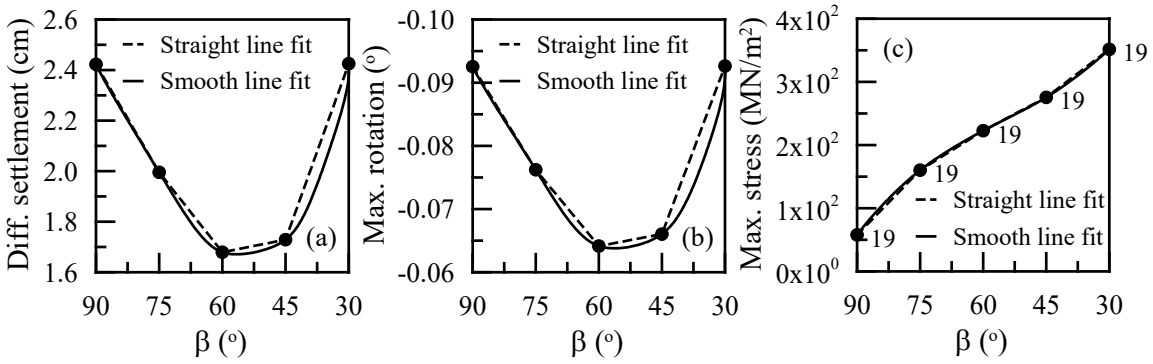

Figure 6.5. (a) Differential settlement, (b) Maximum rotation, and (c) Maximum stress

Further, the maximum axial force (AF), shear force (SF), bending moment (BM) observed in the pile head for pile group foundation with different inclination of the outer pile are plotted in Figure 6.6 (a), (b), and (c), respectively. The pile on which the maximum value is observed is also shown in the figure. The variation of maximum AF shown in Figure 6.6 (a) shows that AF increased when the inclination of the outer pile decreased from 90° to 60° and then started decreasing when the inclination further decreased to 30°. The magnitude of the maximum SF increased with the decrease in the inclination of the outer pile as shown in Figure 6.6 (b). However, the decrease in SF is not signification when

the inclination decreased from 45° to 30°. Further, the maximum BM increased with the decrease in the outer pile inclination as shown in Figure 6.6 (c).

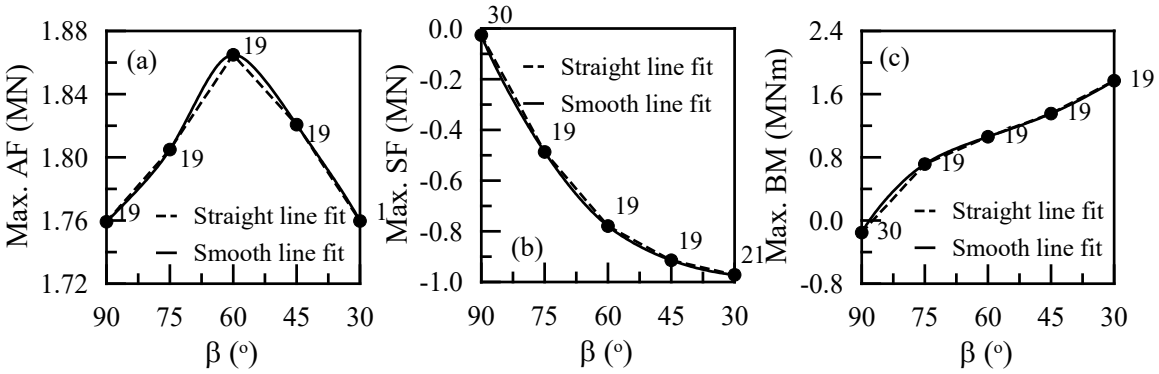

Figure 6.6. (a) Maximum axial force, (b) Maximum shear force, and (c) Maximum bending moment

Further, the variation of the SF and BM along the length of piles for pile number 19 and 30 for different inclination of outer piles are shown in Figure 6.7 and 6.8, respectively. These figures also show the location of the pile and the direction of bending moment applied. Although the length of the pile is 30 m, only the upper 12 m is shown in Figures 6.7 and 6.8 because the SF and BM are zero for the lower portion of the pile. A large variation in SF is observed within the depth of about 9.0 m for all the cases. After about 9.0 m, the SF distribution is the same for all the cases. Further, the magnitude of SF is found to be larger for pile number 19 compared to pile number 30 which is due to the direction of bending moment and lateral load.

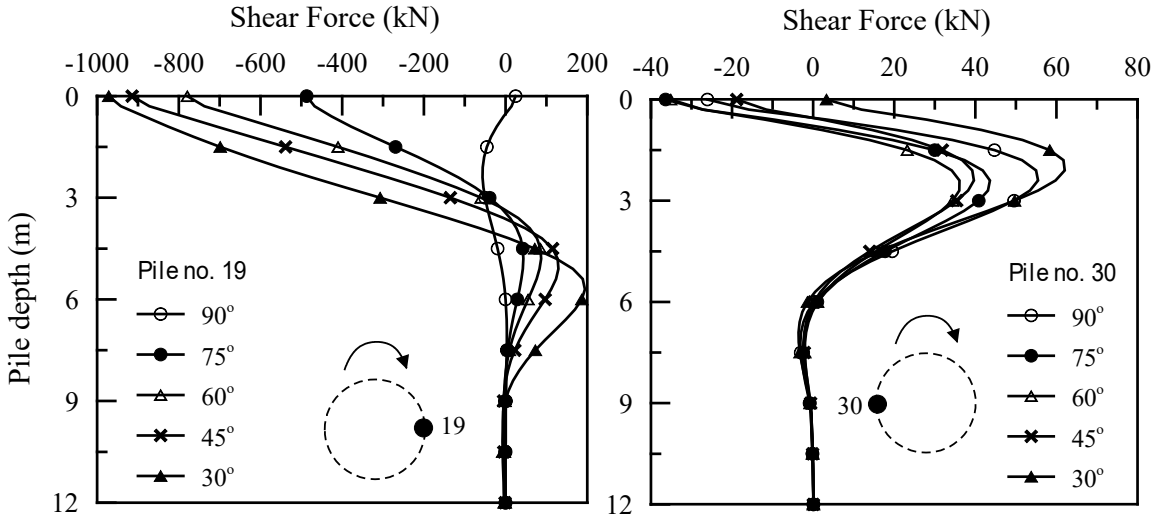

(Note: Actual pile length is 30 m, but only upper 12 m is shown.)

Figure 6.7. Variation of shear force along the length of pile for the extreme piles

Similarly, for the variation of BM along pile 19 and 30 shows larger variation up to the depth of about 7.5 m for all the cases After about 7.5 m, the BM distribution is same for all the cases. Further, the magnitude of BM is larger for pile number 19 compared to pile number 30 which is due to the direction of bending moment and lateral load.

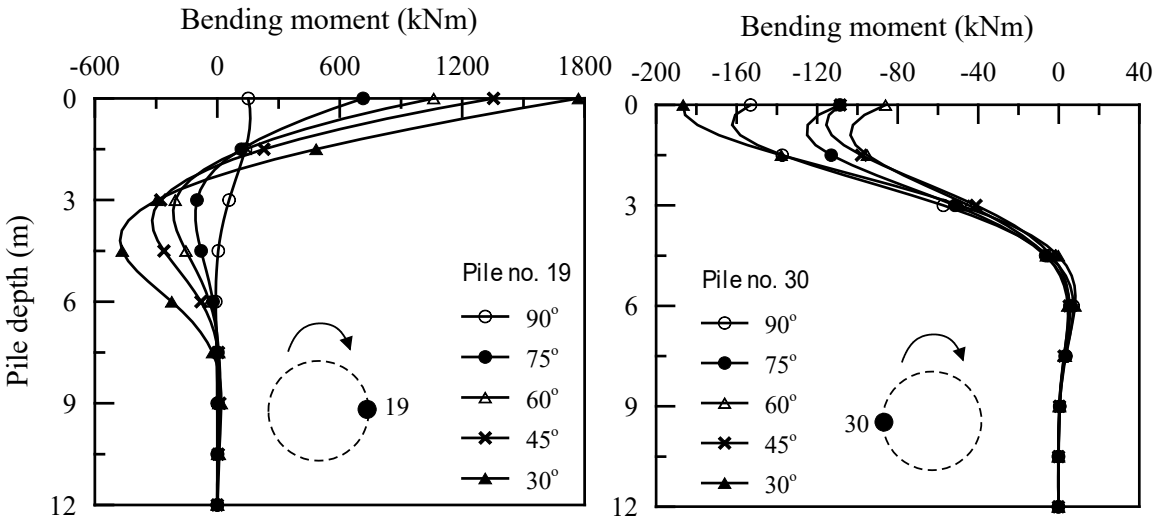

(Note: Actual pile length is 30 m, but only upper 12 m is shown.)

Figure 6.8. Variation of bending moment along the length of pile for the extreme piles

These results provide some idea of how the performance of the foundation can be improved. However, to obtain the foundation that is closer to tree root system and to investigate if there is more efficient configuration, further modification in the pile configuration is required. Hence additional analyses were conducted by further modifying the pile configurations in which piles were reoriented and rearranged along two and three circumferences.

6.4.5 Analysis with modification in the geometry

The pile group foundation with piles arranged along two circumferences was modified by inclining the outer piles alternately at two different angles between 75° and 30°. For example, if pile number 19 (Figure 6.3) is inclined at 75° with the horizontal plane, the next pile, i.e., pile number 20 would be inclined at 60°, then pile number 21 would be at 75° and so on. Following this scheme of modification, additional six models were created with outer piles alternatively inclined at 75°/60°, 75°/45°, 75°/30°, 60°/45°, 60°/30°, and 45°/30° and are listed in Table 6.3.

Table 6.3. Modified models created in GROUP

Model name	β (°)	
	Inner pile	Outer pile (alternate)
D1M06	90	75/60
D1M07	90	75/45
D1M08	90	75/30
D1M09	90	60/45
D1M10	90	60/30
D1M11	90	45/30

A 3D view of the pile group models generated in GROUP is shown in Figure 6.9.

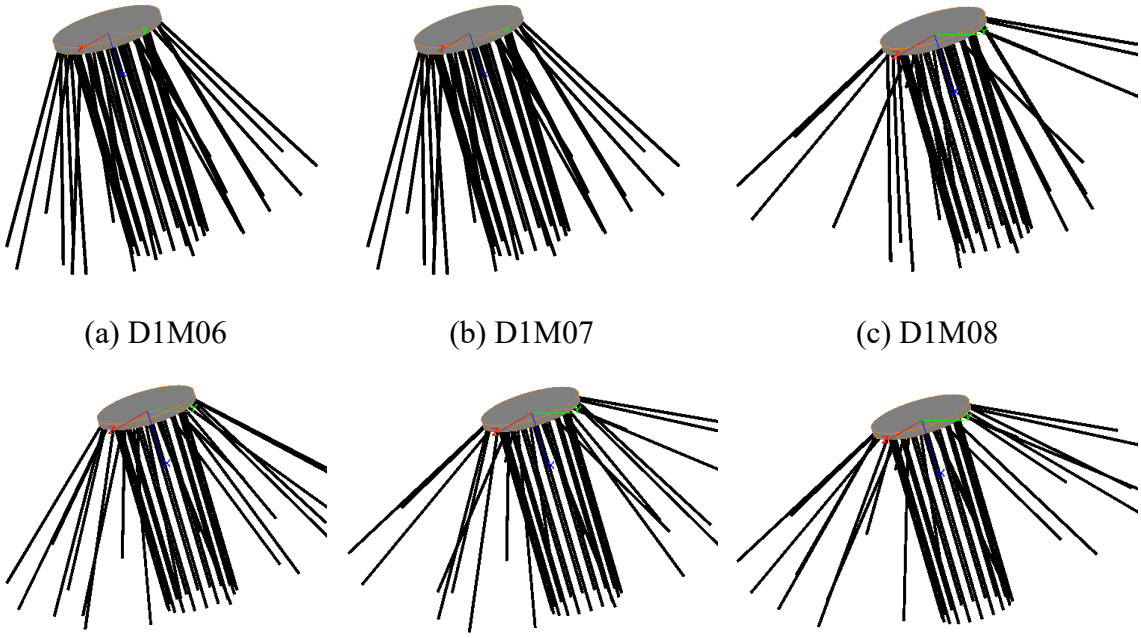

(a) D1M06 (b) D1M07 (c) D1M08

(d) D1M09 (e) D1M10 (f) D1M11

Figure 6.9. 3D view of models with modified configurations generated in GROUP

6.4.5.1 Results and discussions

The maximum settlement, differential settlement, and maximum rotation of the observed in the pile group foundation with the modified orientation are shown in Figure 6.10 (a), (b), and (c), respectively. Both straight line and smooth curve fitting lines are shown in the figure. From Figure 6.10 (a) and (b), it can be seen that the differential settlement and rotation is the lowest for the configuration in which piles inclined alternately at an angle of 60° and 45° with the horizontal plane. Further, the variation of maximum stress induced in the pile for different configuration is plotted in Figure 6.10 (c). For all the configurations, the maximum stress is observed in pile number 20 with the lowest and the highest values observed in the pile group foundation with outer piles inclined at 75°/60° and 75°/30°, respectively.

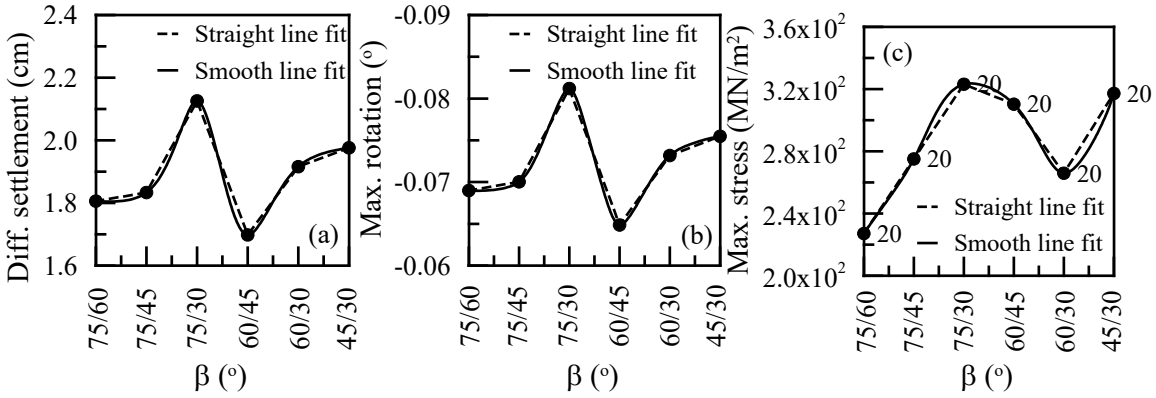

Figure 6.10. Maximum settlement, (b) Differential settlement, and (c) Maximum rotation

The variation of the maximum AF, SF, and BM observed in the pile head are plotted in Figure 6.11 (a), (b), and (c), respectively. The lowest and the highest AF is observed in the pile group foundation with the outer piles inclined at 75°/45° and 45°/30°, respectively. Further, the SF is observed to be the lowest when the outer piles are inclined at 75°/60° and the highest when the outer piles are inclined at 75°/30°, 60°/30°, and 45°/30°. Like SF, BM is also observed to be the lowest when the outer piles are inclined at 75°/60°. While the highest BM is observed in the configurations with outer piles inclined at 75°/30° and 45°/30°.

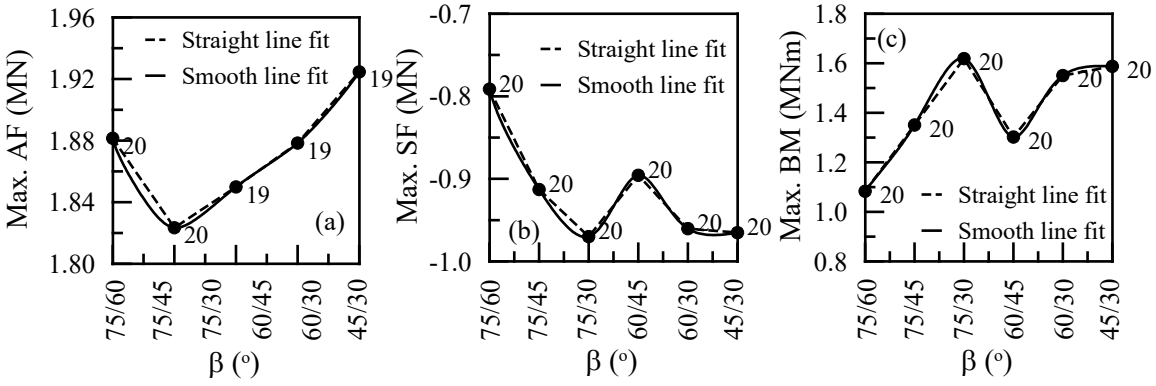

Figure 6.11. (a) Maximum axial force, (b) Maximum shear force, (c) Maximum bending moment, and (d) Maximum stress

Further, the variation of SF and BM along the length of the pile for pile number 19 and 30 (piles at the extreme ends) are shown in Figure 6.12 and 6.13, respectively. Only upper 12 m of the pile is shown in the figure because the SF and BM for the lower portion of the pile are zero. It can be seen in Figure 6.12 that the large variation in SF is observed within the depth of about 7.5 m for all the cases. Below the depth of 7.5 m, the variation of SF is zero. In addition, the magnitude of SF distribution is higher for pile number 19 compared to pile number 30 due to the direction of horizontal load and bending moment.

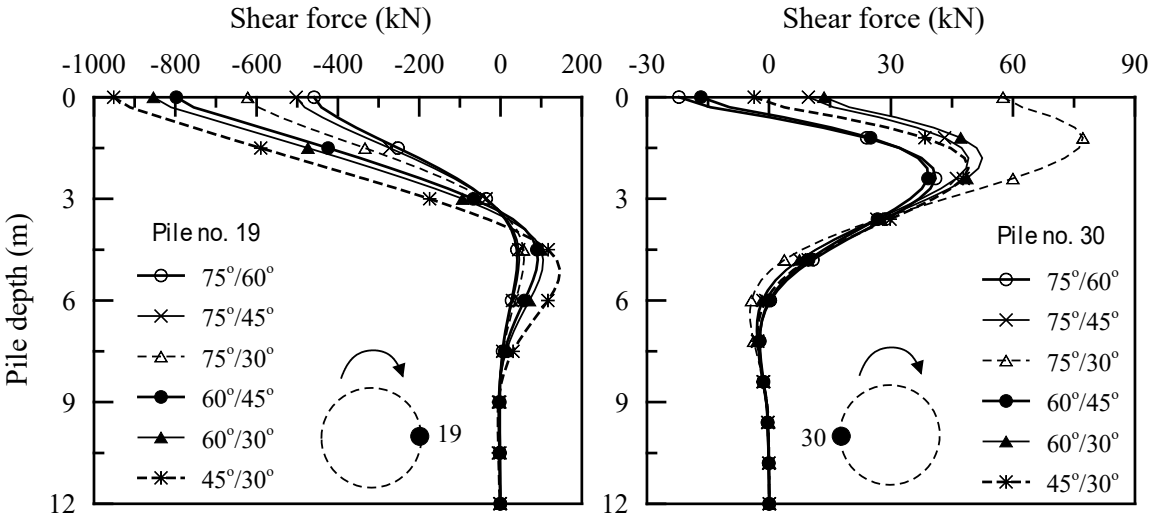

(Note: Actual pile length is 30 m, but only upper 12 m is shown.)

Figure 6.12. Variation of shear force along the length of the pile for the extreme piles

From the variation of BM plotted in Figure 6.13, it can be observed that the BM is induced only on approximately upper 7.5 m length of the pile. Moreover, the magnitude of variation is higher for pile number 19 compared to pile number 30 due to the same reason as mentioned before.

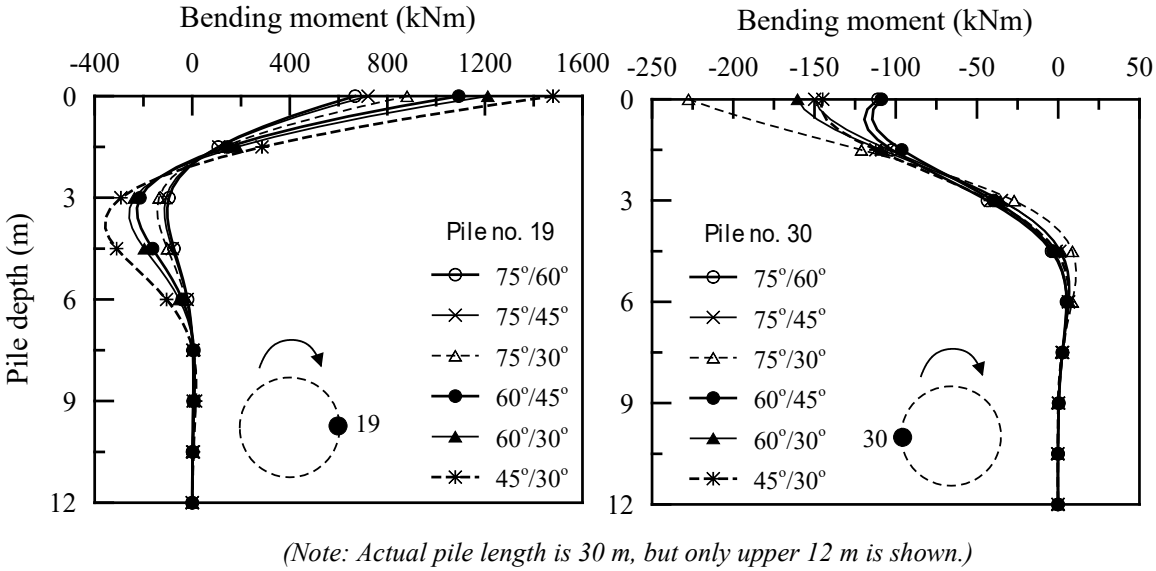

Figure 6.13. Variation of bending moment along the length of the pile for the extreme piles

6.4.6 Analysis with modification in the geometry – 3 circumferences

The initial design of the pile group foundation with piles arranged along two circumferences was modified by rearranging the piles along three circumferences as shown in Figure 6.14. In the pile group foundation with the new arrangement of piles, 8 piles were arranged along the circumference of radius 3.9 m, 12 piles along the circumference of radius 5.3 m, and remaining 20 piles along the circumference of radius 6.7 m at the equal spacing. However, the number and length of pile and radius of the pile cap remained yhe same in the new configuration.

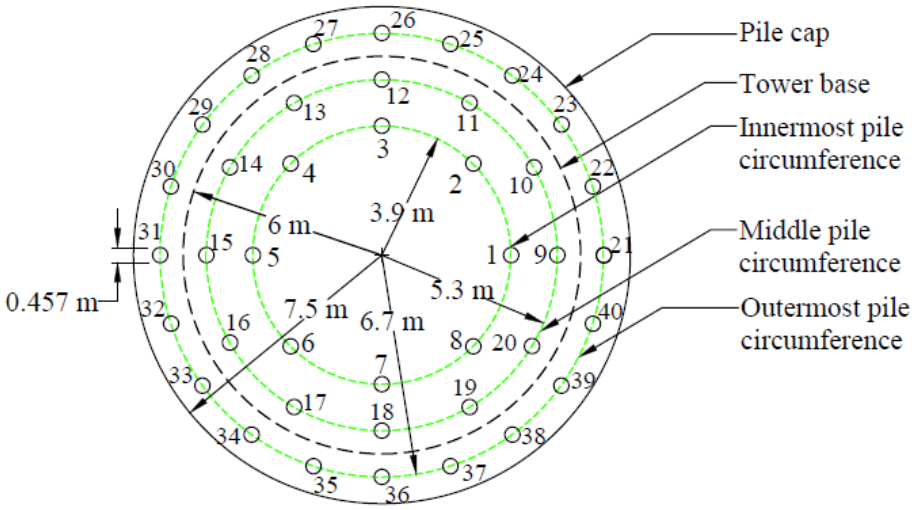

Figure 6.14. Configuration with piles along three circumferences

In the first configuration with the new pile arrangement, all the piles were kept vertical. Then, the other configurations were created by changing the inclination of outermost and middle circumference piles between 30° to 75° keeping in mind that the middle piles can't be inclined at a higher angle than the outermost pile. This exercise was performed to generate the configurations which are closer to the tree root system. Fifteen models were created with this scheme which is listed in Table 6,4 where β is the angle made with the horizontal plane.

Table 6.4. Models with piles along three circumferences

Model name	β (°)		
	Innermost pile	Middle pile	Outermost pile
D2M01	90	90	90
D2M02	90	90	75
D2M03	90	90	60
D2M04	90	90	45
D2M05	90	90	30
D2M06	90	75	75
D2M07	90	75	60
D2M08	90	75	45
D2M09	90	75	30

Table 6.4 (Cont.)

D2M10	90	60	60
D2M11	90	60	45
D2M12	90	60	30
D2M13	90	45	45
D2M14	90	45	30
D2M15	90	30	30

A 3D view of the pile group models generated in GROUP for the models listed in Table 6.4 is shown in Figure 6.15.

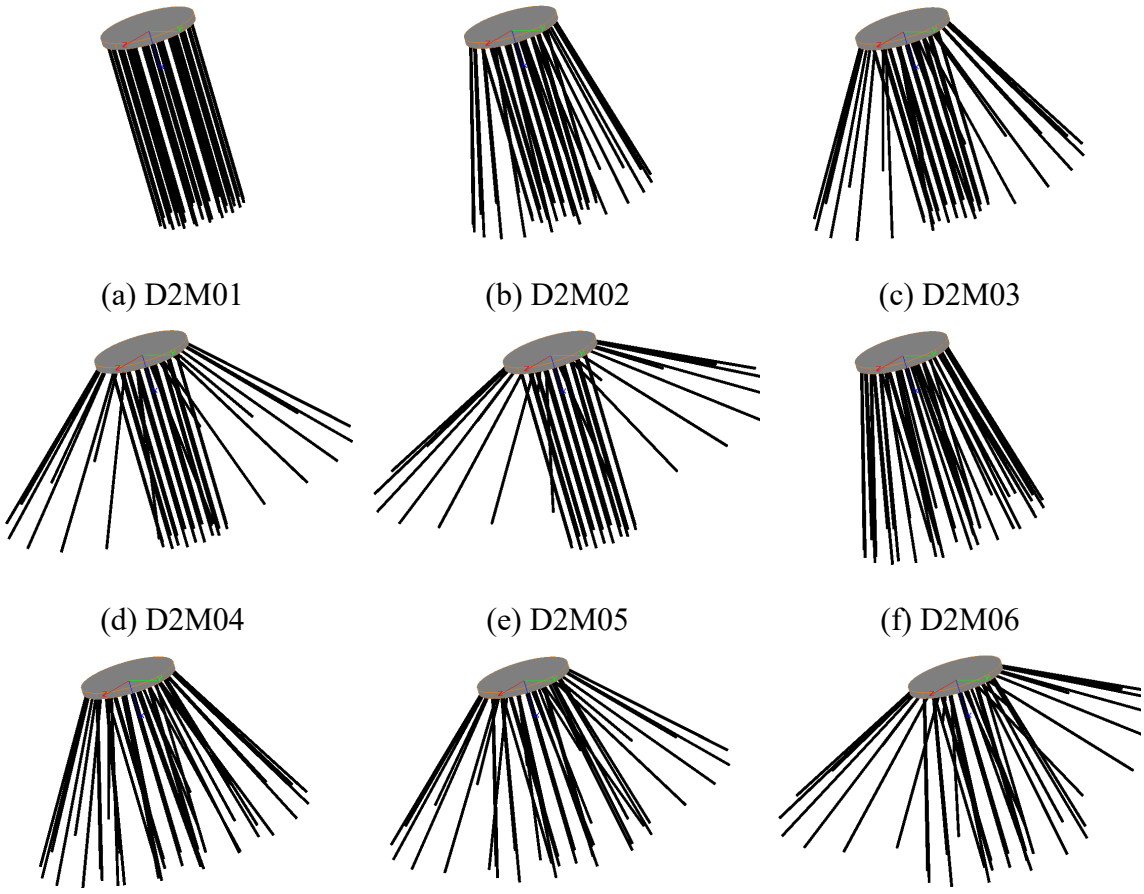

(a) D2M01 (b) D2M02 (c) D2M03

(d) D2M04 (e) D2M05 (f) D2M06

(g) D2M07 (h) D2M08 (i) D2M09

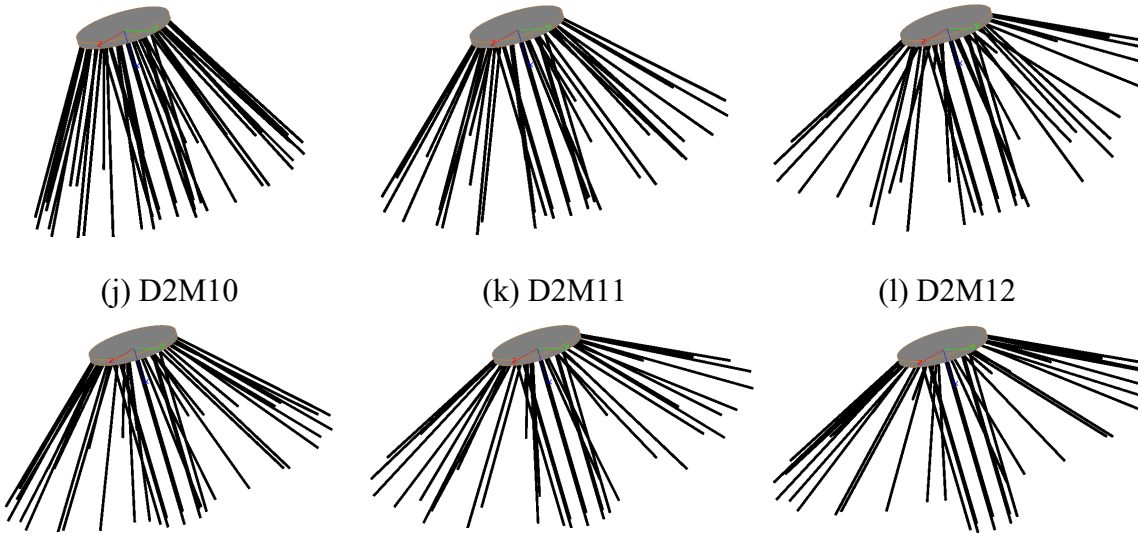

(j) D2M10 (k) D2M11 (l) D2M12

(m) D2M13 (n) D2M14 (o) D2M15

Figure 6.15. 3D view of modified models with piles along three circumferences generated in GROUP.

6.4.6.1 Results and discussions

Like previous cases, the differential settlement, maximum rotation, and maximum stress for different configurations were plotted and shown in Figure 6.16 (a), (b), and (c), respectively. From the Figures 6.16 (a) and (b), it can be observed that the differential settlement and rotation are minimum for the combination of configurations when the outermost piles are inclined at 45° and 60° and the middle piles are inclined at 90°, 75°, 60°, and 45°. On the other hand, the differential settlement and rotation is higher for the cases when the outermost piles are inclined at an angle of 30°. Since the rotation is directly proportional to the differential settlement, a similar response was observed for rotation. The number shown at each data point in Figure 6.16 (c) is the pile number (see Figure 6.14) on which maximum stress is observed. For all configurations, the maximum stress is

observed in pile number 21 which is the extreme pile in the direction of horizontal load and bending moment. While decreasing the inclination of the outermost pile with respect to the horizontal plane from 90° to 30° at the interval of 15° with same inclination of middle piles, the stress is observed to increase.

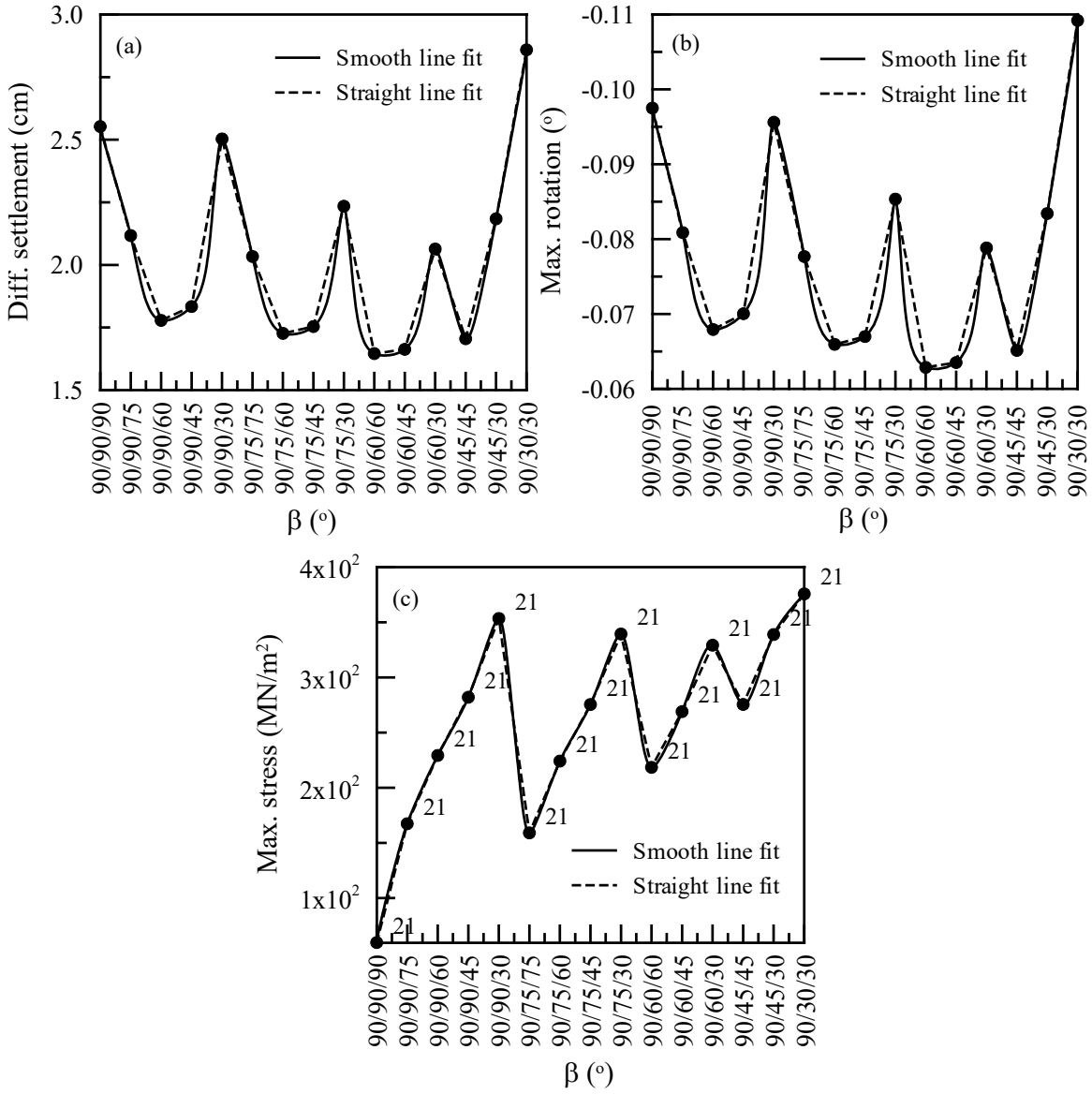

Figure 6.16. (a) Differential settlement, (b) Maximum rotation, and (c) Maximum stress

Further, the variation of the maximum AF, SF, and, BM are plotted in Figure 6.17 (a), (b), (c), respectively. The values shown for each data point in Figure 6.17 are the pile number at which the maximum pile head responses were observed (refer to Figure 6.14 for pile number and location). The lowest AF is observed in 90°/90°/30° (innermost/middle/outermost pile inclination with the horizontal plane) configuration, followed by 90°/90°/90° and 90°/30°/30° configurations. The highest AF is observed in 90°/60°/30° configuration. In summary, the decrease in the outermost piles' inclination tend to increase the AF. Similary the maximum SF observed at the pile head for each configuration are plotted in Figure 6.17 (b). The negative values denote the direction of SF. The lowest SF is observed in the configuration where all the piles are vertical. The highest value of SF is observed in 90°/75°/30°, 90°/45°/30°, 90°/90°/30°, 90°/60°/30°, and 90°/30°/30° (in the order of highest to lowest values) configurations. The SF is observed to be increasing with the decrease in the outermost piles' inclination. The variation pattern of maximum BM observed on the pile head for different configurations (Figure 6.17 (c)) is similar to that of maximum stress. The lowest BM is observed in the configuration with all vertical piles. Decreasing the inclination of the outermost pile with respect to the horizontal plane from 90° to 30° at the interval of 15° with the same inclination of middle piles resulted in the increase in BM.

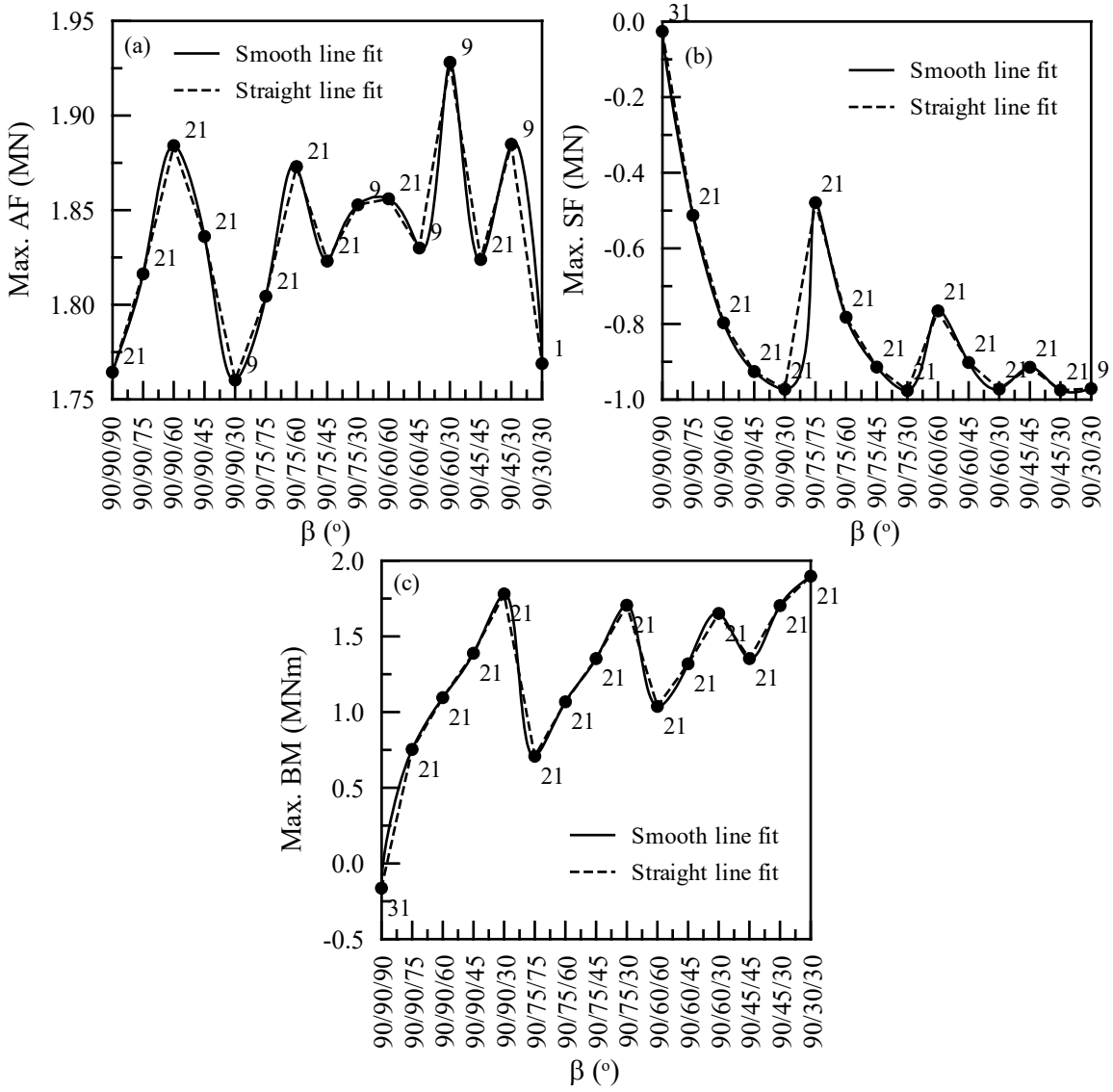

Figure 6.17. (a) Maximum axial force, (b) Maximum shear force, (c) and Maximum bending moment

Further, the variation of the SF and BM for all the configurations of the piled group foundation along the length of the pile for the extreme piles, i.e. pile number 21 and 31 are shown in Figures 6.18 and 6.19, respectively. Similar to previous cases, only upper 12 m is shown because the SF and BM were observed to be zero below 12 m. The location of the pile and the direction of BM applied is also shown in the figure. For pile no. 21, which

lies in the direction of the BM, the configuration with all vertical piles do not appear to show large variation compared to other configurations. This result is consistent with the case with piles arranged along two circumferences with an inclination of 90°. Further, the SF is induced only on the upper approximately 9 m of the pile.

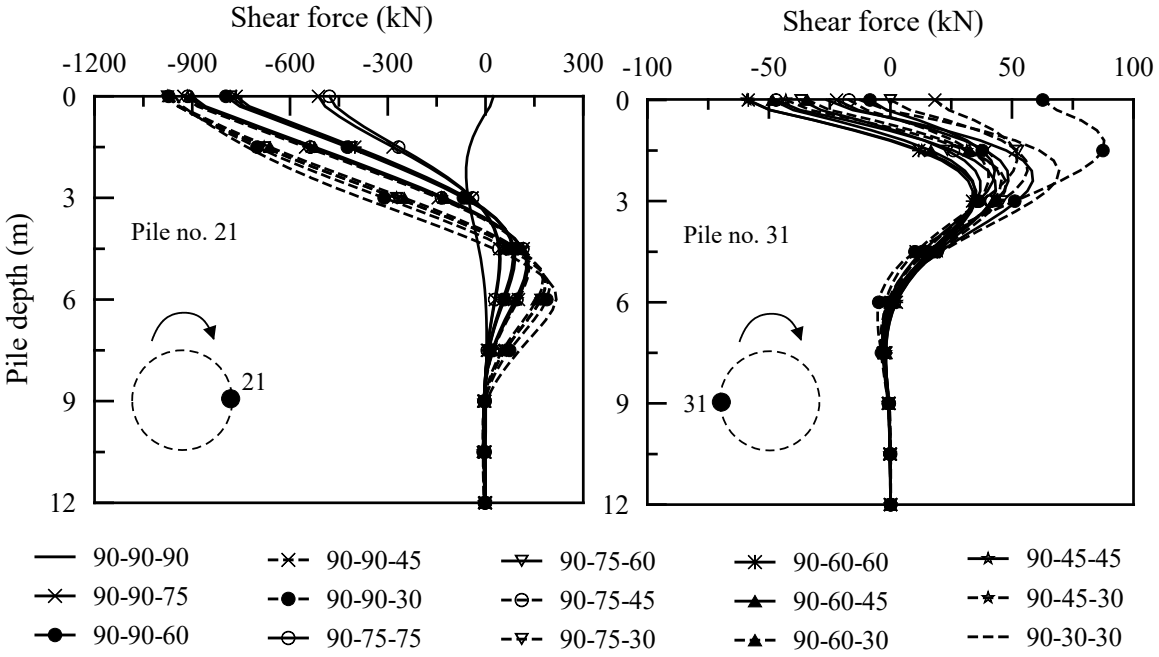

(Note: Actual pile length is 30 m, but only upper 12 m is shown.)

Figure 6.18. Variation of shear force along the length of the pile for the extreme piles

The variation of BM along the pile length (only upper 12 m) for all the configurations is shown in Figure 6.19 for pile number 21 and 31. For pile number 21, the configuration with all vertical piles is not showing much variation compared to other configurations. Similar to SF distribution, the BM is also induced only on the upper 9 m (approximately) of the pile.

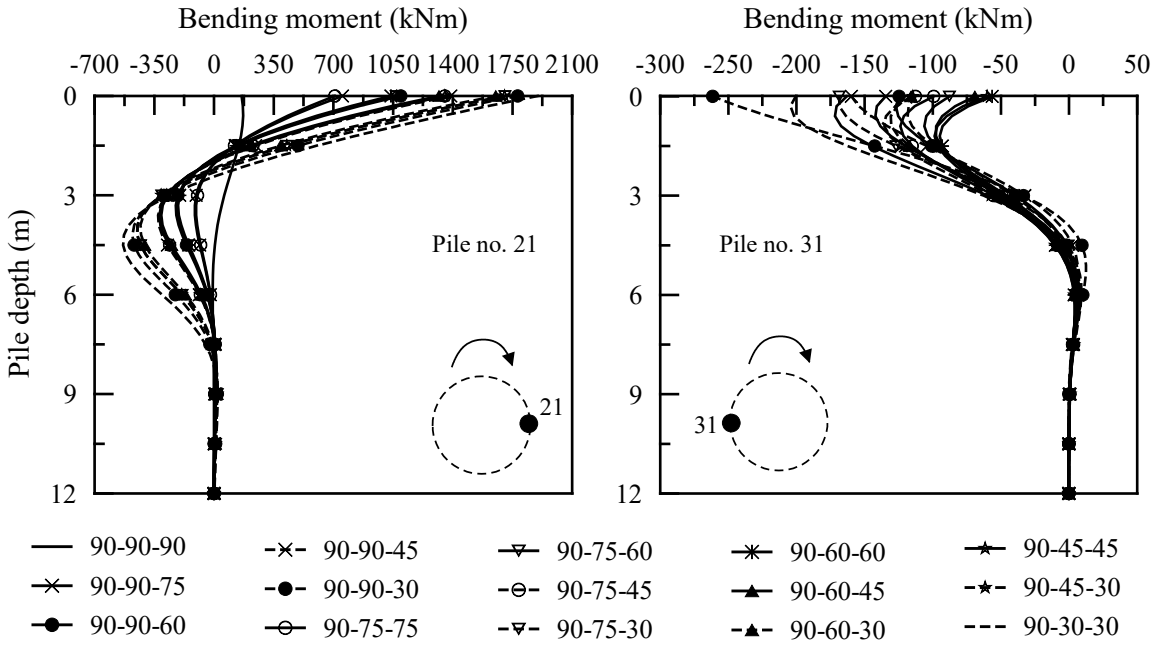

(Note: Actual pile length is 30 m, but only upper 12 m is shown.)

Figure 6.19. Variation of bending moment along the length of the pile for the extreme piles

6.4.7 Summarized discussion

The differential settlement and rotation of different configurations presented above can be used to ensures the serviceability requirement of the foundation. On the other hand, stress, AF, SF, and BM results presented above can be used to ensure the structural safety (not presented in this study) of the foundation under the given design loads.

Further, the results for the configurations with two circumferences are compared as shown in Table 6.5 to investigate the most effective configuration. From Table 6.5, it can be seen that the configuration in which the outer piles are alternately inclined at 60° and 45° is the most effective in terms of the differential settlement. This configuration is still

efficient when compared to all the configurations including the configurations where the piles are arranged along three circumferences.

Table 6.5. Comparison of all configurations with piles along two circumferences

Model name	β (°)		Differential settlement (cm)
	Inner pile	Outer pile	
D1M01	90	90	2.42
D1M02	90	75	2.00
D1M03	90	60	1.68
D1M04	90	45	1.73
D1M05	90	30	2.43
D1M06	90	75/60	1.61
D1M07	90	75/45	1.64
D1M08	90	75/30	1.90
D1M09	**90**	**60/45**	**1.52**
D1M10	90	60/30	1.71
D1M11	90	45/30	1.77

6.5 Finite element analysis

GROUP analysis exhibited promising results. However, GROUP doesn't have advanced features to model a semi-spherical bulb, soil-root interface, and sub-roots. These limitations can be addressed by using an advanced finite element software. In this study, ABAQUS was used to perform the finite element analysis. ABAQUS can model both soil and structural components and the constraints and interactions between soil and structure in an accurate manner. In addition, a 3D numerical model can be developed in ABAQUS which is required for this problem due to asymmetric loading even though the foundation geometry is symmetrical.

6.5.1 Problem formulation

The new modified foundation investigated in this study is intended for a wind turbine tower which is assumed to be constructed in a site composed of stiff clay with unit weight and undrained cohesion of 18 kN/m^3 and 100 kPa, respectively. The vertical load, horizontal load, and bending moment considered for this study are 17.5 MN, 1.1 MN, and 73.5 MNm, respectively.

6.5.2 Identification of simplified configurations

Six simplified configurations were created in which the main roots and sub-roots were attached to the bulb at different locations. The bulb considered in this study was a semi-spherical three-dimensional component with a diameter of 5 m. The first three configurations have six, twelve, and eighteen main-roots (MR) at three different levels as shown in Figure 6.20 (a), (b), and (c), respectively. The first model shown in Figure 6.20 (a) consists of six main roots inclined at an angle of 20° with the horizontal on the top level of the bulb. In the next model as shown in Figure 6.20 (b), an additional six main roots were added to the middle part of the bulb inclined at an angle of 37.5°. Similarly, an additional six main roots were added to the second model at the bottom part of the bulb at an angle of 55° as shown in Figure 6.20 (c). Three additional configurations were developed by adding two sub-roots (SR) per main root at an angle 20° from main root's longitudinal axis. Both main root and sub-root have a tapered cross-section. The main root was considered to have a length of 10 m with a diameter of 0.5 m at the top to 0.12 m at the bottom. Similarly, the SR was considered to have a length of 5 m with a diameter of 0.16 m at the top and 0.08 m at the bottom. A vertical drilled shaft of diameter 1.5 m and

length 10 m was placed at the center of the bulb which contributes to the vertical load capacity. The drilled-shaft serves the purpose of taproot which is a straight root growing vertically downward from the center. The configurations are shown in Figure 6.20.

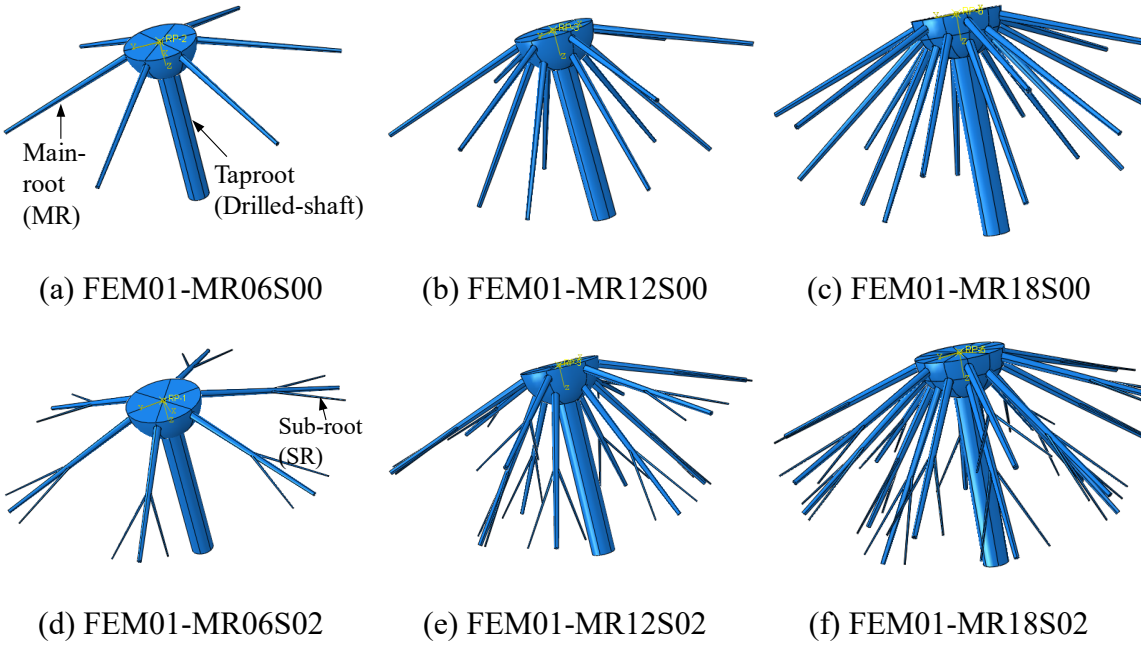

(a) FEM01-MR06S00 (b) FEM01-MR12S00 (c) FEM01-MR18S00

(d) FEM01-MR06S02 (e) FEM01-MR12S02 (f) FEM01-MR18S02

Figure 6.20. Simplified configurations of new foundation after the tree root system

6.5.3 Finite element Analysis of the simplified configurations

A 3D finite element model of the potential foundation system including supporting soil was developed using ABAQUS. The key features of finite element model development are discussed below.

6.5.3.1 Finite element model development and boundary conditions

At first, 3D individual components of the soil-foundation system, i.e. soil, bulb, drilled shaft, and roots (main root and sub-root) were created. Each of the components were represented by a 3D deformable solid element. The diameter of the model domain was considered to be 40 m and the total height was considered to be 25 m. The individual

components were then assembled at their respective locations in the assembly module. Since the soil body is a solid section, it must be modified such that it has space for the foundation components (bulb and roots). To obtain such a section, cut instance technique was used to cut the soil with the foundation which resulted in a new soil part with required spaces for bulb, roots, and taproot. Finally, a new soil part, roots (main root and sub-root), bulb, and drilled shaft were assembled as shown in Figure 6.21. A transparent view of the model is shown in Figure 6.21 to ensure the visibility of the bulb and internal roots. The boundary conditions are also shown in Figure 6.21. The base of the model was fixed, i.e. no translation in x, y, and *z* directions and the vertical sides of the model were fixed in *x* and *y* directions (lateral) and free in the *z*-direction (vertical).

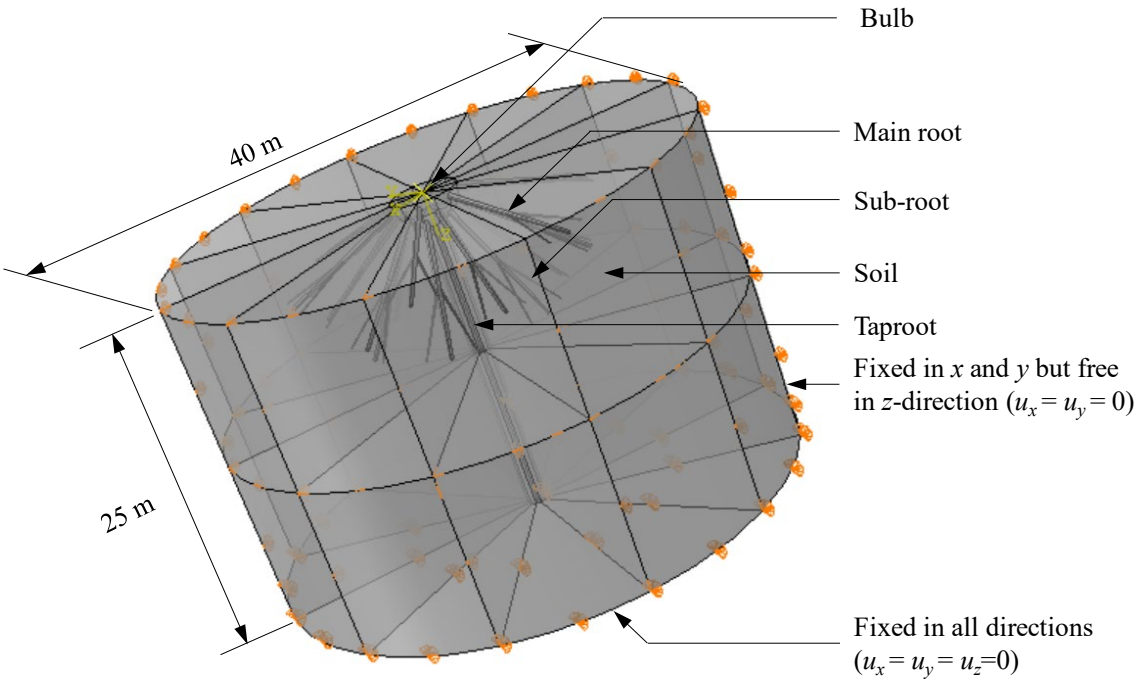

Figure 6.21. 3D model of FEM01-MR18S02 in ABAQUS

6.5.3.2 Constitutive model

All the components of the modified foundation, i.e., soil, bulb, root (main root and sub-root), and drilled shaft were represented by inbuilt linear elastic (LE) constitutive model in ABAQUS. The roots used in this study was considered to be reinforced polymetric pile (RPP). RPP is made of recycled high-density polyethylene (HDPE) reinforced with fiber reinforced polymer or steel rods (Iskander, 2012). It is very light and can contain a small percentage of glass fibers to enhance strength (Iskander, 2012). Since it is made of recycled polymers, it is environment-friendly too. Further, it performs better than timber, steel, and concrete piles in waterfront areas. Therefore, the applicability can be extended to the offshore wind turbine as well. The reason for using the RPP for this study is because this research will be extended in the future where the material properties of the roots will be changed from the conventional material and analyzed.

The appropriate properties of all the components are listed in Table 6.1. The properties of RPP were obtained from Iskander (2012). It should be noted that ABAQUS doesn't have any unit system. Hence it is important to ensure that the values of each parameter entered are consistent unit so that the units of the results can be properly interpreted. The units used in Table 6.6 are one of the sets of consistent units suggested by ABAQUS.

Table 6.6. Structural components model parameters

Component	Density (kg/m^3)	Young's modulus (N/m^2)	Poisson's ratio
Bulb	2549.3	3.28×10^{10}	0.15
Drilled shaft	2549.3	3.00×10^{10}	0.15
Root (RPP)	81.6	1.02×10^{9}	0.46
Soil	1835.5	3.05×10^{7}	0.45

6.5.3.3 Spatial discretization

The geometry of the proposed foundation is very complicated. For such complicated geometry, it was not possible to use a hexahedral element, which is efficient in terms of processing time, to discretize the model even after partition. Therefore, in this study, a 10-node quadratic tetrahedron element (C3D10) was used to discretize the simulation domain. While meshing, the partitioning technique was used to simplify the simulation domain as much as possible. It facilities the user to have control over the desired number of elements at the desired locations. In addition, finer mesh was generated in the areas where the stress concentration was predicted to be higher. The finite element mesh generated for the model FEM01-MR18S02 is shown in Figure 6.22. The soil is not shown in Figure 6.22 to show the foundation components.

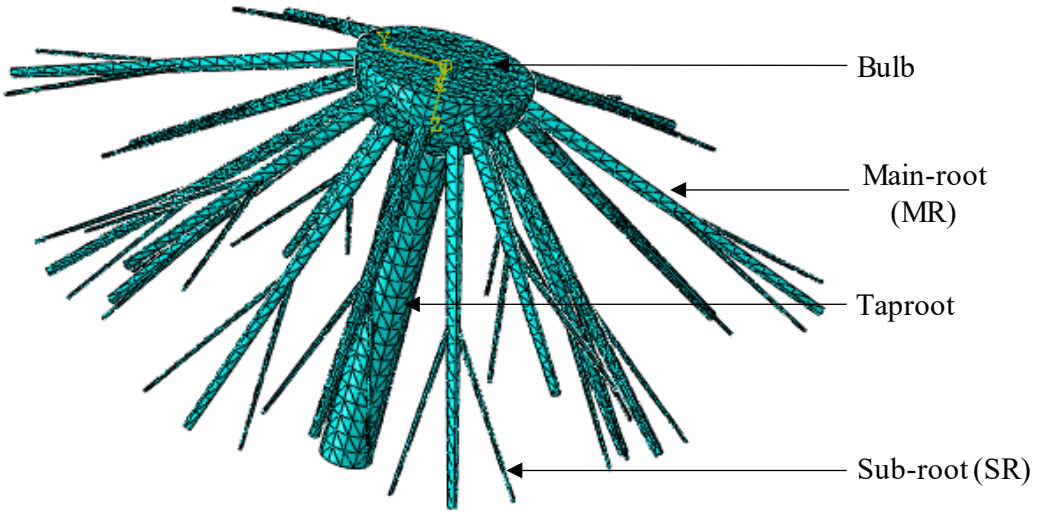

Figure 6.22. Finite element mesh of model FEM01-MR18S02

6.5.3.4 Soil-root interface modeling

The identified interfaces in the proposed foundation are; soil-root, soil-bulb, bulb-root, and bulb-drilled shaft, bulb-soil and root-root (main root-sub-root). The load transfer mechanism from the superstructure to the bulb, from bulb to roots and soil, and from roots to soil is affected by the way these interfaces are modeled. For this study, surface to surface based tie constraint was used for all interfaces. A tie constraint ties two surfaces in contact together throughout the simulation. It makes the translation and rotation motion equal for the surfaces in contact.

6.5.3.5 Key steps of the simulation

The analysis was carried out in three steps; the initial step, geostatic step, and loading step. The initial step is the default step in ABAQUS which is created automatically. In the initial step, the boundary conditions, interactions, and constraints are already activated which are propagated into the next step. The geostatic step establishes the equilibrium of gravitational loads and forces and verifies the initial stresses. The last step is the loading step where the design loads (vertical load, horizontal load, and bending moment) were applied in the desired directions and locations. The vertical load was applied as the vertical pressure on the top surface of the bulb, the horizontal load was applied as surface traction on the top surface of the bulb, and the bending moment was applied as a point load at the center of the bulb. After successfully developing a 3D model of the piled-raft foundation, a job was created and submitted for the analysis in Palmetto cluster which is Clemson University's high-performance computing resource.

6.5.4 Results and discussions

The deformed mesh with the resultant deformation contour for all the simplified configurations is shown in Figure 6.23. The values of the resultant deformation, *U* shown in Figure 6.23 is in meter. In Figure 6.23, the sub-roots are not visible because they are hidden inside the soil. It can be observed in Figure 6.23 that the roots on the direction of the bending moment have bent. The main roots at the top portion of the bulb have bent more than the main roots at the lower portion. Further, it can be noticed that the resultant deformation decreased when a greater number of main roots are added. On the other hand, the addition of sub-roots had an insignificant reduction in the resultant displacement.

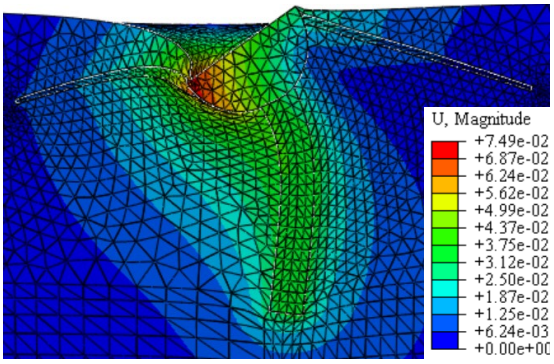

(a) FEM01-MR06S00

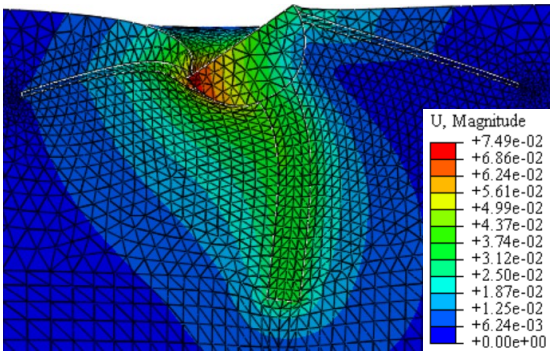

(d) FEM01-MR06S02

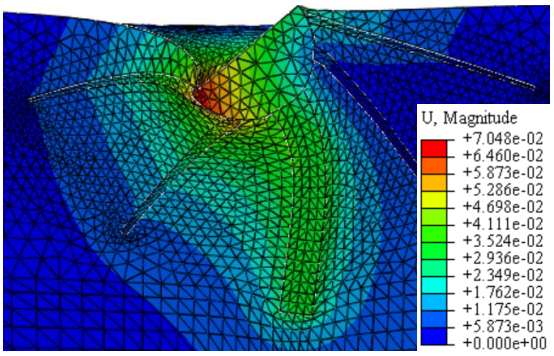

(b) FEM01-MR12S00

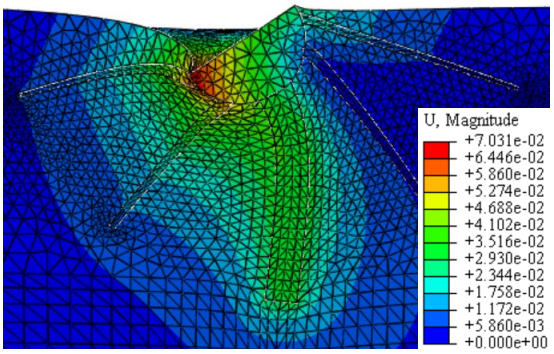

(e) FEM01-MR12S02

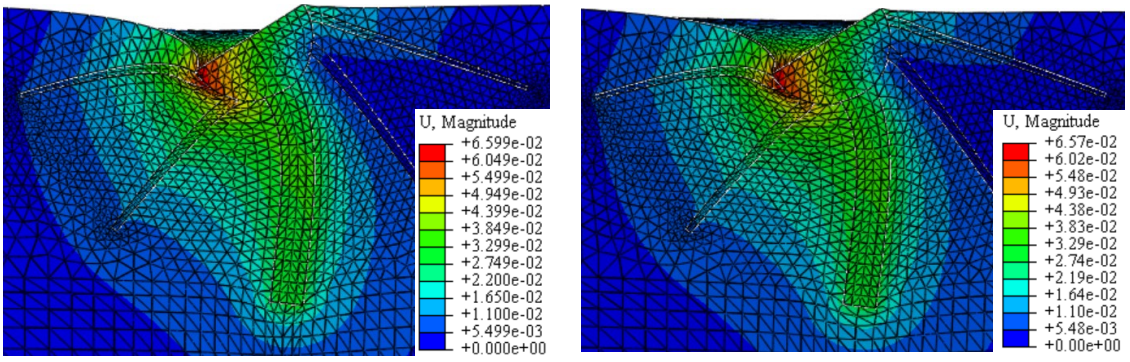

(c) FEM01-MR18S00 (f) FEM01-MR18S02

Figure 6.23. Deformed shape with resultant displacement contours (Deformation scale factor = 50)

The computed differential settlement and horizontal displacement obtained from ABAQUS for all the configurations were compared and presented graphically in Figure 6.24. The results showed that the addition of main roots contributed to a higher improvement in the performance, whereas, the contribution of sub-roots was insignificant.

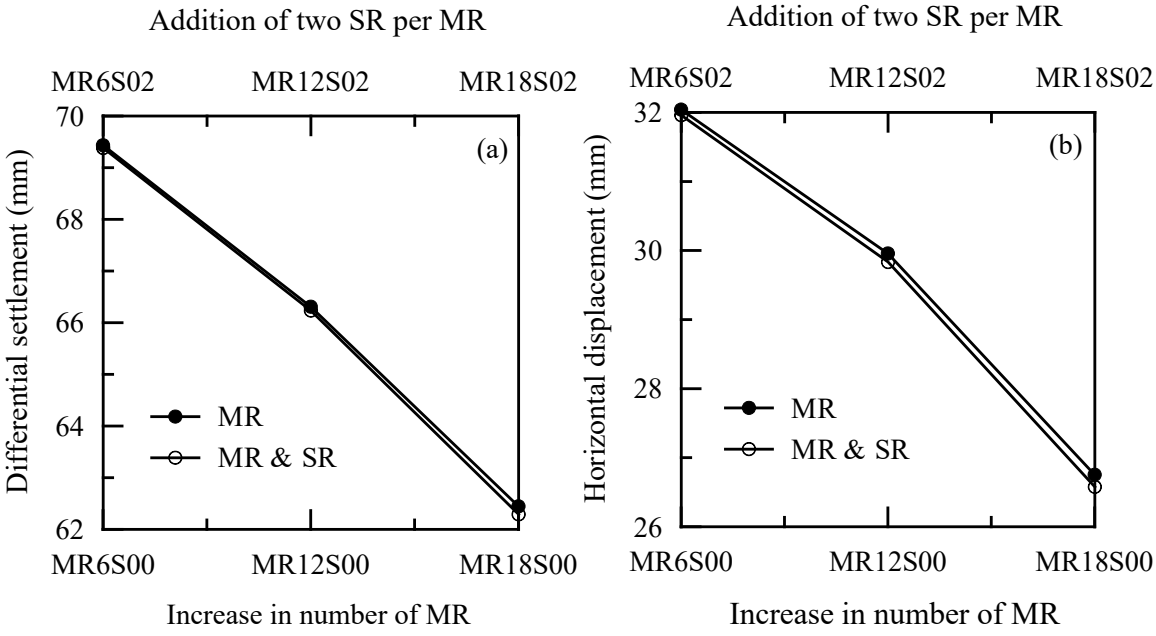

Figure 6.24. Comparison of performance for different configurations (a) differential settlement and (b) horizontal displacement

6.6 Future work

Based on the preliminary analysis, it can be concluded that the new foundation doesn't require the sub-roots. However, to make a strong recommendation, more extensive research is required in this area. The following future works are suggested.

- Creating additional configurations which will involve the change in length, size, orientation, and cross-section (tapered vs. constant section) of the roots
- Changing the material properties of roots
- Modeling the soil-root interfaces using appropriate interface properties
- Performing the coupled analysis including wind turbine on the top.
- Performing the analysis for different site conditions
- Addressing the constructability of the new foundation with unconventional geometry

6.7 Conclusion

In this study, the analysis on the development of a new foundation after the tree root system subjected to a combined vertical load, horizontal load, and bending moment is presented. Since the natural tree root system is very complicated and the exact replication of such configuration will not practically possible to construct, simplified configurations were created and analyzed in ABAQUS. The configurations consisted of different numbers of main roots and sub-roots at different angles. The results showed that the increase in the number of main roots resulted in the improvement of the performance under combined loading. However, the addition of sub-roots had insignificant improvement in the performance. In order to recommend an effective configuration of the new foundation

through biomimicry, an extensive study is required involving the change in number, orientation, and size of roots and also change in material properties of the roots. Moreover, it is crucial to address the construction issues of the proposed potential foundation.

CHAPTER 7

CONCLUSIONS AND RECOMMENDATIONS

7.1 Conclusions

The motivation of this research is coming from the need for increasing sustainable and clean energy production from wind to meet the ever-increasing global energy demand. Building a taller wind turbine tower can increase the production of wind energy due to high wind speed but presents significant challenges in designing cost-effective and safe foundation. The design challenges are addressed in this dissertation by performing a simplified analytical design, robust design optimization, and finite element analysis of piled-raft foundation for a tall wind turbine of height 130 m. The wind turbine tower is assumed to be constructed in site with multilayered soil, clayey soil, and sandy soil.

A simplified geotechnical design of a piled-raft foundation for a tall wind turbine subjected to combined load (vertical load, horizontal load, and bending moment) is presented in this dissertation. The analytical design of the piled-raft foundation is complicated due to a lack of understanding of the complex three-dimensional soil-structure interaction. As a result, it is not possible to estimate the load shared between raft and piles. The design challenges increase when the foundation is subjected to a combined load. The design procedure for the piled-raft foundation available in the literature only incorporates the vertical load. However, the differential settlement induced due to bending moment is critical for the tall wind turbine. This issue is addressed in this study. A new method to calculate the differential settlement due to the bending moment is proposed in this study.

The analytical design procedure for the piled-raft foundation involved safety and serviceability checks. It was found that the differential settlement controlled the final design.

The wind turbine is constructed in a wind farm which extends over a large area. Such large area may have variation in wind speed and strength parameter of the soil. Both of these parameters have a significant impact on the design of the piled-raft foundation. Designing location specific foundation for each wind turbine in a wind farm will require extensive subsurface exploration and a lot of time which have a direct impact on the cost of the project. Therefore, to design an optimum piled-raft foundation applicable for the whole wind farm, a reliability-based robust design optimization using Non-dominated Sorting Genetic Algorithm – II (NSGA-II) and Monte Carlo simulation is presented in this dissertation. In the design optimization, the wind speed and strength parameter of soil are considered as random variables and radius of raft, number of piles, and length of pile are design variables. The total cost of the foundation and the standard deviation of the differential settlement are considered as the two objectives to satisfy. This procedure resulted in many safe designs which were presented graphically in the form of Pareto front. The Pareto front showed a clear trade-off relationship between the two objectives. It can be used by an engineer as a design tool to select the design as per the safety requirement and cost limitation. It should be noted that the multi objective design optimization performed in this study are based on response function (differential settlement function) obtained from the analytical design. Similar procedure can be followed to perform the optimization using the response function based on finite element analysis.

The simplified analytical design of the piled-raft foundation is not accurate because the three-dimensional soil-structure interaction is not incorporated. Therefore, in this study, a finite element analysis of the piled-raft foundation subjected to the combined load is performed. The soil-structure interaction was incorporated in the finite element modeling by defining the interaction properties in the normal and tangential direction at the contacts. The parametric study conducted by varying the friction coefficient showed that the response was insensitive to the friction coefficient. However, the results may be different for other problems. The comparison the results from finite element analysis with the analytical design results showed that the analytical design procedure predicted a higher vertical settlement and horizontal displacement and lower differential settlement and rotation. Similar results were observed while conducting the parametric study by varying wind speed and undrained cohesion except for the highest wind speed and lowest undrained cohesion.

Moreover, a preliminary study on the development of a new foundation for a wind turbine through biomimicry is presented in this dissertation. Since wind turbine is comparable to the coconut tree, sabal palm tree, and Palmyra tree and they are exposed to similar loads, the roots of such trees were studied to develop a new foundation. The roots of these trees have complicated geometry. Therefore, in this study simplified configurations of the new foundation were created with different number and orientation of main roots and sub-roots. The results showed that the increase in the number of main roots improved the performance while adding sub-roots to the main root didn’t have significant improvement.

7.2 Limitations

Although this dissertation has contributed to the existing literature, the following limitations of the results are identified.

- The validation of the analytical design procedure presented in this study is not performed
- The Pareto fronts developed in this research for different soils are based on certain range of soil strength parameter and wind speed. The results may be different for other ranges
- The finite element model of piled-raft foundation is developed carefully by accurately modeling the soil-structure interface. However, it is required to validate the finite element modeling procedure

7.3 Recommendations

Although great advancements have been made in the analytical design and finite element analysis of the piled-raft foundation and this study contributes to the better understanding of the piled-raft foundation design, further study in this field is necessary. Moreover, the development of the new foundation through biomimicry is an interesting idea and preliminary study is presented in this dissertation, still, more extensive study is required. Therefore, based on this study, it is recommended to explore the following areas.

7.3.1 Validation of fully coupled finite element model

The finite element analysis of the piled-raft foundation presented in this study is not fully coupled, i.e. the wind turbine tower was not created, and the results are not validated. Therefore, it is recommended to conduct a fully coupled finite element analysis

of the piled-raft foundation. Creating a fully coupled model will require proper interaction between the tower and the raft. A fully coupled model will provide a realistic load transfer from the tower to the foundation. Most importantly, it is highly recommended to validate the finite element modeling technique with the experimental results.

7.3.2 Dynamic analysis of the piled-raft foundation

All the analyses of the piled-raft foundation are performed for the static loading condition. However, the wind load is dynamic in nature and produces vibration in the tower body. Moreover, the wind farm may be constructed in a seismically active area. In such cases, a dynamic analysis of the piled-raft foundation is necessary.

7.3.3 Extensive study on biomimicry

The concept of the development of a new cost-effective foundation through biomimicry of the tree root system is an interesting and novel concept. This dissertation presents preliminary study results on this research topic. However, there are many areas to be explored on this topic. The recommended future works on this topic include;

- Creating additional configurations of the potential foundation by changing length, size, number, orientation, and cross-section (tapered/constant section) of the roots
- Conducting the analysis by using different material properties for roots at different site conditions
- Incorporating proper interaction properties at soil-root interfaces
- Investigating the constructability of the potential new foundation
- Estimating and comparing the cost of the proposed foundation with the conventional foundation

REFERENCES

ASCE (American Society of Civil Engineers) (2010). "Minimum Design Loads for Buildings and Other Structures." *Standard ASCE/SEI 7-10*, ASCE, Reston, VA, USA, ISBN 978-0-7844-1085-1.

Ben-Hassine, J. and Griffiths, D.V. (2012). "Reliability Based Design of Foundations Subjected to Combined Loading with Applications to Wind Turbine Foundations." *Proceedings of the 11th International Congress on Numerical Methods in Engineering and Scientific Applications*, CIMENICS 2012, (eds E. Davila et al.), Pub. Sociedad Venezuela de Metodos Numericos en Ingenieria, CI 17-23.

Bosworth, S., El-Sayed, H.S., Ismail, G., Ohmer, H., Stracke, M., West, C. and Retnanto, A. (1998). "Key Issues in Multilateral Technology." *Oilfield Review*, 10(4), 14-28.

Bowles, J. E. (1987). "Elastic Foundation Settlement on Sand Deposits." *Journal of Geotechnical Engineering,* 113(8), 846–860.

BP (2017). "BP Statistical Review of World Energy June 2018."

Burland, J.B. (1995). "Piles as Settlement Reducers." *18th Italian Congress on Soil Mechanics*, Keynote Address, Pavia, Italy.

Burrall, M., DeJong, J.T., Wilson, D., Martinez, A., and Huang, L. (2018). "Vertical pullout tests of tree root systems for bio-inspired foundation idea development." *Proc. Biomed. and Bioinsp. Geotech. (B2G) Conf.,* Atlanta, GA.

Chan, C.M., Zhang, L.M. and Ng, J.T., (2009). "Optimization of pile groups using hybrid genetic algorithms." *Journal of Geotechnical and Geoenvironmental Engineering*, 135(4), 497-505.

Coduto, D.P. (2001). "Foundation Design: Principles and Practices." 2nd Edition, *Prentice Hall*, Upper Saddle River, NJ, USA, ISBN 0-13-589706-8.

Das, B.M. (2011). "Principles of Foundation Engineering." 7th edition, *Cengage Learning*, Stamford, CT, USA, ISBN 978-0-495-66812-1.

Das, B. M. (2016) "Principles of Foundation Engineering." 8th edition, *Cengage Learning*.

Deb, K. and Gupta, S. (2011). "Understanding knee points in bicriteria problems and their implications as preferred solution principles." *Engineering Optimization*, 43(11), 1175-1204.

Deb, K., Pratap, A., Agarwal, S., and Meyarivan, T. (2002). "A fast and elitist multi objective genetic algorithm: NSGA-II." *IEEE Transactions on Evolutionary Computation*, 6(2), 182–97.

DeJong, J.T., Burrall, M., Wilson, D.W., and Frost, J.D. (2017). "A Bio-Inspired Perspective for Geotechnical Engineering Innovation." *Geotechnical Frontiers 2017*, GSP 280, 862-870.

Deka, R. (2014). "Different Analysis Methods of Piled Rafts." *International Journal of Engineering Technology, Management and Applied Sciences*, 2(4).

Duncan, J.M. (2000). “Factors of Safety and Reliability in Geotechnical Engineering.” *Journal of Geotechnical and Geoenvironmental Engineering*, 126(4), 307-316.

Duncan, J.M. and Buchignani, A. N. (1976). “An Engineering Manual for Settlement Studies.” Department of Civil Engineering, University of California, Berkley.

Duryea, M. L. and Kampf, E. (2017). “Selecting Coastal Plain Species for Wind Resistance.” *IFAS Extension*, University of Florida.

Fellenius, B.H. (1999). “Basics of foundation design.” 2nd edition, *BiTech Publishers*, Richmond, British Columbia.

Fenton, G.A. and Griffiths, D.V. (2008). “Risk Assessment in Geotechnical Engineering.” *John Wiley & Sons*, Inc., Hoboken, NJ, USA, ISBN 978-0-470-17820-1.

Gong, W., Khoshnevisan, S., & Juang, C. H. (2014). “Gradient-based design robustness measure for robust geotechnical design.” *Canadian Geotechnical Journal*, 51(11), 1331-1342.

Griffiths, D.V., Fenton, G.A. and Manoharan, N. (2002). “Bearing capacity of a rough rigid strip footing on cohesive soil: A probabilistic study.” *Journal of Geotechnical and Geoenvironmental Engineering*, 128(9), 743-755.

Grunbeg, J. and Gohlmann, J. (2013). “Concrete Structures for Wind Turbines.” *Wilhelm Ernst & Sohn*, Berlin, Germany, ISBN 978-3-433-03041-7.

Gudmundsdottir, B. (1981). “Laterally loaded piles.” M.S. thesis, University of Alberta, Edmonton, Alberta, Canada.

GWEC (Global Wind Energy Council). (2015). “Global Wind Report 2015.”

Haldar, A. and Mahadevan, S. (2000). “Probability, Reliability, and Statistical Methods in Engineering Design.” *John Wiley & Sons*, Inc., 605 Third Avenue, New York, NY, ISBN 0-471-33119-8.

Hemsley, J.A. (2000). “Design applications of raft foundations.” *Thomas Telford Ltd*., Heron Quay, London, ISBN 0727727656.

Hough, B.K. (1957). “Basic soils engineering.” *The Ronald Press Company*, New York, USA.

International Energy Agency (IEA), 2018. “Global Energy & CO2 Status Report 2017.”

Iskander, M.G. (2012). “Sustainable Piling Made of Recycled Polymers: State of the Art Review.” *Journal of ASTM International*, 9(2), Paper ID JAI103677.

Janbu, N., Bjerrum, L., and Kjaernsli, B. (1956). “Veiledning vedlosning av fundamentering-soppgaver.” *Norwegian Geotechnical Institute*, 18, 30–32.

Jozefiak, K., Zbiciak, A., Maslakowski, M., and Piotrowski, T. (2015). “Numerical modelling and bearing capacity analysis of pile foundation.” *XXIV R-S-P seminar, Theoretical Foundation of Civil Engineering (24RSP) (TFoCE 2015)*, 111(2015), 356-363.

Juang, C.H., Fang, S.Y., Tang, W.H., Khor, E.H., Kung, G.T.C., and Zhang, J. (2009). “Evaluating model uncertainty of an SPT-based simplified method for reliability analysis for probability of liquefaction.” *Soils and Foundations*, 49(12), 135-152.

Juang, C.H., Schuster, M., Ou, C.Y. and Phoon, K.K. (2011). "Fully-probabilistic framework for evaluating excavation-induced damage potential of adjacent buildings." *Journal of Geotechnical and Geoenvironmental Engineering*, 137(2), 130-139.

Juang, C. H., and Wang, L. (2013). "Reliability-based robust geotechnical design of spread foundations using multi-objective genetic algorithm." *Computers and Geotechnics*, 48, 96–106.

Juang, C.H., Wang, L. Liu, Z., Ravichandran, N. Huang, H., and Zhang, J. (2013). "Robust design of drilled shafts in sand: New design perspective." *Journal of Geotechnical and Geoenvironmental Engineering*, 139(12), 2007-2019.

Juang, C.H., Wang, L., Hsieh, H.S. and Atamturktur, S. (2014). "Robust geotechnical design of braced excavations in clays." *Structural Safety*, 49, 37-44.

Khoshnevisan, S., Wang, L., and Juang, C.H. (2016). "Simplified procedure for reliability-based robust geotechnical design of drilled shafts in clay using spreadsheet." *Georisk: Assessment and Management of Risk for Engineered Systems and Geohazards*, 10(2), 121-134, DOI: 10.1080/17499518.2016.1146305.

Kim, K.N., Lee, S.H., Kim, K.S., Chung, C.K., Kim, M.M. and Lee, H.S., (2001). "Optimal pile arrangement for minimizing differential settlements in piled raft foundations." *Computers and Geotechnics*, 28(4), 235-253.

Kulhawy, F.H., and Mayne, P.W. (1990). "Manual on estimating soil properties for foundation design." *Report EL-6800 Electric Power Research Institute*, Palo Alto, CA, USA.

Kulhawy, F.H. and Phoon, K.K., (1996). "Engineering judgment in the evolution from deterministic to reliability-based foundation design." *Proceedings of Uncertainty,* 96, 29-48.

Lee, J.H., Kim, Y., and Jeong, S. (2009). "Three-dimensional analysis of bearing behavior of piled raft on soft clay." *Computer and Geotechnics*, 37(2010), 103–114.

Leung, Y.F., Klar, A. and Soga, K., (2009). "Theoretical study on pile length optimization of pile groups and piled rafts." *Journal of Geotechnical and Geoenvironmental Engineering*, 136(2), 319-330.

Lewin, T.J. (2010). "An investigation of design alternatives for 328-ft (100-m) tall wind turbine towers." Master's Thesis, Iowa State University, Ames, IA, USA.

Liu, X., Cheng, G., Wang, B., and Lin, S. (2012). "Optimum Design of Pile Foundation by Automatic Grouping Genetic Algorithms." *International Scholarly Research Network*, 2012, Article ID 678329.

Malhotra, S (2011). "Selection, Design and Construction of Offshore Wind Turbine Foundations, Wind Turbines." Dr. Ibrahim Al-Bahadly (Ed.), *InTech*, ISBN 978-953-307-221-0.

Mayne, P. W., and Kemper, J. B. (1988). "Profiling OCR in stiff clays by CPT and SPT." *Geotechnical Testing Journal*, 11(2), 139–147

Meyerhof, G.G. (1963). “Some Recent Research on the Bearing Capacity of Foundations.” *Canadian Journal*, 1(1), 16-26.

Morgan E. C., Lackner, M., Vogel, R.M., and Baise, L.G. (2010). “Probability distributions for offshore wind speeds.” *Energy Conversion and Management*, 52(2011), 15-26.

Overgård, I.E.V., Depina, I., Eiksund, G. (2016). “Reliability-based design of a monopile foundation for offshore wind turbines based on CPT data.” *Proceedings of the 17th Nordic Geotechnical Meeting*, Reykjavik, Iceland, 495-502.

Phoon, K.K. (2008). “Reliability-Based Design on Geotechnical Engineering: Computations and Applications.” *Taylor and Francis*, CRC Press.

Phoon, K.K., Kulhawy, F.H. and Grigoriu, M.D. (2003a). “Development of a reliability based design framework for transmission line structure foundations.” *Journal of Geotechnical and Geoenvironmental Engineering*, 129(9), 798-806.

Phoon, K.K., Kulhawy, F.H. and Grigoriu, M.D. (2003b). “Multiple resistance factor design for shallow transmission line structure foundations.” *Journal of Geotechnical and Geoenvironmental Engineering*, 129(9), 807-818.

Poulos, H.G. and Davis, E.H. (1980). “Pile foundation analysis and design.” *John Wiley*, New York, USA.

Poulos, H.G. (2001a). “Methods of Analysis of Piled Raft Foundations.” A Report Prepared on Behalf of Technical Committee TC-18 on Piled Foundations, *International Society of Soil Mechanics and Geotechnical Engineering*.

Poulos, H.G. (2001b). "Piled raft foundation: design and applications." *Geotechnique*, 51(2), 95-113.

Prakoso, W.A., and Kulhawy, F.H. (2001). "Contribution to piled-raft foundation design." *Journal of Geotechnical and Geoenvironmental Engineering*, 127 (1), 17-24.

Rahbari, P., Ravichandran, N., and Juang, C.H. (2017). "Robust Geotechnical Design of a Retaining Wall Subjected to Earthquake Loads." *Geotechnical Frontiers*, GSP 278, 149-158.

Rahbari, P., Ravichandran, N., and Juang, C.H. (2018). "Seismic Geotechnical Robust Design of Cantilever Retaining Wall Using Response Surface Approach." *Journal of GeoEngineering* Accepted for publication.

Raju, V.S. (2015). "Piled Raft." Prof. V.S. Raju Consultants, *Geotechnical and Structural Engineers*.

Randolph, M.F. (1994). "Design methods for pile groups and piled rafts." *State-of-the-Arts Report, 13th International Conference on Soil Mechanics and Foundation Engineering*, New Delhi, India, 5, 61-82.

Reul, O. (2004). "Numerical study of the bearing behavior of piled rafts." *International Journal of Geomechanic*s, 10.1061/(ASCE)1532-3641(2004)4:2(59), 59–68.

Reul, O. and Randolph, M.F. (2003). "Piled rafts in overconsolidated clay: comparison of in situ measurements and numerical analyses." *Geotechnique*, 53(3), 301-315.

Roa, K.N.S.V. (2011). "Foundation Design: Theory and Practice." 1st edition, *John Wiley and Sons (Asia) Pte Ltd*, 2 Clementi Loop, #02-01, Singapore 129809, ISBN- 13: 978-470-82534-1.

RSMeans Building Construction Cost Data 2013, *Construction Publishers & Consultants*, Norwell, MA, ISBN 978-1-936335-56-5.

Sawada, K. and Takemura, J. (2014). "Centrifuge model tests on piled raft foundation in sand subjected to lateral and moment loads." *Soils and Foundations*, 54(2), 126-140.

SCDOT Geotechnical Design Manual Version 1.1 (2010). "Chapter 7 – Geomechanics."

Schuster, M.J., Juang, C.H., Roth, M.J.S. and Rosowsky, D.V. (2008). "Reliability analysis of building serviceability problems caused by excavation." *Geotechnique*, 58(9), 743-749.

Shrestha, S. (2015). "Design and Analysis of Foundation for Onshore Tall Wind Turbines." M.S. thesis, Clemson University, Clemson, SC, USA.

Shrestha, S. and Ravichandran, N. (2016). "Design and Analysis of Foundations for Onshore Tall Wind Turbines." *Geo-Chicago 2016 GSP 270*, Chicago, IL, USA, 217-226.

Shrestha, S., Ravichandran, N., and Rahbari, P. (2017). "Geotechnical Design and Design Optimization of Pile-Raft Foundation for Tall Onshore Wind Turbines in Multi-Layered Clay." *International Journal of Geomechanics*, 18(2).

Sinha, A. and Hanna, A. M. (2016). "3D Numerical Model for Piled Raft Foundation." *International Journal of Geomechanics*, 17(2), 04016055-1-9.

U.S. Army Corps of Engineers (1990). "Engineering and Design – Settlement Analysis." Engineering Manual, No. 1110-1-1904.

Valliappan, S., Tandjiria, V. and Khalili, N., (1999). "Design of raft–pile foundation using combined optimization and finite element approach." *International journal for numerical and analytical methods in geomechanics*, 23(10), 1043-1065.

Vesic, A.S. (1973). "Analysis of Ultimate Loads of Shallow Foundations." *ASCE Journal of the Soil Mechanics and Foundation Division*, 99(SM1), 45-73.

Vesic, A.S. (1975). "Bearing Capacity of Shallow Foundations." Foundation engineering Handbook, 1st edition, *Van Nostrand Reinhold Company*, Inc., New York, USA.

Wade, D. D. and Langdon, O. G. (1990). "Sabal palmetto (Walt.) Lodd. Ex J. A. & J. H. Schult. cabbage palmetto." In: Burns, Russell M.; Honkala, Barbara H., technical coordinators, *Silvics of North America*, Vol. 2, Hardwoods. Agric. Handb. 654, Washington, DC, U.S. Department of Agriculture, Forest Service, 762-767.

Wagner, H.J. and Mathur, J. (2013). "Introduction to Wind Energy Systems: Basics, Technology and Operation, 2nd Edition." *Springer*, Verlag Berlin Heidelburg, ISBN 9783642329753.

Wang, Y., Au, S.K. and Kulhawy, F.H. (2011). "Expanded reliability-based design approach for drilled shafts." *Journal of Geotechnical and Geoenvironmental Engineering*, 137(2), 140-149.

Wang, L., Gong, W., Luo, Z., Khoshnevisan, S., and Juang, C.H. (2015). "Reliability-Based Robust Geotechnical Design of Rock Bolts for Slope Stabilization." *Geotechnical Special Publication*, 1926-1935.

Wolff, T. F. (1989). "Pile Capacity Prediction Using Parameter Functions." *Predicted and Observed Axial Behavior of Piles, Results of a Pile Prediction Symposium*, sponsored by the Geotechnical Engineering Division, ASCE, Evanston, IL, June 1989, ASCE Geotechnical Special Publication (23), 96 – 106.

WPC, A Terracon Company (2010). "Geotechnical Engineering Report: Clemson Wind Turbine Testing Facility North Charleston, South Carolina." WPC Project No. EN105060.

Zhang, J., Zhang, L.M. and Tang, W.H. (2011). "Reliability-based optimization of geotechnical systems." *Journal of Geotechnical and Geoenvironmental Engineering*, 137(12), 1211-1221.